



CENTER FOR INFRASTRUCTURE ENGINEERING STUDIES

FRP Repair and Health Monitoring of Railroad Steel Bridges

by

GRADUATE RESEARCH ASSISTANTS:

Anja Frauenberger

Xiangdong Liu

Lakshmanan Meyyappan

Jose Mata

Tarun Gupta

FACULTY ADVISORS:

Pedro F. Silva

Cihan H. Dagli

Hardy J. Pottinger

Antonio Nanni

INDUSTRY COLLABORATOR:

Ward N. Marianos, Jr.

DISCLAIMER

The contents of this report reflect the views of the author(s), who are responsible for the facts and the accuracy of information presented herein. This document is disseminated under the sponsorship of the Center for Infrastructure Engineering Studies (CIES), University of Missouri-Rolla, in the interest of information exchange. CIES assumes no liability for the contents or use thereof.

The mission of CIES is to provide leadership in research and education for solving society's problems affecting the nation's infrastructure systems. CIES is the primary conduit for communication among those on the UMR campus interested in infrastructure studies and provides coordination for collaborative efforts. CIES activities include interdisciplinary research and development with projects tailored to address needs of federal agencies, state agencies, and private industry as well as technology transfer and continuing/distance education to the engineering community and industry.

Center for Infrastructure Engineering Studies (CIES)

University of Missouri-Rolla

223 Engineering Research Laboratory

1870 Miner Circle

Rolla, MO 65409-0710

Tel: (573) 341-6223; Fax -6215

E-mail: cies@umr.edu

FRP REPAIR AND HEALTH MONITORING OF RAILROAD STEEL BRIDGES

by

*Anja Frauenberger*¹

*Xiandong Liu*¹

*Lakshmanan Meyyappan*¹

*Jose Mata*¹

*Tarun Gupta*¹

*Pedro F. Silva*²

*Cihan H. Dagli*³

*Hardy J. Pottinger*⁴

*Antonio Nanni*⁵

*Ward N. Marianos, Jr.*⁶

¹ Graduate Research Assistant

² Assistant Professor of Civil Engineering
Associate Director of Repair of Buildings and Bridges Center – RB²C

³ Professor of Engineering Management
Director Smart Engineering Systems Lab - SESL

⁴ Associate Professor of Electrical Engineering

⁵ Vernon and Maralee Jones Endowed Professor of Civil Engineering
Director Center for Infrastructure Engineering Sciences – CIES

⁶ Associate, Modjeski and Masters, Inc.

Final Report

Report No. CIES 03-44

**Center for Infrastructure Engineering Studies
University of Missouri – Rolla**

January 2003

ABSTRACT

A large number of our nation's bridges must be replaced or are in need of major repair/rehabilitation because they do not conform to current demands due to deterioration caused by aging or environmental conditions, heavier vehicles and increased traffic volume. Since a replacement alternative usually involves high costs and/or substantial interference with the normal traffic flows, strengthening is many times one of the most effective alternatives. As many bridges remain in continuous service despite aging and associated potential for damage accumulation and/or collapse, the Federal Railroad Administration (FRA) has identified as one of its strategic priorities the health monitoring of these structures to ensure a safe mode of operation. As such, a research program funded by FRA was initiated at the University of Missouri Rolla (UMR). The main objectives of this research program are as follows: (1) demonstrate the use of fiber reinforced polymers (FRP) composites in the repair/rehabilitation of railroad steel bridges with highly corroded steel members, and (2) health monitoring of railroad steel bridges to ensure a safe mode of operation of these bridges.

Compared to the application of FRP composites to other traditional materials, research examining the prospects of the combination of FRP and steel has been limited. Considering the fact that many bridges that are in need of rehabilitation and strengthening are steel bridges, it is imperative to increase the amount of research in this area. In this research project, the following strengthening issues applied to steel structures were investigated; (i) bond characterization, (ii) flexural strengthening, and (iii) strengthening of highly corroded axially loaded steel members using carbon FRP (CFRP).

Development of health monitoring technologies capable of continuously monitoring the structural performance of the civil infrastructure on a real-time basis is becoming an important research area. In this research program, the main components used in the development of a field deployable remote system for health monitoring consisted of: (i) wireless sensors for data collection, and (ii) soft computing tools for data processing, which involved classification, decision, pattern recognition and process control of the collected data.

Test results have confirmed the advantages of FRP composites applied to the repair/rehabilitation of steel bridges and field deployable remote systems for the health monitoring. This final report presents the results from this research project funded by FRA.

ACKNOWLEDGEMENTS

The research presented in this report was sponsored by the Federal Railroad Administration (FRA) and the UMR University Transportation Center (UTC), and their financial assistance is acknowledged. In addition, the authors would like to thank Fyfe Inc., Glasforms Inc., Sika, Structural Composites Inc., MO-SCI, Buildex Inc., USG Inc., and HCA Inc. for the contribution of materials.

TABLE OF CONTENTS

Abstract.....	v
Acknowledgements.....	vii
Table of Contents.....	viii
List of Figures.....	xvii
List of Tables.....	xxii
1. Introduction.....	1
1.1. Background.....	1
1.1.1. Repair/Rehabilitation of Steel Members with FRP Composites.....	1
1.1.2. Health Monitoring of Steel Bridges using Neural Networks.....	2
1.2. Research Objectives.....	3
1.3. Report Layout.....	4
1.4. Summary of Major Research Findings.....	5
1.4.1. Repair/Rehabilitation of Steel Members with FRP Composites.....	5
1.4.2. Health Monitoring of Steel Bridges using Neural Networks.....	5
2. Literature Review.....	7
2.1. Repair/Rehabilitation of Structures using FRP Composites.....	7
2.1.1. Performance of Adhered FRP Composites.....	7
2.1.1.1. Bond of FRP onto Concrete Surfaces.....	7
2.1.1.2. Bond of FRP onto Steel Surfaces.....	7
2.1.1.2.1. Bonded Length.....	7
2.1.1.2.2. Galvanic Corrosion.....	8
2.1.1.2.3. Surface Preparation.....	9
2.1.1.2.4. Thermal Effects.....	9
2.1.1.3. Other Aspects Regarding the Application to Steel.....	10
2.1.1.4. CFRP-Steel Bond Related Analytical Model.....	11
2.1.2. Traditional Steel Strengthening Methods For Flexural Members.....	13
2.1.2.1. Welding Steel Cover Plates.....	14
2.1.2.2. Bolting Steel Cover Plates.....	14
2.1.2.3. Adhering Steel Cover Plates.....	15
2.1.3. FRP Strengthening Methods For Flexural Members.....	15
2.1.3.1. Tension Flange Strengthening with Unidirectional Laminates.....	15

2.1.3.2. Tension Flange Strengthening using Alternative FRP Reinforcement Methods.....	16
2.1.4. FRP Strengthening Methods For Compression Members	18
2.1.4.1. Expansive Light-Weight Concrete.....	18
2.1.4.2. Local Bond-Slip Relationship between Steel and Concrete	18
2.1.4.3. Composite Column Construction.....	21
2.1.5. FRP Applications to Metallic Structures - Case Studies	21
2.1.5.1. Tickford Bridge.....	21
2.1.5.2. Slattocks Canal Bridge.....	22
2.1.5.3. Hythe Bridge.....	22
2.1.6. Design Guidelines Applicable to Metallic Structures.....	23
2.2. Health Monitoring of Steel Bridges.....	24
2.2.1. Sensor Technology.....	24
2.2.1.1. Temperature Sensors.....	24
2.2.1.2. Wind Pressure Transducer Sensors.....	24
2.2.1.3. Global Positioning Systems	25
2.2.1.4. Vibration Induced Sensors.....	25
2.2.1.5. Input Excitation Methods.....	25
2.2.1.6. Non-Destructive Technologies	27
2.2.2. Soft Computing Tools.....	28
2.2.2.1. Neural Network Systems for Health Monitoring of The civil infrastructure	28
2.2.2.2. Evaluation Methodology.....	29
2.2.2.3. Neural Networks	29
3. Bond Characterization	31
3.1. Introduction.....	31
3.1.1. Background.....	31
3.1.2. Objectives	31
3.1.2.1. Specimen Type.....	31
3.1.2.2. Bonded Length.....	32
3.1.2.3. Wraps.....	32

3.1.2.4. FRP Laminate Type	32
3.1.2.5. Adhesive Type	32
3.1.2.6. Adhesive Thickness	32
3.1.2.7. Surface Preparation	32
3.1.2.8. Curing Time	33
3.1.3. Research Findings	33
3.1.4. Chapter Layout.....	34
3.2. Experimental Program	34
3.2.1. Introduction.....	34
3.2.2. Problem Statement	34
3.2.3. Specimen Description and Instrumentation	35
3.2.3.1. Specimen Types	35
3.2.3.1.1. Discontinuous Specimens	35
3.2.3.1.2. Continuous Specimen	37
3.2.3.2. Specimen Characterization Factors.....	37
3.2.3.2.1. Wraps	37
3.2.3.2.2. FRP Laminate Type	39
3.2.3.2.3. Adhesive Type	39
3.2.3.2.4. Adhesive Thickness	40
3.2.3.2.5. Surface Preparation	41
3.2.3.2.6. Curing Time	41
3.2.3.3. Specimen Notation.....	41
3.2.4. Test Matrix	43
3.2.5. Specimen Preparation	44
3.2.6. Test Setup.....	46
3.3. Experimental Results	47
3.3.1. Introduction.....	47
3.3.2. General Observations.....	47
3.3.2.1. Failure Modes	47
3.3.2.1.1. Failure Mode S.....	47
3.3.2.1.2. Failure Mode SF	47

3.3.2.1.3. Failure Mode F.....	48
3.3.2.1.4. Failure Mode +w.....	48
3.3.2.2. Test Series I.....	49
3.3.2.3. Test Series II.....	52
3.3.2.4. Test Series III.....	53
3.3.2.5. Test Series III _T – Time Dependency.....	59
3.3.2.6. Test Series III-W ₁	60
3.3.2.7. Test Series III-W ₂	62
3.3.2.8. Test Series Continuous Specimens.....	65
3.3.3. Load-Strain Response.....	67
3.3.3.1. Test Series I.....	67
3.3.3.2. Test Series II.....	68
3.3.3.3. Test Series III.....	69
3.3.3.4. Test Series III _T – Time Dependency.....	75
3.3.3.5. Test Series III-W ₁	76
3.3.3.6. Test Series III-W ₂	77
3.3.3.7. Test Series Continuous Specimen.....	78
3.4. Discussion of Results.....	79
3.4.1. Brittle Strain Response.....	80
3.4.2. Ductile Strain Response.....	82
3.5. Summary and Conclusions.....	83
3.5.1. Summary.....	83
3.5.2. Conclusions.....	85
3.5.2.1. Specimen Type.....	85
3.5.2.2. Bonded Length.....	86
3.5.2.3. Wrapping the Specimens.....	86
3.5.2.4. FRP Laminate Type.....	86
3.5.2.5. Adhesive Type.....	87
3.5.2.6. Adhesive Thickness.....	87
3.5.2.7. Surface Preparation.....	88
3.5.2.8. Curing Time.....	88

3.5.3. Recommendations for Future Research Projects	88
4. Flexural Tests.....	90
4.1. Introduction.....	90
4.1.1. Background.....	90
4.1.2. Objectives	90
4.1.3. Research Findings.....	90
4.1.4. Chapter Layout.....	91
4.2. Experimental Program	91
4.2.1. Introduction.....	91
4.2.2. Problem Statement	91
4.2.3. Retrofit Scheme	92
4.2.4. Experimental Setup.....	95
4.2.4.1. Test Specimen and Material.....	95
4.2.4.2. Theoretical Prediction.....	96
4.2.4.3. Surface Preparation.....	97
4.2.4.4. Test Setup.....	97
4.2.4.5. Instrumentation	99
4.2.4.6. Design of the Test Specimen Using the Proposed Retrofit Scheme	101
4.3. Experimental Results	101
4.3.1. Test Unit 1.....	101
4.3.2. Test Unit 2.....	102
4.3.3. Test Unit 3.....	104
4.3.4. Test Unit 4.....	105
4.4. Discussion of Experimental Results	105
4.5. Conclusions.....	107
5. Axially Loaded Members	108
5.1. Introduction.....	108
5.1.1. Background.....	108
5.1.2. Objectives	109
5.1.3. Research Findings.....	109
5.1.4. Chapter Layout.....	109

5.2. Expansive Light-Weight Concrete.....	110
5.2.1. Objective.....	110
5.2.2. Background.....	110
5.2.3. Expansive Cement Blend.....	111
5.2.4. Expansion Test.....	111
5.2.4.1. Test Specimens	112
5.2.4.2. Materials	112
5.2.4.3. Mix-design, Test Setup and Materials	113
5.2.4.4. Specimen Curing Environment.....	115
5.2.4.5. Test Results, Discussion and Conclusions.....	115
5.2.5. GFRP Confined Concrete Compression Test	119
5.2.5.1. Test Specimens	119
5.2.5.2. Test setup and Test Matrices.....	119
5.2.5.3. Test Results, Discussions, and Conclusions	120
5.2.6. Relationship between Internal Pressure Developed in the Concrete and Confining Stiffness	121
5.2.6.1. Test Specimens and Instrumentations.....	121
5.2.6.2. Test Results, Discussion and Conclusions.....	122
5.2.7. Summary.....	123
5.3. Local Bond-Slip Relationship between Smooth Steel Bars and FRP Confined Expansive Light-Weight Concrete.....	124
5.3.1. Objective.....	124
5.3.2. Background.....	124
5.3.3. Test Specimens and Materials	125
5.3.3.1. GFRP Pipes.....	125
5.3.3.2. Steel Bars	125
5.3.3.3. Light-weight Concrete	125
5.3.4. Test Setup and Instrumentation	127
5.3.5. Test Results and Discussion.....	127
5.3.6. Analytical Model	129
5.3.7. Conclusions.....	132

5.4. FRP Retrofit Scheme for Corroded Steel Columns	132
5.4.1. Objective	132
5.4.2. Test Specimens and Test Matrix	132
5.4.3. Test Setup and Instrumentation	136
5.4.4. Test Results and Discussions	138
5.4.5. Conclusions	140
5.4.6. Analytical Model	140
5.4.6.1. Composite Column	140
5.4.6.2. Development Length	141
5.4.6.3. Elastic Buckling	144
5.4.6.4. Inelastic Buckling	148
5.4.6.5. Analytical Results and Conclusions	148
5.5. Summary	150
5.6. Design Guidelines	151
5.6.1. Cross Section of Retrofit Material	152
5.6.1.1. Area Requirement	152
5.6.1.2. Stiffness Requirement	153
5.6.1.3. Structural Requirement	153
5.6.2. Length of Retrofit Material	154
5.6.3. Thickness of FRP Pipe	154
6. Displacement Sensing	156
6.1. Introduction	156
6.1.1. Background	156
6.1.2. Objectives	156
6.1.3. Research Findings	156
6.1.4. Chapter Layout	157
6.2. Relative Displacement Sensors (GPS)	157
6.2.1. Test Description	157
6.2.2. Results	158
6.2.3. Conclusion	158
6.3. Dynamic Response Sensors	159

6.4. Wireless Instrumentation	160
6.4.1. Objective	160
6.4.2. Background	161
6.4.3. Bluetooth Enabled Devices	161
6.4.4. A Prototype: Smart Wireless Sensor Cluster (SWSeC).....	163
6.4.4.1. Microcontroller	163
6.4.4.2. Bluetooth Enabled Radio: ROK 101 007.....	165
6.4.4.3. Establishing a Bluetooth Connection.....	166
6.4.4.4. Interfacing the Controller with Bluetooth.....	169
6.4.4.5. Hardware Design	170
6.4.4.6. Smart Wireless Sensor Cluster.....	172
6.4.4.7. Instrumentation Field Test	173
6.4.4.7.1. Objective	173
6.4.4.7.2. Setup	173
6.4.4.7.3. Results.....	174
6.4.5. Final Design: ASUL	175
6.4.5.1. C8051F123 Microcontroller	175
6.4.5.2. Taiyo Yuden EYSF2SAXX.....	176
6.4.5.3. EYSF2SAXX: Changes to the Source Code	176
6.4.5.4. Hardware Design	177
6.4.5.5. ASUL Cluster.....	179
6.4.6. Complete Wireless Solution Description.....	179
6.4.6.1. System Test Setup.....	180
6.5. Conclusions.....	182
7. Smart Health Monitoring System	183
7.1. Introduction.....	183
7.1.1. Background.....	183
7.1.2. Objective.....	183
7.1.3. Research Findings.....	184
7.1.4. Chapter Layout.....	185
7.2. Overall System.....	185

7.3. Data Acquisition and Analysis.....	186
7.4. Damage Detection.....	194
7.5. Fuzzy Logic Decision System	196
7.6. Neural Network Prediction System	200
7.7. Conclusions.....	203
7.7.1. Recommendations for Future Research Projects	203
8. Conclusions and FUTURE RESEARCH NEEDS.....	204
8.1. Conclusions.....	204
8.1.1. Repair/rehabilitation of steel members with FRP composites:.....	204
8.1.2. Health monitoring of steel bridges using Neural Networks:	205
8.2. future Research needs	206
8.2.1. Repair/rehabilitation of steel members with FRP composites:.....	206
8.2.2. Strengthening of timber and concrete bridge members with FRP composites:	206
8.2.3. Improving blast resistance of railroad bridge members with FRP composites:	207
8.2.4. Health monitoring of steel bridges using Neural Networks:	207
List of References	209

LIST OF FIGURES

Figure 2-1 Deformations for Rigid – Deformable Joint	12
Figure 2-2 Geometry of Adhesive Joint.....	13
Figure 2-3 Bond Stress Dependencies	13
Figure 2-4 Reinforcement Schemes (Gillespie et al, 1996).....	16
Figure 2-5 Defined Functions	20
Figure 2-6 Tickford Bridge.....	21
Figure 2-7 Hythe Bridge	23
Figure 2-8 Davis 7911 Anemometer.....	24
Figure 3-1 Discontinuous Specimen.....	36
Figure 3-2 Continuous Specimen – Geometry and Instrumentation	37
Figure 3-3 Wrapping Schemes.....	38
Figure 3-4 Specimen Preparation (using Enforce CFL)	45
Figure 3-5 MTS 880 and Data Acquisition.....	46
Figure 3-6 Failure Mode S.....	48
Figure 3-7 Failure Mode SF.....	48
Figure 3-8 Failure Mode F.....	49
Figure 3-9 Failure of Wraps (+w).....	49
Figure 3-10 Test Results – Test Series I.....	50
Figure 3-11 Test Results – Test Series II.....	53
Figure 3-12 Test Results – Test Series III.....	55
Figure 3-13 Failure of CFRP 200/2000 -Sikadur [®] 30 Specimens	57
Figure 3-14 Test Results – Test Series III _T	60
Figure 3-15 Increase of Bonded Area by Ramps.....	60
Figure 3-16 Test Results – Test Series III-W ₁	61
Figure 3-17 Test Results – Test Series III-W ₂	64
Figure 3-18 Failure of Continuous Specimen.....	66
Figure 3-19 Strain Profiles – Test Series I.....	67
Figure 3-20 Strain Profiles – Test Series II	68
Figure 3-21 Strain Profiles – Specimen III-1 to III-6	70

Figure 3-22 Strain Profile– Specimen III-7	71
Figure 3-23 Strain Profiles – Specimen III-8 to III-10	72
Figure 3-24 Strain Profiles – Specimen III-11 to III-12	73
Figure 3-25 Strain Profiles – Tests III-13	74
Figure 3-26 Strain Profiles – Test Series III _T (Cont.).....	76
Figure 3-27 Strain Profiles – Test Series III-W ₁ (Continuation)	77
Figure 3-28 Strain Profiles – Test Series III-W ₂ (Continuation)	78
Figure 3-29 Strain Profiles – Specimen C-1	78
Figure 3-30 Strain Profiles – Specimen C-2.....	79
Figure 3-31 Typical Strain Profiles.....	80
Figure 3-32 Bond Stresses – Brittle Response.....	81
Figure 3-33 Bond Stresses – Ductile Response	82
Figure 4-1 Retrofitted Cross-Section.....	92
Figure 4-2 Moment Curvature Analysis for W12 x 14 Section.....	94
Figure 4-3 M_R/M_D for different levels of Corrosion vs. Section Modulus.....	95
Figure 4-4 Test Setup (Liu, 2002).....	98
Figure 4-5 Test Setup.....	98
Figure 4-6 Lateral Support Setup (Liu, 2002)	99
Figure 4-7 View of Lateral Support Setup.....	99
Figure 4-8 Strain Gage Locations (Liu, 2002).....	100
Figure 4-9 Distribution of LVDT (Liu, 2002)	100
Figure 4-10 Failure Mode of Test Unit 1	102
Figure 4-11 Test Unit 1	102
Figure 4-12 Failure Mode of Test Unit 2.....	103
Figure 4-13 Test Unit 2.....	103
Figure 4-14 Failure Mode of Test Unit 3.....	104
Figure 4-15 Test Unit 3.....	104
Figure 4-16 Test Unit 4.....	105
Figure 4-17 Strain-Location – Test Unit 3.....	106
Figure 4-18 Strain-Location – Test Unit 4.....	106
Figure 5-1 Typical Built-up Steel Column of Steel Railway Bridge.....	108

Figure 5-2 Test Specimens.....	112
Figure 5-3 Strain Gages on Specimens of the Seven Groups	115
Figure 5-4 Force Balance Mechanism	116
Figure 5-5 Stress Developed in GFRP Pipes vs. Time	116
Figure 5-6 Internal Pressure of the Concrete vs. Time	116
Figure 5-7 Internal Pressure of Concrete vs. Calcium Aluminate Cement Percentage in Total Cement Weight	117
Figure 5-8 Internal Pressure of Concrete vs. Sulfur Trioxide Percentage in Total Cement Weight	117
Figure 5-9 Internal Pressures of Concrete at Different Height Locations vs. Time (Group VI)	117
Figure 5-10 Internal Pressure of Concrete at Different Height Locations vs. Time (Group VII)	117
Figure 5-11 Instrumentation of the Compression Test	119
Figure 5-12 Typical Failed Specimens	120
Figure 5-13 Longitudinal Stress vs. Longitudinal Strain.....	121
Figure 5-14 Longitudinal Stress vs. Transverse Strain.....	121
Figure 5-15 Lateral Strain vs. Time	123
Figure 5-16 Stress in Pipe vs. Time	123
Figure 5-17 Internal Pressure vs. Time.....	123
Figure 5-18 Stabilized Internal Pressure vs. Confining Stiffness ($E*2t/D$).....	123
Figure 5-19 Test Specimens.....	126
Figure 5-20 Test Setup and Instrumentations	127
Figure 5-21 Load vs. Free End Slip of Group I	129
Figure 5-22 Load vs. Free End Slip of Group II.....	129
Figure 5-23 mBEP Local Bond Slip Laws for Group I	131
Figure 5-24 mBEP Local Bond Slip Laws for Group II.....	131
Figure 5-25 Test Specimens.....	133
Figure 5-26 Fabrication Schemes of FRP Jackets	134
Figure 5-27 Notch Details.....	135
Figure 5-28 Test Setup.....	136
Figure 5-29 Distributions of LVDTs and Strain Gages	137

Figure 5-30 Failed Specimens	138
Figure 5-31 Load vs. Deflection	140
Figure 5-32 Load Transfer Mechanisms of Typical Composite Column and Jacketed Composite Column.....	142
Figure 5-33 Defined Functions	143
Figure 5-34 Assumed Stiffness Distribution and Deflection Shape for Test Unit 3 to 7	145
Figure 5-35 Influence of Residual Stress on Average Stress-strain Curve.....	148
Figure 5-36 Comparison between Experimental and Theoretical Buckling Loads	149
Figure 5-37 Ultimate Load (P) vs. Slenderness Parameter (L) for a Steel Column	151
Figure 5-38 Structural construction requirement for the retrofitted material	154
Figure 6-1 UMR Smart Bridge Test	158
Figure 6-2 PVDF Sensor.....	159
Figure 6-3 Crossbow Technology.....	161
Figure 6-4 ROK 101 007	163
Figure 6-5 C8051 Block Diagram.....	165
Figure 6-6 Ericsson Development Kit	166
Figure 6-7 Connection Establishment Process	168
Figure 6-8 Prototype Schematic.....	171
Figure 6-9 Smart Sensor Cluster.....	172
Figure 6-10 Teardrop Bridge	173
Figure 6-11 Testing Teardrop Bridge	174
Figure 6-12 Peak Vibration.....	175
Figure 6-13 Taiyo Yuden EYSF2SAXX	176
Figure 6-14 ASUL Schematic.....	178
Figure 6-15 ASUL cluster.....	179
Figure 6-16 Remote PC	180
Figure 6-17 Cluster AZUL.....	180
Figure 6-18 ASUL Test Configuration.....	181
Figure 6-19 HP54600 Test V Plot	181
Figure 6-20 ASUL Test V Results.....	182
Figure 7-1 Teardrop Bridge	184

Figure 7-2 Overall System	186
Figure 7-3 Teardrop Bridge – Sensor Locations.....	187
Figure 7-4 Sensor Locations	188
Figure 7-5 Sensor Output.....	189
Figure 7-6 Un-calibrated Sensor Output.....	190
Figure 7-7 Calibrated Sensor Output	191
Figure 7-8 Power Spectrum Values	193
Figure 7-9 Sensor Locations	195
Figure 7-10 Power Spectrum Comparison.....	196
Figure 7-11 Membership Values	198
Figure 7-12 Backpropagation Architecture	201
Figure 8-13 Manually Investigating the Tightness of Eyebars in Steel Bridges	206

LIST OF TABLES

Table 2.1 Temperature Ranges (AASHTO)	10
Table 3.1 Bonded Length Type	36
Table 3.2 Wrapping Scheme	38
Table 3.3 FRP Laminate Properties	39
Table 3.4 Adhesive properties	40
Table 3.5 Test Matrix	43
Table 3.6 Test Results – Test Series I	50
Table 3.7 Test Results – Test Series II	52
Table 3.8 Test Results – Test Series III	54
Table 3.9 Test Results – Test Series III _T	59
Table 3.10 Test Results – Test Series III-W ₁	61
Table 3.11 Test Results – Test Series III-W ₂	64
Table 3.12 Test Results – Continuous Specimens	65
Table 4.1 Properties of CFRP Laminates	96
Table 4.2 Test Matrix	96
Table 4.3 Theoretical Properties of a W12 x 14	96
Table 4.4 Test Results	107
Table 5.1 Properties of the GFRP Pipe	112
Table 5.2 Cumulative Percentage Passing of Aggregate	113
Table 5.3 Compositions of the Seven Cement Blends	114
Table 5.4 Concrete Mix Design for 1 yard ³ (0.76 m ³)	114
Table 5.5 Test Matrix	115
Table 5.6 Slumps and Densities for the Seven Groups of Concrete	118
Table 5.7 Results of GFRP Confined Concrete Tests	120
Table 5.8 Properties of Test Specimens	122
Table 5.9 Compositions of the Cement Blend	122
Table 5.10 Properties of the GFRP Pipe	125
Table 5.11 Properties of Steel Bar	125
Table 5.12 Engineering Properties of the GFRP Confined Concrete	126

Table 5.13 Test Matrix.....	126
Table 5.14 Test Results.....	128
Table 5.15 Calibrated Parameters of mBEP Model.....	130
Table 5.16 Anchorage Length Examples.....	131
Table 5.17 Test Matrix.....	133
Table 5.18 Properties of GFRP Pipe.....	134
Table 5.19 Engineering Properties of GFRP Confined Concrete.....	134
Table 5.20 Properties of Steel Material.....	135
Table 5.21 Notch Details.....	136
Table 5.22 Test Results.....	139
Table 5.23 Development Length Results of the Specimens.....	144
Table 5.24 Theoretical Buckling Load.....	149
Table 6.1 GPS Displacement Solution Cost.....	159
Table 6.2 PVDF Properties.....	160
Table 7.1 Data Details.....	189
Table 7.2 Power Spectrum Summary.....	195

1. INTRODUCTION

1.1. BACKGROUND

The main objectives of this research program funded by FRA were as follows: (1) demonstrate the use of FRP composites in the repair/rehabilitation of railroad steel bridges with highly corroded steel members, and (2) health monitoring of railroad steel bridges to ensure a safe mode of operation of these bridges. The principal recipients of the outcomes from this project will be the railroad owners, in that they will have more economical and efficient technology for the maintenance of their bridge inventory and for its safe operation. The main outcome of this research program is the development of recommended specifications, supporting tests, and field procedures to be integrated into existing practice.

1.1.1. REPAIR/REHABILITATION OF STEEL MEMBERS WITH FRP COMPOSITES

More than thirty percent of bridges in the United States are steel bridges. More than forty percent of these bridges are considered either structurally deficient or functionally obsolete. For the state of Missouri, these numbers look even more alarming. More than fifty percent of all bridges are made of steel, and fifty percent of these bridges are structurally deficient or functionally obsolete according to the Federal Highway Administration (FHWA) (FHWA 2001). Due to deterioration caused by aging or environmental conditions, heavier vehicles and increased traffic volume, these bridges do not conform to current demands and must be replaced or are in need of strengthening.

A replacement alternative will most likely involve high costs and closure of traffic for long periods, or at least, substantial interference with the normal traffic flows. Because of these reasons, strengthening appears to be an attractive alternative. A traditional retrofit method for repairing corroded and/or structurally deficient steel members consists of attaching cover plates to these members through bolts or welding. There are many disadvantages associated with these methods, such as: (1) the procedure is labor intensive and time consuming, (2) it requires drilling and extensive lap splice detailing, (3) traffic may have to be interrupted for a period of time, (4) there is a potential for weld fatigue cracking at the cover plate ends and a region of high stress concentrations may develop near the bolts, and (5) increase in the weight of the members. In this context, the use of fiber reinforced polymer (FRP) materials emerges as an alternative with great

potential. Their high strength, high fatigue resistance, low weight and corrosion resistance make them very attractive for the strengthening of the civil infrastructure. Once the composite is applied, no temporary scaffolding is needed to hold the FRP in place until the epoxy has cured. Thereby, the impact on traffic is low when compared to conventional methods.

Reinforcing concrete structures with FRP composites is nowadays a widely accepted and practiced strengthening method with design guidelines been developed and published in recent years (ACI 440.2R-02, 2002; ACI 440R, 1996; CAN/CSA-S806-02, 2002; JSCE, 1997; FIP Task Group 9.3, 1999). However, research has also been conducted on the strengthening of masonry with FRP composites (Tumialan, 2001; Li, 2002). Research, however, examining the prospects of the application of FRP on steel has been limited. Considering the fact that many bridges that are in need for rehabilitation and strengthening are steel bridges, it is imperative to increase the amount of research in this area. In this research project the following carbon FRP (CFRP) strengthening issues relative to steel structures were investigated; (1) bond characterization (2) flexural strengthening, and (3) strengthening of highly corroded axially loaded steel members.

1.1.2. HEALTH MONITORING OF STEEL BRIDGES USING NEURAL NETWORKS

In this research project, wireless sensors and soft computing tools were investigated to construct a field deployable remote wireless data collection system for health monitoring of bridges. Health monitoring of the civil infrastructure is an important research area because of its continuous use despite aging and associated potential for damage accumulation. Hence, the ability to continually monitor the structural performance of these systems on a real-time basis is becoming very important for their safe operation. The main components necessary in the development of a practical real-time structural health monitoring system may consist of sensors for data collection, and soft computing tools for data processing, which involves classification, decision, pattern recognition and process control of the collected data.

The sensors required for data collection should be such that they can relay, on a real-time basis, the collected data to smart engineering tools like fuzzy logic and neural network. Key measurands that are necessary for the proper evaluation of the performance of steel bridges are: (a) temperature induced deformations; (b) wind induced deformations; (c) vibrations induced

deformations; (d) long term degradation due to corrosion and/or fatigue induced deformations; and (e) impact damage.

Soft computing tools are becoming commonly used in the engineering community in developing health monitoring systems. Some examples of soft computing tools are neural networks, fuzzy logic, genetic algorithms, expert systems and artificial intelligence. Recently, hybrid architectures using two or three of the aforementioned smart tools are also common as they yield more efficient results. Fuzzy logic and neural networks are used to make predictions because of their inherent robustness and their abilities to handle nonlinearities and uncertainties in structural behavior. Since health monitoring of the civil infrastructure may be performed continuously on a real-time basis, the amount of data that needs to be processed and analyzed is large. Thus, it is of essential importance to add smart engineering system concepts and tools that can process the extensive amounts of data. Analysis may be done using a smart health monitoring system that uses neuro-fuzzy hybrid architecture. The neuro-fuzzy hybrid architecture will provide the data analysis needed for the health monitoring system.

Neural network models have been studied and used extensively in the last decade in order to achieve human-like intelligence and process data. Typical applications include: classification, decision making, financial analysis, medical diagnostics, optimization, pattern recognition, process control, robotics and automation, signal processing, targeted marketing, and time series prediction. In this project, some of the attractive features of neural network models that were investigated include those with the potential for classification, decision, pattern recognition and process control.

1.2. RESEARCH OBJECTIVES

Advanced composites made of fibers embedded in a polymeric resin, also known as FRP materials, have emerged as an alternative and practical solution to steel and its inherent corrosion problems. Since there are no nationally accepted specifications for construction process control of repairs with FRP composite materials, there is a need to develop such specifications to ensure acceptable performance of structures repaired with FRP. Development of retrofit techniques using FRP composite materials for application to corroded steel members is one of the objectives of this research program.

Another objective of this research program is to design a suitable configuration and construct a field deployable remote wireless data collection system for health monitoring. There is a large number of sensor technologies that are promising for displacement sensing in health monitoring. These include thermocouples, anemometers, accelerometers and global positioning system technologies. Data received from these sensors can be collected remotely and a smart health monitoring system can be used to process the data. In order to develop a reliable health monitoring system, it is also of essential importance to add a smart system-engineering concept for the health monitoring of railroad bridges. In this project, this was achieved through a Neuro-Fuzzy Hybrid architecture for data mining and detection of safe and/or unsafe modes of operation.

1.3. REPORT LAYOUT

In Chapter 1 background information related to the needs for repair/rehabilitation of railroad steel bridges with FRP composites, and health monitoring of railroad steel bridges to ensure a safe mode of their operation is presented. Chapter 2 contains pertinent literature review for all major topics investigated in this research project. It presents conventional steel strengthening methods as well, as past research findings for strengthening of the civil infrastructure with FRP composites. Additionally, ways for bridge monitoring and the use of Neural Networks for damage detection of structures are presented.

Chapters 3, 4 and 5 discuss major experimental results related to the feasibility of using FRP composites for the repair/rehabilitation of steel members with section losses due to corrosion. Chapter 3 deals with the bond characterization of precured FRP laminates adhered to steel. The use of FRP composites for the flexural strengthening of steel members is discussed in Chapter 4. Then, a retrofit technique utilizing FRP composites for the upgrade of existing axially loaded members in compression is presented in Chapter 5.

Health monitoring is the key issue addressed in Chapters 6 and 7. Whereas in Chapter 6 the displacement sensor system that was used in this project is discussed, Chapter 7 deals with the overall data acquisition and analysis. Finally, Chapter 8 contains a brief summary of conclusions for this research project and lists research areas that need to be addressed in the future.

1.4. SUMMARY OF MAJOR RESEARCH FINDINGS

In this section, major research findings are presented in two sections according to the primary objectives of this research program, namely: (1) the repair rehabilitation of steel members with FRP composites, and (2) the health monitoring of steel bridges using neural networks.

1.4.1. REPAIR/REHABILITATION OF STEEL MEMBERS WITH FRP COMPOSITES

- Two different bond behavior types, depending upon the used adhesive, were observed in this research project. They were characterized as: (1) brittle, designated as Case 1, and (2) ductile, designated as Case 2. Future design methodologies should be based on an allowable stress/strain approach for Case 1, as the effective development length is relatively short and does not affect the bond strength. This case was implemented in the flexural retrofit of steel members with simulation of highly corroded tension flanges. In case of a ductile bond behavior, a design approach based on the rupture of the FRP laminate using a certain bonded length may be appropriate. However, due to the potential for high strain levels that will develop at the rupture of FRP laminates (typically higher than the yield strain for steel), additional criteria will have to be considered, such as buckling of the compression flange, buckling of the web, and lateral torsional buckling of the structural member.

- In the flexural strengthening tests, a retrofit scheme was employed considering a bond performance according to Case 1. Test results indicate that indeed in all tested specimens, the FRP laminates applied to the steel members failed by debonding, after a certain bond stress limit was exceeded, which was dictated by the properties of adhesive used. However, test results indicate that the load capacity of the test units was within the desired load capacity levels.

- The retrofit of axially loaded steel members using FRP pipes filled with expansive concrete evolved as a promising new technology. Overall, test results indicated that a restoration of the ultimate load capacity of a deficient steel column was attainable. Design guidelines were developed for the retrofit of stocky and slender columns, and future research will have to prove their accuracy.

1.4.2. HEALTH MONITORING OF STEEL BRIDGES USING NEURAL NETWORKS

- Although Global Positioning Systems (GPS) appear to be a promising solution to obtain accurate relative displacement measurements, their use in this research project was not possible

due to high costs. Instead, research in this project used PVDF vibration sensors in combination with a wireless sensor data acquisition cluster. This system provides reliable data sets for the continuous health monitoring of steel bridges. For future applications, the addition of temperature and wind loading sensors may improve the sensor system. The electronic platform required for the wireless PVDF sensor networks has been developed at UMR. This wireless acquisition cluster consisted of Bluetooth-compliant radios, coupled with microcontrollers and a solar power supply.

- Continuous data analysis was accomplished with a software program developed at UMR. This continuous data analysis used a non-destructive evaluation technique, which did not cause disruption on the normal traffic flow. In addition, due to its high sensitivity small damages are likely to be detected using this system.

- After performing an extensive literature review, it was clear that vibration based structural health monitoring systems presented a number of advantages over other conventional methods. Test results indicated that this type of system was simple to implement, inexpensive, small enough to be mobile, and more effective for real-time structural health monitoring. This system provided the user with continuous data sets, which can be processed and analyzed by a neuro-fuzzy architecture system. Ambient excitation methods are more realistic and accurate for test data collection.

2. LITERATURE REVIEW

2.1. REPAIR/REHABILITATION OF STRUCTURES USING FRP COMPOSITES

2.1.1. PERFORMANCE OF ADHERED FRP COMPOSITES

2.1.1.1. Bond of FRP onto Concrete Surfaces

Although this research project dealt only with repair rehabilitation of steel members using FRP composite materials, it was useful from a research perspective to conduct a brief literature review on current state-of-the-art related to some aspects of FRP applications to concrete structures.

A research project conducted at the University of Missouri – Rolla (Miller, 1999) dealt with the bond performance between CFRP sheets and concrete. Factors such as the bonded length, compressive strength of the concrete and the stiffness of the CFRP sheets were examined. Flexure specimens were chosen with a hinge placed at the center of the beam to focus the crack development only in the mid-span of the beam. This was achieved to ensure that crack development in the bonded length could be prevented. In addition, these specimens were constructed with an unbonded length of FRP of 4in (10.2cm) at the center of the span with the main objective of measuring the FRP strain, and to more precisely calculate the load on to the CFRP sheets. Overall, 27 specimens were tested and the following conclusions were drawn: (1) the bonded length did not affect the bond strength, as the effective bonded length was less than the bonded lengths examined in this project, resulting in the same failure load for all different specimens, (2) the surface preparation is of significant importance, and (3) the stiffness and thickness of the FRP sheets affects the overall specimen performance. These conclusions were useful in the design of the test units for this FRA research project.

2.1.1.2. Bond of FRP onto Steel Surfaces

In order to obtain a durable bond between steel and FRP composite, various factors have to be considered. In the next sections some of the most significant factors namely: bonded length, galvanic corrosion, surface preparation, and thermal effects are discussed in further detail.

2.1.1.2.1. Bonded Length

Research on the bonded length of CFRP strips to steel has been conducted at the University of Minnesota and was reported in Nozaka (2001). The application of the strips to fatigue cracked steel bridge girders was investigated. One focus of this research was to establish the effective

bond length (development length), which is defined as the shortest bond length engaging the largest possible strength of the FRP. The failure mode in all specimens was characterized by fracture of the FRP. The effective bonded length was 8in (20.3cm) using the CFRP laminate Tyfo[®] UC and the adhesive DP-460NS.

Several other research projects were undertaken at the University of Delaware. Miller (2000) investigating the development length of CFRP plates bonded to steel surfaces. Six continuous double-sided reinforced specimens were tested in tension to determine the rate of force transfer. To replicate the full-scale rehabilitation a glass fabric layer was placed in the adhesive line. Two different adhesives were investigated. An analytical model proposed by Albat and Romilly (1999) was used to analyze the adhesive shear stress and CFRP sheet strain distributions. Experimental results showed good agreement between the analytical and the experimental data. Major research findings, from both the analytical model and the experimental results, indicated that the development length for the chosen material combinations was 4in (10.2cm).

Research by Miller (2000) was relevant to the work conducted under this research program. In this research project FRP laminates were applied with three different bonded lengths to examine the overall specimen performance and to establish a value for the development length, which depends on the FRP laminate and the adhesive used.

2.1.1.2.2. Galvanic Corrosion

Galvanic corrosion of a material is defined as an increase of corrosion above the normally observed rate. It is due to the difference in conductivity of at least two materials. If an electrolyte (e.g. water) is also present, one material becomes the anode and the other one the cathode and electron exchange occurs. As such, the steel oxidizes and corrosion occurs at a higher rate. As steel and carbon have different conductivities galvanic corrosion becomes a concern. This problem is widely addressed in West (2001).

This research dealt with the enhancement of the bond between CFRP laminates and steel. Amongst others the impact of galvanic corrosion was covered. By simply placing an adhesive layer between the carbon and the steel, research by West (2001) concluded that it was sufficient to prevent galvanic corrosion. However, as discontinuities in the adhesive line may open the chance for galvanic corrosion, it was suggested to place a fiberglass scrim layer between the steel

and the CFRP. Experimental tests were conducted and proved the relevance of this measure. The use of an insulating glass layer was also recommended by Moy (2001) and Miller (2000).

In this research project, funded by FRA, the problem of galvanic corrosion was also addressed by testing the performance of Glass-Carbon Hybrid FRP laminates on steel. However, no environmental based tests were conducted up to date to examine in more detail the problem of galvanic corrosion.

2.1.1.2.3. Surface Preparation

Steel: In order to increase the good strength between the steel substrate and the FRP composite adequate surface preparation is crucial. Rust, paint, and other deposits have to be removed from the steel surface. This can be done by sandblasting, as reported in Ammar (1996), Al-Saidy (2001), and Tavakkolizadeh (2002). Another method is shot-blasting the members, as reported in Moy and Nikoukar (2002). As an enhancement to the bond strength, the application of silane coupling agents to the clean steel surface was examined by McKnight et al. (1994) and Ammar (1996). Experimental results indicated that an increase in the bond performance was achieved.

FRP Composite: Commonly available FRP laminates may be divided in two groups. The first group includes those laminates that have one face already prepared for application. This face is roughened in order to ensure the highest possible bond strength between the adhesive layer and the laminate. The second group includes those laminates with both shiny sides from the pultrusion process. In these cases, the laminates have to be manually roughened before their application. This can be accomplished either by using sandpaper or sandblasting, as reported in Ammar (1996) and Tavakkolizadeh (2002).

In this FRA research project, four different laminates were used. Three CFRP laminates had a roughened side, and no special surface preparation was required. On the other hand, the Glass-Carbon-Hybrid FRP required roughening of the hybrid glass side, which was accomplished by the use of sandpaper.

2.1.1.2.4. Thermal Effects

According to the AASHTO LRFD Bridge Design Specifications, temperature changes must be considered when designing bridges. Two climatic conditions are defined: moderate and cold. In

Table 2.1 temperature ranges for different construction materials are listed. It can be seen that steel is more temperature sensitive than other materials. Therefore, adhesives, used to bond steel cover plates or FRP composites to steel, are subjected to high temperatures affecting the joint strength, as reported in Albrecht et al. (1984) (see also section 2.1.2.3). Further, it is necessary to recognize that the coefficients of thermal expansion for steel and FRP composites differ greatly. The coefficient of thermal expansion for mild steel is about $12 \times 10^{-6}/K$ whereas the value for FRP plates can be significantly less, or even within a negative range. Consequently, due to temperature variations, significant stresses will develop in the adhesive leading to premature debonding of the FRP laminate. Therefore, it is vitally important to address temperature effects characterizing the general bond behavior of FRP on steel. However, this topic has not been researched extensively.

Table 2.1 Temperature Ranges (AASHTO)

Climate	Steel or Aluminum	Concrete	Wood
Moderate	0 to 122 °F (-18 to 50 °C)	10 to 81 °F (-12 to 27 °C)	10 to 75 °F (-12 to 24 °C)
Cold	-31 to 122 °F (-35 to 50 °C)	0 to 81 °F (-18 to 27 °C)	0 to 75 °F (-18 to 24 °C)

Denton (2002) proposed a closed-form solution to investigate interfacial shear stresses and normal stresses within the elastic range to study the effect of temperature changes. Example calculations using this approach resulted in values for the interfacial shear stresses as high as 4920psi (33.9MPa). In this study, a high modulus CFRP plate with an elastic modulus of 50Msi (350GPa), a width of 9.5in (24cm), and a thickness of 0.47in (12mm) were used. It is clear that for these stress levels temperature changes introduce substantial interfacial shear stresses that can lead to the premature debonding failure of the FRP laminates.

Temperature effects were not implemented in this FRA experimental program, as the goal of this project was primarily to analyze the bond performance of FRP laminates on steel under normal laboratory conditions. Further research will indeed have to cover these temperature effects.

2.1.1.3. Other Aspects Regarding the Application to Steel

Research has also been conducted examining the applicability of FRP composites to steel, in particular adhesive selection. These are addressed next. Liby (1993) examined the feasibility of

the application of CFRP laminates to steel composite girders. Overall six girders were tested, reinforced with CFRP laminates of 80 and 200mils (2 and 5mm) thickness. In some tests, additional bolting was also provided. For peeling restraint additional clamps were attached at the ends of the laminates. It was observed that a significant strength increase was only accomplished beyond the steel yield point, which was due to the use of a relatively flexible adhesive. In addition, the ultimate capacity of the steel composite bridge girder was increased significantly.

Ammar (1996) considered several aspects of the rehabilitation of degraded steel bridge girders. Besides surface preparation, issues such as the selection of the most suitable adhesive, crack growth of reinforced and un-reinforced specimens (fatigue life), and economics of this rehabilitation type were investigated. Small-scale girder rehabilitation tests were conducted as well as full-scale rehabilitation. Research results indicate that tapering the ends of the laminate or clamping them to the tension flange of a beam resulted in an increase of the ultimate load. In addition, an increase in stiffness, yield load as well as the retention of the ductility of the steel beams was observed.

2.1.1.4. CFRP-Steel Bond Related Analytical Model

Numerous models accounting for the shear stress concentrations at the ends of the bonded regions have been developed. For the shear stress analysis in this research project the modification of Volkersen shear lag analysis (in MIL-HDBK-17-3E. Polymer Matrix Composites) was chosen and is introduced in this section. The application of this model is limited to uniform adhesive joint thickness. However, it accounts for variable adherent stiffness and thickness as well, at different applied loads and bonded lengths. The consideration of the adherent thickness is important for FRP composites because they are relatively soft in directions where the matrix controls the overall composite behavior. Therefore, transverse shear and normal thickness stresses affect the overall shear stress behavior significantly and have to be accounted for in addition to axial stresses.

With regard to the different stiffness ratios of the adherents, three scenarios are possible:

- two ideally rigid adherents
- one ideally rigid and one deformable adherent
- two deformable adherents

Henceforth, the stiffness ratio, B , for both adherents is calculated using the following expression:

$$B = E \cdot t \quad \text{Eq. 2.1}$$

Where E the Young's Modulus and t the thickness of the considered adherent. The steel-FRP laminate joints in this research project are classified as Case (b), where the stiffness ratio B_U for the upper adherent (FRP) is smaller than the stiffness ratio B_L for the lower adherent (steel). Due to the elongation of the FRP laminate the shear strain at the right end of the bond layer increases significantly (see Figure 2-1).

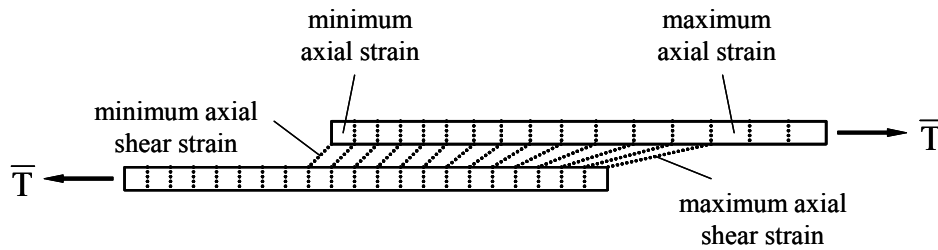


Figure 2-1 Deformations for Rigid – Deformable Joint

Considering a joint geometry, as illustrated in Figure 2-2, the shear stress τ_b may be calculated as follows:

$$\tau_b(x) = \beta \cdot \bar{\sigma}_x \left[\frac{1}{1 + \rho_B} \frac{\cosh\left(\frac{\beta(x-L)}{\bar{t}}\right)}{\sinh\left(\frac{\beta \cdot L}{\bar{t}}\right)} + \frac{1}{1 + \rho_B} \frac{\cosh\left(\frac{\beta \cdot x}{\bar{t}}\right)}{\sinh\left(\frac{\beta \cdot L}{\bar{t}}\right)} \right] \quad \text{Eq. 2.2}$$

Where:

$$\beta = \sqrt{G_a \frac{\bar{t}^2}{t_a} \left(\frac{1}{B_U} + \frac{1}{B_L} \right)} \quad \text{Eq. 2.3}$$

$$\bar{t} = \frac{t_U + t_L}{2} \quad \text{Eq. 2.4}$$

$$\bar{\sigma}_x = \frac{\bar{T}}{\bar{t}} \quad \text{Eq. 2.5}$$

$$\rho_B = \frac{B_L}{B_U} \quad \text{Eq. 2.6}$$

In the expressions above, L is the bonded length, G_a is the shear modulus and t_a is the thickness of the adhesive, and \bar{T} the load applied at each adherent.

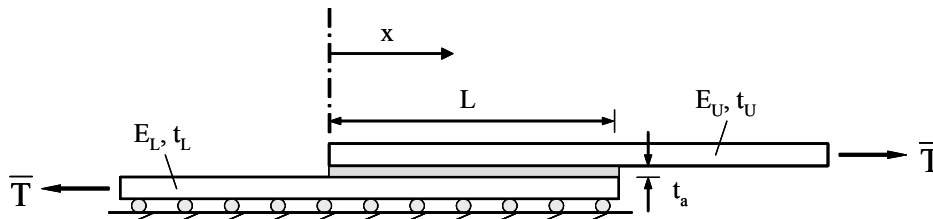


Figure 2-2 Geometry of Adhesive Joint

Figure 2-3 shows the dependency of the bond stresses on the adhesive thickness and the E-Modulus of the adhesive according to the analytical model described in this section. As expected, an increase in the adhesive bond line thickness leads to a decrease in the bond stresses. Furthermore, a stiffer adhesive results in higher bond stresses.

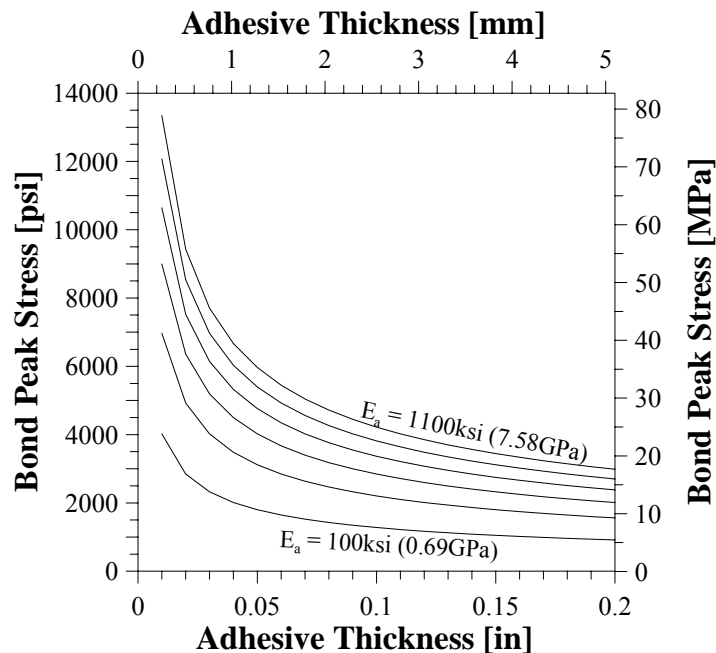


Figure 2-3 Bond Stress Dependencies

2.1.2. TRADITIONAL STEEL STRENGTHENING METHODS FOR FLEXURAL MEMBERS

One of the most common strengthening methods to increase the load carrying capacity of composite steel beams is to: (1) attach steel cover plates by the means of welding or bolting steel cover plates to the beam, and (2) adhere steel cover plates with or without the additional use of bolts. These two strengthening methods are discussed next.

2.1.2.1. Welding Steel Cover Plates

Welding steel cover plates to the flange of flexural members is a commonly used procedure to strengthen and rehabilitate steel structures (Klaiber, 1987; Reid, 2001). The addition of steel cover plates increases the section modulus and hence the flexural capacity. However, some of the disadvantages of this procedure are: (1) intense traffic control may be necessary during the strengthening procedure, (2) the enlargement of the structural member may reduce the bridge clearance, and (3) the additional weight of the cover plates will impose larger load demands requiring larger member sizes and in turn affecting the serviceability of the strengthened structural member. Additionally, as presented in Ghosh (2000), the existing steel members may contain high carbon contents, which is one of the leading causes of premature fracture during welding. Furthermore, significant residual stresses develop due to the high temperatures necessary during the welding process, which will cause a reduction in the fatigue life of the structure. The combination of one or more of these disadvantages makes the retrofit of steel members with FRP composites a very attractive alternative.

2.1.2.2. Bolting Steel Cover Plates

The principle for bolting steel cover plates is the same as for welding plates, as described in Section 2.1.2.1. An increase of the section modulus results in an increase of the flexural capacity of the member (Klaiber, 1987). Issues like traffic control, bridge clearance and added weight are still some disadvantages of this strengthening alternative; however, problems related to a reduction in the fatigue life are not as critical.

In order to bolt steel plates, existing members must be drilled first, which reduces the member section modulus. Furthermore, depending on the bolt connection scheme, as investigated by Ghosh (2000), slip between the connected members results in a non-uniform stress distribution and stress concentrations at the holes. As such, friction grip joints are recommended. In order to ensure a proper contact mechanism, this connection type requires careful tightening of the bolts, which leads to extra labor costs and time to the retrofit operation. This connection type is also highly dependent upon the surface condition at the interface of the connected members. In many instances dirt, oil, deposits or other foreign materials are present in corroded steel members, which will prevent the necessary friction mechanism from developing because there is no

uniform surface to develop a proper uniform friction mechanism. As such, this strengthening method is often not considered suitable for the strengthening of corroded steel members.

2.1.2.3. Adhering Steel Cover Plates

Problems previously described related to welding and bolting of steel cover plates has lead to research on the use of adhesives to bond steel cover plates to strengthen and rehabilitate existing corroded steel members. Adhering steel plates results in a more even force transfer along the steel plates and fewer stress concentrations. Adhesively bonded joints with or without additional bolting at the ends of the new steel plates (where the peeling forces are highest) were extensively researched by Albrecht et al. (1984), Albrecht (1987), Albrecht and Sahli (1988). These researchers have concluded that the use of an adhesively bonded joint in combination with bolts increases the fatigue life of a structure by a factor of 20 over that of conventionally welded cover plates.

Bonding steel cover plates to a steel member with an adhesive reduces stress concentrations as the stresses are evenly distributed along the plate. However, this method also holds some disadvantages. Although minimum impact, the steel cover plate thickness reduces the clearance of a structure. But, the steel cover plates will add significant weight to the structure, which influences its serviceability and dynamic performance, limiting the size of the steel cover plates. Furthermore, due to the weight of the cover plates, scaffolding is necessary to hold the steel cover plates in place while the adhesive cures in place, which has limited the implementation of this strengthening method.

2.1.3. FRP STRENGTHENING METHODS FOR FLEXURAL MEMBERS

2.1.3.1. Tension Flange Strengthening with Unidirectional Laminates

Liby (1993) conducted experimental and analytical studies on wide flange steel beams strengthened with carbon fiber reinforced plastic laminates (CFRP) and acting compositely with concrete slabs. The experimental program consisted of composite W8×24 steel sections assembly with a 28in (70cm) wide, 4.5in (11.4cm) thick reinforced concrete slab test specimen. CFRP laminates 6.5in (16.5cm) wide and 146in (365cm) long were attached to the tension flange using the FR-1272 two-part epoxy adhesive. A total of 13 tests were carried out under this research program.

Tests results indicated that the use of 0.08in (0.2cm) thick CFRP laminate leads to an increase in both the elastic and the ultimate capacity of the composite sections; but only a negligible increase in stiffness was observed. In contrast, using 0.2in (0.5cm) thick CFRP laminates a substantial increase in stiffness was also observed, in addition to both an increase in the yield and the ultimate load capacity. Test results indicated that the majority of the load transfers to the CFRP laminate occurred only after the tension flange had yielded. In these tests, failure was preceded by large deflections. This study indicates that it is feasible to use CFRP laminates to strengthen steel composite bridges provided that durability of the adhesive is assured and measures are taken to ensure that there is no galvanic corrosion action due to the direct contact between the CFRP laminate and steel.

2.1.3.2. Tension Flange Strengthening using Alternative FRP Reinforcement Methods

Gillespie, et al. (1996) investigated the rehabilitation of steel beams using composite materials (FRP). The specimens were W8×10 girders of A709 grade 36 steel. Four reinforcement schemes were designed to improve the flexural performance of the tested steel girder shape. These researchers carried out tests examining four different reinforcement schemes, as shown in Figure 2-4).

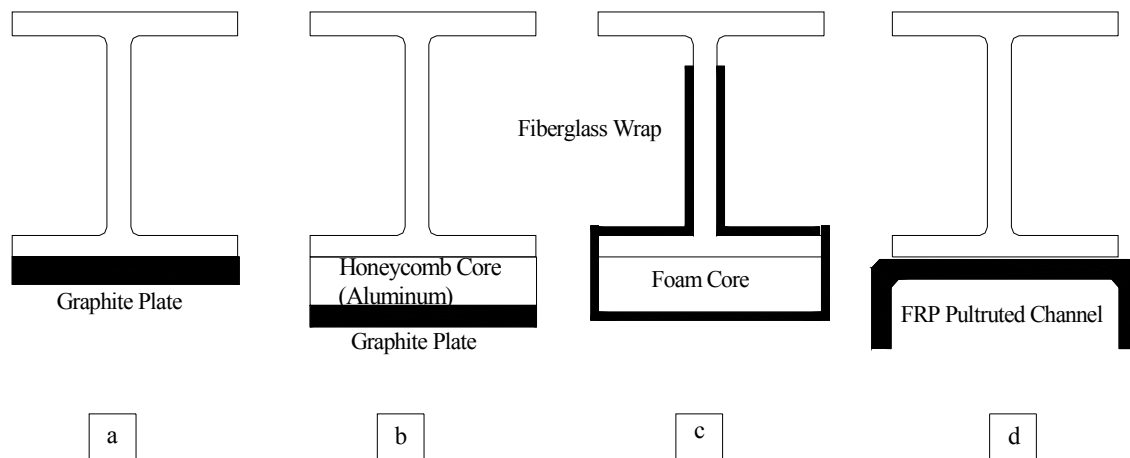


Figure 2-4 Reinforcement Schemes (Gillespie et al, 1996)

The first reinforcement scheme was a unidirectional carbon-fiber composite plate bonded directly to the tension flange of the beam using a two-part epoxy adhesive (see Figure 2-4a). The second reinforcement scheme used the same composite plate but took advantage of an aluminum

honeycomb structure to space the composite plate farther away from the steel section (see Figure 2-4b). For these two cases the thickness of the composite was 0.18in (4.5mm). In the third scheme a ± 45 degree E-Glass fabric was wrapped around the bottom flange and the web of the W-section, but a foam core was adhesively bonded to the bottom flange (see Figure 2-4c). The fourth scheme utilized a pultruded E-Glass channel, which was adhesively bonded and mechanically fastened with self-tapping screws (see Figure 2-4d).

The specimens were tested under (1) service load, and (2) up to ultimate strength. The service load tests showed that the adhesively bonded composite plates indeed increased the bending stiffness of the tested specimens ranging from 11 to 30% and therewith demonstrated the effectiveness of strengthening of steel members with FRP composites. In the strength load tests the strength of the members was defined as the load carried by the section at yield of the tension flange. The tests were continued past the yield point up to ultimate failure of the section. The test results indicated that a strength increase ranging from 37 to 71% was achieved.

To maximize the potential of the composite materials, the most desirable failure mode is to cause the fibers in the composite to fracture at the location of maximum moment. This results in the largest amount of ductility and the largest increase in ultimate strength over the elastic range. This is analogous to achieving the plastic moment capacity in a compact, braced steel girder. The failure mode of greatest concern with the bonded composites is failure of the adhesive bond. This failure occurs due to concentrations of shear and peeling stresses acting at the termination of the composite patch. The key to prevent this failure mode in cases where shear stresses and curvatures are large at the termination of the composite, is to taper the composite over a sufficient length.

Gillespie, et al. (1996) in their research used full-scale members taken from service. The size of the virgin girder was similar to a W24 \times 84. Due to corrosion present in these full-scale members, the tested girders exhibited 20 to 30% stiffness losses. A CFRP retrofit scheme was selected to achieve a maximum stiffness increase and minimum weight increase through comparison. Twelve strips of CFRP sheets were bonded to the tension flange (six strips on the inner flange surface and six strips on the outer flange surface) by using a two-component epoxy adhesive paste. Test results showed that the CFRP sheets led to an 11% increase in stiffness of the

rehabilitated girder over the non-rehabilitated girder. The load capacity of the corroded girder was also increased by 14% after rehabilitation. Researchers under this research program have also investigated the crack propagation after rehabilitation. Test results showed that the CFRP retrofit scheme was also adequate in reducing the fatigue crack growth of corroded steel members.

2.1.4. FRP STRENGTHENING METHODS FOR COMPRESSION MEMBERS

2.1.4.1. Expansive Light-Weight Concrete

Shrinkage is a time-dependent phenomenon that is observed in normal concrete. Shrinkage results from excess water that evaporates from the surface when exposed to air, and the concrete shrinks in volume. In post-tensioned construction, tendons present in ducts are usually grouted with a hydraulic cement grout type to avoid shrinkage of the grout inside the ducts. The purpose of grouting the ducts with this grout type is to protect the tendon from corrosion and to provide and maintain bond between the tendon and concrete. Research work on expansive concrete follows the ASTM C845 “Expansive Hydraulic Cement”, which limits the expansion of concrete between 0.04% and 0.1%. ASTM C157 and C806 provide the guidelines for measuring the length change of hardened hydraulic-cement mortar and concrete, and restrained expansion of expansive cement mortar. The work conducted in this FRA research project on expansive light weight concrete was largely based on these ASTM guidelines, which are further elaborated in section 5.2.

2.1.4.2. Local Bond-Slip Relationship between Steel and Concrete

Bond of reinforcement is intrinsically a three-dimensional problem. In the analytical approaches, it is usually separated into two bi-dimensional problems, which considers modeling in the transverse and longitudinal plane. Modeling in the transverse plane uses many of the same concepts as those employed in the field of fracture mechanics. The first model proposed by Tepfer (1973) was largely based on the slip-modulus theory, which assumes a linear relationship between local bond stress and local slip to describe the bond stresses distribution along the longitudinal direction of the reinforcement in the concrete. In later years, modeling in the longitudinal plane has been approached by establishing non-linear equations for local bond-slip relationship and solving numerically the differential equation for bond, which takes into account the boundary conditions. The most commonly used model for steel bars is the Bertero-

Eligehausen-Popov (BEP) (Eligehausen et al. 1983) model. This model has been incorporated into CEB-FIP Model code 90, using different numerical values for the parameters related to confined and unconfined concrete. The mBEP model is given by:

$$\tau(s) = \tau_0 \left(\frac{s}{s_0} \right)^\alpha \left(1 - \frac{s}{\bar{s}} \right) \quad \text{Eq. 2.7}$$

This expression includes four unknown parameters: τ_0 , s_0 , α , and \bar{s} . If s_0 is set to be equal to the unit length, then the above expression can be transformed into a simple expression, which includes three unknown parameters: C , α , and \bar{s} , as follows:

$$\tau(s) = Cs^\alpha \left(1 - \frac{s}{\bar{s}} \right) \quad \text{Eq. 2.8}$$

Where τ is the shear stress acting on the contact surface between bar and concrete, and s is the slip that is the relative displacement between the bar and the concrete. The differential equation governing the bond of a bar embedded in concrete can be derived from the equilibrium and compatibility equations on a finite element of rod of length dx , along with the assumptions that the rod is linearly elastic and the concrete strain is negligible if compared to that of the rod. Russo et al. (1990) has proposed the following differential equation:

$$\frac{d^2s(x)}{dx^2} = \frac{\pi d_b}{E_b A_b} \cdot \tau(s) \quad \text{Eq. 2.9}$$

Where d_b is the bar diameter, E_b is the modulus of elasticity of the bar, A_b is the cross section area of the bar, and x is the longitudinal direction of the bar.

A rigorous numerical method to calibrate parameters of a given local bond-slip relationship using experimental results of pullout tests was developed by Focacci et al. (2000). In this report, this method was adopted to find the parameters of the local bond-slip relationship (mBEP model between hot-rolled smooth steel bar and FRP confined light-weight concrete). The defined functions in this method are shown in Figure 2-5.

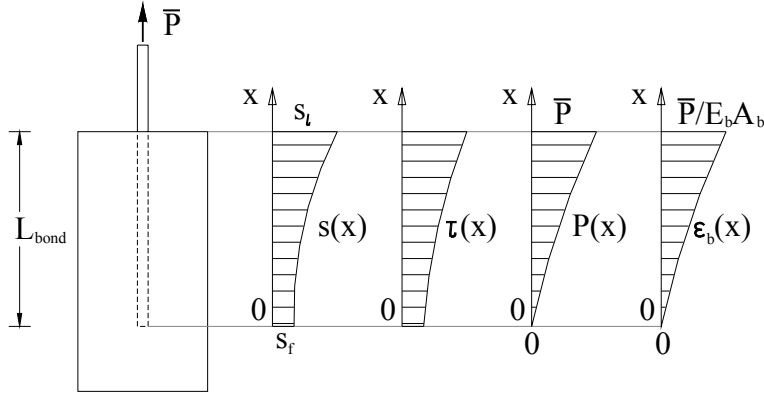


Figure 2-5 Defined Functions

In Figure 2-5, $s = s(x)$ is the slip along the bar, $\tau = \tau(x)$ is the bond shear stress along the bar, $P = P(x)$ is the normal pull out force along the bar, $\varepsilon_b = \varepsilon_b(x)$ is the bar strain along bar's longitudinal direction. These formulas can be stated using the following expressions:

$$\left\{ \begin{array}{l} s = s_f \\ P = 0 \\ \varepsilon_b = 0 \end{array} \right. \text{ at } x = 0; \quad \left\{ \begin{array}{l} s = s_l \\ P = \bar{P} \\ \varepsilon_b = \bar{P} / E_b A_b \end{array} \right. \text{ at } x = L_{bond} \quad \text{Eq. 2.10}$$

The numerical method can be explained as follows. For a given bonded length, the differential equation with known local bond-slip relationship can be solved numerically for increasing values of the free end slip with the boundary conditions given by:

$$\left\{ \begin{array}{l} s(0) = s_f \\ \left. \frac{ds}{dx} \right|_{x=0} = \varepsilon_b(0) = 0 \end{array} \right. \quad \text{Eq. 2.11}$$

Once $s = s(x)$ is known, $\varepsilon_b = \varepsilon_b(x)$, and $P = P(x)$ will be derived. At $x = L_{bond}$, the slip is s_l (load end slip), and the load is the pull out applied on the bar. By comparing these analytical results of (P, s_l, s_f) to experimental pull out test results conducted under this FRA research project, a best-guess set of unknown parameters for local bond-slip relationship was derived and is presented in further detail in section 5.3.

2.1.4.3. Composite Column Construction

The combined structural use of steel and concrete was first encountered almost as soon as the two materials became widely available to structural engineers. The first systematic tests of composite columns were conducted at Columbia University's Civil Engineering Laboratory in 1908 by W.H. Burr. In 1936, the American Institute of Steel Construction (AISC) adopted a revised version of its 1923 Standard Specification under the title Specification for Design, Fabrication and Erection of Structural Steel for Buildings. The document included a new Section 8: Composite Beams, specifying general requirements for the use of steel beams encased in concrete. Now various codes provide the guidelines for design of composite beams and columns. For columns, LRFD is the preferred method when the percentage of steel is large. In this FRP research program the composite action of FRP circular pipes and steel columns under axial compressive loads was investigated and research results are presented in section 5.4

2.1.5. FRP APPLICATIONS TO METALLIC STRUCTURES - CASE STUDIES

2.1.5.1. Tickford Bridge

The Tickford Bridge (Figure 2-6a) is located at Newport Pagnell in the United Kingdom (UK). Constructed in 1810 it is believed to be the oldest working cast iron bridge in the world (<http://www.ciria.org.uk>).



Figure 2-6 Tickford Bridge

When this bridge showed signs of weakness, and was not able to carry normal traffic, a weight restriction was imposed on traffic crossing this bridge. Not recognizing this as the final solution, Maunsell Ltd, a civil and structural engineering consultant in the UK, was hired to analyze the structure in order to find the best strengthening method. For historic and aesthetic reasons, conventional repair methods were not applicable. Therefore, carbon fiber fabric of the Japanese reinforcement system Replark[®] was chosen. This wet lay-up system could be wrapped around the contours of the three largest spandrel rings and the lower main chord. In order to prevent galvanic corrosion, a continuous filament polyester drape veil was installed between the iron and the FRP sheets. After the application process in 1999, the whole structure was repainted. As the maximum reinforcement thickness was 0.4in (10mm), the overall aesthetics of the bridge was not significantly affected.

2.1.5.2. Slattocks Canal Bridge

The Slattocks Canal Bridge was built in 1936 and is located in Rochdale, U.K. (<http://xnet.mouchel.com>). This steel girder and concrete deck bridge has a clear span of 25ft (7.62m). An assessment showed that the bridge needed strengthening to carry 90 kip (40ton) vehicles. The consulting group Mouchel proposed the strengthening scheme, which consisted of pre-cured CFRP plates. This method enabled the contractor Balvac to work beneath the bridge while vehicles up to 37.5 kips (17tons) kept using the bridge during normal hours of operation. The 0.3in (8mm) thick and 3.9in (10cm) wide CFRP plates were bonded to the bottom flanges of the beams with a structural adhesive. After application in the spring of 2000 the headroom under the bridge was reduced by only 0.4in (10mm), which did not affect the navigable clearance for the canal. Another advantage of this technique was the cost, as the strengthening with CFRP plates was \$32,000 less expensive than proposed alternatives.

2.1.5.3. Hythe Bridge

The Hythe Bridge was built in 1874 and is located in Oxford, U.K., as shown in Figure 2-7 (<http://xnet.mouchel.com>). This two-span cast iron structure was strengthened with prestressed composite materials in 1999 in order to make the bridge accessible to traffic up to 90 kips (40tons), which conforms with the European vehicle weight standard. Four narrow plates of prestressed CFRP were applied to eight inner cast iron beams out of ten total beams on each span. This new technique of in situ prestressing was developed by the consulting group Mouchel.

The application was done by the contractor Balvac. Continuous traffic flow and lower reduction in headroom were parameters making the Oxfordshire County Council opt for this technique.



Figure 2-7 Hythe Bridge

2.1.6. DESIGN GUIDELINES APPLICABLE TO METALLIC STRUCTURES

As the strengthening of metallic structures with FRP composites is still relatively new, there is a lack in design guidelines that can substantiate the body of knowledge to influence the usage of FRP as a plausible FRP retrofit scheme, and as such much research is needed. The only source found, was the “ICE design and practice guides” edited by Moy (2001) and published in the U.K. It offers recommendations regarding the structural strengthening or repair of metallic components of onshore structures, using FRP composites. It covers aspects related to the exposure to different environments such as temperature, moisture, chemicals, ultraviolet radiation and fire, all issues that will have to be considered in the design process. The composite design, strain and thermal compatibility, as well as ultimate strength capacity of the FRP are also covered. In addition, factors accounting for long-term degradation, adhesive joint design, which address the limitation or reduction of peel stresses and galvanic corrosion, are covered. Elastic and elasto-plastic design methods are presented discussing the features of cast iron, wrought iron and steel. Basic approaches for the Finite Element Design are introduced. Further, manufacturing, quality inspection and repair methods are discussed. This publication covers the main principles and important aspects of the strengthening of metallic structures.

2.2. HEALTH MONITORING OF STEEL BRIDGES

2.2.1. SENSOR TECHNOLOGY

2.2.1.1. Temperature Sensors

Traditional temperature sensors can be categorized in thermo-resistive, thermoelectric contact (thermocouple), semiconductor pn-junction, optical, acoustic, and piezoelectric temperature sensors (Fradon, 1997). Thermo-resistive sensors can be further categorized as: resistance temperature detectors (RTD), silicon resistive, and thermostat temperature sensors. Optical sensors can be further categorized as: fluoroptic, interferometric, and thermochromic. Thermo-contact sensors are most often used for structural temperature monitoring. They require careful attention to the design of electronic signal conditioning circuits for noise-free measurements. Dallas semiconductor (<http://www.dalsemi.com>) produces a simple 1-wire digital thermometer (DS1822) with a 36°F (2°C) accuracy over a range of 14°F (-10°C) to 185°F (85°C). It uses a silicon resistive technique to measure temperature. Signal conditioning is integral to the chip and the interface is a simple 1-wire plus ground reference with power extracted from the signal line.

2.2.1.2. Wind Pressure Transducer Sensors

The Davis 7911 Anemometer (http://www.davisnet.com/product_documents/weather) is a typical wind-vane style wind pressure transducer. A drawing showing a roof-top installation is shown in Figure 2-8. Figure 2-8b depicts a close up view of the Davis 7911 anemometer. A system like this, or a similar system, will need to be installed per bridge. Wind speed data will be collected by the local host processor and relayed periodically to the remote data collection site.

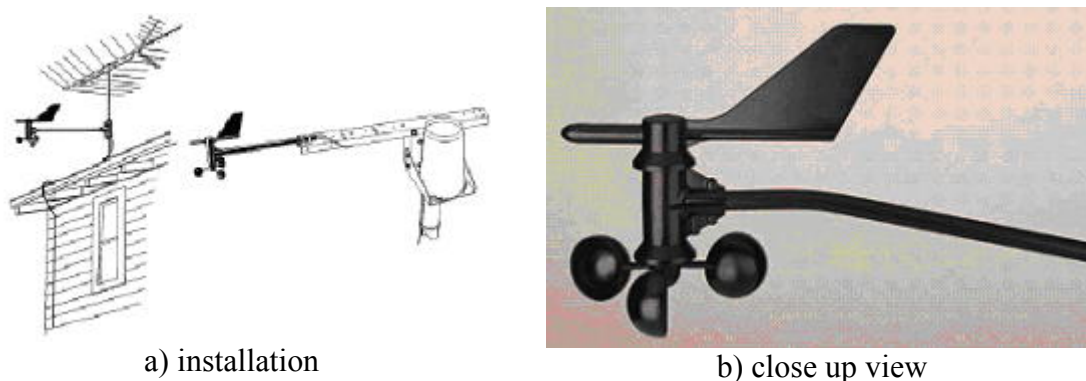


Figure 2-8 Davis 7911 Anemometer

2.2.1.3. Global Positioning Systems

Fuzino et al. (2000) have shown the application of GPS in the measurement of wind-induced semi-static lateral displacements of a bridge girder. Two sets of GPS antennas and receivers were placed at the midspan of the girder and in the office. It was shown that the measured lateral displacements agree very well with the values predicted by three-dimensional finite element analysis, proving the reliability of the GPS as a valuable tool for the health monitoring of bridges. The usage of GPS in the health monitoring of bridges avoids the need for installation of strain gages or other less reliable measuring devices that often require intense installation labor and wiring. Furthermore frequency analysis of the dynamic component of the data indicates that the natural frequencies of the low modes can be identified accurately using current GPS technology. Major disadvantages in the usage of GPS are high costs and cannot be used in closed spaces. These issues are further addressed in this final report in section 6.2.

2.2.1.4. Vibration Induced Sensors

Research work by Doebling et al. (1996) demonstrated the advantages of using vibration signatures for structural health monitoring. The basic premise of vibration based structural health monitoring is that damage in a structure or change in the physical properties (i.e., stiffness, mass and/or damping) will, in turn, alter the dynamic response of any structure.

The vibration-based technique allows for monitoring the structure on a global basis. More over, the cost of such a method is significantly less than other methods, because all that is needed to collect the vibration data are some standard vibration sensors. Vibration sensors usually cost less than other sensors and are readily available in the market. These sensors are small in size and can be easily attached to the structure. Health monitoring of a structure using vibration sensors can be considered as a nondestructive method; however, the recorded data is very sensitive and each sensor monitors only a small region of a structure. Using a cluster of sensors it is possible to monitor an entire structure. This nondestructive technique was implemented in this research program and research results are described in section 6.3.

2.2.1.5. Input Excitation Methods

In the research work by Charles, R. et al. (1999) various excitation methods were used to provide the necessary structural dynamic excitation. The data acquisition process involves devising a method to collect test data and finding a suitable location for mounting the sensors on the

structure. In order to collect vibration data, a structure must be subjected to dynamic excitation. Excitation methods can be broadly classified in two categories namely; measured input excitation methods and ambient excitation methods. As the name suggests in the case of the measured input excitation method, the input is measured and is applied at a single location. In the case of ambient excitation methods, the input to the structure is not measured directly. In general, the measured input excitation methods are used for smaller structures and bridges while the ambient excitation methods are used for larger structures, suspension type and cable-stayed bridges.

In order to analyze the modal characteristic or resonant frequencies it is required that all the characteristics of the input forcing function be known. This is possible only in the case of the measured input excitation methods. But this method has few drawbacks, which makes ambient excitation methods more commonly used. Measured excitation method though easy is not very realistic especially when it comes to large structures. In most cases for measured input excitation methods, the structure is usually out of operation while tests are conducted, which causes disruptions to the normal traffic flow. Also when using measured excitation methods, some ambient excitations are present, which makes the process of data classification rather difficult leading naturally to undesirable results. Ambient excitation can be defined as the excitation undergone by the structure under its normal operating conditions. Ambient excitation methods are commonly used for large structures, however they can also be used for small structures. In the following paragraphs a few methods used to perform the measured input excitation and ambient excitation will be discussed.

Some commonly used measured excitation inputs are impact, step relaxation and shakers. Impact excitation has a number of advantages because it; (1) is easy to control the input parameters, (2) is portable, and (3) has a fast setup and response time. However, this method becomes very labor intensive if there is the need to use this method on a large structure, and multiple impacts can sometimes cause damage to the structure. In the case of step relaxation method, a static force is applied to a point on a structure and then it is suddenly released. Shakers on the other hand are excitation devices that are positioned along the length of a bridge, which imposes a continuous dynamic force on the structure at a known frequency. Both step relaxations and shakers have similar advantages and disadvantages as the impact input method.

One of the most commonly used ambient excitation methods for bridges is the test vehicle method. In this method a test vehicle is driven over a bridge at different speeds and vibration is collected. For further analysis different vehicles are used as test vehicles. The test vehicle excitation is more realistic because it is more close to the type of excitation a bridge will undergo under normal operations. This is a very good dynamic load because it acts upon the entire length of a bridge, and not at a specific location, as the case for the measured input excitation methods. Some of the disadvantages of this method are that; (1) the collected vibrations using a test vehicle are not only dependent on the bridge but also related to the test vehicle, and (2) the natural frequency can vary slightly under different traffic conditions on the bridge.

2.2.1.6. Non-Destructive Technologies

This research work conducted by Charles, R. et al. (1999) summarizes some advantages and disadvantages of using different types of non-destructive technologies for monitoring of the structural performance of the civil infrastructure. A wide variety of such systems are non-destructive in nature and consist of: acoustic or ultrasonic, X-radiography, eddy-currents, microwaves, magnetic fields, thermal fields and many more. All of these methods have some disadvantages even though they may provide significant detail regarding the nature and localization of damage. Some disadvantages of these systems that may not be practical for the application to the health monitoring of bridge structures are: (1) most of these system are used only on a local basis, and (2) require direct access to the structure. These requirements are not always practical, because they may involve traffic closures or disruptions during inspection and testing and for this reason some non-destructive techniques are insufficient and not widely used in real-time health monitoring of the civil infrastructure. In addition, data collection requires using and installing bulky equipment in the field, which may not always be possible. The cost involved with collecting data is also a significant factor in choosing non-destructive technology to perform the health monitoring of a structure.

Structural health monitoring of civil infrastructure is a very challenging task because major requirements are that; (1) it must be a non-destructive method, (2) it must be sensitive, (3) it must be able to detect small damages such as cracks, de-laminations or loose connections, (4) it must be able to monitor a certain minimum area of the structure as opposed to a point measurement, (5) ease of data collection and storage is important, and (6) it must be easy to pre-

process and analyze the data using smart system engineering concepts. Among all the methods investigated in the literature, the vibration based structural health monitoring technique (see section 2.2.1.5) meets with most of the above-mentioned requirements for a real-time health monitoring system and, as such, was selected in this research program.

2.2.2. SOFT COMPUTING TOOLS

Many civil and mechanical systems are in continuous use despite aging and associated potential for damage accumulation. Hence, the ability to monitor the structural health of these systems on a real-time basis is becoming very important. As previously stated, one of the main goals of this research program was to develop a practical real-time structural health monitoring system using smart systems engineering concepts and tools. In order to achieve these goals, extensive literature review was performed. The main goal of the literature review was to collect sufficient information to select the best possible and most cost effective solution to evaluate on a real-time basis the structural performance of a bridge structure. The nature of the selected method should be such that it can feed data continuously to a smart engineering tool system like fuzzy logic and neural network. The challenges faced while using the different kinds of data and method, and how it is dealt with, is also briefed in the literature review. Previous research in these areas covers a wide spectrum of analytical and experimental techniques in health monitoring, which are presented next.

2.2.2.1. Neural Network Systems for Health Monitoring of The Civil Infrastructure

Research works by Battani, M. et al. (1998) highlights the advantages of using fuzzy logic for damage detection in bridges. The main characteristic of fuzzy logic that has made it popular is its effectiveness and ease in handling non-linearities and uncertainties. Conventional decision making systems and control systems are not the most popular methods because they rely on the accuracy of the modeling of the system dynamics. Since complex structures encountered in the real world exhibit significant non-linearities and uncertain parameters, designing an accurate dynamic model is not always possible using these conventional decision methods. For these reasons, fuzzy logic methods are frequently used because, they do not require accurate dynamic models, they are much closer to human thinking and natural language than conventional logical systems, and (3) they provide an effective means of capturing the approximate, inexact nature of the real world. The basic idea of a fuzzy logic system is to incorporate the expert experience of a

human operator in the design of the controller in controlling a process whose input-output relationship is described by a collection of fuzzy rules involving linguistic variables rather than a complicated dynamic model.

2.2.2.2. Evaluation Methodology

Heywood et al. (2000) has presented an evaluation methodology applicable to obtain a bridge's *fitness-for-purpose*, on the basis of the collected health monitoring data. The *fitness-for-purpose* evaluation (FPE) of bridges is defined as the ratio of the available live load capacity to the estimated value, and can either be derived from the conventional theory or from the health monitoring data, given by the corresponding formulas:

$$FPE_{theory} = \frac{\text{Ultimate live load capacity expressed as a strain}}{\text{Theoretical ultimate limit state live load strain}} \quad \text{Eq. 2.12}$$

$$FPE_{HM} = \frac{\text{Ultimate live load capacity expressed as a strain}}{\text{Measured Ultimate limit state live load strain}} \quad \text{Eq. 2.13}$$

In order for the bridge to be considered fit for operation, these two expressions should give a value greater than one. In the opposite case, special action should be taken in order to retrofit the bridge structure. This paper illustrates four case studies showing that the concept of the FPE can be useful in practical applications of bridge health monitoring.

2.2.2.3. Neural Networks

Masri et al. (1996) demonstrated the successful use of Neural Networks in the damage detection of structures. Relatively small changes in the structural parameters are detectable, even when the vibration measurements are noise-polluted. The factors that influence the choice of a system identification approach for damage detection in structures are summarized below:

- Variety of materials of construction
- Level of damage and deterioration of concern
- Types of sensors used
- Nature of the instrumentation network
- Extent of available knowledge concerning the ambient dynamic environment
- Degree of measurement noise pollution

- Spatial resolution of the sensors
- Configuration and topology of the test structure
- Sophistication of available computing resources
- Complexity of the detection scheme
- Degree of a priori information about the condition of the structure
- Selected threshold level for detecting perturbations in the system condition
- Depth of knowledge concerning the failure modes of the structure

This paper establishes firmly the use of neural networks in civil engineering applications. In addition, literature review indicates the extensive use of the fuzzy logic, neural networks, and hybrid fuzzy-neural network architectures for bridge engineering applications.

After performing the extensive literature review it is clear that vibration based structural health monitoring has a number of advantages over the other conventional methods. It is simple, inexpensive, small and more effective for real-time structural health monitoring. This provides us with continuous data, which can be processed and analyzed by the neuro-fuzzy architecture. The ambient excitation methods are more realistic and accurate for test data collection. Of the various ambient excitation methods the test vehicle base method is simple and reliable to use. A cluster of sensors attached to different truss members can effectively help in monitoring the health of the entire bridge. The use of fuzzy logic and neural network makes it robust and helps in handling the non-linearities associated with the structural behavior. These issues were addressed in this research program and research results are presented in Chapter 7.

3. BOND CHARACTERIZATION

3.1. INTRODUCTION

3.1.1. BACKGROUND

Some research has been conducted in the United States (Liu, 2001; Liby, 1993; West, 2001; Ammar, 1996; Al-Saidy, 2001), Japan (Nakagoshi, 2000)) and Great Britain (Moy, 2001) on FRP materials applied to steel members, but much more research is needed to substantiate some of the findings in these research programs. In addition design standards must also be amplified beyond existing ones. The available research shows that many influencing factors have not been addressed sufficiently. These include the bond between FRP and steel, and the affects of temperature (Denton, 2002). Presented in this report are issues related to the bond performance between steel and FRP laminates, and objectives related to these issues are presented next.

3.1.2. OBJECTIVES

Bond between FRP and steel has been identified as one of the main variables controlling the behavior of FRP-strengthened steel members. The primary objective of this research was to characterize the bond performance between FRP laminates and steel, taking into consideration the following factors:

- Specimen type
- Bonded length
- Wrapping of specimens with CFRP sheets for adhesion enhancement
- FRP laminate type
- Adhesive type
- Adhesive thickness
- Surface preparation
- Curing time

3.1.2.1. Specimen Type

Seven different series of specimens were tested. Six series consisted of discontinuous and one series of continuous specimens. Discontinuous specimens were designed to simulate the worst-case scenario of a completely corroded steel member in need of FRP bridging and thereby considering the effects of stress concentrations at these discontinuities. The specimens were designed such that failure was controlled by debonding or rupture of the FRP laminates, without

yielding to occur in the steel. For these reasons, the specimens were reusable. Furthermore, one continuous specimen was tested to determine the influence of the introduced stress concentrations caused by the gap in the discontinuous specimens. All tests were performed under static conditions. A detailed description of the specimens is given in Section 3.2.3.

3.1.2.2. Bonded Length

In order to obtain data related to the bond stress distribution along the FRP laminate, three different bonded lengths were tested: 3, 6 and 9in (7.6, 15.2 and 22.9cm).

3.1.2.3. Wraps

To determine if the performance of an upgraded specimen can be improved, additional wraps made of CFRP sheets were applied to the 9in (22.9cm) specimens.

3.1.2.4. FRP Laminate Type

All laminates used in this research project were precured laminates, produced by pultrusion. Besides conventional, widely available carbon-FRP laminates (CFRP), a glass-carbon hybrid FRP (GC-Hybrid FRP) laminate, specifically designed for the application to steel, was also used. This hybrid FRP was chosen, in order to address galvanic corrosion, which may occur due to direct contact between carbon fibers and steel.

3.1.2.5. Adhesive Type

As FRP reinforcement is usually designed for use on concrete, another aspect of this program was to identify the most suitable adhesive for the application of FRP laminates to steel. Different types of adhesive were tested in order to examine the performance of the adhesive.

3.1.2.6. Adhesive Thickness

Another major factor influencing the bond behavior between FRP and steel is the adhesive thickness. In this research program the adhesive thickness was controlled by glass beads placed in the adhesive line. A detailed description of the glass beads used is given in Section 3.2.3.

3.1.2.7. Surface Preparation

Surface preparation was also another factor considered in this research program. Specimens free of corrosion were cleaned with a wire brush to remove any impurities (see Section 3.2.3.2.5). In future research projects corroded steel members should be tested.

Furthermore, the impact of sanding the GC-Hybrid FRP laminates prior to application was investigated, as these laminates do not have a ?? for the application roughened side.

3.1.2.8. Curing Time

This factor was found to be of importance at a later stage of the program, after the load-strain response for fully cured specimens was either linear (indication for a brittle epoxy) or non-linear and fanned (indication for a more plastic epoxy). An additional test series was initiated investigating the time dependent strength development of the adhesive.

3.1.3. RESEARCH FINDINGS

The following general findings were obtained from this experimental program:

- 1) Laminate debonding from the steel plate will occur at the location of stress concentrations such as the end of the laminate or discontinuities in the steel.
- 2) An increased bonded length results in a higher failure load and FRP peak strains. However, the effective development length remains nearly unaffected.
- 3) Wrapping the specimens with CFRP-sheet strips did not affect failure load and peak strains significantly.
- 4) The FRP laminate type had minor impact on the overall specimen performance. The test results for the precured GC-Hybrid laminate were in a comparable range to the used CFRP laminates, and therefore its future application to steel members looks promising.
- 5) The adhesive is the factor affecting the overall bond performance most. Two different bond behaviors were observed in this research project – brittle and ductile. Further investigation will have to show which type is preferable for the strengthening of steel and which design approach has to be considered.
- 6) Adhesive thickness: In case of the epoxy Tyfo[®] MB an adhesive thickness of 80mils (2mm) is preferable to a thickness of 10mils (0.25).
- 7) Sanding the GC-Hybrid laminates did not affect the overall specimen performance significantly.

3.1.4. CHAPTER LAYOUT

Section 3.1 gives some background information on the needs for the strengthening of steel structures and concerning the use of FRP composites in Civil Engineering applications. Furthermore, the objectives of this report are presented and a short summary of the topics covered is given. In Section 3.2, the different materials used in this project are characterized, specifically FRP materials, epoxies and the different types of steel. Furthermore, this section describes the experimental program. It includes tests addressing different specimen types, bonded length, number of wraps, FRP and adhesive type, adhesive thickness, surface preparation, and the strength development of the adhesive as a function of time. In Section 3.3, the results of the experimental program are presented. Section 3.4 presents the discussion of the experimental data and analysis of the bond behavior. Finally, Section 3.5 contains the summary, conclusions and recommendations for future research.

3.2. EXPERIMENTAL PROGRAM

3.2.1. INTRODUCTION

In this section the experimental program is described, along with the problem statement (Section 3.2.2). Section 3.2.3 contains the description and instrumentation of the different specimens and characterization of the various bond-influencing factors considered in this research. Subsequently, in Section 3.2.4, all materials used in this research project are characterized, and their properties listed. The test matrix is introduced in Section 3.2.4, followed by the description and designation of the different specimens (Section 3.2.5.) Finally, in Section 3.2.6 the test setup is described.

3.2.2. PROBLEM STATEMENT

The use of FRP as the strengthening material for steel structures is a relatively new strengthening scheme. Although extensive research has been carried out on the strengthening of steel structures, some the structural performance influencing factors have not yet been addressed sufficiently. These include bond characteristics between FRP and steel. In this program, research focused on establishing a strain limit level that can be incorporated in a design methodology, as a function of the bond influencing factors studied herein. Furthermore, the effective development length for the application of FRP laminates to steel was studied.

Definition of the development length is the shortest bonded length necessary to attain failure of reinforcement under a certain load (Miller, 1999). All the stress transfer takes place within this length, and an increase in bonded length beyond the development length does not lead to any significant increase in load.

Bond failure between FRP and steel is characterized by a sudden failure resulting from either fracture of the adhesive or separation of the steel and the FRP laminate from the adhesive. Experimental results presented in Section 3.3.2 indicate that debonding failure occurred due to the separation at the interface of the adhesive to the FRP or the adhesive to the steel. As stated in Moy (2001) the shear stresses in the adhesive layer will place an upper limit on the stiffness or thickness of the FRP composite. Therefore, a limitation of the longitudinal shear stress can prevent debonding failure.

In this program, research focused on establishing a reliable strain limit level at bond failure that can be used in a design scheme for the rehabilitation of steel members. Design of a retrofit/rehabilitation scheme to strain levels below the expected strain levels at bond failure can be used such as in an Allowable Stress Design. This approach is similar to the strain limit approach presented in the ACI 440.2R-02 (2002). In this project four different precured FRP laminate types and five different adhesives were investigated, and the test results are reported in Section 3.3.

3.2.3. SPECIMEN DESCRIPTION AND INSTRUMENTATION

3.2.3.1. Specimen Types

Seven different series of specimens were tested. Six series consisted of discontinuous specimens and one of a continuous specimen. The discontinuous specimens were designed to simulate the worst-case scenario of a completely corroded steel member. The continuous specimen was developed to investigate the bond performance for different specimen types.

3.2.3.1.1. Discontinuous Specimens

Six test series were investigated using discontinuous specimens. These specimens consisted of two steel plates (Grade 36) separated by a gap, and connected with FRP laminates on either side of the steel plates, see Figure 3-1a and c. This gap was 1 in (2.5cm) and was used to simulate the aforementioned worst-case scenario of a completely corroded steel member. The steel plates

were 5in (12.7cm) wide with lengths of 25in and 18in (63.5cm and 45.7cm). Different bonded lengths were investigated. The connecting FRP laminates had a width of 1.5in (3.8cm), and an overall length of 19, 22, 25in (48.3, 55.9, 63.5cm) on the side where strain gages were installed. On the side where no strain gages were installed the bonded length was maintained 28in (71.1cm) between all specimens.

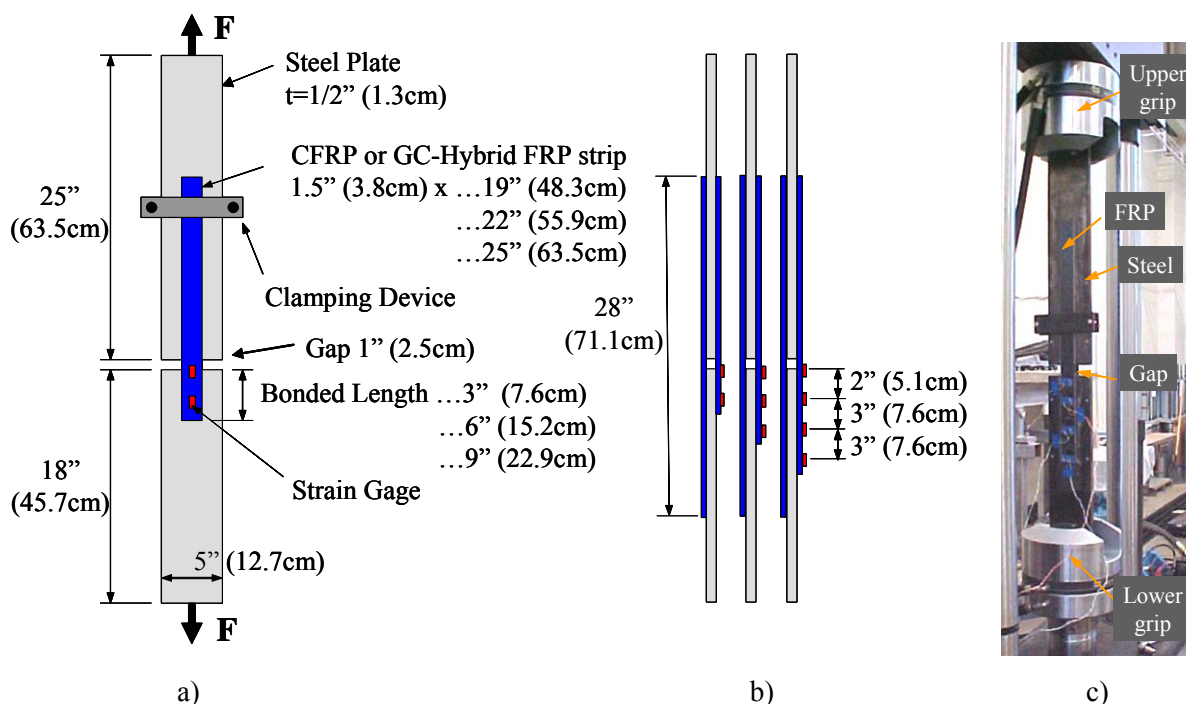


Figure 3-1 Discontinuous Specimen

As previously discussed six test series used this specimen type. These test series consisted of specimens with different bonded lengths. As shown in Figure 3-1a these bonded lengths were 3in (7.6cm), 6in (15.2cm) and 9in (22.9cm). To facilitate the reference in future sections these test series were designated as Type I, II and III, respectively, see Table 3.1.

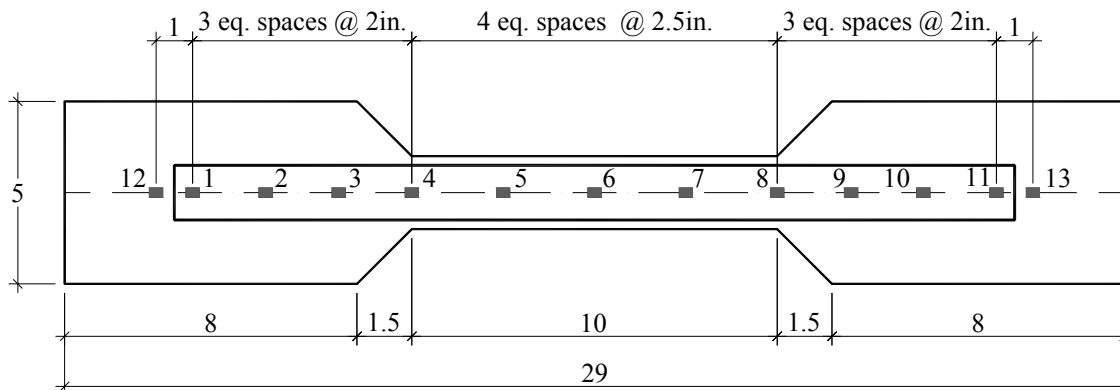
Table 3.1 Bonded Length Type

Specimen Notation	Bonded Length	
	in	cm
I	3	7.6
II	6	15.2
III	9	22.9

All test units were instrumented with strain gages, which were installed along the investigated bonded length side to obtain strain profiles. The locations of the strain gages are shown in Figure 3-1b.

3.2.3.1.2. Continuous Specimen

To study the influence of stress concentrations in the gap region this specimen type was designed. Two specimens were investigated in this test series using the same steel plate. This specimen type was continuous, as shown in Figure 3-2, and hence the introduction of stresses due to the discontinuity was avoided. The specimen consisted of steel Grade 36 and was 0.25in (0.6cm) thick. The specimen dimensions are shown in Figure 3-2, as well as the strain gage locations. The FRP laminate, this time applied to only one side of the specimen, was positioned symmetrically with respect to the centerline of the steel plate, and therefore the bonded length was the same on either side of the laminate. The overall FRP length was 23in (58.4cm).



Note: all dimensions are in inches
 Plate Thickness: 0.25in
 Steel Grade: A36

Unit Conversion:
 1 in. = 2.54 cm

Figure 3-2 Continuous Specimen – Geometry and Instrumentation

3.2.3.2. Specimen Characterization Factors

Besides the already described differences in specimen type and bonded length, other factors were taken into consideration, and are described next

3.2.3.2.1. Wraps

To investigate increase in failure load of steel members retrofitted with precured FRP laminates CFRP sheet strips were wrapped around the specimen. In this test series only discontinuous

specimens were used. The application of 1 wrap or 2 wraps was characteristic for these two series. Due to the impracticality of wrapping the specimens of Type I and II, only the specimens of Type III, which had a bonded length of 9in (22.9cm), were wrapped with the 1in (2.5cm) wide CFRP sheets (see Figure 3-3). As such these series were designated as type III-W₁ and III-W₂, respectively, for the 1-wrap and 2-wraps specimens (see Table 3.2).

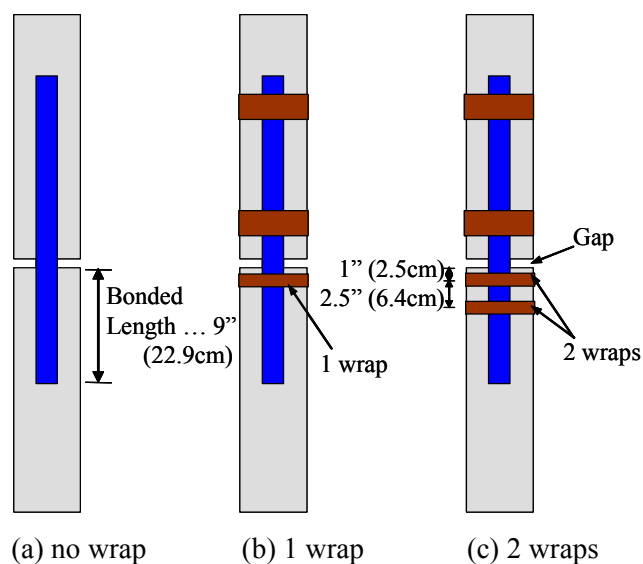


Figure 3-3 Wrapping Schemes

Table 3.2 Wrapping Scheme

Specimen Notation	Bonded Length		Number of wraps
	in	cm	
III-W ₁	9	22.9	1
III-W ₂	9	22.9	2

The wraps consisted of two layers of 1in. (2.5cm) wide CFRP sheet. The wrapping sheets were not overlapped around the steel plate, and a 1in. (2.5cm) gap was left between the ends of the sheets. This design detail was implemented to duplicate a retrofit condition for a W-section, where the web would prevent a continuous wrap. To prevent failure at the side where no strain gages were installed, two continuous double-layered 3in (7.6cm) wide wraps were applied to the specimen.

3.2.3.2.2. FRP Laminate Type

Four different laminate types were used in this research project. One type was a special manufactured Glass-Carbon-Hybrid FRP, provided by Glasforms, Inc., and was used to protect the steel from galvanic corrosion, which is likely to occur as a direct contact of carbon and steel. This laminate was manufactured with a thin layer of glass fibers on one side. This was in contrast to other research projects, where a glass scrim layer is used between the steel and carbon, as reported in Section 2.3.2.1. The other laminates tested, were the CFRP 200/2000 provided by Structural Composites, Inc., Tyfo[®] UC CFRP laminate provided by Fyfe Inc. and the CarboDur[®] S1012 provided by Sika Inc.

Table 3.3 FRP Laminate Properties

Specimen Notation	Laminate Type	Ultimate Strength		Young's Modulus		Thickness		Elongation at Break
		ksi	MPa	ksi	GPa	in	mm	[%]
H	GC-Hybrid FRP	250	1724	18,000	124	0.053	1.35	1.4
C	S&P CFRP 200/2000	360	2500	29,000	200	0.055	1.4	- *)
T	Tyfo [®] UC	405	2790	22,500	155	0.075	1.9	1.8
S	Sika CarboDur [®] S1012	440	3050	23,600	165	0.047	1.2	1.7

*) not available

Table 3.3 indicates the properties of these four laminate types as well as the notation for specimen reference. The properties for the GC-Hybrid FRP were determined based on an average of 4 tensile tests. The ends of these laminates were patched with GFRP sheets and saturant to prevent high compression of the fibers in the transverse direction due to gripping from the testing machine. Material properties for all other laminates were provided by the manufacturer.

3.2.3.2.3. Adhesive Type

Since the application of FRP composites to steel is in its development stages, the available adhesives are mostly tailored for the strengthening and repair applications to concrete structures. One of the main goals of this research project was to investigate the most suitable adhesive for the application of FRP laminates to steel. Five adhesives were investigated: (1) En-Force CFL, (2) Sikadur[®] 30, (3) Sikadur[®] 31, (4) Tyfo[®] MB, and (5) S&P Resin 220.

Table 3.4 Adhesive Properties

Specimen Notation	Adhesive Type	E- Modulus (UMR)		E-Modulus (Manufacturer)	
		ksi	GPa	ksi	GPa
1	En-Force CFL	275	1.9	-	-
2	Sikadur [®] 30	900	6.21	1700	11.7
3	Sikadur [®] 31	400	2.77	1050	7.22
4	Tyfo [®] MB	-	-	8400	58
5	S&P 220	1150	7.93	-	-

The epoxy En-Force CFL is part of the SCI CFRP laminate 200/2000 composite strengthening system of Structural Composites, Inc. The epoxy Sikadur[®] 30 and 31 are both applicable to steel according to the manufacturer, and were therefore included in this research project. The fourth adhesive tested, was Tyfo[®] MB and is manufactured by the company Fyfe. Epoxy adhesive S&P resin 220, provided by S&P in Switzerland, was also used in this project. As depicted in Table 3.4 the adhesive types En-Force CFL, Sikadur[®] 30 and 31, Tyfo[®] MB and S&P Resin 220 were designated as 1, 2, 3, 4 and 5, respectively.

The??? in Table 3.4 given E-Moduli for the adhesives were obtained from tests conducted at UMR or provided by the manufacturer, if applicable. Tests at UMR were conducted according to ASTM D 790-02 in flexural three-point bending. The specimens were prepared and cured at ambient lab temperature. The epoxy was mixed as described in Section 3.2.5 and spread on a plastic sheet by means of a spatula. After sprinkling glass beads in a diameter of 80mils (2mm) to obtain a constant adhesive line thickness the epoxy was covered with another plastic sheet and pinned down with a steel plate. The epoxy plates were left to cure for at least 2 weeks, before coupons of the size 0.5in x 2in (13mm x 51mm) were cut with a band saw. The coupons were tested in three-point bending with a span of 1in (25mm). A number of 8 coupons were tested for each epoxy and the E-Modulus was determined by averaging the results for those coupons. It becomes apparent that the glass beads affected the material properties significantly, as stress concentrations were introduced.

3.2.3.2.4. Adhesive Thickness

The adhesive thickness was also investigated in this research program as one of the bond influencing factors. It was controlled in some specimens by glass beads, whereas in other specimens the adhesive thickness was not controlled. This was done in order to obtain a

correlation between specimens with a controlled adhesive thickness of known dimension and an unknown adhesive thickness. The glass beads used in this experimental program had diameters of 10mils (0.25mm), 80mils (2mm) and 140mils (3.5mm). The specimen designation was 10, 80 and 140, respectively. Specimens with an uncontrolled adhesive thickness were designated as 0. A full description of specimens used in this research project is given in Section 3.2.4.

3.2.3.2.5. Surface Preparation

Surface preparation involves cleaning of the steel plates to provide a proper surface for the application of the adhesive. The steel plates for all specimens were cleaned by means of a wire brush and a solvent in order to remove all loose particles and oil. The FRP surface preparation depended upon the laminate type, as already described in Section 2.1.3.2.2. Whereas the CFRP laminates already come from the manufacturer with a roughened face for the application of the adhesive, the GC-Hybrid FRP laminate was smooth on both faces. Therefore, the GC-Hybrid FRP specimens were assembled using sanded laminates, and some laminates were left as is.

3.2.3.2.6. Curing Time

In order to investigate the bond performance of retrofitted steel members as a function of the adhesive curing time, specimens were tested after different curing periods. This time variable was introduced after it was observed that strain profiles of tested specimens varied significantly from test to test, and one plausible reason could be the difference in curing time. For example, for the specimens tested after only seven days the adhesive was still malleable, whereas for specimens tested after 2 weeks the adhesive was significantly more brittle. In the specimen notation superscripts (+) and (-) were introduced to distinguish between the test results for cured and insufficiently cured specimens. Additionally, a new test series 1D was conducted to examine the time dependent strength development for this epoxy. That series was designated as Test Series III_T and is reported in Section 3.3.2.5.

3.2.3.3. Specimen Notation

Overall 56 specimens were tested to investigate the influence of the different variables described in the previous sections. To facilitate the reference to each specimen tested under different conditions the following notation was adopted:

- 1) The first variable in the specimen notation depicts the bond length type for discontinuous specimens as I, II and III. For the continuous specimen, since only one bonded length was considered, the specimen was simply designated as “C”.
- 2) The second variable in the specimen notation refers to specimens with wraps. Wrapped specimens were defined as III-W₁ and III-W₂ for one and two wraps, respectively. Unwrapped specimens were not notated.
- 3) The third variable depicts the FRP laminate type used for the specimen fabrication. The designations H, C, T and S are used as indicated in Table 3.3, and stand for GC-Hybrid FRP, CFRP 200/2000, Tyfo[®] UC and Sika Carbodur[®] S1012, respectively.
- 4) The fourth variable refers to the GC-Hybrid FRP surface. The laminates were defined as “n” or “s” for a non-sanded and sanded FRP face. The CFRP specimens were not notated.
- 5) The fifth variable refers to the adhesive type used for the specimen fabrication. The adhesive types En-Force CFL, Sikadur[®] 30 and 31, Tyfo[®] MB and S&P Resin 220 were designated as 1, 2, 3, 4 and 5, respectively, as indicated in Table 3.4.
- 6) The sixth variable depicts the diameter of the glass beads and therewith the adhesive thickness. The use of glass beads of a diameter of 10mils (0.25mm), 80mils (2mm) and 140mils (3.5mm) was designated as 10, 80 and 140, respectively. Specimens with an uncontrolled adhesive thickness were designated as 0.
- 7) The seventh variable refers to the curing state of the specimen. The superscript (-) depicts a still malleable adhesive at the day of testing, whereas the superscript (+) refers to a fully cured specimen.

The following example illustrates the used specimen notation. A specimen is referred to as: III-D-Hs1-80⁺. This means that:

- the bonded length for this discontinuous specimen was 9in (22.9cm),
- no wraps were applied,

- the sanded GC-Hybrid FRP was adhered to the steel by means of 80mils (2mm) thick epoxy En-Force CFL,
- the epoxy was sufficiently cured.

3.2.4. TEST MATRIX

Seven series of specimens were tested to characterize the bond performance of FRP on steel, as shown in Table 3.5.

Table 3.5 Test Matrix

Specimen Notation		Specimens Tested	Comments
Bond Type	Characteristics		
I	Hn 1-0b ⁺	1	Figure 3-3a
	Hs 1-80 ⁻	1	
	Hs 1-80 ⁺	3	
	C 1-0b ⁺	1	
II	Hn 1-0b ⁺	1	
	Hs 1-80 ⁺	3	
	C 1-0b ⁺	1	
III	Hn 1-0b ⁺	1	
	Hs 1-0b ⁺	1	
	Hs 1-80 ⁻	1	
	Hs 1-80 ⁺	3	
	Hs 1-140 ⁺	1	
	Hs 4-80 ⁺	2	
	C 1-0b ⁺	1	
	C 2-80 ⁺	3	
	C 3-80 ⁺	3	
	T 4-10 ⁺	2	
	T 4-80 ⁺	3	
	S 3-80 ⁺	2	
III _T	Hs 1-80	9	
III-W ₁	Hs 1-0b ⁺	1	Figure 3-3b
	Hs 1-80 ⁺	4	
III-W ₂	Hn 1-0b ⁺	1	Figure 3-3c
	Hs 1-80 ⁺	5	
	C Hs 1-80 ⁺	2	Figure 3-2
	Σ =	56	

Six test series consisted of discontinuous specimens. A seventh series consisted of continuous specimens. Table 3.5 illustrates the specimen notation and the number of specimens tested under each condition. For the relevant characteristics such as adhesive type three specimens were prepared. However, in some cases one specimen did not fail in the expected manner (e.g. III Hs

4-80⁺) and only two test are reported. In the case of the wrapped specimens more than three tests were conducted as the data was not consistent, and no conclusions could be drawn.

3.2.5. SPECIMEN PREPARATION

This section depicts the steps that were carried out to prepare the specimens:

- 1) All steel plates were mechanically cleaned by means of an electric wire brush until a near white finish was observed.
- 2) Next, the specimens were assembled for the FRP application (Figure 3-4a). Two steel angles 1x1x24in (2.5x2.5x61cm) were used to connect one 18in (45.5cm) long and a 25in (63.5cm) long plate. A stable but removable connection for the steel plates was necessary, because no loads should be applied to the FRP prior to testing. In addition, it was necessary to prevent damage of the adhesive layer during transportation and installation in the testing machine.
- 3) The surfaces were wiped with a cloth moistened with Acetone. This step was repeated until the cloth remained clean. The surface of the FRP strips also was cleaned with Acetone. Subsequently, the bonded length was marked on the specimens (Figure 3-4b).
- 4.a) Epoxy En-Force CFL is a two-component epoxy and consists of two components, namely: A and B. Component A is soft and of a beige color. Component B is rather sticky and darkish green (Figure 3-4c). The mixing ratio of component A to component B is 2:1. Both components were premixed separately, as recommended by the manufacturer. After that, component B was added to component A and the epoxy was mixed for approximately 3 minutes until the color streaks had disappeared (Figure 3-4d). Then, the epoxy was applied to the steel by the means of a plastic spatula (Figure 3-4e).
- 4.b) The adhesives Sikadur[®] 30 and 31, and the S&P Resin 220, are also two-component epoxy adhesives. Sikadur[®] 30 and S&P Resin 220 have a mixing ratio of component A to B of 3:1 by weight and volume. The mixing ratio for the Sikadur[®] 31 of component A to B is 1:1 by volume. The application procedure was the same as for the Enforce CFL.

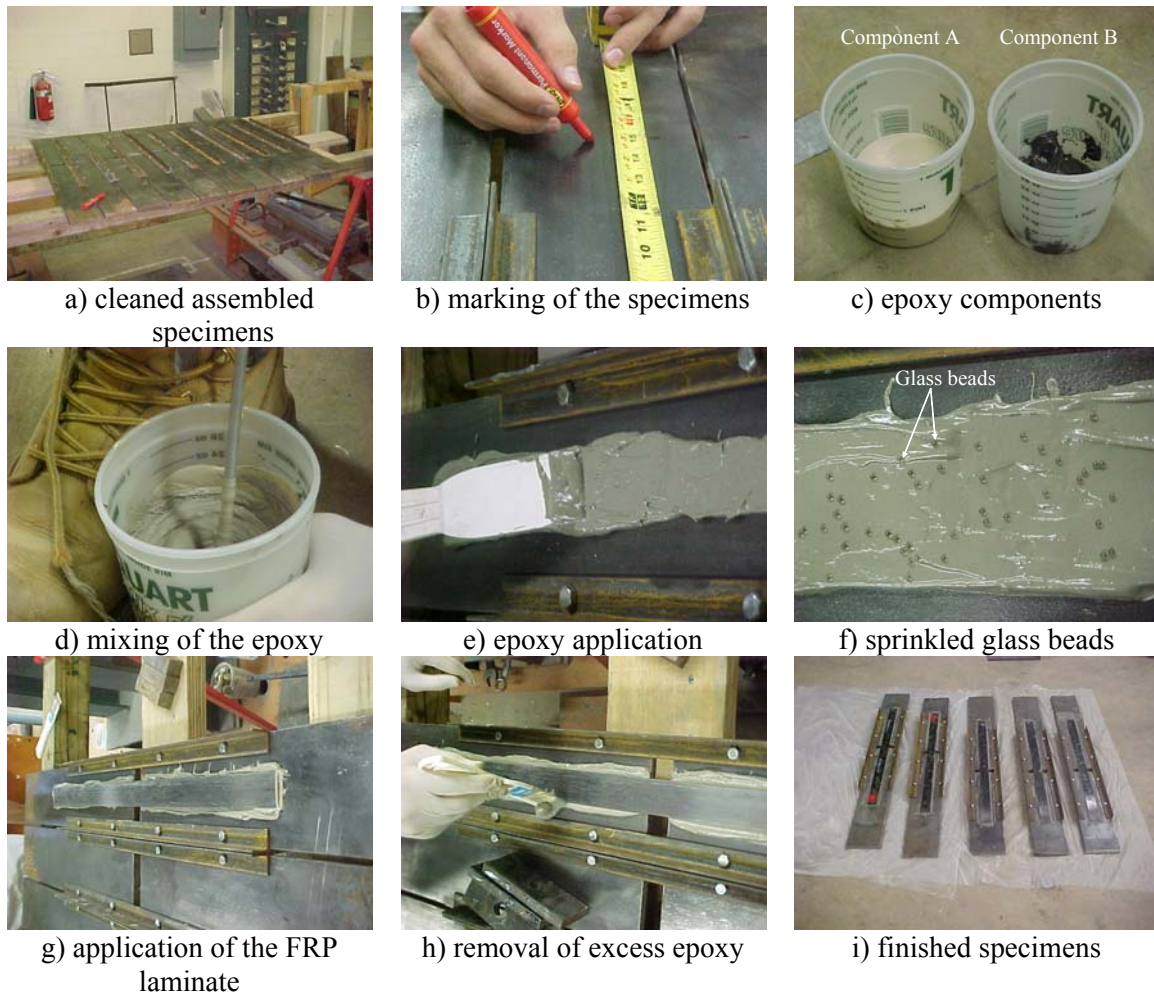


Figure 3-4 Specimen Preparation (using Enforce CFL)

- 4.c) Tyfo[®] MB is also a two-component epoxy, but no mixing manually is necessary as this epoxy is delivered in cartridges and applied with an epoxy gun. The advantage of this product is that it allows for an easier application. In addition, the components are always mixed properly and in a constant ratio. With regard to the specimen preparation the only difference is the application of the epoxy, which is applied in a zigzag manner and spread with a spatula.
- 5) Wherever used, glass beads were sprinkled on the epoxy to assure a constant adhesive line (Figure 3-4f). The FRP strip was applied and pressed down until all excessive epoxy was released (Figure 3-4g). The released epoxy was then carefully removed with a spatula (Figure

3-4h) and the specimen was clamped to ensure the contact of the FRP and the adhesive in order to prevent voids.

- 6) After one day the specimen was turned over and the process was repeated on the reverse side of the specimen. The finished specimens prior to strain gage application are shown in Figure 3-4i.
- 7) In the case of the wrapped specimens, spacers made of 1in (2.5cm) square steel tubes were used to assemble the specimens. This was done to provide clearance between the steel plates and the steel angles for proper wrapping of the specimen. The application process is as described before. The wraps consisted of two 1in. (2.5cm) wide 11in. (27.9cm) long CFRP sheet strips, which were adhered to the specimen by the means of saturant.
- 8) The last step of the specimen preparation was the application of the strain gages.

3.2.6. TEST SETUP

All specimens were tested in the MTS 880, which is a universal testing machine manufactured by MTS and used for tensile as well as compressive tests (Figure 3-5). All tests were conducted under static loading up to failure. The specimens were tested in load control.

Prior to testing a specimen the following installation and preparation steps were undertaken: (1) the lower gripping device was raised to maximum, (2) the specimen was placed, (3) the grips were closed, and (4) the upper part of the machine was locked. (5) The strain gages were connected to the external strain gage channels of the machine and



Figure 3-5 MTS 880 and Data Acquisition

balanced to zero. (6) The steel angles, holding the steel plates together, were removed. (7) To

prevent dispersion of debris after bond failure an additional clamping system consisting of 2 small steel plates and two bolts with wing nuts was attached to the upper part of the specimen. (8) After setting up the data acquisition the specimen was tested.

3.3. EXPERIMENTAL RESULTS

3.3.1. INTRODUCTION

In the following chapter test results and failure modes from the experimental program are presented. Description of test results will be given for the observed behavior considering the different bond influencing factors that were discussed in Chapter 3.2.

Results will be presented by test series, as introduced in Section 3.2.3.3. These will be differentiated between discontinuous specimens according to the bonded length types, the time dependent series and the wrapping scheme.

In Section 3.3.2 the failure modes, failure loads and maximum measured FRP strains are presented. Observations made during testing or the specimen preparation, are also noted.

3.3.2. GENERAL OBSERVATIONS

3.3.2.1. Failure Modes

Before listing the results for the examined specimen types the observed failure modes are classified. Based on test results three main failure modes were observed. These failure modes were characterized by peeling off the laminate, never by FRP rupture. In all specimens the peeling started at the location of the stress concentrations – the discontinuity. For wrapped specimens an additional character is introduced to describe the state of the wraps after failure.

3.3.2.1.1. Failure Mode S

This failure mode occurs at the interface between the steel and the epoxy. This failure mode is defined when less than 25 percent of the epoxy remains on the steel plates (see Figure 3-6).

3.3.2.1.2. Failure Mode SF

This failure mode stands for a dual failure at the interface between the steel and the epoxy as well as at the interface between the FRP and the epoxy. The percentage of the epoxy remaining on the steel plate was defined to be between 25 and 75 percent (see Figure 3-7).

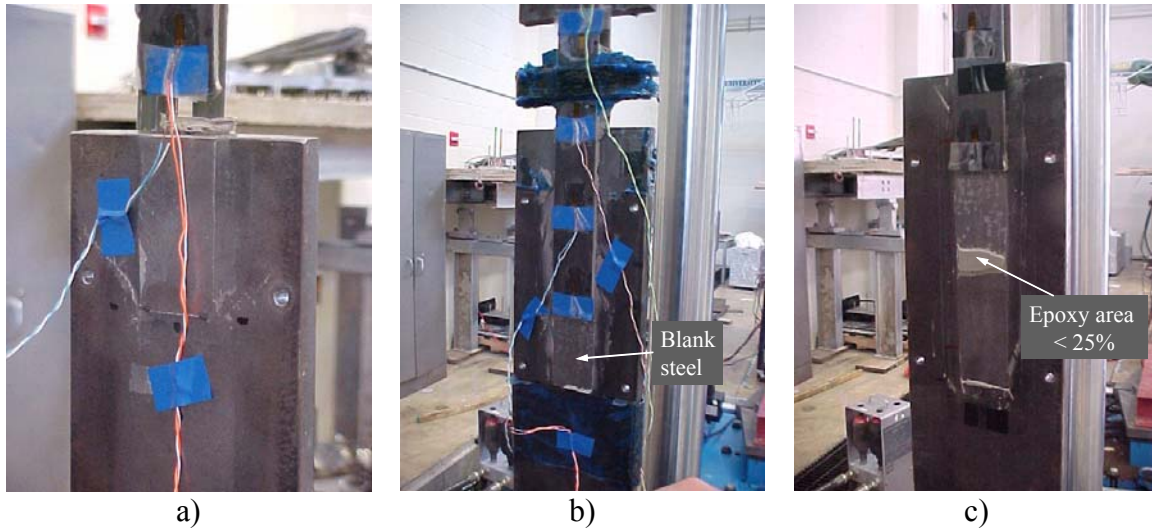


Figure 3-6 Failure Mode S

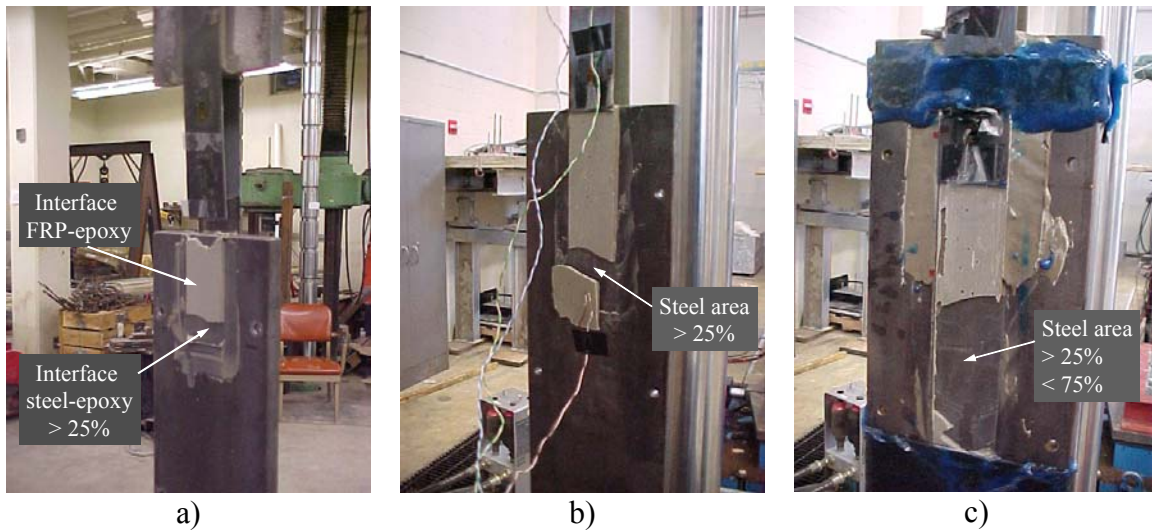


Figure 3-7 Failure Mode SF

3.3.2.1.3. Failure Mode F

This failure mode refers to the failure at the interface between the FRP and the epoxy, which is the case if the percentage of the epoxy remaining on the steel plate was more than 75 percent. In some cases glass fibers remained on the epoxy, but these cases are not defined separately (see Figure 3-8).

3.3.2.1.4. Failure Mode +w

This failure mode was introduced to give additional information concerning the state of the wraps at failure. It is only used in combination with the aforementioned three failure modes. The

additional letter +w is hereby used to indicate that at least one of the wraps failed, as shown in Figure 3-9. If this information is not given, the specimen failed by the FRP sliding out of the wrap.

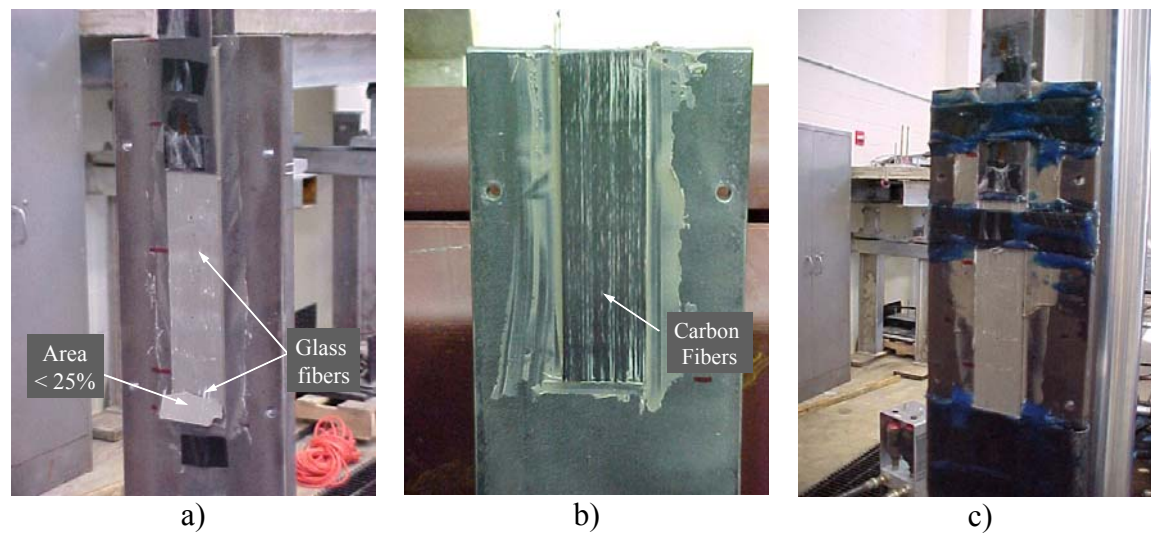


Figure 3-8 Failure Mode F

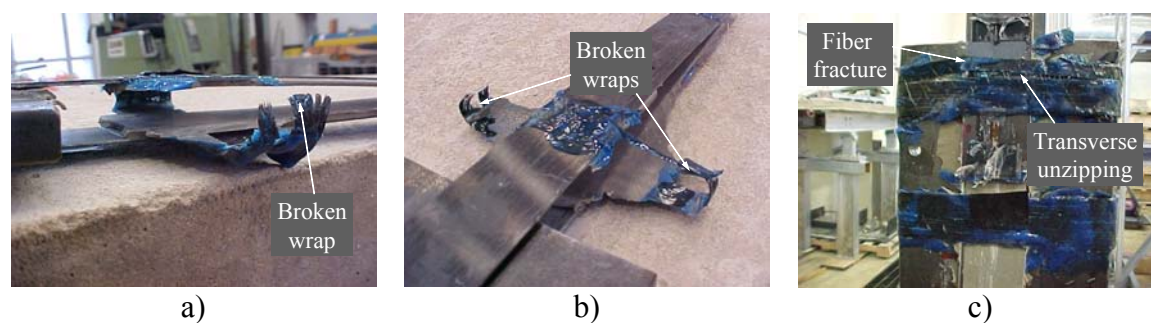


Figure 3-9 Failure of Wraps (+w)

3.3.2.2. Test Series I

A total number of six specimens were tested in this test series. As described in Section 3.2 these specimens were fabricated with a bonded length of 3in (7.6cm), and as such they were designated as Type I (see Table 3.1). In this test series five specimens were fabricated with GC-Hybrid FRP laminate, and one specimen was fabricated with the CFRP 200/2000 laminate. All specimens were prepared with the epoxy En-Force CFL.

A numerical and graphical description of the test data is presented in Table 3.6 and Figure 3-10, respectively.

Table 3.6 Test Results – Test Series I

Specimen	Specimen Type	Failure Load		Microstrain	Failure Mode
		kips	KN		
I-1	I-Hn 1-0b ⁺	11.5	51	3900	SF
I-2	I-Hs 1-80 ⁻	9.3	41	2600	S
I-3.1	I-Hs 1-80 ⁺	15.1	67	5200	F
I-3.2	I-Hs 1-80 ⁺	13.1	58	- ¹⁾	F
I-3.3	I-Hs 1-80 ⁺	12.1	54	4200	F
I-4	I-C 1-0b ⁺	12.4	55	3400	S

¹⁾ strain gage malfunction

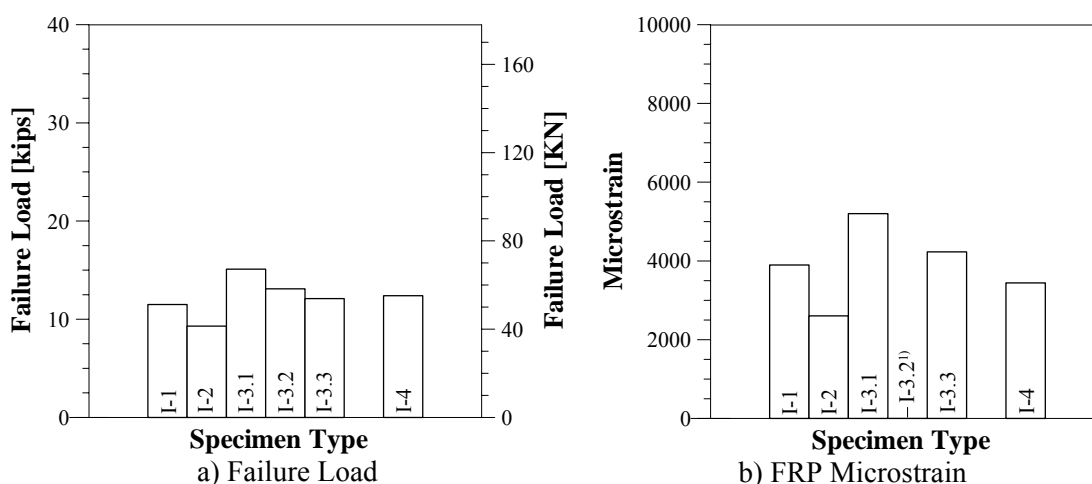


Figure 3-10 Test Results – Test Series I

As indicated in Table 3.6, in Specimen I-1 the GC-Hybrid FRP laminate was not sanded prior to the application. No beads were used to obtain a constant adhesive thickness. This specimen cured for more than a month, and post-test inspection revealed that the adhesive was brittle. As such it was notated with the subscript (+) to indicate that the adhesive had properly cured. This specimen experienced dual bond failure at the interfaces between the FRP and the epoxy and the steel and the epoxy (see Figure 3-7a), and was described as exhibiting Failure Mode SF.

In Specimen I-2 the GC-Hybrid FRP laminate was sanded prior to the application. Glass beads of a diameter of 80mils (2mm) were used to obtain a constant adhesive thickness. Post-test inspection indicated that the epoxy was still malleable and as such was designated with the subscript (-). Since the properly cured adhesive is brittle, the malleability of the examined

adhesive indicated that the curing process was incomplete. However, this specimen was tested after 7 days considering the curing time recommendation provided by the En-Force manufacturer. Since this specimen was cured under laboratory conditions, it may be suggested that for steel a different curing time may need to be adopted. The failure mode of Specimen I-2 can best be characterized as Failure Mode S (see Figure 3-6a), since failure occurred at the interface between the steel and the epoxy. In addition, comparing the results with those of Specimen I-1, lower strain values observed during testing may suggest that the curing time may play a significant role in the bond performance of FRP to steel applications.

All Specimens I-3.1 to I-3.3 were prepared with sanded GC-Hybrid laminates, and glass beads of a diameter of 80mils (2mm). Post-test inspection indicated that the epoxy was properly cured. All experienced the same failure mode, which occurred at the interface between the FRP and the epoxy (Failure Mode F, see Figure 3-8a). Remnants of glass fibers could be found on the epoxy. This clearly indicates that the failure occurred due to peeling off of the FRP laminate. In Specimen I-3.2 the strain gage located at position 1 was not functioning properly, and no strain data was recorded.

Specimen I-4 was the only specimen fabricated with the CFRP 200/2000. Glass beads of a diameter of 80mils (2mm) were used to obtain a constant adhesive thickness. Post-test inspection indicated that the epoxy was properly cured. This specimen experienced failure at the interface between the steel and the epoxy (Failure Mode S, see Figure 3-6a). Carbon fibers remained on the epoxy.

Evaluating the chart in Figure 3-10, and by comparing results for the Specimens I-1, I-2 and I-3 it may be concluded that the curing time impacts the failure load, peak strains and failure mode. Based on these test results Test Series III_T was introduced to investigate the effects of curing time on the bond performance of FRP to steel applications. Test results for Series III_T are presented in Section 3.3.2.5.

Comparing the results for the Specimens I-1 and I-3, sanding the GC-Hybrid laminates resulted in an increase of the failure load and the peak strain. This observation will be evaluated in further detail for Test Series II and III.

Comparing the results for the Specimens I-1, I-3 and I-4, it may be concluded that the use of GC-Hybrid FRP results in a better bond performance of the specimen. This observation is meaningful, because this laminate not only improves the bond performance, which is an important consideration, but also protects the steel against galvanic corrosion.

3.3.2.3. Test Series II

A total number of five specimens were tested in this test series. As described in Section 3.2 these specimens were fabricated with a bonded length of 6in (15.2cm), and as such they were designated as Type II (see Table 3.1). In this test series four specimens were fabricated with GC-Hybrid FRP laminate, and one specimen was fabricated with the CFRP 200/2000 laminate. All specimens were prepared with the epoxy En-Force CFL.

A numerical and graphical description of the test data is presented in Table 3.7 and Figure 3-11, respectively.

As indicated in Table 3.7, in Specimen II-1 the GC-Hybrid FRP laminate was not sanded prior to the application. No beads were used to obtain a constant adhesive thickness. This specimen cured for more than a month, and post-test inspection revealed that the adhesive was inflexible and brittle. As such it was notated with the subscript (+) to indicate that the adhesive had properly cured. This specimen experienced a failure at the interface between the FRP and the epoxy (see Figure 3-8a), and was described as exhibiting Failure Mode F.

All Specimens I-2.1 to I-2.3 were prepared with sanded GC-Hybrid laminates, and glass beads of a diameter of 80mils (2mm). Post-test inspection indicated that the epoxy was properly cured. Although each specimen experienced a different failure mode by definition, in all cases epoxy remained on the steel and the FRP laminate, and remnants of glass fibers were found on the epoxy. However, similar failure loads were observed.

Table 3.7 Test Results – Test Series II

Specimen	Specimen Type	Failure Load		Microstrain	Failure Mode
		kips	KN		
II-1	II-Hn 1-0b ⁺	11.6	52	3600	F
II-2.1	II-Hs 1-80 ⁺	15.0	67	4900	S
II-2.2	II-Hs 1-80 ⁺	14.7	65	4400	SF
II-2.3	II-Hs 1-80 ⁺	16.5	73	5500	F
II-3	II-C 1-0b ⁺	11.9	53	2500	F

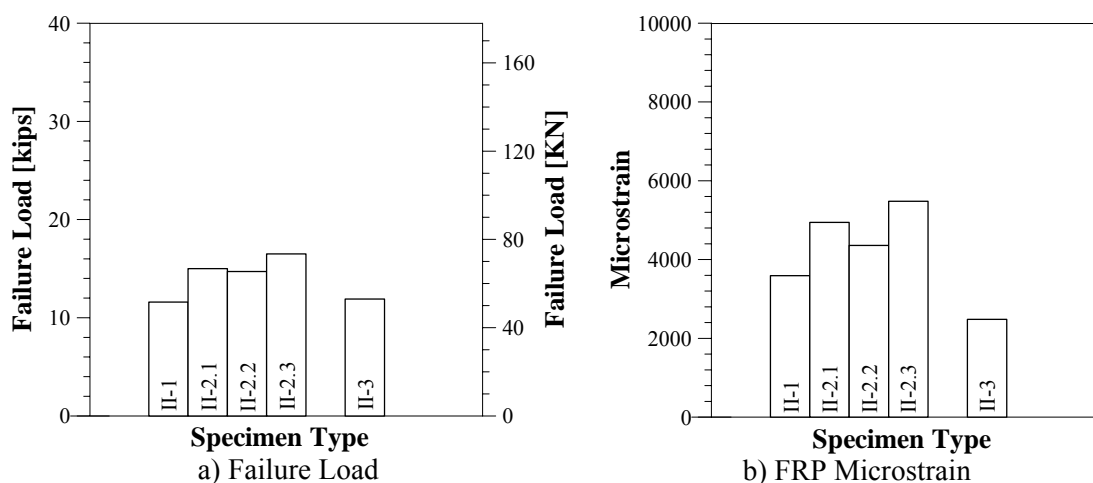


Figure 3-11 Test Results – Test Series II

Specimen II-3 was the only specimen fabricated with the CFRP 200/2000. Glass beads of a diameter of 80mils (2mm) were used to obtain a constant adhesive thickness. Post-test inspection indicated that the epoxy was properly cured. This specimen experienced failure at the interface between the FRP and the epoxy (Failure Mode F, see Figure 3-8b). Carbon fibers remained on the epoxy.

Comparing results between Specimens I-1 and II-2, by sanding the GC-Hybrid FRP laminates an increase in failure load and peak strain was obtained. However, since the curing times were not the same for all specimens this conclusion needs to be further validated. Additional information will be presented for the test series in the following sections. Furthermore, it may be concluded that the failure mode and the recorded loads and strains are not interdependent.

Once again, comparing results for Specimen II-1 and II-2 with II-3, the GC-Hybrid FRP reinforced specimens displayed higher peak strains.

3.3.2.4. Test Series III

A total number of 26 specimens were tested in this test series. As described in Section 3.2 these specimens were fabricated with a bonded length of 9in (22.9cm), and as such they were designated as Type III (see Table 3.1). In this test series nine specimens were fabricated with GC-Hybrid FRP laminate. For seven of these specimens the epoxy En-Force CFL was used, and for the other two the epoxy Tyfo[®] MB. Ten specimens were reinforced with the CFRP 200/2000

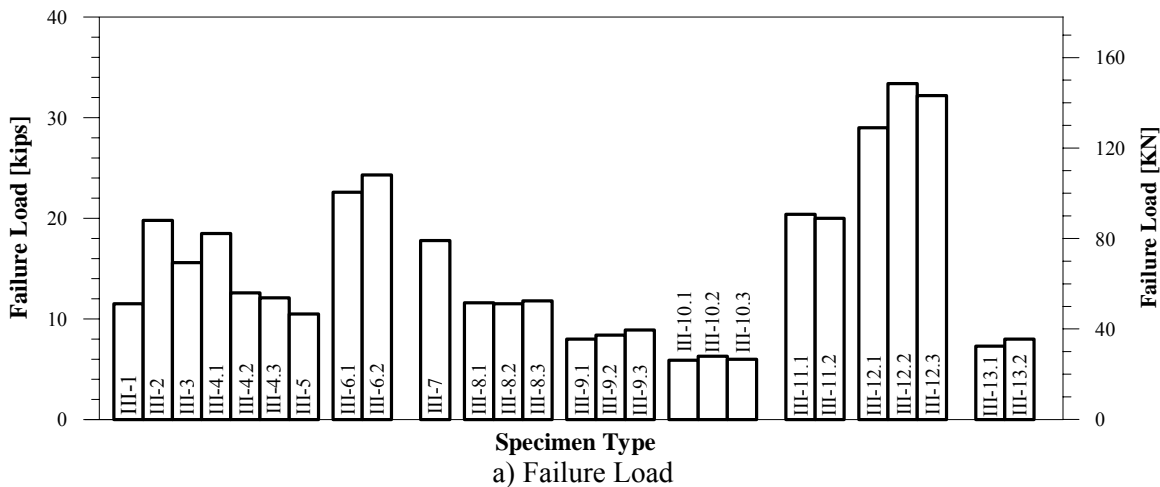
laminate. Out of these, one specimen was prepared with the En-Force CFL, and each three with Sikadur[®] 30 and 31, and S&P Resin 220. Furthermore, five specimens with two different adhesive thickness were prepared with the CFRP laminate Tyfo[®] UC and the epoxy Tyfo[®] MB. Lastly, two specimens were fabricated with Sika CarboDur[®] S1012 and Sikadur[®] 31.

A numerical and graphical description of the test data is presented in Table 3.8 and Figure 3-12, respectively. As indicated in Table 3.8, in Specimen III-1 the GC-Hybrid FRP laminate was not sanded prior to the application. No beads were used to obtain a constant adhesive thickness. This specimen cured for more than a month, and post-test inspection revealed that the adhesive was inflexible and brittle. As such it was notated with the subscript (+) to indicate that the adhesive had properly cured. This specimen experienced a failure at the interface between the FRP and the epoxy (see Figure 3-8a), and was described as exhibiting Failure Mode F.

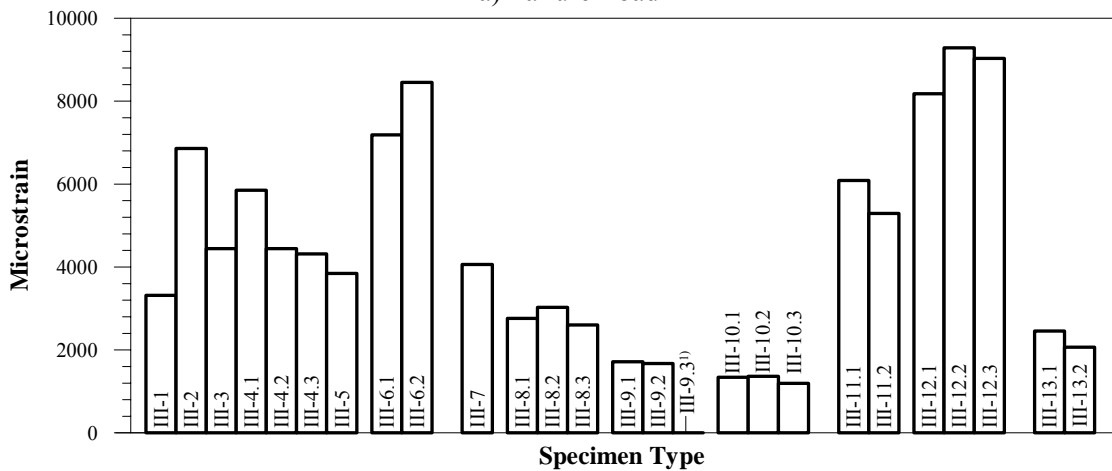
Table 3.8 Test Results – Test Series III

Specimen	Specimen Type	Failure Load		Microstrain	Failure Mode
		kips	KN		
III-1	III-Hn 1-0b ⁺	11.5	51	3300	F
III-2	III-Hs 1-0b ⁺	19.8	88	6800	S
III-3	III-Hs 1-80 ⁻	15.6	69	4400	S
III-4.1	III-Hs 1-80 ⁺	18.5	82	5800	S
III-4.2	III-Hs 1-80 ⁺	12.6	56	4400	F
III-4.3	III-Hs 1-80 ⁺	12.1	54	4300	S
III-5	III-Hs 1-140 ⁺	10.5	48	3800	F
III-6.1	III-Hs 4-80 ⁺	22.6	101	7200	F
III-6.2	III-Hs 4-80 ⁺	24.3	108	8500	F
III-7	III-C 1-0b ⁺	17.8	79	4100	F
III-8.1	III-C 2-80 ⁺	11.6	52	2800	F
III-8.2	III-C 2-80 ⁺	11.5	51	3000	F
III-8.3	III-C 2-80 ⁺	11.8	52	2600	F
III-9.1	III-C 3-80 ⁺	8.0	36	1700	F
III-9.2	III-C 3-80 ⁺	8.4	37	1700	F
III-9.3	III-C 3-80 ⁺	8.9	40	- ¹⁾	F
III-10.1	III-C 5-80 ⁺	5.9	26	1300	F
III-10.2	III-C 5-80 ⁺	6.3	28	1400	F
III-10.3	III-C 5-80 ⁺	6.0	27	1200	F
III-11.1	III-T 4-10 ⁺	20.4	91	6100	F
III-11.2	III-T 4-10 ⁺	20.0	89	5300	F
III-12.1	III-T 4-80 ⁺	29.0	129	8200	F
III-12.2	III-T 4-80 ⁺	33.4	149	9300	F
III-12.3	III-T 4-80 ⁺	32.2	143	9000	F
III-13.1	III-D S 3-80 ⁺	7.3	32	2500	F
III-13.2	III-D S 3-80 ⁺	8.0	36	2100	F

1) strain gage malfunction



a) Failure Load



b) FRP Microstrain

Figure 3-12 Test Results – Test Series III

In Specimen III-2 the GC-Hybrid FRP laminate was sanded prior to the application. But beads of 80mils (2mm) diameter were used to control the adhesive thickness. Post-test inspection indicated that the epoxy was properly cured. This specimen experienced a failure at the interface between the steel and the epoxy (see Figure 3-6c), and was described as exhibiting Failure Mode S.

In Specimen III-3 the GC-Hybrid FRP laminate was sanded prior to the application. Glass beads of a diameter of 80mils (2mm) were used to obtain a constant adhesive thickness. Post-test inspection indicated that the epoxy was still malleable and as such was designated with the

subscript (-). The failure mode of Specimen III-3 can best be characterized as Failure Mode S (see Figure 3-6a), since failure occurred at the interface between the steel and the epoxy.

In Specimen III-4.1 the GC-Hybrid FRP laminate was sanded prior to the application. Glass beads of 80mils (2mm) diameter were used to control the adhesive thickness. Post-test inspection indicated that the epoxy was properly cured. This specimen experienced a failure at the interface between the steel and the epoxy (see Figure 3-6a), and was described as exhibiting Failure Mode S.

Specimens I-4.2 and I-4.3 were prepared with sanded GC-Hybrid laminates, and glass beads of a diameter of 80mils (2mm). Post-test inspection indicated that the epoxy was properly cured. Although each specimen experienced a different failure mode, in both cases similar failure loads and peak strains, significantly lower than the values for Specimen III-4.1, were observed.

In Specimen III-5 the GC-Hybrid FRP laminate was sanded prior to the application. Glass beads of 140mils (3.5mm) diameter were used to control the adhesive thickness. The epoxy was properly cured. This specimen experienced failure at the interface between FRP and epoxy (see Figure 3-8a), at very low load and strain levels. Improper bond between the FRP and the epoxy was found upon close examination of the failed specimen, shown in a big void. Careful clamping of the specimens has to be assured, especially for the use of GC-Hybrid FRP. This laminate type is always arched due to the different coefficients of thermal expansion of the two used fibers and the resultant different temperature dependent behavior. During the manufacturing process the carbon fibers contract upon contact with the hot matrix and the glass fibers expand. During the cooling process this the carbon fibers expand and the glass fibers shorten, which results in a curved laminate.

Specimens III-6.1 and III-6.2 were prepared with sanded GC-Hybrid laminates, and glass beads of a diameter of 80mils (2mm). But, another epoxy was used – Tyfo[®] MB. Post-test inspection indicated that the epoxy was properly cured. Both specimens failed at the interface between the FRP and the epoxy (see Figure 3-8a), which is described as Failure Mode F. Further, in both specimens at least one of the laminates ruptured longitudinally. Very high failure loads and peak strains were observed. The post-test inspection also showed that the sanding pattern of the FRP was imprinted in the epoxy, an observation that could not be made for the other used epoxies.

Specimen III-7 was the only specimen fabricated with the CFRP 200/2000 and En-Force CFL. Glass beads of a diameter of 80mils (2mm) were used to obtain a constant adhesive thickness. Post-test inspection indicated that the epoxy was properly cured. This specimen experienced failure at the interface between the FRP and the epoxy (Failure Mode F, see Figure 3-8b). Carbon fibers remained on the epoxy. Considerably high failure load and peak strains were observed.

All Specimens III-8.1 to III-8.3 were prepared with CFRP 200/2000 laminates and the epoxy Sikadur[®] 30. Glass beads of a diameter of 80mils (2mm) were used to control the adhesive thickness. Post-test inspection indicated that the epoxy was properly cured. All specimens failed at the interface between the FRP and the epoxy (Failure Mode F). However, additional observations could be made, and are illustrated in Figure 3-13. At the discontinuity failure occurred in the epoxy itself, for about a length of 0.5in (1.2cm). Following this is an area (Area I), where no fibers are attached to the epoxy, but a thin epoxy layer was found on the FRP laminate. This area stretches about 2-3in (5.1-7.6cm). Then follows the already in other CFRP specimens observed area (Area II), where carbon fibers remain on the epoxy. The failure loads and peak strains were very consistent for all specimens tested but not at a very high.

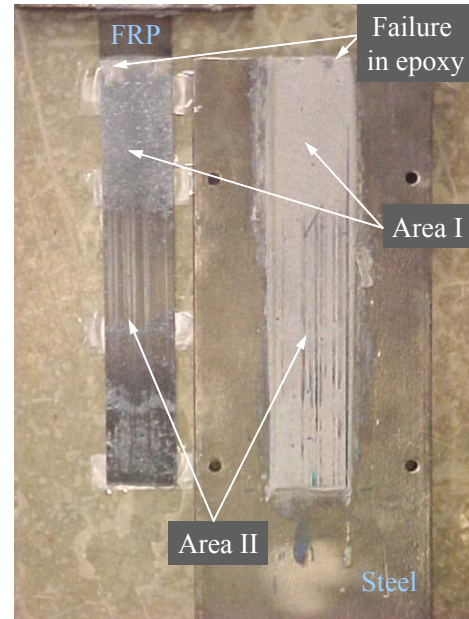


Figure 3-13 Failure of CFRP 200/2000 -Sikadur[®] 30 Specimens

All Specimens III-9.1 to III-9.3 were prepared with CFRP 200/2000 laminates and the epoxy Sikadur[®] 31. Glass beads of a diameter of 80mils (2mm) were used to control the adhesive thickness. Post-test inspection indicated that the epoxy was properly cured. All specimens failed at the interface between the FRP and the epoxy (Failure Mode F). Very low failure loads and peak strains were observed.

All Specimens III-10.1 to III-10.3 were prepared with CFRP 200/2000 laminates and the epoxy S&P Resin 220. Glass beads of a diameter of 80mils (2mm) were used to control the adhesive

thickness. Post-test inspection indicated that the epoxy was properly cured. All specimens failed at the interface between the FRP and the epoxy (Failure Mode F). Again, very low failure loads and peak strains were observed.

All Specimens III-11.1 to III-11.3 were prepared with the CFRP laminate Tyfo[®] UC and the epoxy Tyfo[®] MB. Glass beads of a diameter of 10mils (0.25mm) were used to control the adhesive thickness, as this value was recommended by the manufacturer. Post-test inspection indicated that the epoxy was properly cured. All specimens failed at the interface between the FRP and the epoxy (Failure Mode F). Further, in all specimens at least one of the laminates ruptured longitudinally. Carbon fibers remained on the epoxy. High failure loads and peak strains were observed.

All Specimens III-12.1 to III-12.3 were also prepared with the CFRP laminate Tyfo[®] UC and the epoxy Tyfo[®] MB. However, this time glass beads of a diameter of 80mils (2mm) were used to control the adhesive thickness. Post-test inspection indicated that the epoxy was properly cured. All specimens failed at the interface between the FRP and the epoxy (Failure Mode F). Further, in all specimens at least one of the laminates ruptured longitudinally. Carbon fibers remained on the epoxy. Very high failure loads and peak strains were observed.

Specimens III-13.1 and III-13.2 were fabricated with the CFRP laminate Sika CarboDur[®] S1012 in combination with Sikadur[®] 31. Glass beads of a diameter of 80mils (2mm) were used to control the adhesive thickness. Post-test inspection indicated that the epoxy was properly cured. All specimens failed at the interface between the FRP and the epoxy (Failure Mode F). Low failure loads and peak strains were observed.

Comparing results between Specimens III-1 and III-2, by sanding the GC-Hybrid FRP laminates an increase in failure load and peak strain was obtained. However, since for the Specimen III-4.2 also Failure Mode F was observed, no conclusion may be inferred for the failure mode as a result of sanding the GC-Hybrid FRP laminate.

Comparing results between Specimens III-3 and III-4.1 a higher curing time results in an increase in failure load and peak strain. However, Specimen III-4.3 was cured sufficiently but the

peak strains were similar to those for Specimen III-3, and the failure load was even lower. Therefore, no immediate conclusion may be drawn about the impact of the curing time.

Further, comparing the Specimens III-11 and III-12 it may be concluded that an increased adhesive thickness results in higher failure loads and peak strains. However, further research will have to be conducted to investigate the optimum adhesive thickness depending upon the adhesive used.

3.3.2.5. Test Series III_T – Time Dependency

A total number of 9 specimens were tested in this test series, which was initiated after obtaining experimental results reported in the previous sections. As described in Section 3.2 these specimens were fabricated with a bonded length of 9in (22.9cm). All specimens were fabricated with GC-Hybrid FRP laminate and the epoxy En-Force CFL. The specimens are designated as Type III_T (see Section 3.2.3.2.6).

A numerical and graphical description of the test data is presented in Table 3.9 and Figure 3-14, respectively.

Comparing the test results for different curing times it may be concluded that (1) an increase in failure load and peak strains will occur during the first 10 days after the FRP application, and (2) past a curing time of 10 days the failure loads and peak strains will decrease converging towards a final value. However, only a small number of tests were carried out and the data for a curing time of more than 10 days was not consistent. Therefore, further tests have to be undertaken to investigate this time dependent behavior. It may be found that the curing time recommended by the manufacturer (7 days) is insufficient for the application of this epoxy to steel members, and another recommendation will have to be established.

Table 3.9 Test Results – Test Series III_T

Specimen	Specimen Type	Failure Load		Microstrain FRP	Failure Mode
		kips	KN		
III _T -1	4 days	11.7	52	4700	S
III _T -2	5 days	13.1	58	4800	S
III _T -3	7 days	18.6	83	7100	S
III _T -4	9 days	24.9	111	8500	F
III _T -5	11 days	23.8	106	8400	F
III _T -6	15 days	19.8	88	6300	SF

III _T -7	18 days	11.9	53	3900	S
III _T -8	21 days	21.7	97	7000	SF
III _T -9	30 days	14.4	64	5200	F

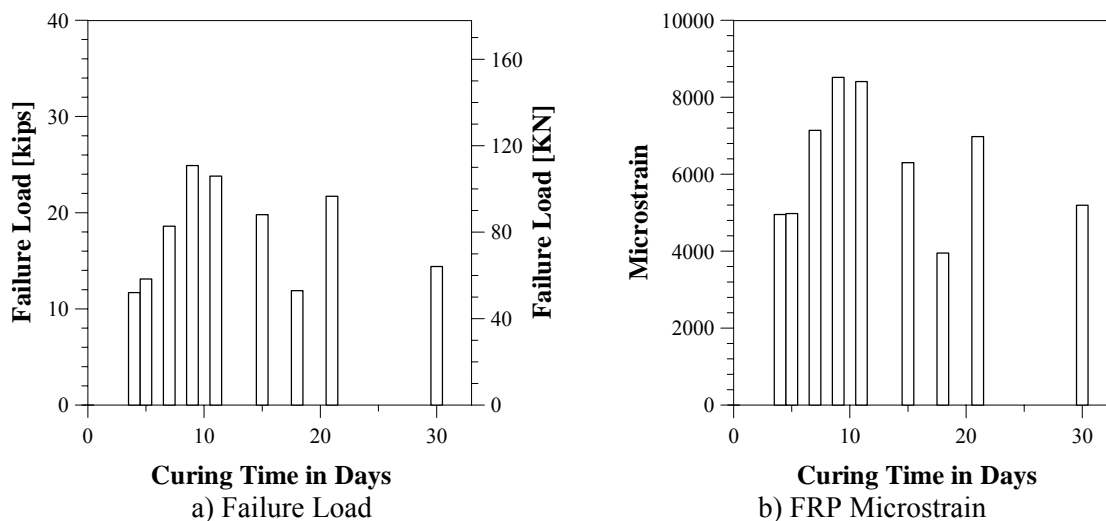


Figure 3-14 Test Results – Test Series III_T

3.3.2.6. Test Series III-W₁

A total number of 5 specimens were tested in this test series. As described in Section 3.2 these specimens were fabricated with a bonded length of 9in (22.9cm) and one wrap, and as such they were designated as Type III-W₁ (see Table 3.2). All specimens were prepared using the GC-Hybrid FRP laminate and the epoxy En-Force CFL.

A numerical and graphical description of the test data is presented in Table 3.10 and Figure 3-16, respectively.

As indicated in Table 3.10, in Specimen III-W₁-1 the GC-Hybrid FRP laminate was sanded prior to the application. No beads were used to obtain a constant adhesive thickness. The epoxy had cured sufficiently at the time of the test. This specimen experienced a failure at the interface between the steel and the epoxy (Failure Mode S). This specimen was one of the first wrapped specimens fabricated. Large ramps

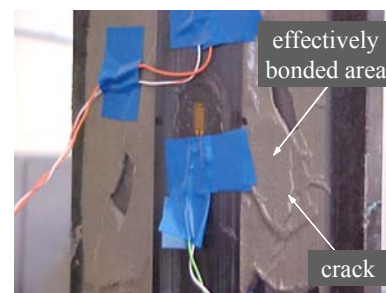


Figure 3-15 Increase of Bonded Area by Ramps

were applied, and post-test inspection revealed that these ramps might have increased the bonded area, resulting in a higher failure load and peak strain. Figure 3-15 depicts the crack pattern around the laminate and the increased bonded area. As a result of this observation all other specimens were prepared with localized ramps.

Table 3.10 Test Results – Test Series III-W₁

Specimen	Specimen Type	Failure Load		Microstrain	Failure Mode
		kips	KN		
III-W ₁ -1	III-W ₁ -Hs 1-0b ⁺	23.7	105	7700	S
III-W ₁ -2.1	III-W ₁ -Hs 1-80 ⁺	21.2	94	7300	S+w
III-W ₁ -2.2	III-W ₁ -Hs 1-80 ⁺	21.7	97	7400	S+w
III-W ₁ -2.3	III-W ₁ -Hs 1-80 ⁺	14.2	63	5300	SF
III-W ₁ -2.4	III-W ₁ -Hs 1-80 ⁺	14.2	63	5600	F+w

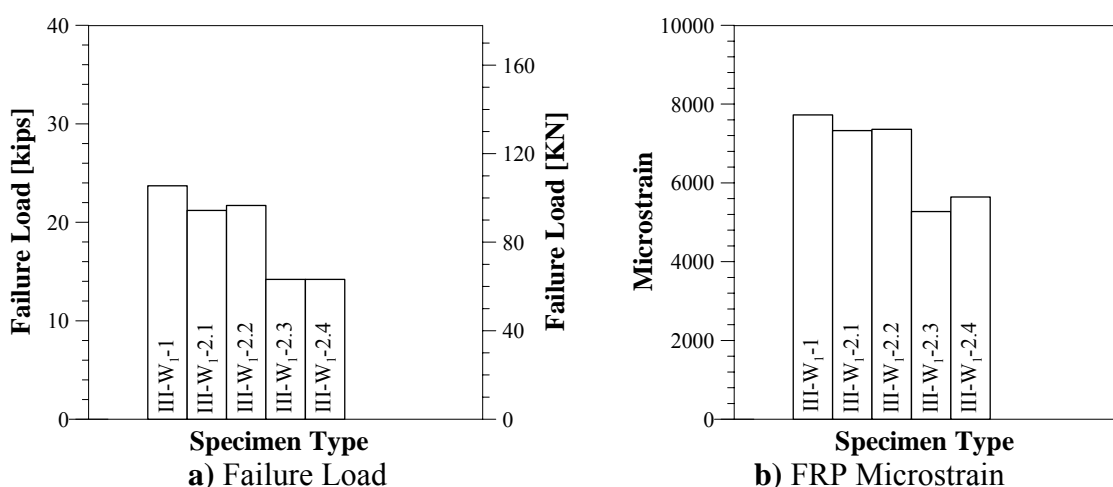


Figure 3-16 Test Results – Test Series III-W₁

In Specimen III-W₁-2.1 the GC-Hybrid FRP laminate was sanded prior to the application. Beads with a diameter of 80mils (2mm) were used to obtain a constant adhesive thickness. The epoxy had cured sufficiently at the time of the test. This specimen experienced a failure at the interface between the steel and the epoxy, plus braking of the wrap (Failure Mode S+w). A problem had occurred in the application of the wrap. While curing, one of the ends of the wrap came loose. The end was cut of and a new wrap (only one-layer) was applied. Failure occurred at this side of the wrap. Figure 3-9a shows the failed wrap.

In Specimen III-W₁-2.2 the GC-Hybrid FRP laminate was sanded prior to the application. Beads with a diameter of 80mils (2mm) were used to obtain a constant adhesive thickness. The epoxy had cured sufficiently at the time of the test. This specimen experienced a failure at the interface between the steel and the epoxy, plus braking of the wrap (Failure Mode S+w). The wrap broke at both sides as indicated in Figure 3-9b.

In Specimen III-W₁-2.3 the GC-Hybrid FRP laminate was sanded prior to the application. Beads with a diameter of 80mils (2mm) were used to obtain a constant adhesive thickness. The epoxy had cured for more than a month. This specimen experienced a dual failure at the interface between the steel and the epoxy and the FRP and the epoxy. The wrap was intact and the failure mode was characterized as Failure Mode SF.

In Specimen III-W₁-2.4 the GC-Hybrid FRP laminate was sanded prior to the application. Beads with a diameter of 80mils (2mm) were used to obtain a constant adhesive thickness. The epoxy had cured for more than three months. This specimen experienced a failure at the interface between the FRP and the epoxy. Little transverse unzipping occurred in the wrap (see Figure 3-9c) and the failure mode was characterized as Failure Mode F+w.

Comparing Specimen III-W₁-2.1 and III-W₁-2.2 with Specimen III-W₁-2.3 and III-W₁-2.4 it may be concluded that the curing time has significant impact. In all specimens the epoxy was inflexible and brittle upon examination, but still the observed failure loads and peak strains differed greatly. It may therefore be concluded that in fact there is a decrease in failure load and peak strain for specimens with a longer curing period. Further tests have to be carried out to investigate this time dependency.

Comparing the specimens of this test series with the specimens of Test Series III that were prepared with the same materials, it may be concluded only a small increase in peak strain was obtained due to the wrap.

3.3.2.7. Test Series III-W₂

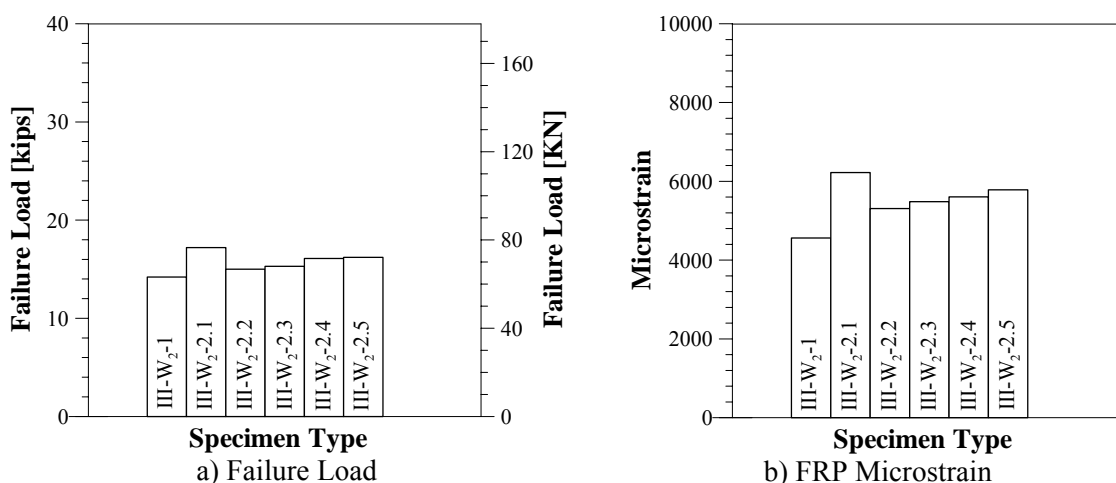
A total number of 6 specimens were tested in this test series. As described in Section 3.2 these specimens were fabricated with a bonded length of 9in (22.9cm) and two wraps, and as such they

were designated as Type III-W₂ (see Table 3.2). All specimens were prepared using the GC-Hybrid FRP laminate and the epoxy En-Force CFL.

A numerical and graphical description of the test data is presented in Table 3.11 and Figure 3-17, respectively.

Table 3.11 Test Results – Test Series III-W₂

Specimen	Specimen Type	Failure Load		Microstrain	Failure Mode
		kips	KN		
III-W ₂ -1	III-W ₂ -Hn 1-0b ⁺	14.2	63	4600	F
III-W ₂ -2.1	III-W ₂ -Hs 1-80 ⁺	17.2	78	6200	F
III-W ₂ -2.2	III-W ₂ -Hs 1-80 ⁺	15.0	67	5300	F
III-W ₂ -2.3	III-W ₂ -Hs 1-80 ⁺	15.3	68	5500	SF+w
III-W ₂ -2.4	III-W ₂ -Hs 1-80 ⁺	16.1	72	5600	F
III-W ₂ -2.5	III-W ₂ -Hs 1-80 ⁺	16.2	72	5800	F

**Figure 3-17 Test Results – Test Series III-W₂**

As indicated in Table 3.11, in Specimen III-W₂-1 the GC-Hybrid FRP laminate was not sanded prior to the application. No beads were used to obtain a constant adhesive thickness. The epoxy had cured sufficiently at the time of the test. This specimen experienced a failure at the interface between the FRP and the epoxy, and the failure mode is therefore characterized as Failure Mode F (see Figure 3-8c).

In Specimen III-W₂-2.1, III-W₂-2.2, III-W₂-2.4 and III-W₂-2.5 the GC-Hybrid FRP laminate was sanded prior to the application. Beads with a diameter of 80mils (2mm) were used to obtain a constant adhesive thickness. The epoxy had cured sufficiently, in the case of Specimen III-W₂-2.4 and III-W₂-2.5 for than 3 months. All specimens experienced a failure at the interface between the FRP and the epoxy, characterized as Failure Mode F (see Figure 3-8c).

In Specimen III-W₂-2.3 the GC-Hybrid FRP laminate was sanded prior to the application. Beads with a diameter of 80mils (2mm) were used to obtain a constant adhesive thickness. The epoxy

had cured sufficiently. This specimen experienced dual failure at the interfaces between the FRP and the epoxy and between the steel and the epoxy (see Figure 3-7c). Additionally, transverse unzipping of the first wrap occurred (see Figure 3-9c). The failure mode was characterized as Failure Mode SF+w.

Comparing all Specimens III-W₂-2.1 to III-W₂-2.5, it may be concluded that failure load and peak strains and the observed failure mode are not interdependent.

Comparing the specimens of this test series with the specimens of Test Series III and III-W₂ that were prepared with the same materials, it may be concluded that no increase in failure load and peak strains was obtain by applying to wraps. In fact, the recorded loads and strains were lower than in the other test series. More tests will have to be carried out to investigate if a bond enhancement with wraps is possible.

3.3.2.8. Test Series Continuous Specimens

A total number of 2 specimens were tested in this test series. As described in Section 3.2 these specimens were prepared with sanded GC-Hybrid FRP laminates and the epoxy En-Force CFL. Glass beads with a diameter of 80mils (2mm) were used to control the adhesive thickness. The laminate was applied only to one side of the steel. A numerical description of the test data is presented in Table 3.12.

Table 3.12 Test Results – Continuous Specimens

Specimen	Specimen Type	Failure Load		Microstrain	Failure Mode
		kips	KN		
C-1	C52 Hs 1-80 ⁺ -1	33.6	149	7400	S
C-2	C52 Hs 1-80 ⁺ -2	40.9	182	3300	S

Specimen C-1 failed in the interface between the steel and the epoxy (see Figure 3-18a), although some epoxy pieces came loose from the FRP. The failure mode was characterized as Failure Mode S. After debonding of the FRP laminate, the steel yielded in its narrowed midsection and experienced an elongation of 1in (2.5cm). It was decided to retest this specimen, as else wise the steel plate was still intact.

Specimen C-2 was the retested Specimen 1. Again, the specimen failed at the interface between the steel and the epoxy (see Figure 3-18a). The failure mode was characterized as Failure Mode S. After debonding of the FRP laminate, the steel yielded in its narrowed midsection and fractured.

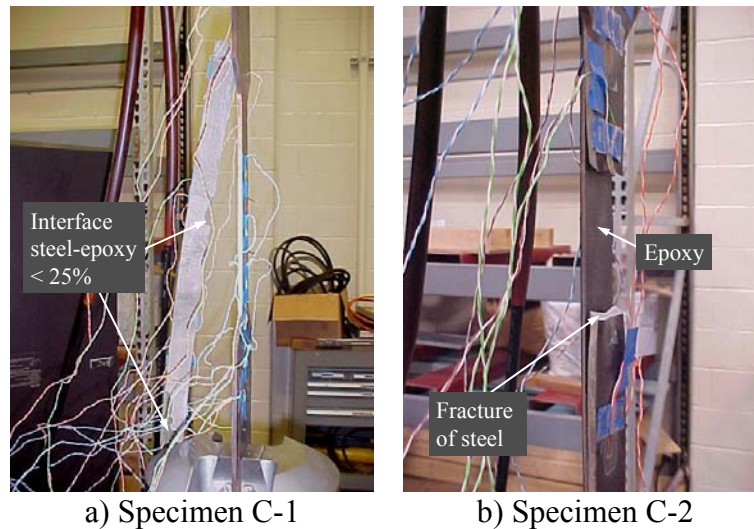


Figure 3-18 Failure of Continuous Specimen

Comparing the test results for the continuous and discontinuous specimens it was found that the same failure mode was observed for all tested specimens. The failure always occurred in the interface between the steel and the adhesive and/or the FRP and the adhesive.

3.3.3. LOAD-STRAIN RESPONSE

The data collected from the strain gages applied to the specimens was used to develop strain profiles. Hereby, the strain was plotted versus the distance of the strain gage to the discontinuity. Curves for different load levels were plotted to illustrate the strain redistribution for increasing load levels.

3.3.3.1. Test Series I

The strain profiles, for the six specimens tested, are displayed in Figure 3-19. It is noticeable that high strains occurred at the discontinuity. In contrast, at a bonded length of 2in (5.1cm) low strains compared to strains at the discontinuity were recorded, which shows a small redistribution of the load over the overall bonded length. However, at this location the strain reached values near 1000 microstrain indicating that minimum force transfer occurred beyond this point.

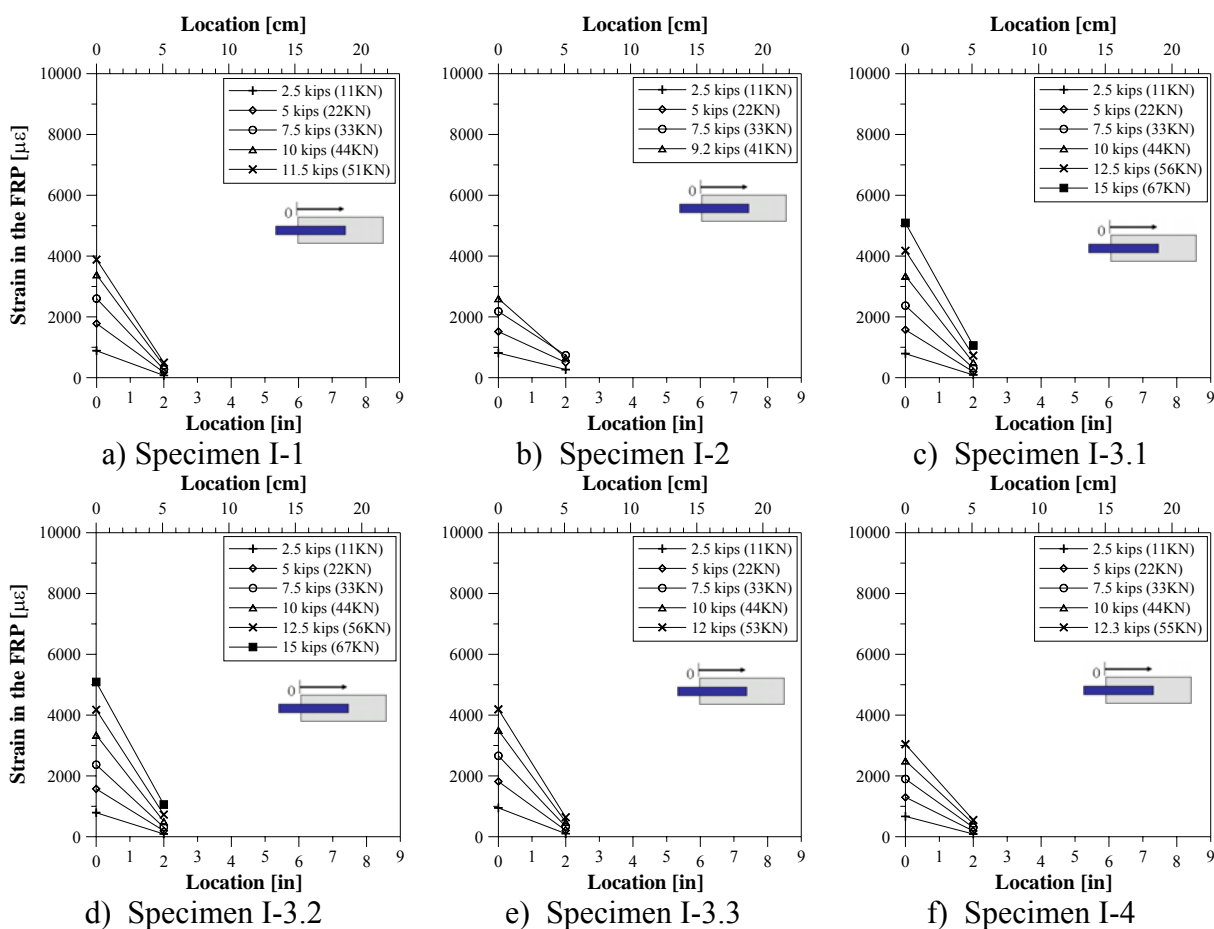


Figure 3-19 Strain Profiles – Test Series I

It is further noticeable, that for the CFRP 200/2000 laminate reinforced specimen lower strains were recorded at the same load level as for specimens reinforced with the GC-Hybrid FRP laminates, which is due to the higher E-Modulus of the CFRP laminates.

3.3.3.2. Test Series II

The strain profiles, for the five specimens tested, are displayed in Figure 3-20. Once again it is clear that significantly higher stresses were recorded at the discontinuity than at the other locations. It can further be seen that at 5in (12.7cm) bonded length almost no strain could be recorded in the FRP laminates. Again for the CFRP 200/2000 laminate reinforced specimen lower strains were recorded at the same load level as for specimens reinforced with the GC-Hybrid FRP laminates.

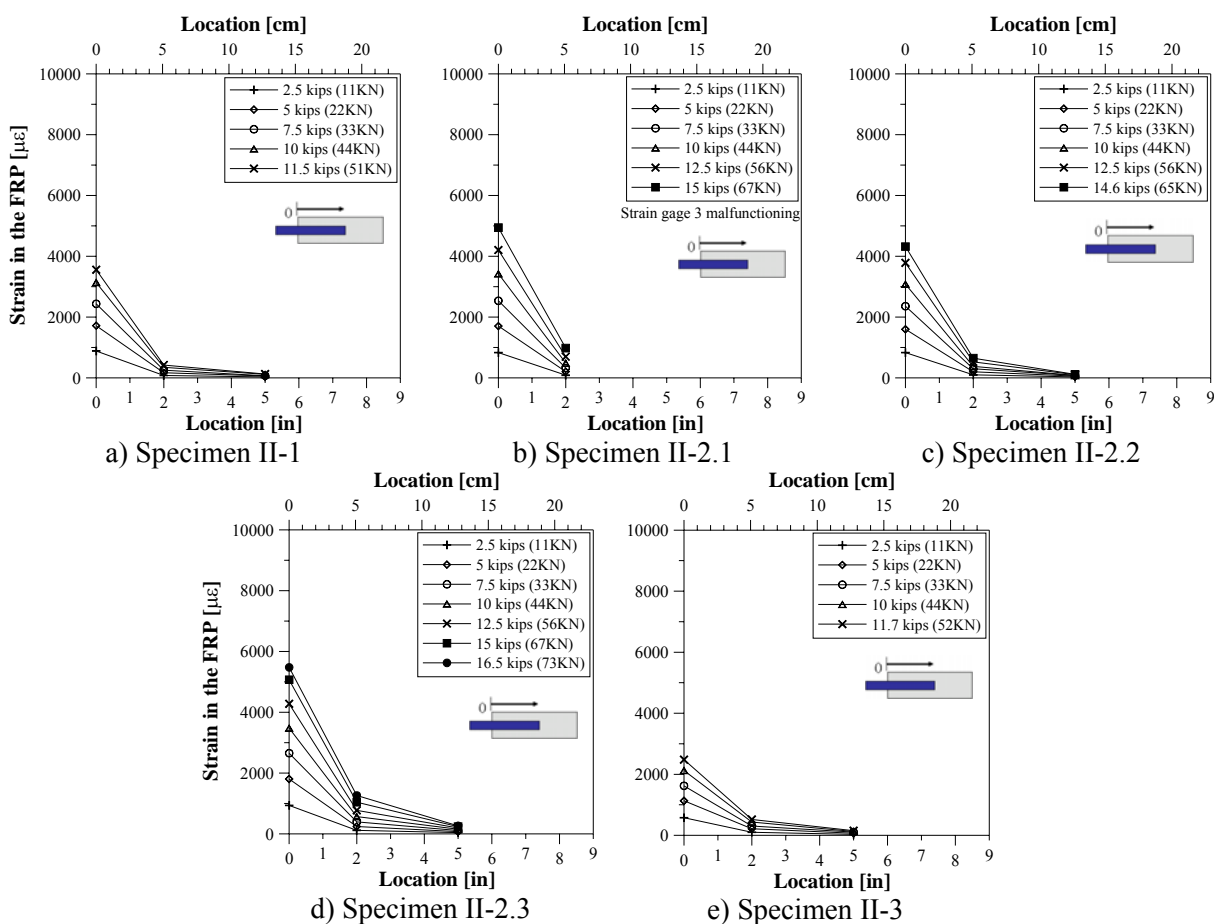


Figure 3-20 Strain Profiles – Test Series II

Comparing the strain profiles for Test Series I and II it can be concluded that the bonded length does not affect the strain distribution over a certain distance, as the curves for both bonded lengths are similar. However, due to the increased bonded length additional stresses were transferred as indicated in the strain profiles beyond 3in (7.6cm), and by higher recorded loads.

3.3.3.3. Test Series III

In this test series 26 specimens were tested, examining the influence of the use of different FRP and adhesive types, and adhesive line thickness.

Figure 3-21a to Figure 3-21g indicate the strain profiles for GC-Hybrid / En-Force CFL reinforced specimens. It becomes apparent that two different strain distributions along the laminate occurred, depending upon the response of the adhesive used.

In Specimen III-2, III-3 and III-4.1 the strain decreased almost consistently over the bonded length. Specimen III-3 was characterized previously as insufficiently cured, and is therefore not further discussed. Although, in Specimen III-2 and III-4.1 the adhesive was cured, the plots for these specimens are similar to Specimen III-3. However, higher strains at the same load level and a higher failure load were recorded. For these two specimens special attention is turned to the graphs at loads close to specimen failure. It is noticeable that a significant increase in strain towards the center of the bonded length occurred at this load stage.

The second type of strain distribution agrees with the responses observed for all specimens in Test Series I and II and was observed for Specimen III-1, III-4.2 and III-4.3, as well as III-5. It is characterized by high strains at the discontinuity and a rapid strain decrease over the first 2in of the bonded length.

Comparing test results for Specimen III-1 to III-4.3 it is clear that with increasing curing time a lower redistribution of the strains over the bonded length takes place, which is shown by the drop in strain towards the end of the laminate.

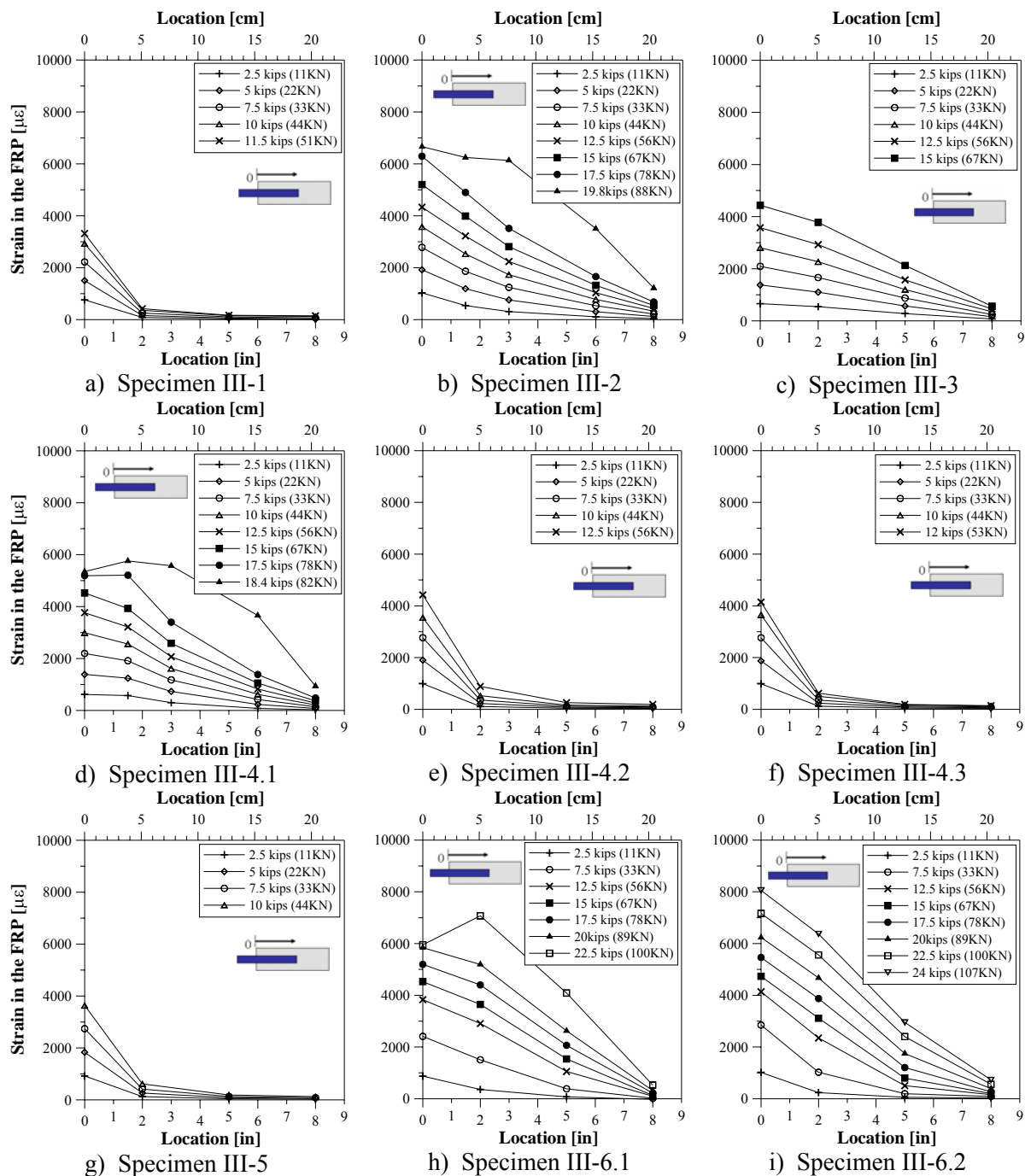


Figure 3-21 Strain Profiles – Specimen III-1 to III-6

Figure 3-21h and Figure 3-21i indicate the graphs for the GC-Hybrid FRP / Tyfo[®] MB reinforced specimens. Once again an almost consistent decrease in strain occurred away from the discontinuity. The graphs corresponding to lower loads are almost parallel indicating that the bond stress transfer is constant. However, in Specimen III-6.1 close to failure a significant increase in strain towards the center of the bonded length occurred. Overall, it may be concluded that the epoxy Tyfo[®] MB results in stress transfer along the laminate very different from the Enforce CFL.

Figure 3-22 and Figure 3-23 illustrate the strain profiles for CFRP 200/2000 reinforced specimens. For these specimens overall four different adhesives were used, as indicated in Section 3.3.2.4.

In the case of Specimen III-7 (see Figure 3-22) the laminate was adhered by the means of Enforce CFL. The strain-location curve agrees well with the response for Specimen I-4 and I-3. A significant drop in strain occurred within the first 2in (5.1cm) of the bonded length indicating a rather brittle adhesive.

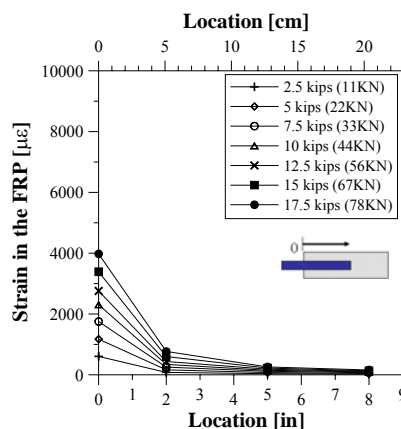


Figure 3-22 Strain Profile– Specimen III-7

For the fabrication of Specimens III-8 (Figure 3-23a to c) the epoxy Sikadur[®] 30 was used. Again a significant drop in strain within the first 2in of the bonded length occurred. The graph for Specimen III-8.2 at a load level of 11.4kips (51KN) already show a slight increase in strain at the location 2in (5.1cm) indicating an increase of the bond stresses which typically happens close to failure.

Figure 3-23d to f illustrate the strain profiles for Specimen III-9.1 to III-9.3, which were fabricated with the epoxy Sikadur[®] 31. Figure 3-23g to i illustrate the strain profiles for Specimen III-10.1 to III-10.3 prepared with S&P resin 220. The curves for these specimens are very similar and resemble those for the Specimens III-8 at lower load levels.

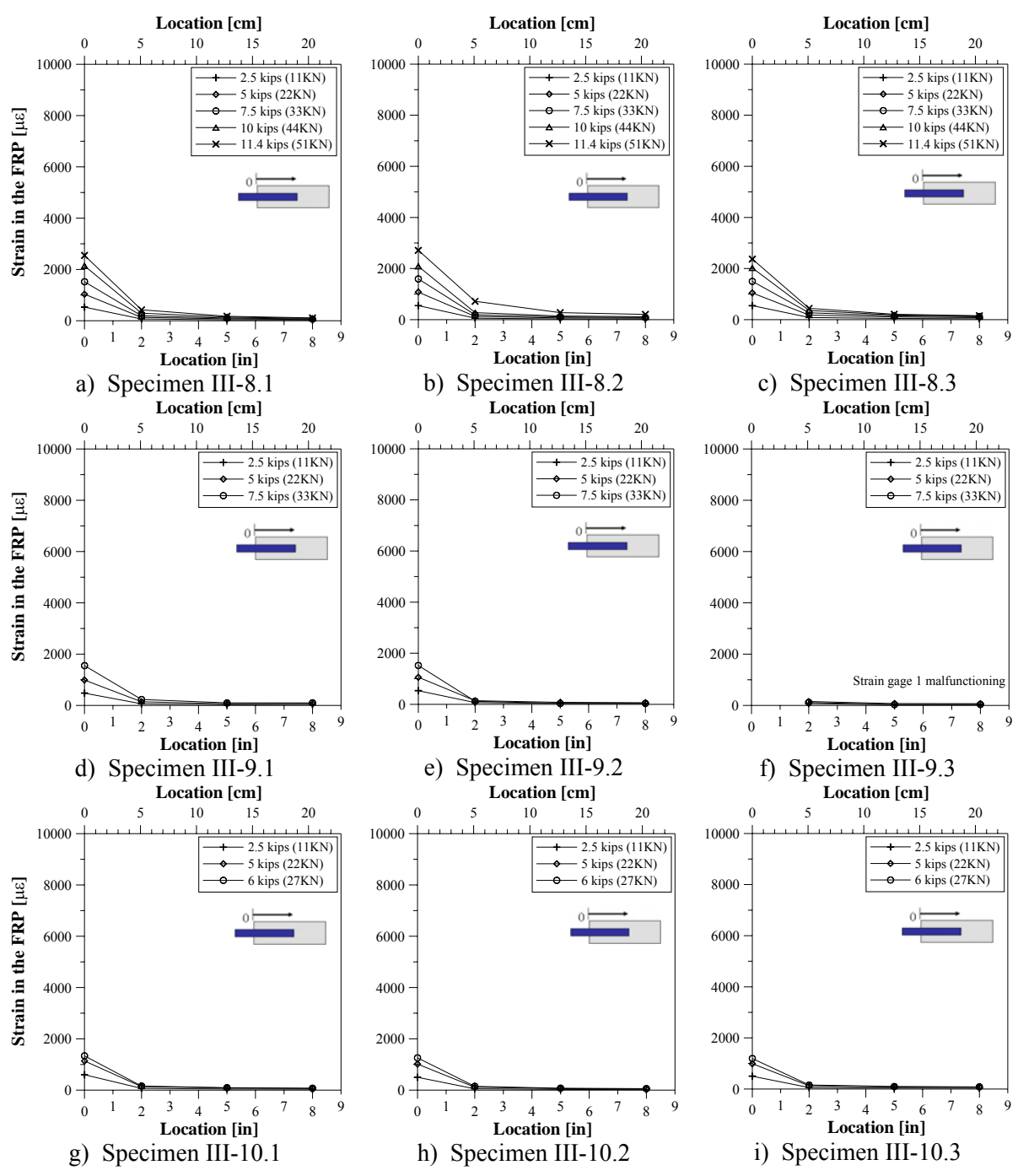


Figure 3-23 Strain Profiles – Specimen III-8 to III-10

The next five specimens, illustrated in Figure 3-24, were fabricated using the adhesive Tyfo[®] MB and the laminate Tyfo[®] UC. Specimen III-11 had an adhesive line thickness of 10mils (0.25mm). Specimen III-12 had an adhesive line thickness of 80mils (2mm). It is noticeable that the strain profiles are almost linear with the maximum strain at the discontinuity. However, close to failure an unproportional increase in strain occurred towards the center of the bonded length (see Figure 3-24a, c and e). In conclusion, the difference in adhesive thickness did not affect the strain value for a certain load; but, for a thicker bond line higher strains and loads were obtained.

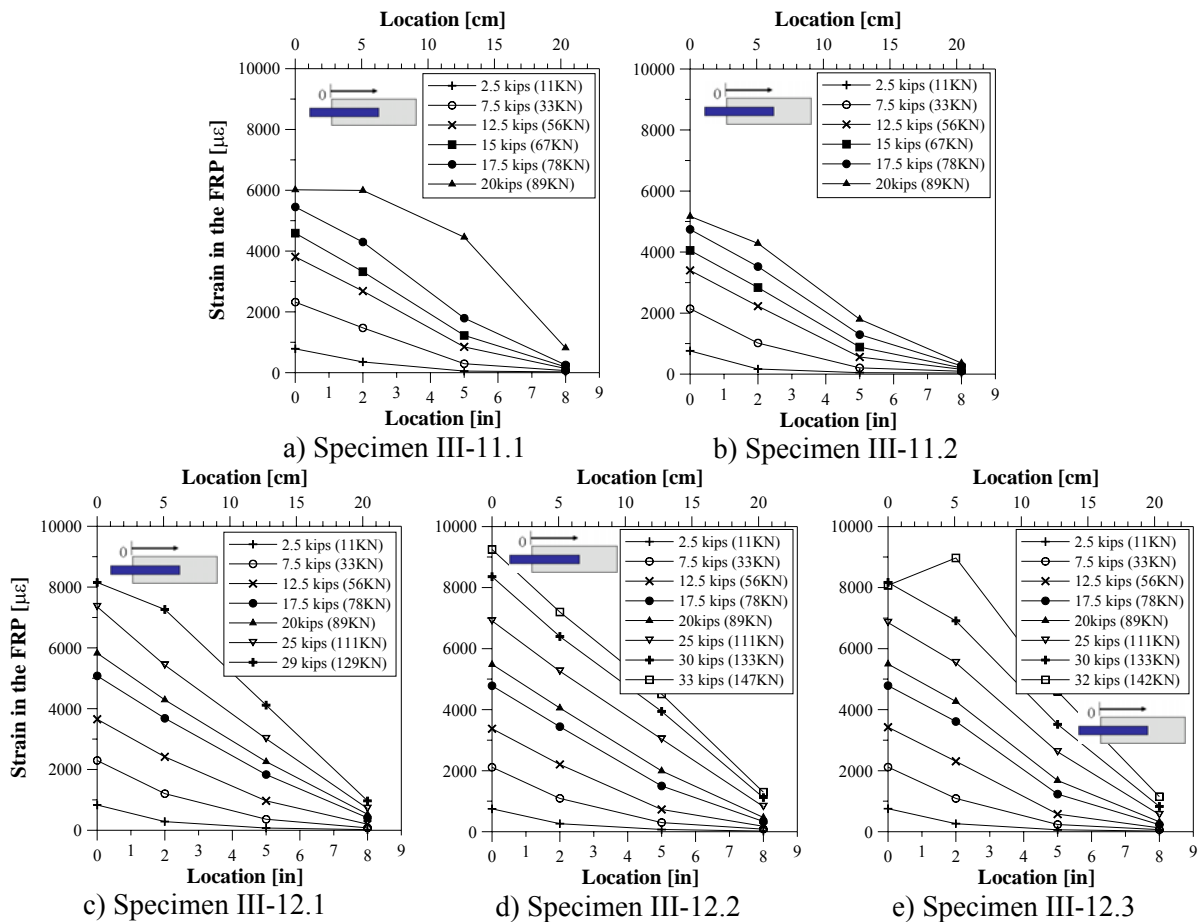


Figure 3-24 Strain Profiles – Specimen III-11 to III-12

Lastly, in Figure 3-25 the strain profiles for specimens fabricated with CFRP Sika CarboDur[®] S1012 and the epoxy Sikadur[®] 30 are indicated. The graph in Figure 3-25b indicates once again brittle adhesive behavior, as a significant drop in strain occurred within the first 2in of the bonded length. However, the graph in Figure 3-25a shows almost linear strain profiles. As only low load and strain levels were reached, and only two specimens were tested no final conclusion may be drawn for this material combination.

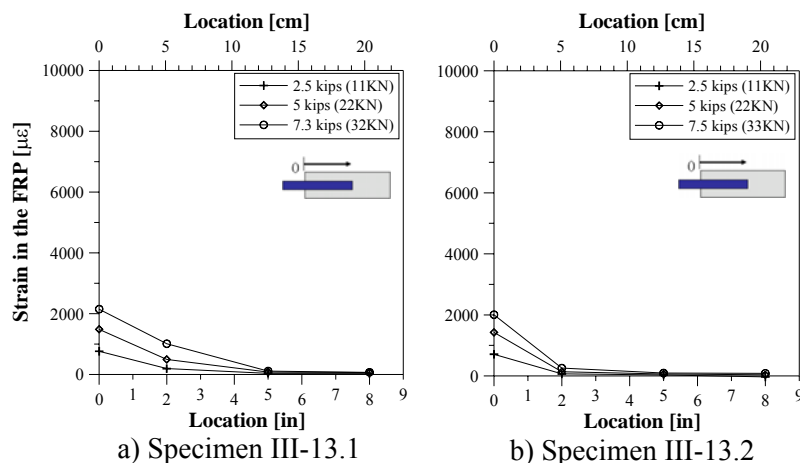


Figure 3-25 Strain Profiles – Tests III-13

Ultimately, the adhesive Tyfo[®] MB distributes the load over a longer bonded length than the other adhesives. Therefore, higher strains and loads were recorded for all specimens prepared with this adhesive. Overall, the adhesive type has considerable influence on the specimen performance, although for the brittle adhesives almost the same strain profiles were obtained. The stiffness of the laminate, however, greatly affects the overall strain behavior, where higher modulus laminates resulted in lower strains at equivalent load levels.

3.3.3.4. Test Series III_T – Time Dependency

All specimens in this section were prepared with the epoxy En-Force CFL. In the following the strain profiles (Figure 3-26) for 9 specimens of age 4 to 30 days are indicated and discussed.

It is noticeable that for an age of up to 9 days the curves are almost linear. However, the curves for less cured specimens tend to be slightly curved upwards (convex progression), whereas specimens of 7 days and older show concave plots. With increasing age the concavity increases also until, for fully cured specimens, at a location of 2in (5.1cm) significantly less strains occur than at the discontinuity. It may therefore be stated that the curves for the 21 day old specimen (Figure 3-26h) are exceptional, and may not be considered to describe the overall strength development of the epoxy. However, as for each curing period only one specimen was tested, at this point no final conclusion is drawn regarding the influence of the curing time.

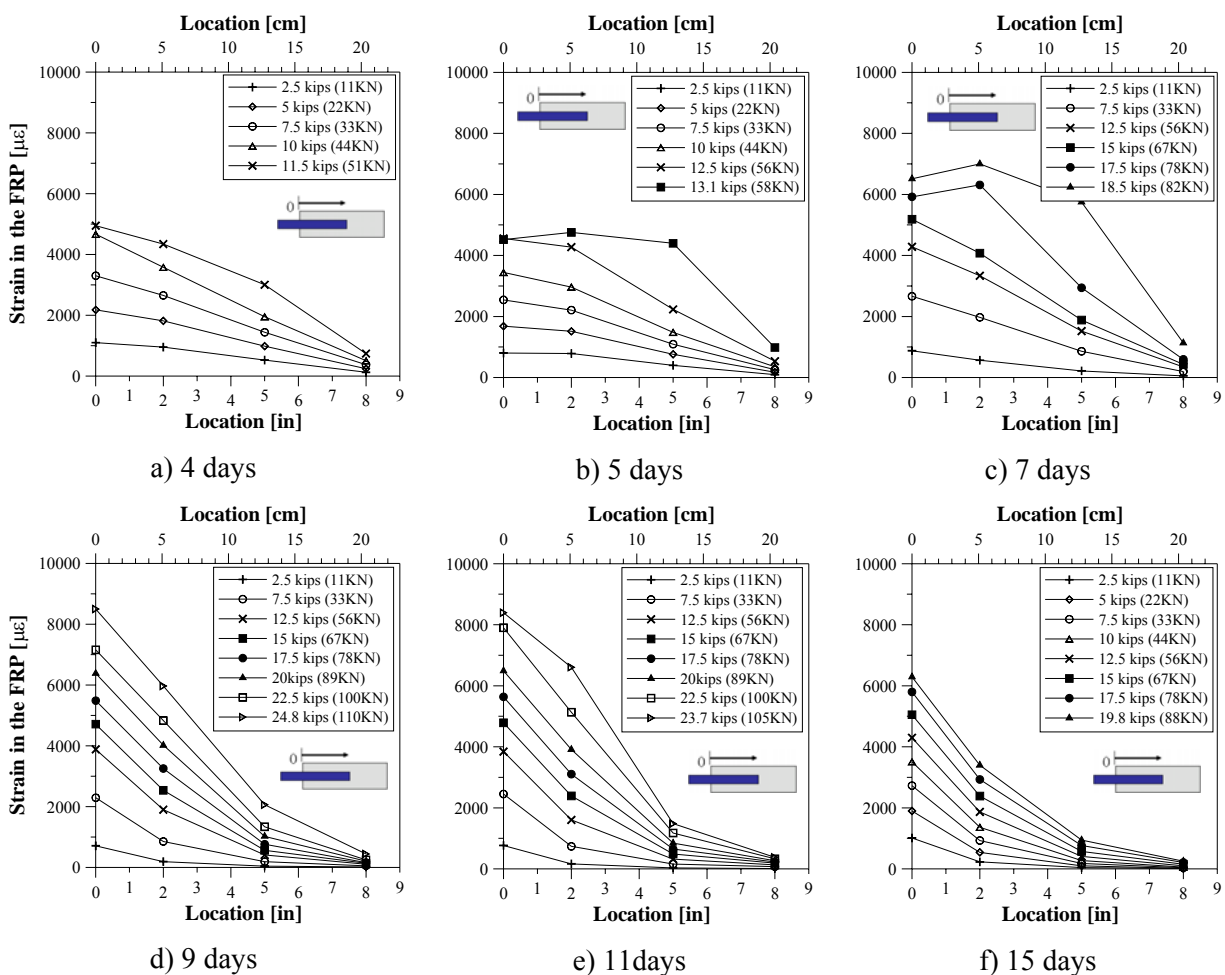


Figure 3-26 Strain Profiles – Test Series III_T

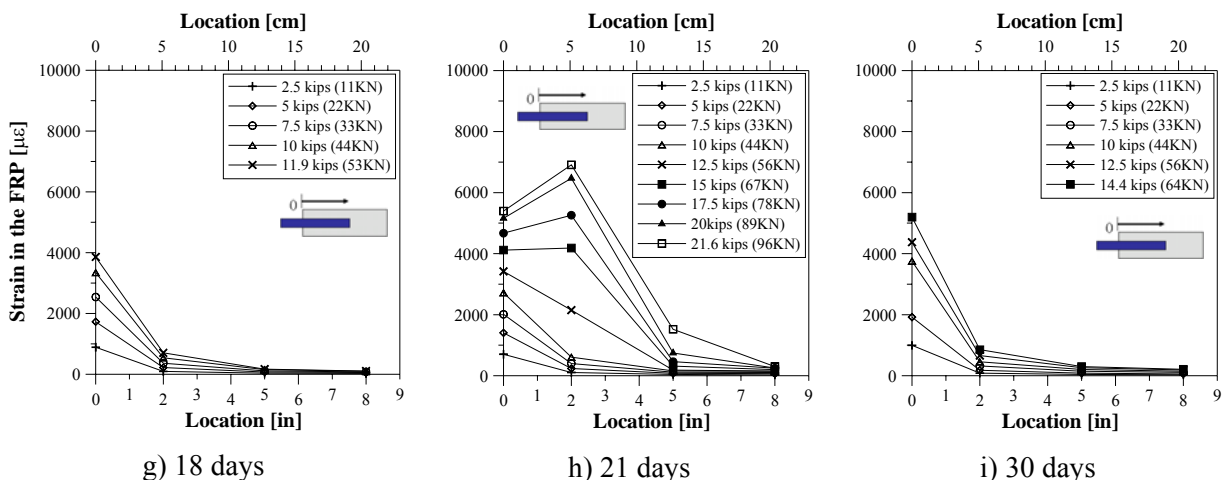


Figure 3-26 Strain Profiles – Test Series III_T (Cont.)

3.3.3.5. Test Series III-W₁

Five specimens with one wrap, applied at 1in (2.5cm) of the bonded length, have been tested. The strain profiles are presented in Figure 3-27. Specimen III-W₁-2.1 and III-W₁-2.2 resulted in curves for a more plastic adhesive with a good strain distribution over the bonded length. Curves for Specimen III-W₁-1, III-W₁-2.3 and III-W₁-2.4 are characterized by a significant drop in strain within the first 2in (5.1cm) bonded length. Comparing the curves with the curves presented in the previous sections it may be concluded that the wraps do not improve the overall specimen performance, as the strain profiles for certain loads are similar. However, as the adhesive resulted inconsistent curves, more tests would have to be conducted to finalize a conclusion.

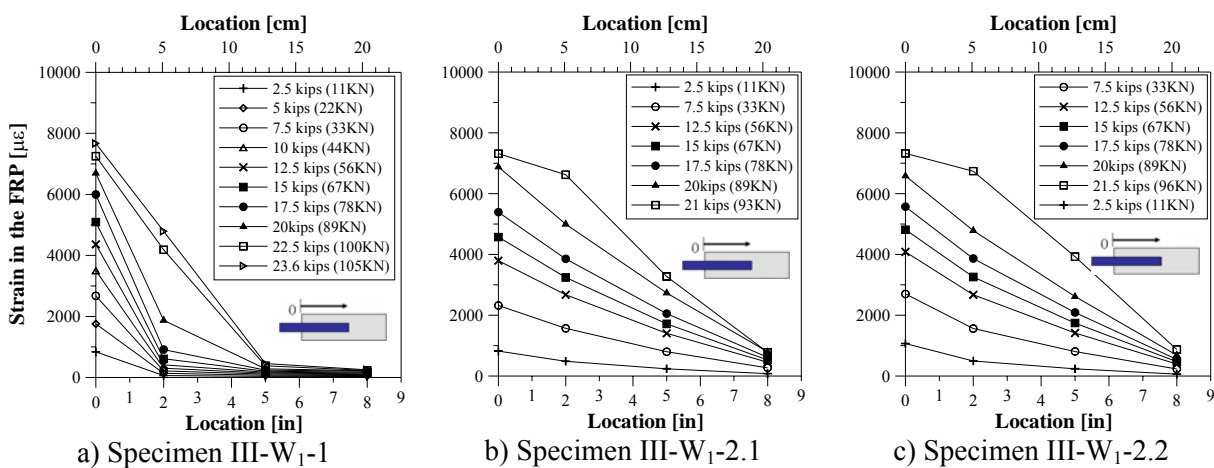


Figure 3-27 Strain Profiles – Test Series III-W₁

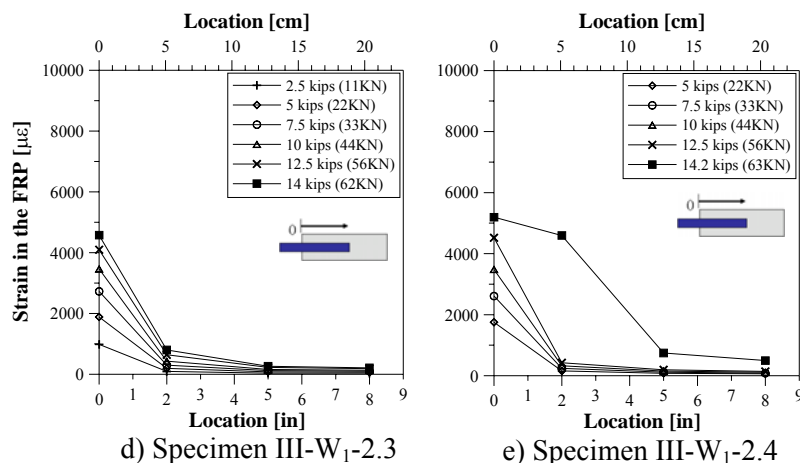


Figure 3-27 Strain Profiles – Test Series III-W₁ (Continuation)

3.3.3.6. Test Series III-W₂

Six specimens with two wraps, applied at 1in (2.5cm) and 3.5in (8.9cm) were tested. The strain profiles are presented in Figure 3-28. Specimen III-W₂-2.1 resulted in curves for a more plastic adhesive with a good strain distribution over the bonded length. The curves for all other specimens indicate brittle adhesive behavior, characterized by a significant drop in strain within the first 2in (5.1cm) bonded length. Comparing the curves with the curves presented in the previous sections it may be concluded that the wraps do not improve the overall specimen performance, as the strain profiles for certain loads are similar. As the adhesive resulted inconsistent curves, more tests would have to be conducted to finalize a conclusion.

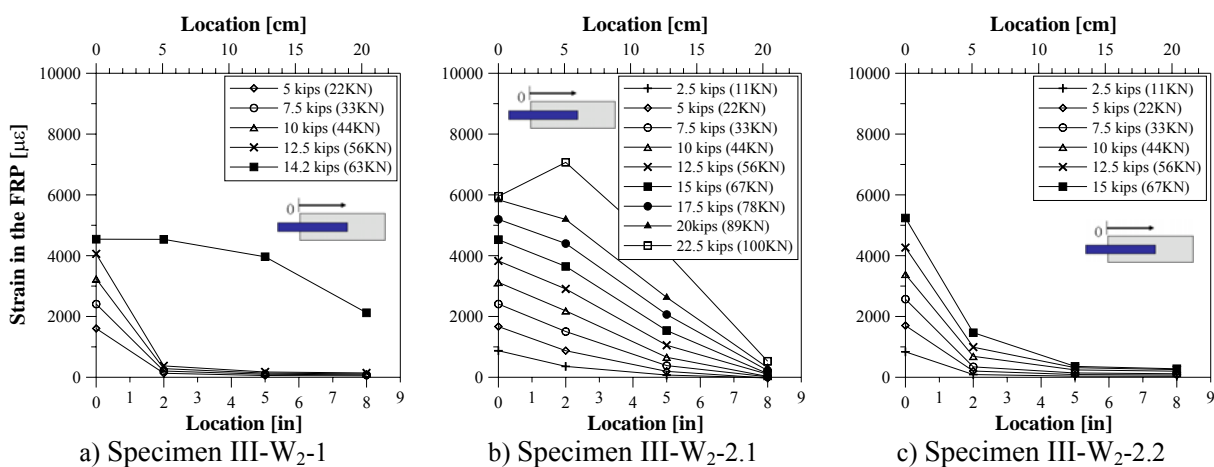


Figure 3-28 Strain Profiles – Test Series III-W₂

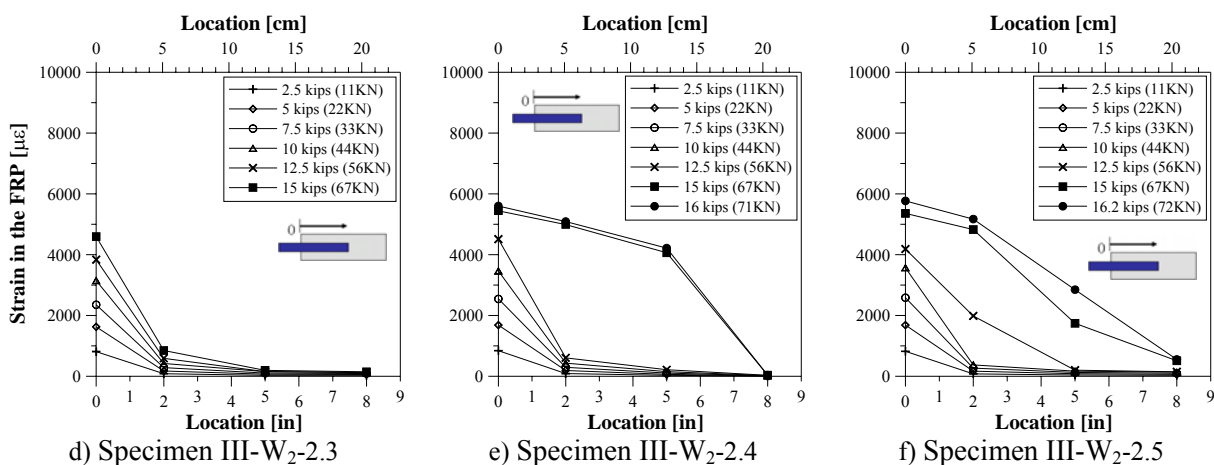


Figure 3-28 Strain Profiles – Test Series III-W₂ (Continuation)

3.3.3.7. Test Series Continuous Specimen

These specimens were, as described in Section 3.3.2.8, reinforced with GC-Hybrid FRP laminates and the epoxy En-Force CFL. Both Specimens failed by debonding of the FRP. It is noticeable that up to a load level of 25kips (111KN) the strain profiles for both specimens are almost identical (see Figure 3-29 and Figure 3-30). For increased loads though the curves differ greatly (incomplete sentence). In Specimen C-1 a sudden increase in FRP strain occurred over the bonded length as well as an abrupt strain increase in the narrow steel part. In Specimen C-2 the steel curves do not experience any abrupt changes due to increased loads.

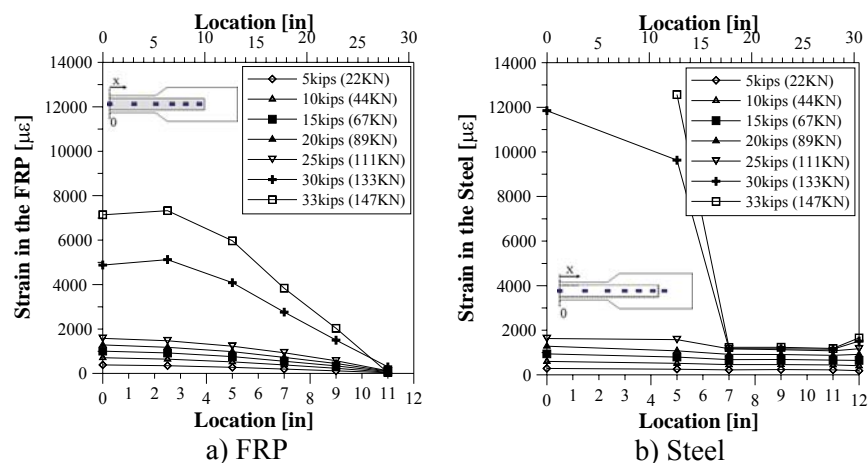


Figure 3-29 Strain Profiles – Specimen C-1

This was to be expected as during the first test the steel was in the range of plastic deformation and therefore the yield strength for Specimen C-2 was higher than for Specimen C-1. In the FRP

an increase in strain of $1000\mu\epsilon$ occurred at the end of the laminate and at the narrow part of the specimen. But overall, the debonding strain for the Specimen C-2 was much lower than for Specimen C-1.

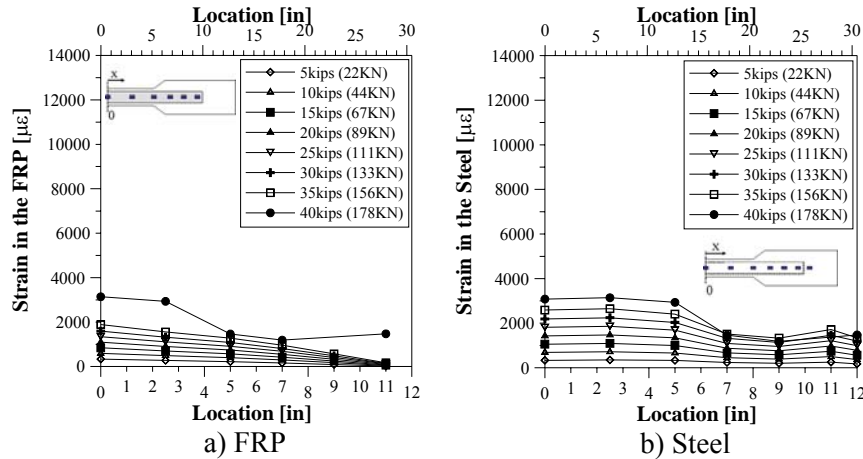


Figure 3-30 Strain Profiles – Specimen C-2

3.4. DISCUSSION OF RESULTS

In this section the two different strain responses will be discussed with regard to bond stress distribution and a simplified design approach is presented. Further, where applicable, the agreement of an analytical model is shown. Throughout this section, the average bond stress between two locations was calculated using the following expression:

$$\mu = t_{frp} E_{frp} \frac{\Delta\epsilon}{\Delta x} \quad \text{Eq. 3.1}$$

Where μ is the bond stress, t_{frp} the FRP thickness, E_{frp} the E-Modulus of the FRP, $\Delta\epsilon$ the strain difference between two gage locations, and Δx the distance between two strain gages.

Although all specimens failed by debonding, two very different strain distributions were observed (see Figure 3-31). One was characterized as brittle because the strain values dropped significantly within the first 2in (5.1cm) (see Figure 3-31a). The other distribution was characterized as ductile because it led to a load transfer over the bonded length (see Figure 3-31b).

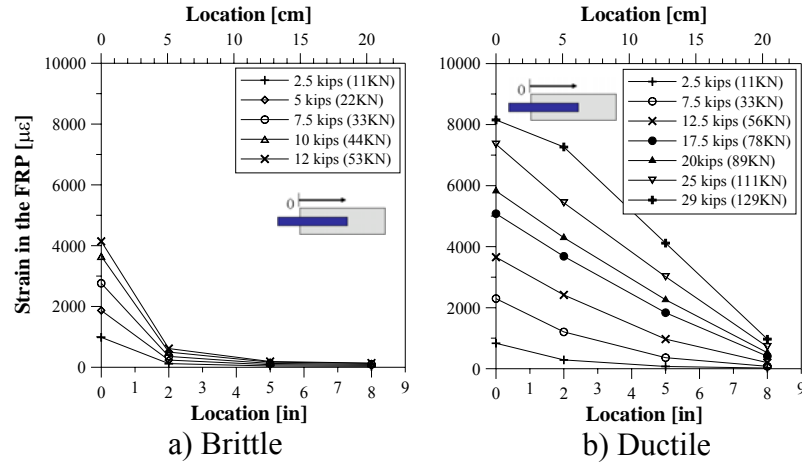


Figure 3-31 Typical Strain Profiles

3.4.1. BRITTLE STRAIN RESPONSE

This response was observed for specimens fabricated with CFRP laminates 200/2000 and the adhesives En-Force CFL, Sikadur 30 and 31 and S&P Resin 220. It was characterized by high peak strains at the discontinuity and comparably low strains at the other strain gage locations.

In Figure 3-32 the experimental bond stresses at a load level of 6 kips (27KN) are plotted together with the curves obtained with the analytical model from Volkersen, which was presented in Section 2.1. It is clear that the experimental average bond stresses do not differ significantly for the various adhesives, but the analytical curves indicate a significant difference in the peak stress values. However, according to the model the development length is expected to be 3 to 5in (7.6 to 12.7cm). The trend is that adhesives with a higher E-Modulus result in higher peak stresses and a shorter effective development length (see curves for Sikadur[®] 30 and S&P Resin 220).

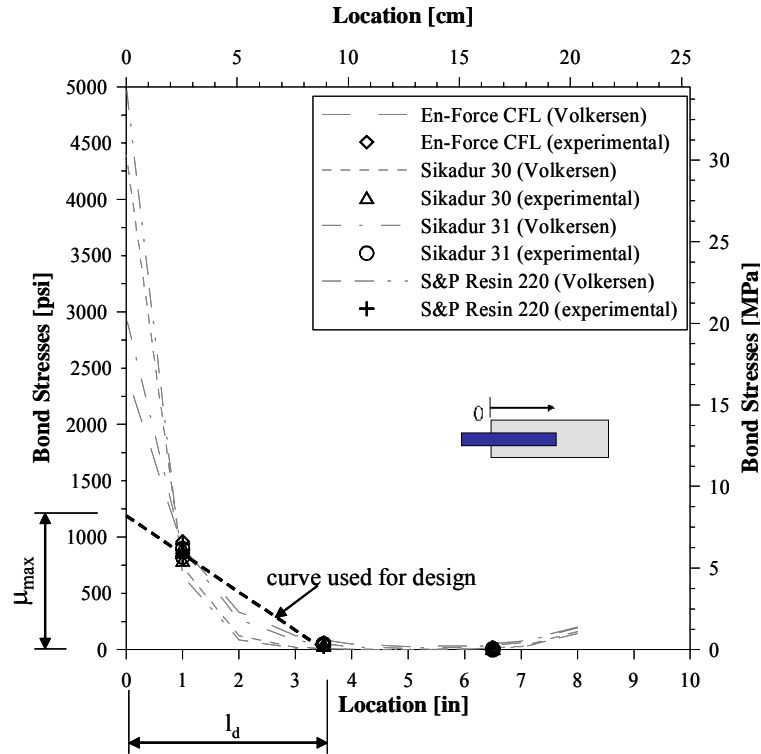


Figure 3-32 Bond Stresses – Brittle Response

Overall, the analytical model shows very good agreement with the experimental data. The placement of the strain gages on the test specimens did not give clarity about the validity of the model for the peak stresses at the discontinuity, however the following may be concluded: (1) the effective development length for all specimens was rather short and the load was mainly transferred within the first 3 to 5in (7.6 to 12.7cm), and (2) high peak stresses occurred at the discontinuity and a rapid drop of the stresses occurred thereafter. Future design should be based on an allowable stress/strain approach. A simplified approach is:

$$f_{frp} = \alpha \cdot \mu_{max} \frac{l_d}{t_{frp}} \quad \text{Eq. 3.2}$$

For adhesives that result in this behavior, where f_{frp} is the limit stress of the FRP, μ_{max} is the debonding stress, α is a factor of safety, l_d is effective development length, and t_{frp} is the FRP thickness. Although, at present, a factor of safety of 1.0 is considered to be appropriate, future

research will have to adjust this value. Also, further investigation is necessary to validate Eq. 3.2 and the analytical model discussed in this section.

3.4.2. DUCTILE STRAIN RESPONSE

This strain response was observed for specimens prepared with Tyfo MB. It was characterized as ductile, as a load transfer over the bonded length took place. Specimens exhibiting this strain distribution failed at much higher load levels, than the brittle specimens.

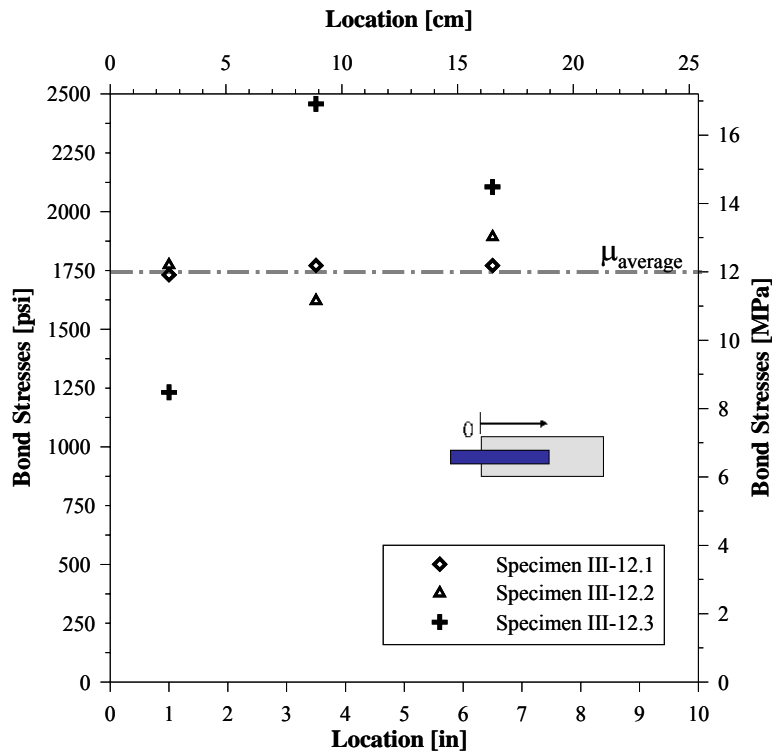


Figure 3-33 Bond Stresses – Ductile Response

Figure 3-33 indicates the maximum bond stresses developed during the loading process for specimens fabricated with the epoxy Tyfo MB and CFRP laminate Tyfo UC. It is noticeable that for Specimen III-12.1 and III-12.2 the bond stress distribution was similar. However, Specimen III-12.3 exhibited a different bond stress behavior, and shall not be further considered, assuming that the other two specimens were typical for this material combination. Evaluating Figure 3-33 it may be concluded that the specimens failed after an average bond stress was achieved along the bonded length. This bond stress is referred to as the average bond stress $\mu_{average}$, and it is

used in the following expression to determine the bonded length l_b to attain rupture of the FRP laminate:

$$l_b = \alpha \cdot t_{frp} \frac{f_{u,frp}}{\mu_{average}} \quad \text{Eq. 3.3}$$

where α is a factor of safety, t_{frp} is the FRP thickness, and $f_{u,frp}$ is the ultimate FRP strength. For steel reinforced with epoxy Tyfo MB and CFRP laminate Tyfo UC, an adhesive line thickness of 80mils (2mm), the average bond stresses in pure tension are 1.75ksi (12MPa) (see Figure 3-33). The FRP laminate used had a thickness of 75mils (1.9mm) and an ultimate strength of 405ksi (2.79GPa) as indicated in Table 3.3. According to Eq. 3.3 a development length of 17.4in (44cm) was computed. However, using adhesives resulting in a ductile strain response, additional aspects will have to be considered. Higher strain levels in the steel, due to higher FRP strains may cause cracking. Fatigue cracks may also develop, and will have to be considered. Additionally, an increase in strain in the bottom flange will lead to an increase of the compression strain in the top flange of structural members and buckling may become an issue. Further research will have to be carried out addressing the above named considerations, validate Eq. 3.3, and factor of safety α to impede formation of buckling zones.

3.5. SUMMARY AND CONCLUSIONS

3.5.1. SUMMARY

While rehabilitation/retrofit of reinforced concrete structures has been extensively researched, and accepted codes of practice are nowadays available (ACI 440.2R-02, 2002), only a limited amount of research has been conducted on the rehabilitation/retrofit of steel structures and in particular steel bridges. The need to upgrade steel bridges stems from the fact that more than thirty percent of the bridges in the U.S. are steel bridges, and more than forty percent of those bridges are considered either structurally deficient or functionally obsolete.

Since conventional strengthening methods present some disadvantages such as: (1) the procedure is labor intensive and time consuming, (2) it requires drilling or extensive lap splicing, (3) traffic must be closed for a longer period of time, (4) there is the potential for weld fatigue cracking at the cover plate ends, and (5) the increased weight of the structures may lead to difficulties in the

member capacity and increases deflection. A innovative strengthening scheme is proposed in this research program which offers the following advantages: (1) the installation of FRP laminates is rather easy and simple to implement in the field, (2) traffic disruptions are minimal, (3) it is durable (Ammar, 1996), (4) a full recovery of the stiffness and the load capacity of the initial steel member may be attained, without significant weight increase (Ammar, 1996). These advantages have been more than demonstrated for the application of FRP composites to reinforced concrete structures.

However, a direct application of this technology for reinforced concrete structures may not be immediately feasible for steel members, and more research is needed to investigate this steel strengthening method. Therefore, in this project some areas were researched that were considered vital in the application of FRP composites to steel structures, such as:

- Specimen type
- Bonded length
- Wrapping of specimens with CFRP sheets for adhesion enhancement
- FRP laminate type
- Adhesive type
- Adhesive thickness
- Surface preparation
- Curing time.

Results from this research program were presented in the previous sections, and the research conclusions along with recommendations for future research are presented in the next sections.

3.5.2. CONCLUSIONS

A total of 56 specimens were tested in this research program. The considered bond influencing factors were as follows:

- Specimen type
- Bonded length
- Wrapping of specimens with CFRP sheets for adhesion enhancement
- FRP laminate type
- Adhesive type
- Adhesive thickness
- Surface preparation
- Curing time.

3.5.2.1. Specimen Type

In this research program, discontinuous and continuous specimens were upgraded with FRP laminates. The discontinuous specimens were fabricated with two longitudinal steel plates separated by a gap of 1in (2.5cm) (see Figure 3-1). These specimens were considered as the worst-case scenario because they can be thought of as a steel member with completely corroded parts of the cross section. As such, stress concentrations were introduced in the region of the gap. In order to evaluate the impact of these stress concentrations on the bond strength and the development length of the FRP laminate, also specimens were investigated without this gap. These specimens were designated as continuous and are discussed in Section 3.1.2.1 (see Figure 3-2). Comparing the test results, presented in Section 3.3.2 and 3.3.3, it was concluded that the bond strength remained unaffected by the introduced stress concentrations. In addition, the same failure mode was observed for all tested specimens. The failure always occurred in the interface between the steel and the adhesive and/or the FRP and the adhesive. Because the discontinuous specimens are less expensive and can be retested more often than continuous specimens, it was decided to concentrate testing this specimen type.

3.5.2.2. Bonded Length

Results obtained by other researchers investigating the application of FRP composites to reinforced concrete structures indicate that the bonded length does not affect the bond strength, but the failure load and peak strains. In order to validate these research results for the application to steel, three different bonded lengths were examined: 3, 6 and 9in (7.6, 15.2, 22.9cm). The specimens were designated for reference as Type I, II and III, respectively. The test results indicated that an increase in bonded length merely affected the failure load and maximum FRP strains. However, the bond stresses remained unaffected.

3.5.2.3. Wrapping the Specimens

All wrapped specimens were prepared using the epoxy En-Force CFL and the GC-Hybrid FRP laminates. Due to the impracticality of wrapping specimens with 3 and 6in (7.6 and 15.2cm) bonded lengths, the bonded length for all specimens was 9in (22.9cm). The wraps consisted each of two 1in (2.5cm) wide CFRP sheet strips. They were discontinuous, as in case of the strengthening of an I- or W-section a continuous wrap will not be possible because of the presence of the web. Since the goal of this research program was to study the application of FRP composites to upgrade I-and W-sections, it was necessary to study the performance of discontinuous wraps.

Although, only a small number of wrapped specimens were tested it could be observed that only a partial increase in failure load and peak strains was obtained. However, the test results varied and further research needs to be conducted to investigate the possibility of bond enhancement due to the application of wraps.

3.5.2.4. FRP Laminate Type

In this research project four different types of FRP laminates were applied: GC-Hybrid FRP, S&P CFRP 200/2000, Tyfo[®] UC and Sika CarboDur[®] S1012. The GC-Hybrid FRP was selected as in previous research a glass scrim layer was used between the steel and the carbon to prevent galvanic corrosion. The other laminates were commonly available CFRP laminates provided by different manufacturers.

So far, only a small number of tests were conducted using different laminates but the same adhesive. However, the test results indicate that higher failure loads and peak strains were

observed for specimens prepared with the Tyfo[®] UC laminates. But as the recorded strains with the lower modulus GC-Hybrid reinforced specimens were only slightly lower, and this FRP type prevents galvanic corrosion, its future application for the strengthening of steel member looks promising. Further research needs to be conducted concentrating on the influence of the FRP laminate stiffness.

3.5.2.5. Adhesive Type

In this research project five different epoxy adhesives were tested: En-Force CFL, Sikadur[®] 30 and 31, Tyfo[®] MB and S&P Resin 220. The tests, examining the impact of the adhesive type on the bond performance, were conducted with discontinuous specimens of Type III, which had bonded length 9in (22.9cm).

Two different types of strain response were observed depending upon the adhesive used. A brittle response was caused by Sikadur[®] 30 and 31 and the S&P Resin 220 and En-Force CFL. This response was characterized by short effective development length and high peak stresses at the discontinuity. A ductile response was observed for specimens fabricated with the epoxy Tyfo[®] MB. It was characterized by a longer effective development length, as the strain was transferred over the whole bonded length. Further, the maximum bond stresses were lower as no localized peaks occurred, as it was the case for aforementioned brittle strain responses.

At this point, no conclusion may be drawn which strain response would be more beneficial for the strengthening of steel members. Further research will have to investigate both responses with regard to peak stresses, the probability of cracking and buckling in the compression flange due to higher strains in the tension flange.

3.5.2.6. Adhesive Thickness

Glass beads were used at a later stage of this project to control the adhesive thickness. Different bead diameters were considered. Most of the specimens were prepared with 80mils (2mm) beads. However, in the case of specimens fabricated with the epoxy Tyfo[®] MB and the CFRP laminate Tyfo[®] UC, also an adhesive thickness of 10mils (0.25mm) was investigated, as this was the thickness recommended by the manufacturer. Although, only a small number of tests were carried out it may be concluded that an adhesive thickness of 80mils (2mm) is more suitable than a thickness of 10mils (0.25mm), as higher peak strains and failure loads were obtained.

3.5.2.7. Surface Preparation

No tests have been carried out in this research project investigating the influence of different steel surface conditions. For all tests non-corroded steel plates were used. Future research will have to verify the feasibility of the findings in this program for the application of FRP laminates to corroded steel members with uneven surfaces.

A small number of specimens were tested to examine the necessity of sanding one face of the FRP laminate prior to application as bond enhancement. All these specimens were fabricated with the GC-Hybrid laminates and the epoxy En-Force CFL. At this point, it may be concluded that sanding the GC-Hybrid laminates does not influence the bond performance significantly. However, more tests have to be carried out to validate this conclusion.

3.5.2.8. Curing Time

In the case of specimens fabricated with GC-Hybrid laminates and En-Force CFL a variety in test results was observed. An additional test series was introduced to investigate the effects of the curing time on the bond performance of FRP laminates to steel applications. The results for this test series were presented in Section 3.3.2.5 and 3.3.3.4. At this point it may be concluded that the failure loads and peak strains will increase within the first 10 days and then decrease. Further, with advanced curing time the force transfer along the bonded length becomes less effective, which was also shown by lower failure loads for longer cured specimens. However, only a small number of specimens were tested and no final conclusion may be drawn yet.

For all other adhesives used in this project no special observations regarding the impact of the curing time were made.

3.5.3. RECOMMENDATIONS FOR FUTURE RESEARCH PROJECTS

With regard to bond influencing factors considered in this research project, further tests will have to be carried out to investigate the impact of (1) FRP laminates with a different stiffness, (2) different adhesive types, henceforth examining brittle and ductile strain responses, (3) different adhesive thicknesses, (4) different surface conditions/treatments of the steel plates, (5) roughening the FRP laminates to enhance the bond.

The results in this research project were obtained for double-lap joints in tension. Future research will have to show the feasibility of these findings for flexural applications. In this context, tests examining the prospect of bond enhancement due to wraps should be carried out.

Another aspect, to be considered, is the long term durability of FRP-steel joints. Factors like chemical environment as well as cyclic temperature changes will have to be investigated. Further, tests should be carried out to verify that galvanic corrosion can be neglected when reinforcing steel members with GC-Hybrid FRP laminates.

Finally, field applications and adequate continuous monitoring would result in a better understanding of the performance of FRP reinforced steel structures.

4. FLEXURAL TESTS

4.1. INTRODUCTION

4.1.1. BACKGROUND

The concept for retrofitting corroded steel members with FRP materials is to strengthen these members with laminates that are adhered to the steel surface with an epoxy paste. This method has many advantages, such as: (1) it is rather easy and simple to implement in the field, (2) traffic disruptions are maintained at minimum levels, (3) it is durable (Ammar, 1996) and (4) it may allow the full recovery in stiffness and moment capacity of the corroded members without significant weight increase (Ammar, 1996). These advantages typically offset the initial costs associated with the costs of using FRP composites.

4.1.2. OBJECTIVES

The main objective of this research program was to develop a competitive technique capable of retrofitting corroded steel flexural members to regain the original design moment capacity of the member within allowable stress levels. In this series of tests, four beams were tested to develop a simple/economic concept for CFRP retrofit of steel girders. Two girders were retrofitted using different lengths of CFRP laminate to investigate the peeling of CFRP laminate at the end of the laminate in different regions of moment and shear.

4.1.3. RESEARCH FINDINGS

Flexural tests conducted in this research program were investigated using the material response presented in section 3.4.1. Flexural test results analyzed according to this material response are very promising towards the development of a rational design approach that considers the material response, as outlined in sections 3.4.1 and 3.4.2. In addition, test results indicate that the retrofit scheme was adequate in retaining the design flexural capacity for corroded steel members. However, additional research is needed to substantiate these findings. Since debonding of the CFRP laminate was the governing failure mode of the retrofitted specimen, it was important to compute the bond stresses at various locations along the length of the CFRP laminate. The corroded specimens were retrofitted using different lengths of the laminate. One test unit was retrofitted by bonding a CFRP laminate along the entire length of the specimen, and failure was characterized by progressive peeling of the bonded CFRP laminate. A second test unit laminate was bonded only along a quarter length of the tested girder, and failure of the

laminates were characterized by sudden peeling. Differences in the registered failure load and mode suggest that the anchorage length of the FRP laminates are crucial in ensuring a proper retrofit scheme, and the development lengths obtained in sections 3.4.1 and 3.4.2 may need to be revisited using flexural tests.

4.1.4. CHAPTER LAYOUT

This part of the report addresses the strengthening of flexural members with FRP composites. In Section 4.1 some background information is given together with the objectives of this research program and the main research findings. Section 4.2 describes the experimental program introducing the retrofit scheme, materials used, and the test setup and design of the test specimens. Section 4.3 contains the experimental results. The discussion of the test results and the conclusions are presented in Sections 4.4 and 4.5, respectively.

4.2. EXPERIMENTAL PROGRAM

4.2.1. INTRODUCTION

The rehabilitation system used consisted of bonding CFRP laminates to the tension flange of corroded steel members. A 4in (10.2cm) notch was introduced at the mid-span of the tension flange to simulate the loss of steel section area due to corrosion. The experimental program consisted of four W12x14 sections, each beam having a length of 108in (274cm). According to the information provided by the manufacturer the yield strength of the steel was 60 ksi (414 MPa). The problem statement and criteria addressed in this research project are presented in the following sections.

4.2.2. PROBLEM STATEMENT

In order to design a retrofit scheme, the aspects of the procedure involved with bonding the CFRP laminates to steel have to be considered. These include the bond behavior of the FRP laminate, force transfer between the CFRP laminate and the steel substrate and the stress levels at which the debonding between the laminate and the steel occurs. During this research program the bond behavior and the stresses in the CFRP laminate were carefully investigated. The bond behavior of the CFRP laminate was studied at UMR and is discussed in Chapter 3 of this report. In this chapter it is focused entirely on stress transfer in CFRP laminate under flexural conditions. Two failure modes are possible in the FRP type retrofit application, namely: (1)

debonding and (2) rupture of the CFRP laminate. In this research project the primary mode of failure of the tested flexural beams was governed by the debonding of the FRP laminate. It was therefore indispensable to place an upper stress limit on the FRP laminate to take this failure into consideration, yet still regaining the flexural capacity of the corroded section.

4.2.3. RETROFIT SCHEME

As previously described the permissible FRP laminate stresses are most crucial for the design process in order to prevent debonding of the FRP laminates at a premature stage. Therefore, design specifications for new steel structures that are based on the load resistance factor design approach (LRFD) are not viable for FRP composite retrofit applications. One of the main reasons is the excessive strain levels that will be imposed on the adhesive. Debonding of the FRP laminates would occur prior to the development of a plastic mechanism, which the LRFD design approach is based on.

Figure 4-1 indicates the retrofitted cross-section and the designation of variables used in the following design approach. Henceforth, A_b^o is the original gross sectional area of the steel member, A_{cor} is the lost area of the tension flange due to corrosion and A_{FRP} is the area of the CFRP laminate.

In order to develop the design methodology the following procedure was implemented for the design of the FRP laminates. The approach is based on balancing the loss of load carrying capacity (Eq. 4.1) and the gain due to the FRP utilizing a stress limit (Eq. 4.2). As such the force loss due to corrosion is:

$$T_L = A_{cor} \alpha f_y$$

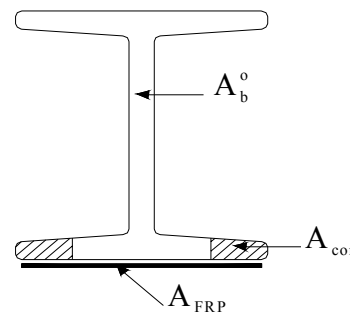


Figure 4-1 Retrofitted Cross-Section

Eq. 4.1

where α and f_y are the stress limit factor of safety and the yield strength of the steel, respectively. Stating that the force gain due to the FRP is:

$$T_g = A_{FRP} f_{FRP}^* \quad \text{Eq. 4.2}$$

where f_{FRP}^* is the debonding stress in the FRP laminate obtained from the tension tests reported in Chapter 3. For a practical design situation, equating Eq. 4.1 with Eq. 4.2, the following expression is obtained, which can be used to determine the required FRP cross sectional area according to the loss due to corrosion:

$$A_{FRP} = \frac{A_{cor} \alpha f_y}{f_{FRP}^*} \quad \text{Eq. 4.3}$$

In order to define the level of safety obtained in this design assumption a moment curvature analysis has been carried out for different W-sections with increasing section modulus by using a computer program developed at UMR. The manufacturer has provided all the parameters used during the analysis. For each section, the moment capacity of the original section, the corroded section and the retrofitted section have been plotted as moment versus curvature. Figure 4-2 indicates the results for a W12 x 14 section. According to this analysis the original section yields at 894 kip-in (101 kNm), which is also the theoretical moment capacity of this section. According to the ASD criteria the design moment cannot exceed 0.6 times the yield moment, given by:

$$M_D = 0.6M_Y \quad \text{Eq. 4.4}$$

where M_D and M_Y are the design moment and the yield moment of the original section, respectively. Therefore for a W12x14 the design moment according to Eq. 4.4 is $M_D = 536$ kip-in (60.5 kNm).

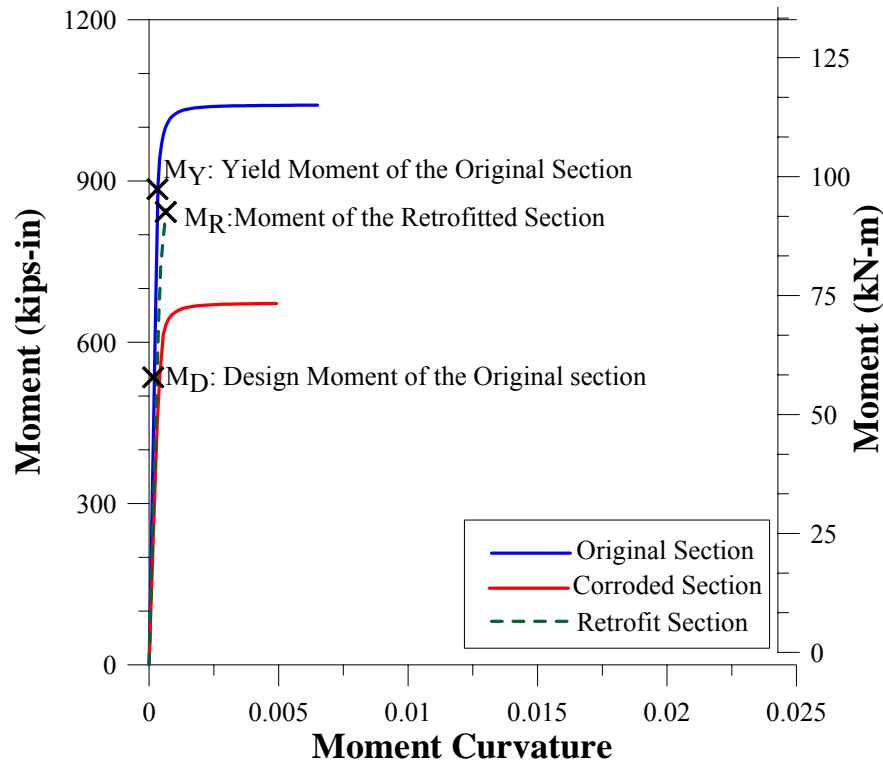


Figure 4-2 Moment Curvature Analysis for W12 x 14 Section

The corroded section was retrofitted by using CFRP laminate with cross-sectional area calculated using the retrofit scheme by Eq. 4.3. During this analysis 100% corrosion of the tension flange was assumed. The retrofitted section's calculated peak capacity at peeling was 843 kip-in (95 kNm), which is greater than M_D . The factor of safety against peeling is equivalent to the strengthening ratio calculated as follows:

$$FS = \frac{M_R}{M_D} = 1.57 \quad \text{Eq. 4.5}$$

where M_R is the moment capacity of the retrofit section. As previously described, the computer program was utilized for different sections and for different levels of corrosion (see Figure 4-3). Analysis indicate that the ratio of moment capacity of the retrofitted section and the design moment of the original section increased only slightly with decrease in the percentage of corrosion as shown in Figure 4-3, and that the factor of safety against peeling in each condition was always above 1.5. These numbers will have to be investigated further.

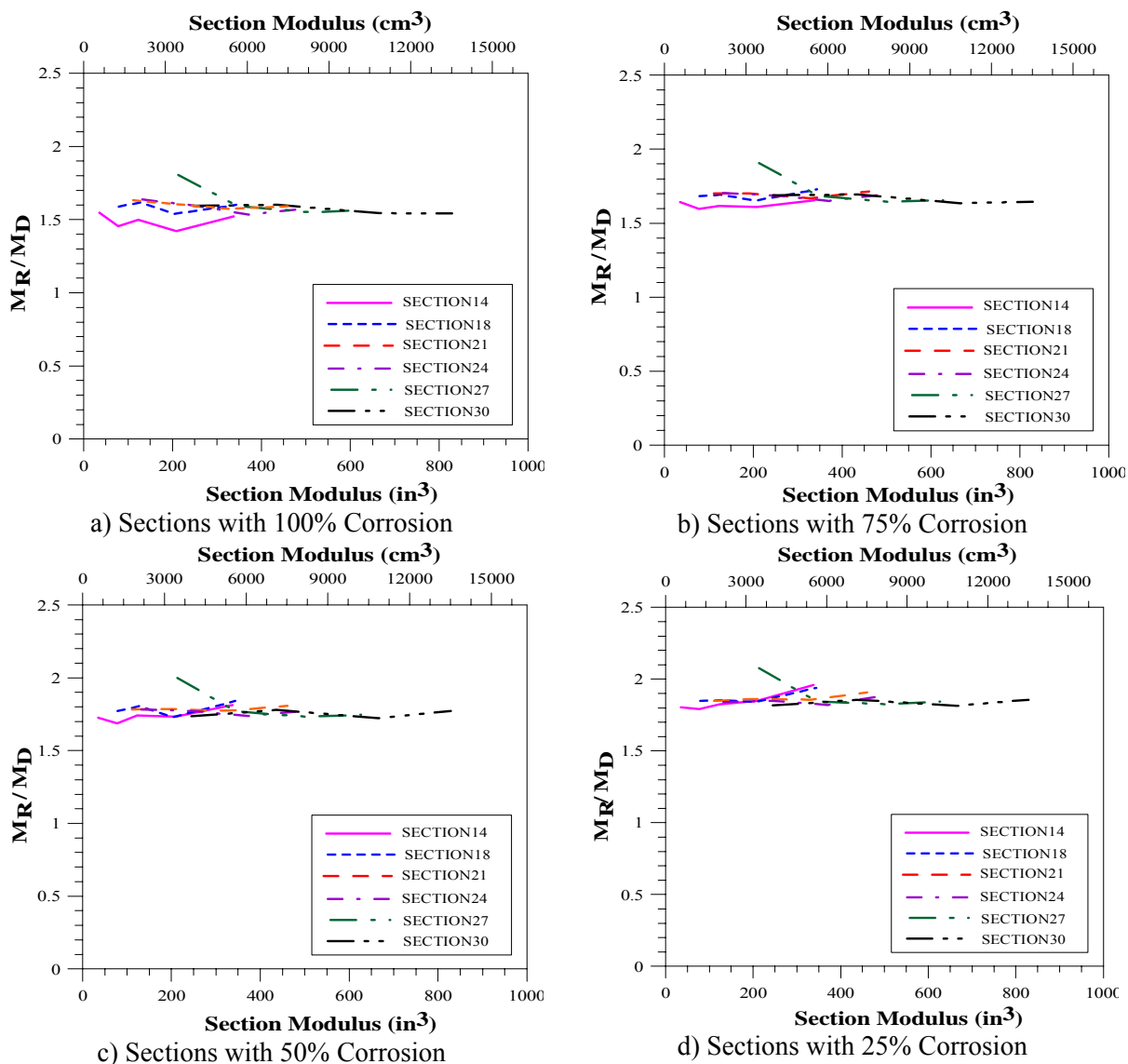


Figure 4-3 M_R/M_D for Different Levels of Corrosion vs. Section Modulus

4.2.4. EXPERIMENTAL SETUP

4.2.4.1. Test Specimen and Material

The experimental program consisted of four W12x14 beams each having a length of 108in (274cm). CFRP laminates 200/2000 provided by Structural Composites Inc. were chosen as strengthening materials. The properties of the FRP laminates are given in Table 4.1.

Table 4.1 Properties of CFRP Laminates

CFRP Laminates 200/2000		
	US System	SI
Modulus of elasticity	>29 Msi	>200 GPa
Tensile strength at break	>360 ksi	>2300 N/mm ²
Width/Thickness	3.94in./0.055in.	100mm/1.4mm
Maximum Elongation At 0.6 - 0.8%	37.1/49.5 k-lb	168/224×10 ³ N

Test Unit 1 was a virgin specimen without the FRP retrofit. The yield point of this specimen was used as a reference point for Test Units 3 and 4. Test Unit 2 was designed with a 4in notch at the mid span of the tension flange to simulate the loss of section area due to corrosion but without the FRP retrofit. Test Units 3 and 4 were designed as Unit 2 but with the FRP retrofit along the entire length and quarter length, respectively, to investigate the feasibility of the retrofit scheme and the impact of the bonded length on the structural performance. The test matrix is shown in Table 4.2.

Table 4.2 Test Matrix

Test Unit	Retrofit	Notch
Unit 1	None	None
Unit 2	None	4 in
Unit 3	Full length	4 in
Unit 4	Quarter length	4 in

Unit Conversion 1in.= 2.54 cm

4.2.4.2. Theoretical Prediction

Utilizing the material properties of the steel sections provided by the manufacturer the load at which the virgin beam would theoretically yield was calculated. The result is indicated in Table 4.3 together with the steel properties.

Table 4.3 Theoretical Properties of a W12 x 14

Yield Strength		Elastic Modulus		Yield Moment		Plastic Capacity	
ksi	MPa	ksi	GPa	Kip-in	kN-m	Kip-in	kN-m
58	400	29000	200	865	98	1008	114

4.2.4.3. Surface Preparation

It is important to remove dust, laitance, grease, curing compounds, waxes, impregnations, foreign particles and other bond inhibiting materials from the surface by blast cleaning or equivalent mechanical means. Steel should be cleaned and prepared thoroughly by blast cleaning. Surface moisture contents need to be less than 5%.

In this experimental program the tension/bottom flange of the beams for Tests Unit 3 and 4 was grinded using sandpaper in order to remove rust and mill scale. Grinding of the surface was accomplished until a near white finish was observed, and a 3mil (0.08mm) anchor X-pattern was imposed, in order to ensure that the epoxy would bond to the rough surface of the steel girder. To fully utilize the strength of the laminate and avoid premature peeling, the surface tensile strength of the bond should be greater than 200 psi (1.4 kPa). After grinding, the steel was wiped with solvent (acetone) in order to remove any oil residue on the surface.

Prior to the application of CFRP laminate, several steps were taken to prepare the retrofit materials. The CFRP laminate was then cut to the appropriate length. After cutting the laminate the bonding surface was sanded or roughed up using scrub pads. The purpose of this procedure is to remove the glossy surface of the laminate for proper bonding with the steel surface. The adhesive is then applied to the underside of the tension flange of the steel section along the required length. The CFRP laminate is then carefully adhered along the length of the beam under the adhesive. The laminate should be clamped with the tension flange of the steel beam to have proper bonding.

4.2.4.4. Test Setup

The test specimens were tested in the Engineering Research Laboratory at the University of Missouri- Rolla (UMR). A typical compression testing machine was used for loading the beam and the load was applied at the mid span (i.e. three point bending). The entire test setup is shown in Figure 4-4 and Figure 4-5.

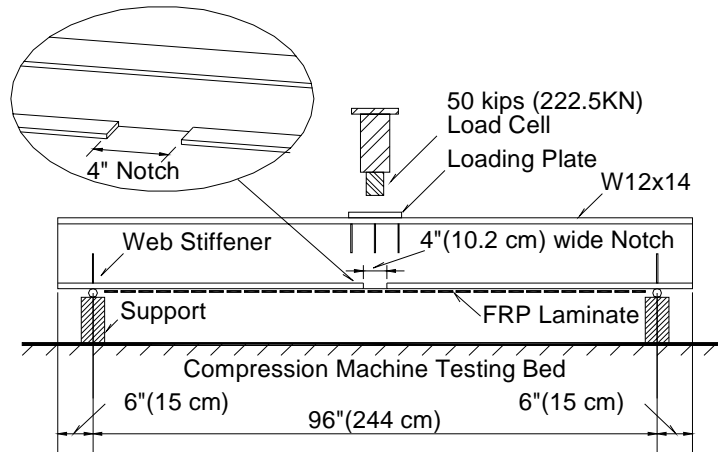


Figure 4-4 Test Setup (Liu, 2002)



Figure 4-5 Test Setup

A simple lateral support system was designed to prevent the premature occurrence of lateral torsional buckling. Four pairs of lateral brace supports were installed to reduce the predisposition for lateral torsional buckling (see Figure 4-6 and Figure 4-7). Two pairs were installed at the supports and the other two were installed at approximately quarter spans. In order to prevent local buckling web stiffeners were also installed at the locations of the applied loads and

supports. A loading plate was inserted between the load cell and the top flange of the specimen to avoid large stress concentration and increase the area of the load transfer to the girder.

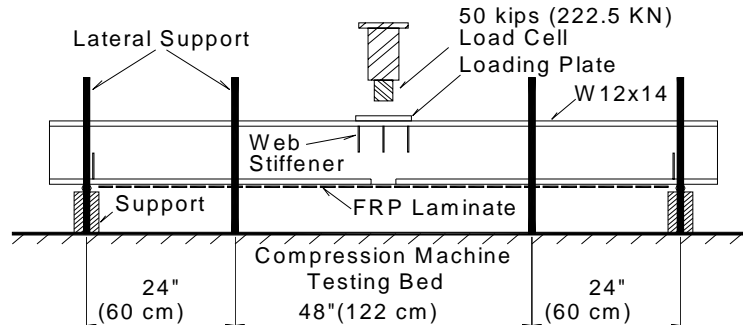


Figure 4-6 Lateral Support Setup (Liu, 2002)



Figure 4-7 View of Lateral Support Setup

4.2.4.5. Instrumentation

Strains were measured at various locations along the length of the beam to determine the maximum strain. Strain gages were installed at 4 separate locations along the girder such as (1) at mid span, (2) 1.5in (3.8cm) from the center line of the girder, (3) 7.5in (19cm) from the center line, and (4) at quarter span. At each of these locations strain gages were installed in different places as indicated in Figure 4-8.

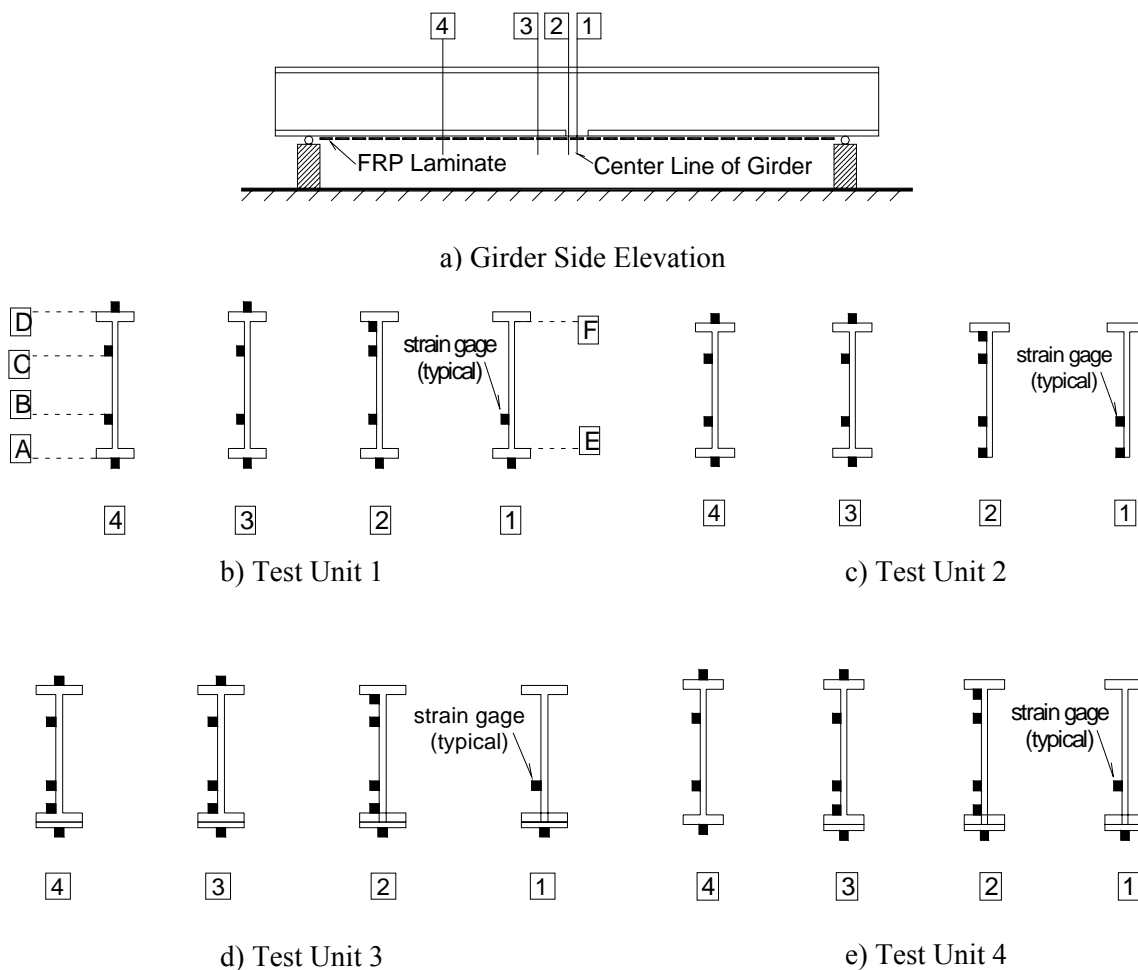


Figure 4-8 Strain Gage Locations (Liu, 2002)

The lateral and vertical deflection of the girder at the mid span and the quarter span were measured by LVDT and the positioning of these LVDT's is shown in Figure 4-9.

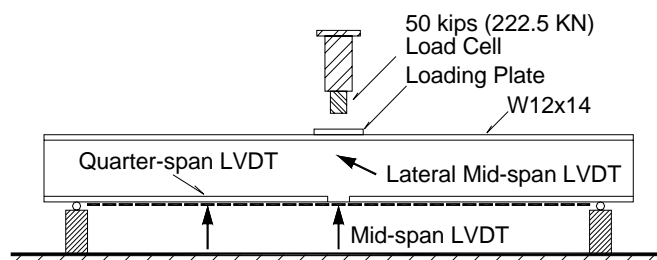


Figure 4-9 Distribution of LVDT (Liu, 2002)

4.2.4.6. Design of the Test Specimen Using the Proposed Retrofit Scheme

The design approach discussed in Section 4.2.3 was used to calculate the required reinforcement for Test Unit 3 and 4. The debonding stress, f_{FRP}^* , was computed according to Eq. 3.2. Using a peak bond stress of 1250 psi (8.5 MPa), a development length at peak stress before peeling of 3.75in (9.5 cm), and thickness of the CFRP laminate equal to 0.055in (1.4mm) (see Table 4.1) the value of f_{FRP}^* in the design scheme was:

$$f_{FRP}^* = \frac{1250 \times 3.75}{0.055} \cong 85 \text{Ksi (588 MPa)} \quad \text{Eq. 4.6}$$

Thus, according to Eq. 4.3 the area of the CFRP laminate required to retrofit the corroded section should be equal to:

$$A_{FRP} = \frac{[(3.97 - 0.20) \times 0.225] \times 0.6 \times 58}{85} = 0.34 \text{in}^2 (2.24 \text{cm}^2) \quad \text{Eq. 4.7}$$

Therefore, the width of the laminate required would be near 6 1/8 in. (16cm). Since the width of the flange for W12x14 section is 3.97in (10cm), the width of the laminate was set at 3.94in (10cm). Thus the objective of the experimental results was to substantiate these analytical studies and to ensure that the moment capacity of the corroded beam can be restored using CFRP retrofit.

4.3. EXPERIMENTAL RESULTS

In this section the experimental results for all four test units are presented. For reference in all plots the design capacity ($0.6P_y$) is indicated as a dashed line.

4.3.1. TEST UNIT 1

The failure mode of Test Unit 1 (control specimen) was lateral torsional buckling (see Figure 4-10). The unit yielded at 35kips (157KN) with a maximum strain of $2300\mu\epsilon$. Figure 4-11 indicates the load-strain and load-deflection curve at mid span. It is important to mention that the lateral torsional buckling developed beyond the observed yield load.



Figure 4-10 Failure Mode of Test Unit 1

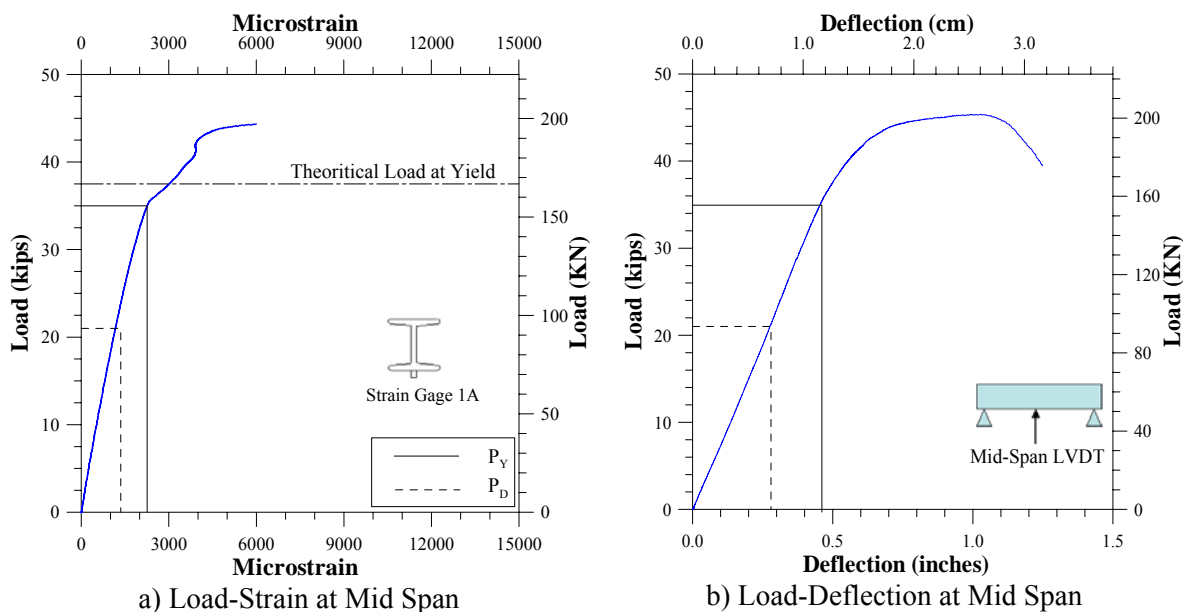


Figure 4-11 Test Unit 1

4.3.2. TEST UNIT 2

Test Unit 2 demonstrated the behavior of a non-retrofitted section with a completely corroded tension flange. A notch of 4in (10.2cm) was introduced as described in Section 4.2.4.1. The failure mode of this specimen was lateral torsional buckling, similar to the failure mode observed in Test Unit 1 (see Figure 4-12). Higher strains were recorded at lower loads as indicated in Figure 4-13a. Although this section capacity was higher than the required P_D level, it is important

to mention that the corresponding safe limit design for the strain level equal to $0.6 \epsilon_y$ was significantly exceeded. The section reached a strain level of $3000 \mu\epsilon$ at the required design level capacity, which is significantly higher than the allowable strain level of $0.6 \epsilon_y$.



Figure 4-12 Failure Mode of Test Unit 2

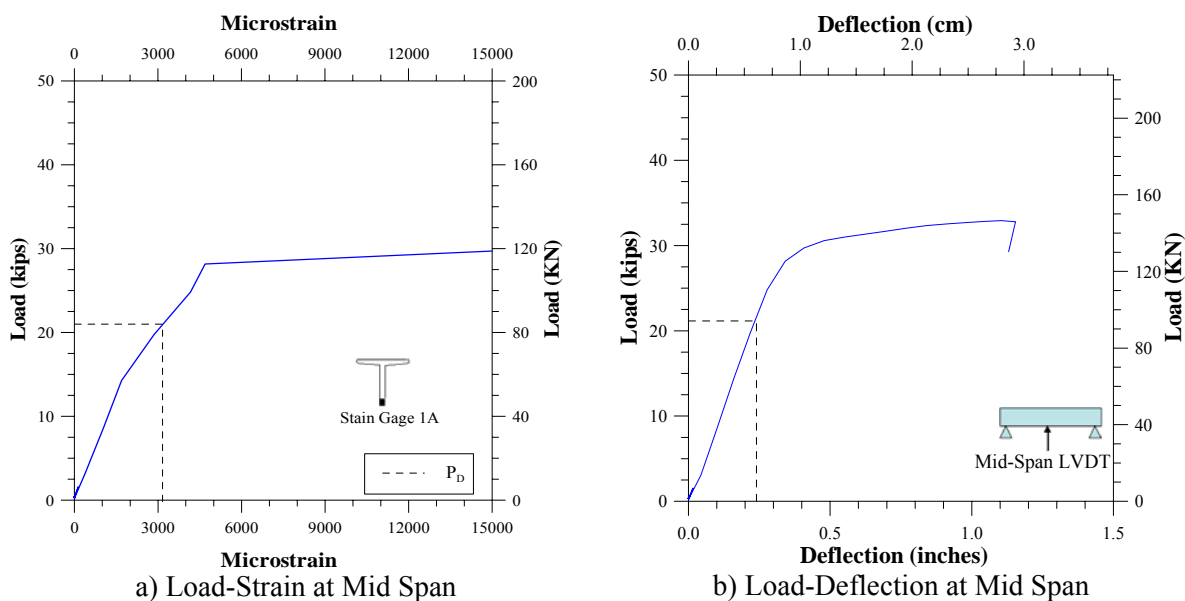


Figure 4-13 Test Unit 2

4.3.3. TEST UNIT 3

This test unit was retrofitted with FRP laminate bonded along the whole beam. The failure mode was characterized by the peeling off of the CFRP laminate (see Figure 4-14). This was due to the high stress concentrations and high shear stresses near the notch area. The load-strain and load-deflection curves are indicated in Figure 4-15.

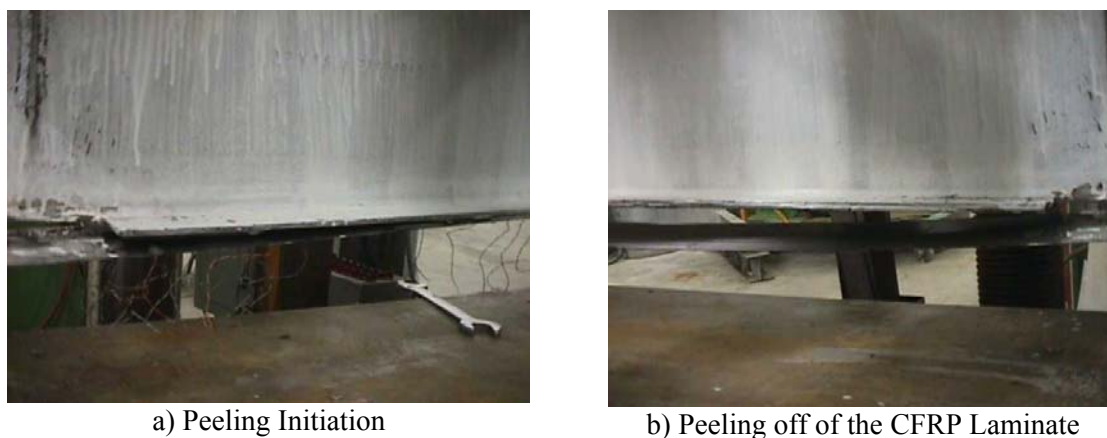


Figure 4-14 Failure Mode of Test Unit 3

According to the proposed retrofit scheme, peeling occurs beyond the required design level. The load at peeling (peak load) 37.6 kips (167 kN) and thus a safety design load of 22 kips (98 kN) was attained.

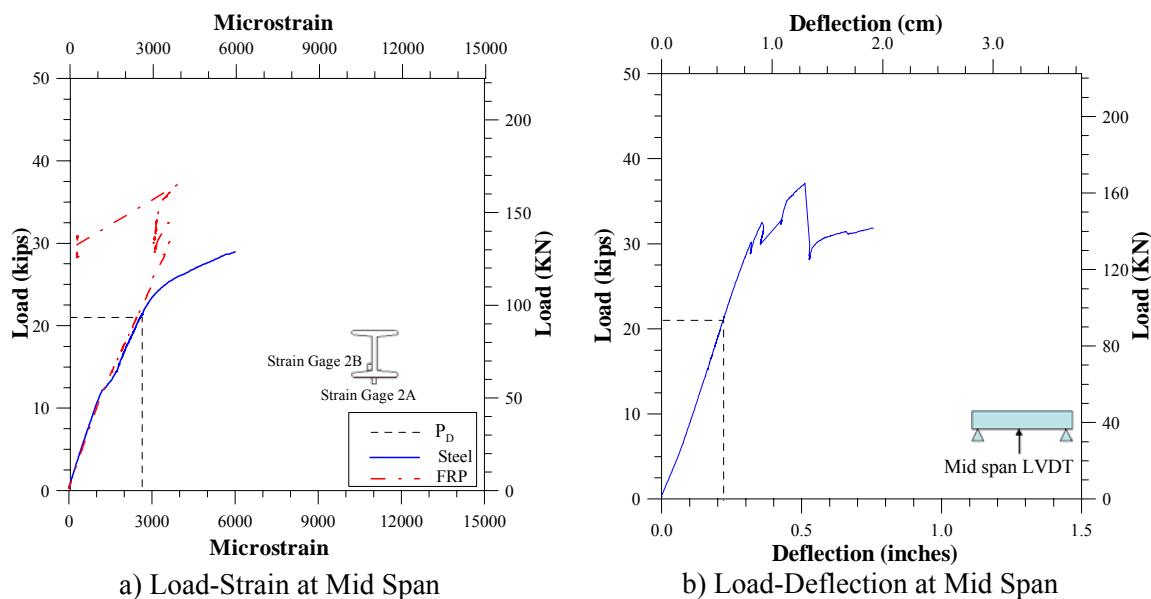


Figure 4-15 Test Unit 3

4.3.4. TEST UNIT 4

In this test unit the CFRP laminate was applied only over a quarter length of the beam. The failure mode was characterized by a sudden peel off as in Test Unit 3. The load-strain and load-deflection curves are shown in Figure 4-16. The load at which peeling occurred was similar to the load that initiated peeling for Test Unit 3. But due to the time taken in Test Unit 3 for the peeling to propagate from the mid-span toward the supports the complete peel off occurred at higher load than in Test Unit 4. The peeling in this case occurred at 33 kips (147 kN).

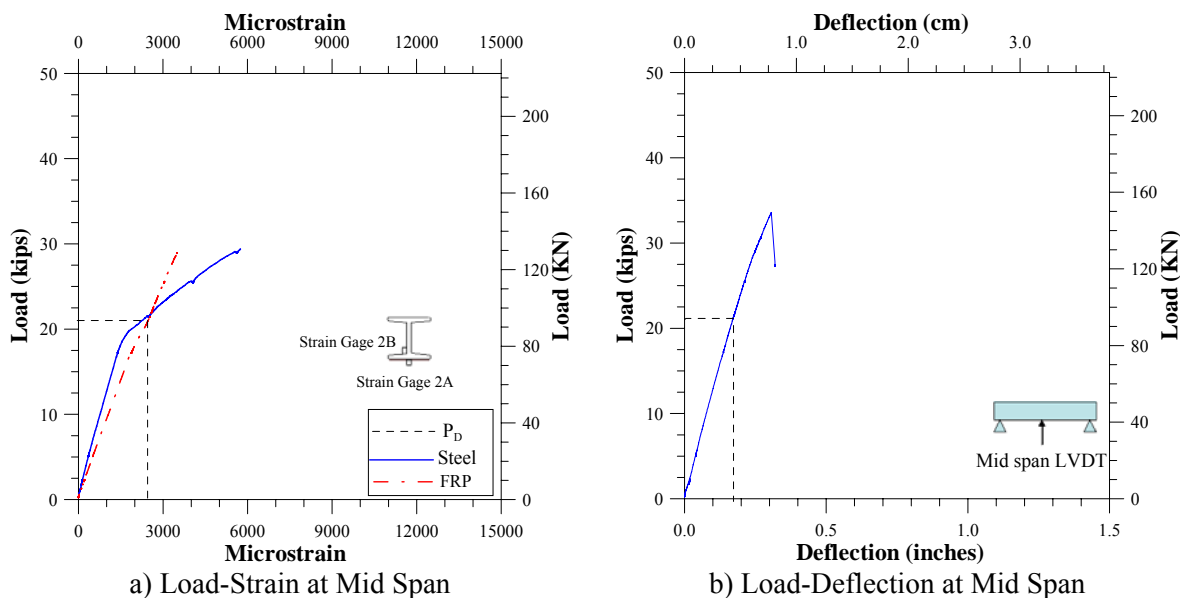


Figure 4-16 Test Unit 4

4.4. DISCUSSION OF EXPERIMENTAL RESULTS

Figure 4-17 and Figure 4-18 indicate the strain profiles for Test Unit 3 and 4, respectively. It is apparent that strains recorded near the notch are significantly higher than those at the end of the laminate for both units. The debonding strain at the notch is slightly greater for Test Unit 4. The debonding stresses for Test Unit 3 and 4 were 107ksi (740MPa) and 120ksi (830MPa), respectively. Both values compared well with the design debonding stress, which was 80 ksi (550 MPa). From Figure 4-17 it may be inferred that the effective development length is greater than 6in (15.2cm). The development length for Test Unit 3 from Figure 4-17 can be taken as approximately equal to 30in (76cm). Therefore, it explains why Test Unit 4 with a bonded length of 6in (15.2cm) failed at a lower load level.

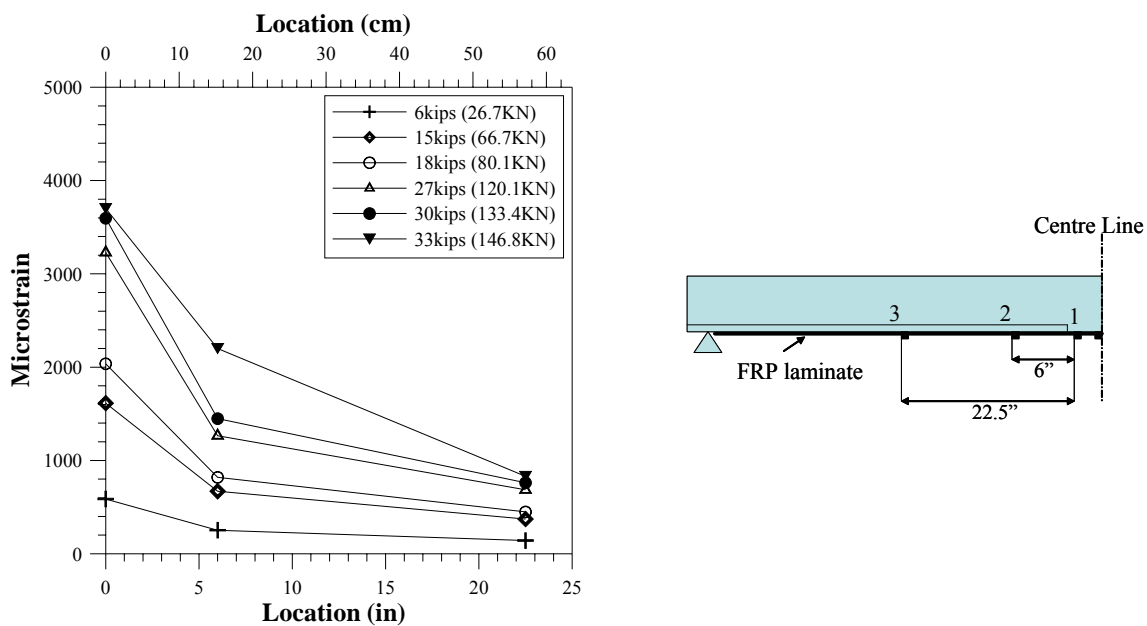


Figure 4-17 Strain-Location – Test Unit 3

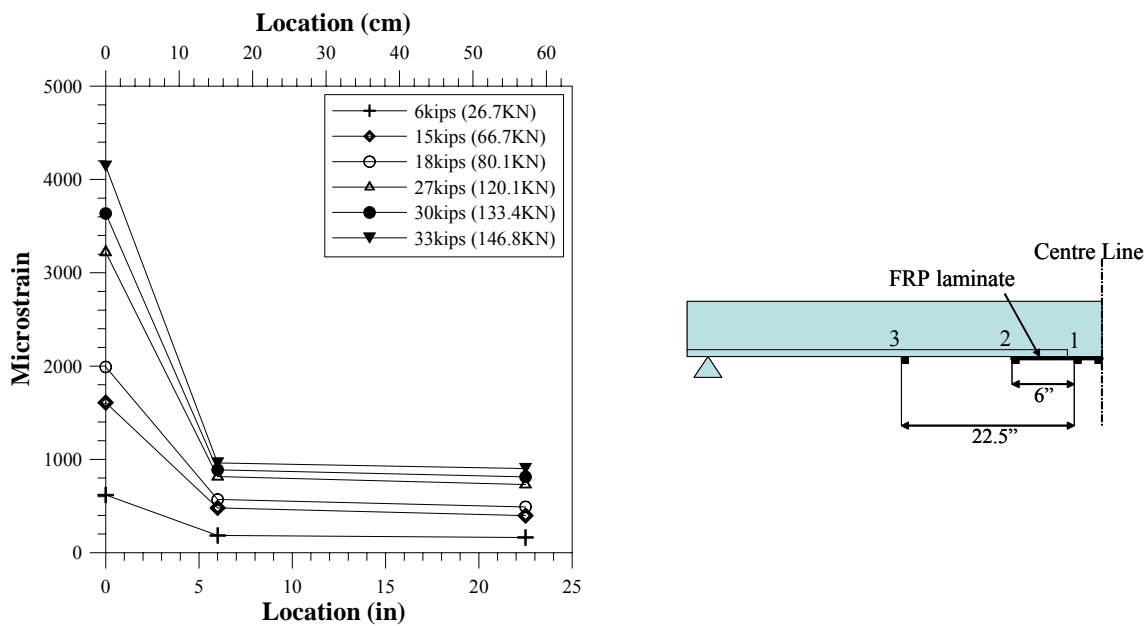


Figure 4-18 Strain-Location – Test Unit 4

In Section 4.2.3 a theoretical approach was introduced to predict the retrofit efficiency. Table 4.4 indicates the test results and the efficiency evaluation for Test Units 3 and 4. The presented efficiencies correspond well with the theoretical value of 1.57 presented in Section 4.2.3. It may be concluded that an increase in bonded length results in an increase of the retrofit efficiency.

Table 4.4 Test Results

Test Unit	P_y/P_R		Mid-Span Deflection		M_y		M_D		M_R		M_R/M_D
	kips	KN	in	cm	Kip-in	KNm	Kip-in	KNm	Kip-in	KNm	
1	35	157	0.45	1.12	840	95	504	57	-	-	-
2	15	67	0.18	0.45	360	41	-	-	-	-	-
3	37.6	167	0.50	1.25	-	-	-	-	902	102	1.78
4	33	147	0.30	0.75	-	-	-	-	792	89.5	1.57

4.5. CONCLUSIONS

In this part of the report rehabilitation of the corroded steel bridge girders using adhesively bonded CFRP laminates has been presented. All the tests performed indicate that by adopting the above retrofit design strategy a promising rehabilitation procedure can be established. It is apparent from the experimental observations that an increase in the moment capacity of the corroded steel bridge girder has been achieved. In addition, the presented results indicate that a safety factor of 1.57 can be achieved by employing the proposed retrofit scheme. Further, in this experimental program a section loss of 100% was considered. Future research will have to address different levels of corrosion to examine the reserve moment capacity beyond the design moment. The use of different adhesives, FRP laminate types, environmental conditioning will also have to be investigated to develop a better understanding of the performance of the FRP retrofitted steel members.

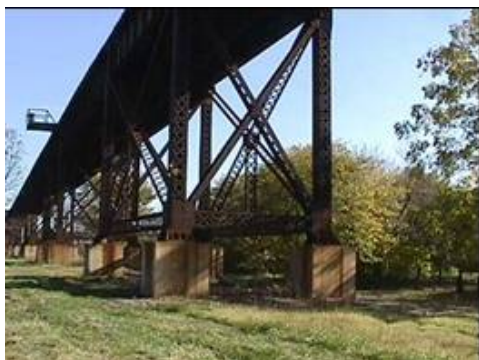
5. AXIALLY LOADED MEMBERS

5.1. INTRODUCTION

5.1.1. BACKGROUND

Throughout the US, there are numerous steel bridges that are at various levels of advanced deterioration. For example, the Macarthur railway steel bridge located in St. Louis, which was built in 1917, shows members with severe corrosion problems. In many of these bridges built-up columns, as shown in Figure 5-1, consist of steel L-angles, I-shapes and plates.

After many years of service and exposure to the environment, corrosion in some of these sections has resulted in loss of axial load capacity and potential for collapse. As shown in Figure 5-1, there is extensive corrosion along the web of the inner I-shape section, in particular above the concrete-filled portion contained by the cover plates. The principal reason for this localized deterioration has been the collection of debris, bird waste and moisture.



a) Bridge Structure



b) Close-Up View Column

Figure 5-1 Typical Built-up Steel Column of Steel Railway Bridge

In many cases, since total replacement is not an option, and traditional retrofit methods are labor intensive and time consuming, an alternative retrofit method using FRP composites may provide a competitive solution that will prolong the usable life of these steel bridges (Tickford Bridge, UK 1999). The concept presented in this research is to strengthen a given deficient built-up column with a two-step procedure: (1) wrapping with open FRP jackets and (2) filling these jackets with expansive light-weight concrete. The attractiveness of this method is that the existing structural members remain untouched. Traditional methods required removal of the steel brace members and application of steel plates to make up for the lost cross section and followed

by drilling, bolting and splice detailing, welding of steel plates, which could result in collapse of the structure. The FRP strengthening method is relatively easy and simple to implement in the field. In addition the expansion of the concrete allows the FRP jacket to provide active confinement to the steel columns.

5.1.2. OBJECTIVES

The main objective of the test program for this task was to develop a retrofit technique capable of upgrading existing axially loaded members in compression, which show significant amounts of cross section loss due to corrosion.

5.1.3. RESEARCH FINDINGS

- 1) Different high-expansion light-weight concretes were achieved by changing the compositions of the cement blends, but the expansion degree was inversely proportional to the modulus of elasticity and compressive strength of this type of concrete.
- 2) The local bond-slip relationship between the expansive light-weight concrete developed in this research project and steel was obtained, and this can be used to determine the engineering problem, such as anchorage length and development length of steel embedded in the concrete. The expansion of the concrete is helpful to increase the bond between concrete and steel.
- 3) Experimental test results showed that this FRP retrofit technology can restore the ultimate load capacity of deficient steel columns to the original value and even higher.

5.1.4. CHAPTER LAYOUT

Section 5.1 gives some background information on the strengthening of axial compression members, the objectives of this research project, and it presents the main research findings. Section 5.2 deals with expansive light-weight concrete, presenting the relationship between the expansion of concrete compositions, and the influence of expansion on the engineering properties of the concrete. The local bond-slip relationship between smooth steel bars and FRP confined expansive light-weight concrete is given in Section 5.3. In Section 5.4 the feasibility of the ??? in this report proposed retrofit technology for corroded steel columns is verified. A summary of all research finding is presented in Section 5.5. Finally, Section 5.6 contains some design guidelines for the retrofit of stocky and slender steel columns.

5.2. EXPANSIVE LIGHT-WEIGHT CONCRETE

5.2.1. OBJECTIVE

In this sub-task, seven types of light-weight expansive concrete mixtures were tested at the University of Missouri-Rolla in order to investigate: a) the relationship between expansion and the compositions of the concrete mixture, and b) the influences of the concrete expansion on the engineering properties of the FRP confined concrete. The expansion of these types of light-weight expansive concrete mixtures resulted from the formation of an expanding agent (ettringite, Mehta, 1986), which is obtained by the reaction of Portland cement, gypsum, calcium aluminate, and water. Different light-weight expansive concrete mixtures were cast into open GFRP pipes and the hoop direction expansion of the GFRP pipes was monitored up to 150 days until the expansion stabilized. At 56 days, the GFRP-confined concrete cylinder specimens were loaded in compression up to failure in order to characterize their engineering properties.

5.2.2. BACKGROUND

The proposed FRP strengthening methodology described above is relatively easy and simple to implement in the field. The expansion of the concrete will increase the friction coefficient between the concrete and steel column, resulting in an increase in the concrete contribution to the combined effective stiffness of the steel composite columns and ultimate load capacities. According to this FRP retrofit method, a higher concrete expansion is desirable because a higher expansion of the concrete will result in a better performance of the retrofitted steel columns and a reduced amount of concrete materials. However the expansion of concrete must be limited to a certain level because it will result in initial confining stresses in the FRP materials that can result in static-fatigue failure such as creep rupture. Furthermore, a light-weight concrete will decrease the extra added weight that must be added to the steel columns and reduce the need to enlarge the foundations.

As mentioned above, a high expansion degree light-weight concrete is desired, but in most previous research (Matusumoto, 1970; Rosetti, et al, 1982; Hoff, 1972; Klein, 1961) an expansive concrete was used that followed the ASTM C845 “Expansive Hydraulic Cement”, which limits expansion to the concrete material between 0.04% and 0.1%. Since this type of concrete cannot provide sufficient expansion to the proposed FRP retrofit method, an investigation on higher expansion light-weight concrete, which is based on a 1975 U.S. patent to

produce "Type M" expansive cement, was carried out. The experimental results from this research are presented in this report.

5.2.3. EXPANSIVE CEMENT BLEND

There are two cement mixtures based on the 1975 U.S. patent to produce "Type M" expansive cement: "shrinkage compensating cement" (ASTM 845) and "self-stressing cement" (higher expansion). Previous researchers worked mostly with shrinkage compensating cement, and just a few researchers dealt with self-stressing cement (Sheigh et al, 1994), and as such research on this type of cement is needed. The compositions of the two cement mixtures according to patent are as follows:

(1) Shrinkage Compensating Cement blend

- a. Sulfur trioxide of Portland cement by ASTM C563
- b. Calcium aluminate cement 2%--9% by weight
- c. Sulfur trioxide 3%--11% by weight
- d. Portland cement to total of 100%

(2) Self-Stressing Cement blend

- a. Sulfur trioxide of Portland cement by ASTM C563
- b. Calcium aluminate cement 6%--17%
- c. Sulfur trioxide 9%--24%
- d. Portland cement to total of 100%

According to the patent, it is recommended that calcium sulfate dehydrate be used up to the addition rate of 10%. If more sulfur trioxide is needed, the remainder should be added as anhydrous calcium sulfate. It is further recommended that the calcium sulfate as hemi-hydrate (often in Portland cement) is less than 60% of the total calcium sulfate in the blend.

5.2.4. EXPANSION TEST

In order to determine the expansion of this light-weight concrete, research was divided in seven test series. Each series used a different concrete mixture.

5.2.4.1. Test Specimens

From a design point of view for the proposed FRP strengthening technology, the internal pressure developed in the concrete is easier to consider than the free expansion degree of the concrete. As a result in these series of tests, seven different light-weight expansive concrete mixtures were cast directly into open GFRP pipes, and the strain gages were applied on the pipes along the hoop direction to monitor any expansion. Hoop stresses developed in the pipes and the internal pressures developed in the concrete were calculated from these hoop direction expansion strains. Properties of the GFRP pipes (provided by the manufacturer) are shown in Table 5.1, and the seven groups of specimens are shown in Figure 5-2. In each test series, three specimens were tested, however only one specimen of each group is shown in Figure 5-2.

Table 5.1 Properties of the GFRP Pipe

	Inside diameter		Height		Thickness		Modulus of Elasticity of hoop direction		Tensile Strength	
	in	mm	in	mm	in	mm	ksi	MPa	ksi	MPa
GFRP pipe	6.4	162	13	330	0.1	2.5	4200	28963	70	483



Figure 5-2 Test Specimens

5.2.4.2. Materials

The mixture for light-weight concrete used: Portland cement (ASTM Type III), calcium aluminate cement, gypsum dehydrate, and anhydrous gypsum. The nominal specific gravities of these constituents were: 3.15, 3.1~3.2, 2.32~2.96, and 2.32~2.96 These properties were provided by the manufacturers. The gypsum was used to provide the sulfur trioxide for the expansive cement blend.

A 1/2"×No. 4 vacuum saturated coarse aggregate and a No.4×0 stockpile saturated fine aggregate were employed. Their specific gravities were 1.52 and 1.71. They were provided by the manufacturers, and their cumulative percentage passing is shown in Table 5.2.

Table 5.2 Cumulative Percentage Passing of Aggregate

Size Designation	Sieve Size								
	3/4in	1/2in	3/8in	No.4	No.8	No.16	No.30	No.50	No.100
1/2" x No.4	100	91	65	4	1				
No.4 x 0			100	95	70	45	26	16	11

(Unit conversion: 1 inch = 25.4 mm.)

U.S. standard sieve size: 3/4 inch (19.05 mm); 1/2 inch (12.7 mm); 3/8 inch (9.525 mm); No.4: 0.187 inch (4.75 mm); No.8: 0.093 inch (2.36 mm); No.16: 0.0464 inch (1.18 mm); No.30: 0.0236 inch (0.6 mm); No.50: 0.0118 inch (0.3 mm); No.100: 0.0059 inch (0.15 mm))

The coarse aggregate was vacuum saturated before leaving the plant and the stockpile was protected from drying by wetting the stockpile occasionally. The fine aggregate was soaked for a week before batching. The following procedures for the fine aggregate are recommended by the manufacturer: (1) Wetting the materials continuously, at least during the day, for about two days. (2) Once the stockpile is fully wetted, reduce this frequency and wet the stockpile only to maintain the material surface wet throughout the pile. This process is continued for a week until the material is wet enough, with enough pores filled, so as to pump the concrete successfully. However in the laboratory the fine aggregate was soaked for one week and drained for one day before batching.

5.2.4.3. Mix-design, Test Setup and Materials

In these series of tests, seven different concrete mixtures were investigated. The compositions of these cement blends are shown in Table 5.3. For the first three series, only gypsum dehydrate was used. According to the patent, it is recommended that gypsum dehydrate be used up to the addition rate of 10%. If more sulfur trioxide is needed, the remainder should be added as anhydrous gypsum. As a result from the fourth to seventh series of tests, both, gypsum dehydrate and anhydrous gypsum, were employed.

The mix designs for these seven types of concrete mixtures are shown in Table 5.4. The water cement ratios were 1:0.32. It can be seen from Table 5.4 that there was considerable absorbed

moisture in the aggregate. This was necessary for pumping purposes. In order to increase the workability of the concrete, a middle range water reducer was used. Even though high workability was desirable, aggregate segregation was a concern when the light-weight aggregates were used. In this above proposed strengthening technology, concrete is cast into relatively narrow space. So the higher the workability of the concrete, the easier the implementation will be in the field.

Table 5.3 Compositions of the Seven Cement Blends

Group	Portland cement type III	Calcium aluminate cement	Sulfur trioxide (SO ₃)	Gypsum dehydrate	Anhydrous gypsum
I	87%	5%	3.7%	8%	/
II	72.5%	6%	10%	21.5%	/
III	49.3%	12%	18%	38.7%	/
IV	30.4%	18%	24%	51.6%	/
V	74.9%	6%	10%	10%	9.1%
VI	66.1%	8%	14%	10%	15.9%
VII	55.3%	12%	18%	10%	22.7%

(The sulfur trioxide was provided by gypsum dehydrate and anhydrous gypsum)

Table 5.4 Concrete Mix Design for 1 yard³ (0.76 m³)

Material	Batch weight	
	lb	kg
Cement	705	320.1
Coarse aggregate @35.6% Moist.	825	374.6
Fine aggregate @25.0% Moist.	938	425.9
Added Water	225	102.2
Mid-range water reducer 997	78 oz	2306 ml

(Unit conversion: 1 yard³ = 0.76 m³, 1 lb = 0.454 kg, and 1 oz = 29.57 ml)

The FRP pipes with open ends were set on a wood plate, and silicon paste was used to seal the seam between the pipe and the wood plate to prevent water leakage during casting of the concrete. Then the light-weight expansive concrete was cast inside the GFRP pipes. Before casting strain gages were installed at mid-height, three-quarter height and 0.5 in (1.3cm) from top locations along the hoop direction of the pipes to measure the hoop direction strains in the pipes as shown in Figure 5-3. There were nine strain gages for each specimen, and each test group had three specimens. The test matrix is shown in Table 5.5, and the locations of the strain gages on typical specimens for the seven groups are shown in Figure 5-3.

Table 5.5 Test Matrix

Test group	Type of the GFRP pipe	Strain gages locations
I	Open pipe	Middle, three quarter and top
II	Open pipe	Middle
III	Open pipe	Middle
IV	Open pipe	Middle
V	Open pipe	Middle, three quarter and top
VI	Open pipe	Middle, three quarter and top
VII	Open pipe	Middle, three quarter and top

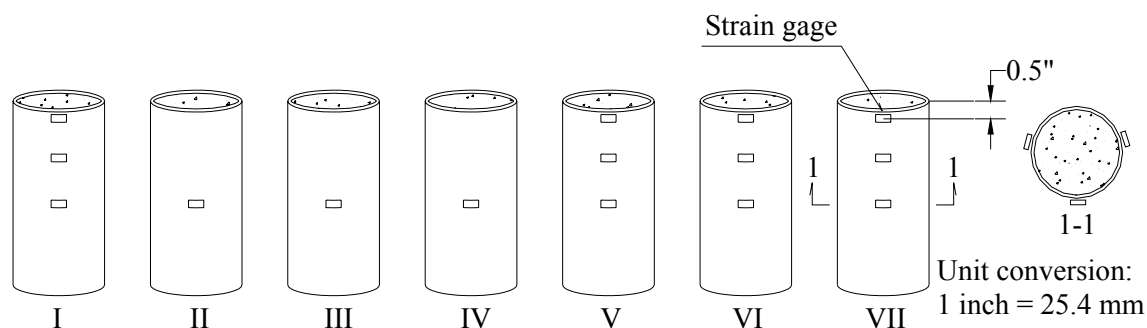


Figure 5-3 Strain Gages on Specimens of the Seven Groups

5.2.4.4. Specimen Curing Environment

After casting, all the specimens were cured for five months in the lab environment until the expansion of the concrete stabilized. The temperature in the lab was near 72°F (22° C).

5.2.4.5. Test Results, Discussion and Conclusions

The hoop direction strains in the pipes were recorded every two days up to five months until they stabilized. The hoop direction stresses developed in the pipes were directly calculated from these strains by multiplying the modulus of elasticity along the hoop direction of the pipes. The internal pressure developed in the concrete was calculated by:

$$P_{concrete} = \frac{\sigma_{FRP} \cdot 2t}{D} \quad \text{Eq. 5.1}$$

where σ_{FRP} is the hoop direction stress developed in the GFRP pipe, $P_{concrete}$ is the internal pressure developed in the concrete, t is the thickness of the GFRP pipe, and D = inside diameter of the GFRP pipe.

The force balance mechanism is shown in Figure 5-4.

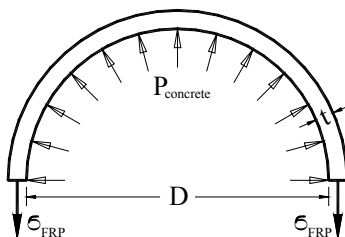


Figure 5-4 Force Balance Mechanism

Hoop stresses developed in the GFRP pipes at center and the internal pressures developed in the concrete for the seven concrete mixtures are shown in Figure 5-5 and Figure 5-6. It can be seen from the figures that the hoop stresses developed in the GFRP pipes or the internal pressure of the concrete increased rapidly in the early stages, then increased slowly and finally stabilized. The internal pressures for the seven groups of expansive concrete varied between 60 psi (0.41 MPa) and approximate 800 psi (5.52 MPa), and the hoop direction stresses developed in the GFRP pipes (confinement pressure) varied from 2 ksi (13.8 MPa) to approximate 25 ksi (172.4 MPa).

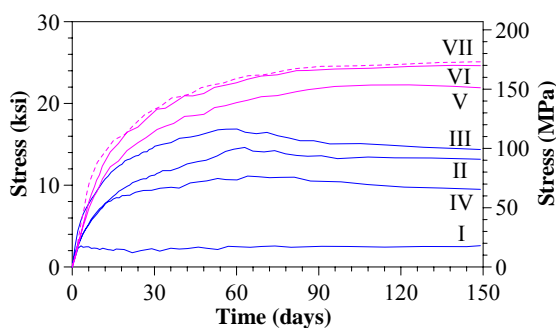


Figure 5-5 Stress Developed in GFRP Pipes vs. Time

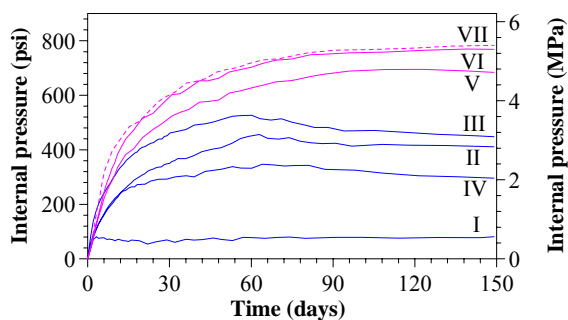


Figure 5-6 Internal Pressure of the Concrete vs. Time

The relationship between the internal pressures and the calcium aluminate cement percentage in total cement weight, and the relationship between the internal pressures and the sulfur trioxide percentage in total cement weight are shown in Figure 5-7 and Figure 5-8 respectively.

For the same stiffness of the confining device used in this project, concrete compositions can be chosen from these two curves according to the desired internal pressure developed in this type of light-weight expansive concrete.

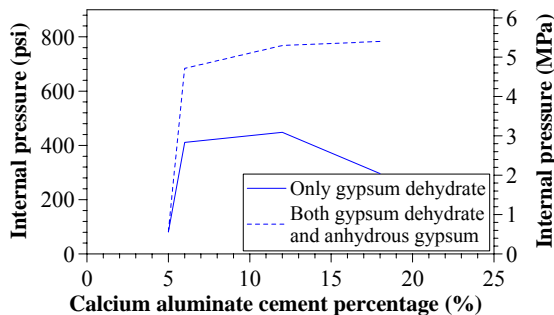


Figure 5-7 Internal Pressure of Concrete vs. Calcium Aluminate Cement Percentage in Total Cement Weight

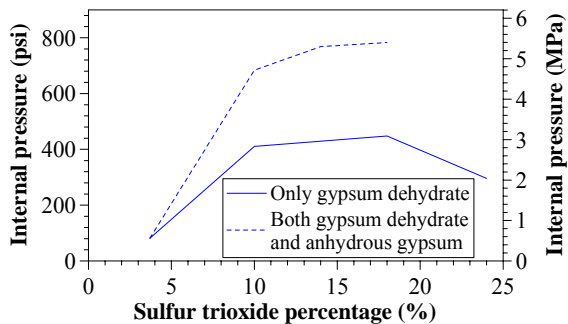


Figure 5-8 Internal Pressure of Concrete vs. Sulfur Trioxide Percentage in Total Cement Weight

The internal pressure distributions along the height of the pipes for test group VI and VII are shown in Figure 5-9 and Figure 5-10.

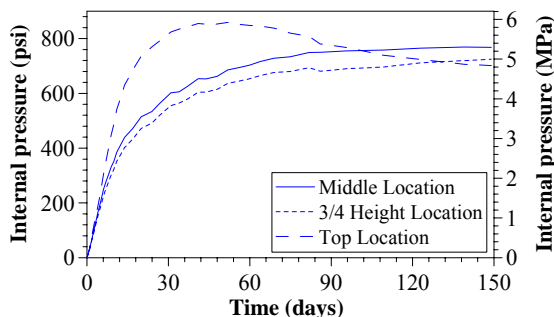


Figure 5-9 Internal Pressures of Concrete at Different Height Locations vs. Time (Group VI)

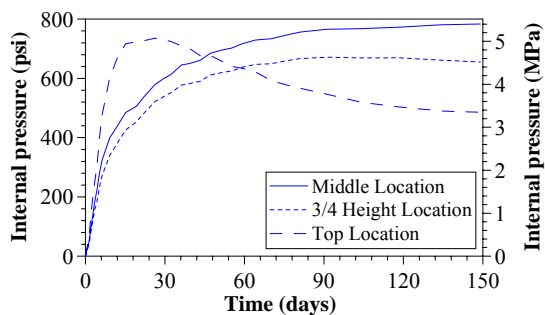


Figure 5-10 Internal Pressure of Concrete at Different Height Locations vs. Time (Group VII)

It can be seen that the ultimate internal pressures developed in the concrete at middle locations were higher than the pressures at 3/4 height and top locations. This phenomenon was due to the different constraining conditions at different locations, since these tests used open GFRP pipes with no constraint along the longitudinal direction. Higher pressures will develop in the central region of the pipes. In the early stages the pressure developed in the concrete at the top location was higher than the pressure developed at other locations which could have resulted from water

concentration content and fine aggregates near the top. However, final internal pressures developed at different locations in the concrete which are consistent with expected distribution. Slumps for the seven concrete groups were measured after mixing and the densities were also recorded at 56 days. Results are shown in Table 5.6.

Table 5.6 Slumps and Densities for the Seven Groups of Concrete

Group	Portland cement type III	Calcium aluminate cement	Sulfur trioxide	Slump		Density	
				in	mm	pcf	kg/m ³
I	87%	5%	3.7%	5	127	105	1683
II	72.5%	6%	10%	3	76.2	103	1651
III	49.3%	12%	18%	2	50.8	103	1651
IV	30.4%	18%	24%	1	25.4	102	1635
V	74.9%	6%	10%	3	76.2	105	1683
VI	66.1%	8%	14%	3	76.2	103	1651
VII	55.3%	12%	18%	2	50.8	103	1651

(The sulfur trioxide was provided by gypsum dehydrate and anhydrous gypsum

Unit conversion: 1 inch = 25.4 mm, and 1 pcf = 16.03 kg/m³)

It was also observed that the workability of the concrete with higher amounts of gypsum and calcium aluminate cement was not satisfactory although the middle range water reducer was used up to the maximum recommended limit during mixing of the concrete. Thus, it may be concluded that higher amounts of gypsum and calcium aluminate cement resulted in lower workability of the concrete mixture as a result of the formation of the expansive agent (ettringite).

Based on these series of tests, the following conclusions can be reached:

- 1) The internal pressure developed in the expansive concrete increased with increasing the amounts of calcium aluminate cement and sulfur trioxide.
- 2) Up to a certain amount of calcium aluminate cement and sulfur trioxide, the pressure increased with increasing calcium aluminate cement and Sulfur trioxide's quantity. After that point, there was a decrease in pressure for increasing the amount of calcium aluminate cement and Sulfur trioxide.
- 3) The stresses developed in the confining device or the internal pressures of the concrete were different at different heights.

- 4) Calcium aluminate cement and Sulfur trioxide decreased the workability of the expansive concrete.
- 5) For a given stiffness of the confining device, the composition of the light-weight expansive concrete can be designed according to the desired internal pressure developed in the concrete.

5.2.5. GFRP CONFINED CONCRETE COMPRESSION TEST

5.2.5.1. Test Specimens

The specimens used in these concrete compression tests were those used during the expansion test series as shown in Table 5.1. However, only two specimens were tested per group. Each test group had two specimens. The GFRP confined light-weight expansive concrete cylinders were cured in the lab for 56 days and then were tested.

5.2.5.2. Test setup and Test Matrices

Axial load was applied directly to the concrete core only. Three strain gages were applied to the GFRP pipes at the middle height to monitor the development of hoop strains. In addition, a longitudinal LVDT was attached to the top of the concrete cylinders to measure the longitudinal displacement. The test setup is shown in Figure 5-11.

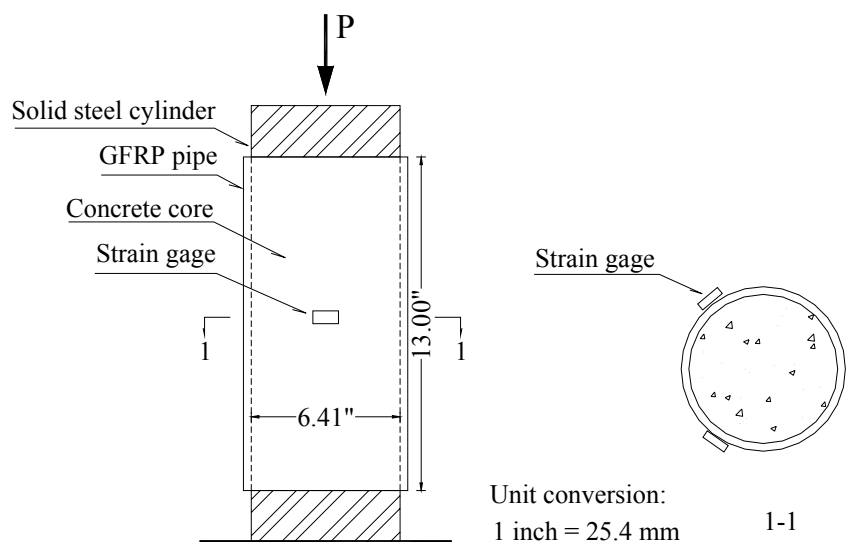


Figure 5-11 Instrumentation of the Compression Test

5.2.5.3. Test Results, Discussions, and Conclusions

The failure mode of the specimens was characterized by fracture of the GFRP pipes along a diagonal line. Four typical failed specimens are shown in Figure 5-12.



Figure 5-12 Typical Failed Specimens

The engineering properties of GFRP confined concrete are shown in Table 5.7. Each test group had two specimens. The modulus of elasticity of the concrete was calculated from the longitudinal stress change divided by the longitudinal strain change in the longitudinal stress range from 0 ksi (0 MPa) to 2 ksi (14 MPa). The elastic modulus of these seven expansive concrete mixtures varied from approximate 70 ksi (483 MPa) to approximate 1600 ksi (11034 MPa). The confined ultimate compressive strength varied from 7 ksi (50 MPa) to 9 ksi (64 MPa).

Table 5.7 Results of GFRP Confined Concrete Tests

Group	Modulus of Elasticity		Compressive Strength	
	ksi	MPa	ksi	MPa
I Calcium aluminate cement 5% Sulfur trioxide 3.7%	1617	11154	9.20	63.4
	1604	11058	9.32	64.3
II Calcium aluminate cement 6% Sulfur trioxide 10%	466	3216	8.89	61.3
	431	2971	8.78	60.5
III Calcium aluminate cement 12% Sulfur trioxide 18%	162	1115	8.00	55.2
	138	953	8.13	56.1
IV Calcium aluminate cement 18% Sulfur trioxide 24%	73	501	7.35	50.7
	81	561	7.35	50.7
V Calcium aluminate cement 6% Sulfur trioxide 10%	591	4077	8.88	61.2
	636	4385	8.84	61.0
VI Calcium aluminate cement 8% Sulfur trioxide 14%	320	2208	8.12	56.0
	334	2302	8.41	58.0
VII Calcium aluminate cement 12% Sulfur trioxide 18%	234	1617	7.25	50.0
	247	1705	8.88	61.2

Longitudinal stresses vs. longitudinal strains and longitudinal stresses vs. transverse strains are shown in Figure 5-13 and Figure 5-14. Results from the second specimen were nearly the same and as such not shown here for brevity.

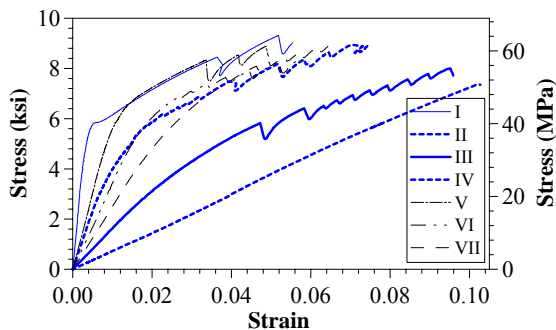


Figure 5-13 Longitudinal Stress vs. Longitudinal Strain

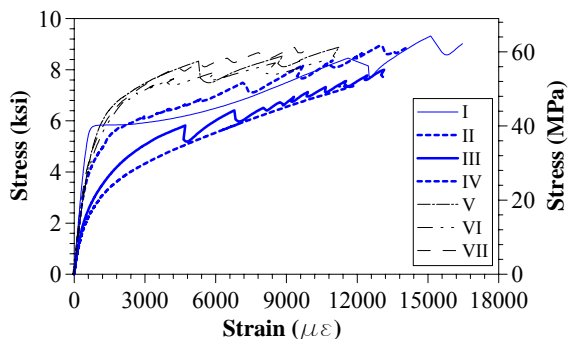


Figure 5-14 Longitudinal Stress vs. Transverse Strain

The following conclusions may be drawn from this series of tests:

- 1) The failure mode of these confined concrete cylinders was by fracture of the GFRP pipes.
- 2) Higher amounts of calcium aluminate cement and sulfur trioxide resulted in higher expansion, lower elastic modulus and compressive strength and decrease the concrete workability.

5.2.6. RELATIONSHIP BETWEEN INTERNAL PRESSURE DEVELOPED IN THE CONCRETE AND CONFINING STIFFNESS

5.2.6.1. Test Specimens and Instrumentations

In order to establish a relationship between internal pressures developed in the concrete and the confinement stiffness, pipes fabricated with different materials were used.

The test specimens for this test series were steel, GFRP and aluminum pipes with different diameters and thickness. The internal pressure developed in the expansive concrete can be related to the modulus of elasticity, thickness and diameter of the pipe as shown in Eq. 5.1, as such the confining stiffness of the pipe was defined as $E*2t/D$ as shown in the following table. The properties of the test specimens are shown in Table 5.8.

Table 5.8 Properties of Test Specimens

Specimen	Modulus of Elasticity		Inside diameter D		Thickness t		Height H		Confining stiffness $E*2t/D$	
	ksi	MPa	in	mm	in	mm	in	mm	ksi	MPa
I (GFRP)	4200	28963	6.4	163	0.1	2.54	13	330	131	903
II (Aluminum)	10000	68960	3.80	96	0.1	2.54	8	203	526	3629
III (Steel)	29000	199984	4.31	109	0.09	2.29	9	229	1211	8354
IV (Steel)	29000	199984	5.90	150	0.132	3.35	12	305	1297	8948

Compositions for the cement mixture for this test series are shown in Table 5.9. Due to the problems with the workability of the concrete experienced in the previous test series, the water cement ratio was increased to 1:0.4 in this test series.

Table 5.9 Compositions of the Cement Blend

Portland cement type III	Calcium aluminate cement	Sulfur trioxide (SO ₃)	Gypsum dehydrate	Anhydrous gypsum
74.9%	6%	10%	10%	9.1%

(The sulfur trioxide was provided by gypsum dehydrate and anhydrous gypsum)

Three strain gages were applied at the middle height of each specimen, and the strains were recorded for about two months until the expansion of concrete stabilized.

5.2.6.2. Test Results, Discussion and Conclusions

The lateral strains and stresses in the pipes and internal pressures developed in the concrete versus time are shown in Figure 5-15 to Figure 5-17. The stresses developed in the pipes or internal pressures developed in the expansive concrete increased rapidly during early stages, then slowed down and finally stabilized. The final internal pressure of concrete vs. confining stiffness curve is shown in Figure 5-18.

Similar to other research findings (Mortazavi, 2001), the following conclusion may be inferred from the presented test results:

- 1) The higher the stiffness of the confinement, the higher internal pressure developed in the confined expansive concrete.

- 2) For a desired internal pressure developed in this type of light-weight expansive concrete, the compositions of the concrete and the type of confining pipe can be decided empirically from curves as shown in Figure 5-7, Figure 5-8 and Figure 5-18.

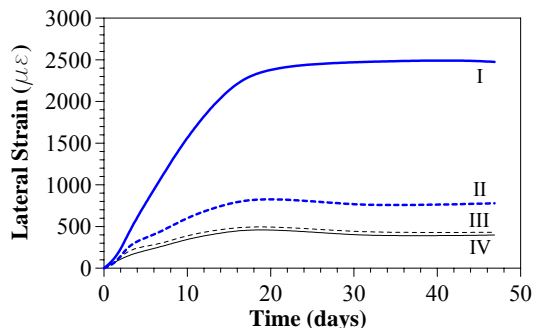


Figure 5-15 Lateral Strain vs. Time

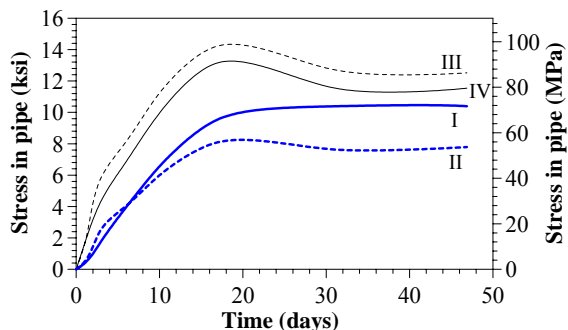


Figure 5-16 Stress in Pipe vs. Time

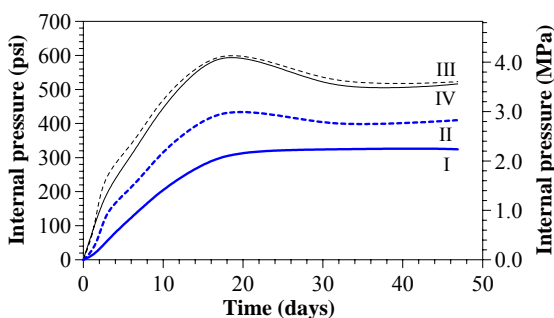


Figure 5-17 Internal Pressure vs. Time

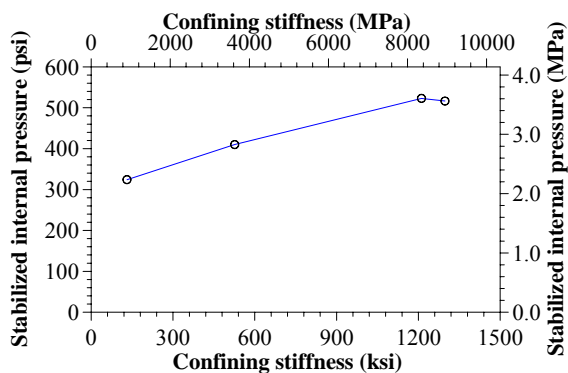


Figure 5-18 Stabilized Internal Pressure vs. Confining Stiffness ($E \cdot 2t/D$)

5.2.7. SUMMARY

In this report, the experimental results of FRP confined high expansion degree concrete were presented. The relationship between expansion of this type of light-weight expansive concrete investigated here and the compositions of the concrete mixtures, engineering properties of these FRP confined expansive concrete, and the relationship between the internal pressure developed in the concrete and confining stiffness were discussed. For a desired internal pressure developed in this type of light-weight expansive concrete, the compositions of the concrete and the properties of confining pipe can be empirically decided from the test results.

This type of light-weight expansive concrete based on type M cement can provide higher expansion than the concrete made according to ASTM C845. The disadvantage was the expansion of this type of concrete results from adding gypsum and calcium aluminate cement to the Portland cement. This condition lowered the modulus of elasticity, and a higher expansion than desired was obtained. More research should be conducted on this topic focusing on how to obtain a higher expansion degree concrete without decreasing the modulus of elasticity significantly.

5.3. LOCAL BOND-SLIP RELATIONSHIP BETWEEN SMOOTH STEEL BARS AND FRP CONFINED EXPANSIVE LIGHT-WEIGHT CONCRETE

5.3.1. OBJECTIVE

Twelve FRP confined concrete cylinders, six of them using light-weight concrete and the remaining six using expansive light-weight concrete, were fabricated with smooth steel bars using different bonded lengths. These specimens were tested and analyzed to better understand bond mechanisms and the influences of different concrete mixtures, FRP confinement and confining pressure on bond performance between smooth steel bars and FRP confined concrete. In addition, an analytical model of bond-slip relationship based on a modified Bertero-Eligehausen-Popov model was evaluated in light of the test results. The parameters of the bond-slip model were calibrated using a numerical approach. The detailed experimental and analytical results are presented in this report.

5.3.2. BACKGROUND

The premise for the success of the proposed FRP strengthening method developed in this report is in the ability to transfer the internal forces from a region of the steel column not retrofitted to one strengthened with the proposed method. Since the transfer of stresses by bond from the steel members to the concrete is of interest, there is a need to determine the local bond slip relationship between the two, especially to evaluate the interaction phenomena between smooth steel materials and the FRP confined concrete mixtures with higher expansion. The advantage of the expansive concrete is that expansion of concrete should increase the friction between the concrete and steel materials, which will translate into shorter transfer length. The problem is however complicated by the fact that expansion in concrete is attained with a loss of stiffness (i.e. reduction of E_c)

5.3.3. TEST SPECIMENS AND MATERIALS

5.3.3.1. GFRP Pipes

In this series of tests, a GFRP pipe was selected because glass-FRP materials are widely used in civil structures and they are relatively inexpensive compared to other types of FRP composites. The properties of the glass FRP pipe (provided by the manufacturer) are shown in Table 5.10.

Table 5.10 Properties of the GFRP Pipe

	Inside diameter		Height		Thickness		Modulus of elasticity of hoop direction		Tensile strength	
	in	mm	in	mm	in	mm	ksi	MPa	ksi	MPa
GFRP pipe	6.4	162	13	330	0.1	2.5	4200	28963	70	483

(Unit conversion: 1 inch = 25.4 mm, and 1 ksi = 6.896 MPa)

5.3.3.2. Steel Bars

Hot-rolled smooth steel bars (not deformed steel bars) were employed in the series of pull-out tests due to the similarity of the surface typical built-up steel column of interest. The properties of the steel bars (developed in the lab) are shown in Table 5.11.

Table 5.11 Properties of Steel Bar

Material	Modulus of elasticity		Tensile yield strength		Diameter	
	ksi	MPa	ksi	MPa	inch	mm
Hot-rolled steel	29000	199984	60	414	0.5	12.7

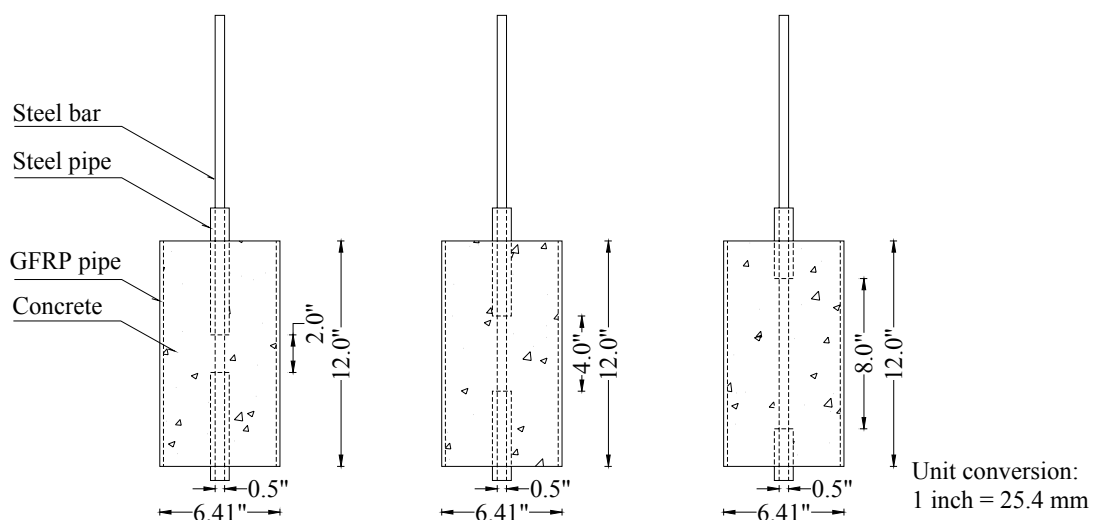
5.3.3.3. Light-weight Concrete

Since a reduction in weight is preferred in retrofit type application, two types of light-weight concrete were investigated in this test series. One was ordinary light-weight concrete without expansion, and the other was expansive light-weight concrete. The mechanical properties of these two concretes, which were measured on cylinder concrete confined with GFRP pipe at 56 days, are shown in Table 5.12.

Test specimens were fabricated with the above mentioned materials. The specimens were GFRP confined concrete cylinders with hot-rolled smooth steel bars in the cylinder center with different bonded lengths. Test specimens are shown in Figure 5-19. Steel pipes as shown in the figure were selected to control the embedment length of the steel bars in the concrete because of the concrete expansion. The test matrix is shown in Table 5.13.

Table 5.12 Engineering Properties of the GFRP Confined Concrete

	Modulus of elasticity		Ultimate compression strength		Density		Stabilized internal pressure	
	ksi	MPa	ksi	MPa	pcf	MPa	psi	MPa
Light-weight concrete	1300	8695	10	69	105	1683	0	0
Expansive light-weight concrete	1000	6896	10	69	105	1683	350	2.4

**Figure 5-19 Test Specimens****Table 5.13 Test Matrix**

Group	Type of concrete	Embedment length		Specimen identification
		in	mm	
I	Light-weight concrete	2	50.8	L2-1
				L2-2
		4	101.6	L4-1
				L4-2
		8	203.2	L8-1
				L8-2
II	Expansive light-weight concrete	2	50.8	EL2-1
				EL2-2
		4	101.6	EL4-1
				EL4-2
		8	203.2	EL8-1
				EL8-2

The adopted specimen notation indicates the type of concrete (L: light-weight concrete; EL: expansive light-weight concrete), the embedment length (first number: 2in, 4in and 8in), and the specimen identification number (1 or 2).

5.3.4. TEST SETUP AND INSTRUMENTATION

The pull-out tests were carried out on the GFRP confined concrete cylinders, and were performed using a testing machine under displacement control. There were three ± 0.05 in DCVTs with $1/10000$ in accuracy in this test setup. The slips at the loaded bar end and unloaded (free) bar end were measured by the first two DCVT1 and DCVT2, and the third DCVT3 was used to measure the deformation of concrete. A strain gage was also applied to the steel bar to record its elongation. The actual load end slip between concrete and steel bar was calculated from the values of DCVT1, DCVT3 and the strain gage. The test setup is shown in Figure 5-20.

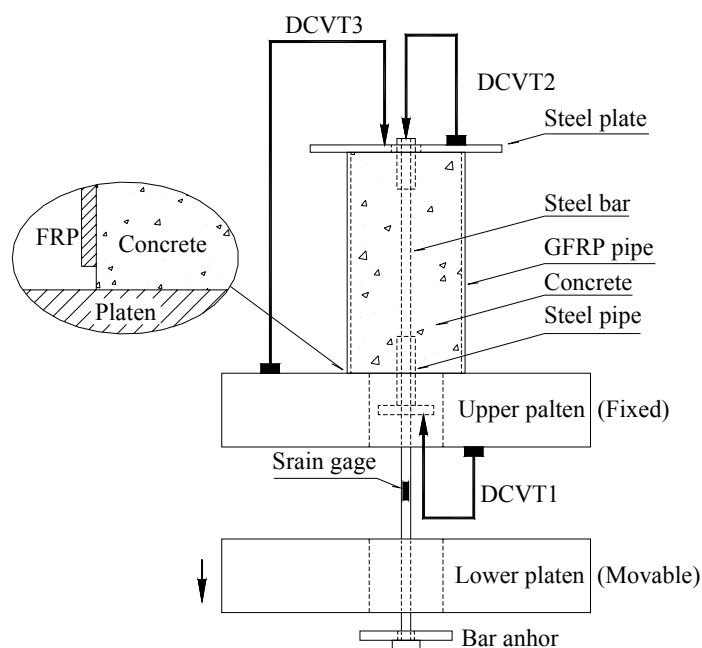


Figure 5-20 Test Setup and Instrumentations

5.3.5. TEST RESULTS AND DISCUSSION

Test results in terms of maximum pull-out load, average bond strength, slip according to peak pull-out load and failure mode are summarized in Table 5.14. Test results indicated that the maximum pull-out loads of the specimens of Group II were slightly higher than Group I. This

can be explained as the expansion of the concrete increased the friction between steel and concrete.

In

Table 5.14, P_{\max} is the maximum pull-out load; $\bar{\tau}_{\max}$ is the maximum average bond strength; s_m is the free end slip of steel bar when pull-out load reaching peak value P_{\max} . The average bond strength $\bar{\tau}_{\max}$ was calculated as follows:

$$\bar{\tau}_{\max} = \frac{P_{\max}}{\pi \cdot d_b \cdot l_b} \quad \text{Eq. 5.2}$$

where d_b is the nominal diameter, and l_b is the bonded length of the bar.

Table 5.14 Test Results

Group	Specimen	P_{\max}		$\bar{\tau}_{\max}$		s_m	
		kips	KN	ksi	MPa	in	mm
I	L2-1	1.65	7.35	0.53	3.63	0.0027	0.068
	L2-2	1.42	6.31	0.45	3.11	0.0090	0.229
	L4-1	3.24	14.42	0.51	3.55	0.0053	0.135
	L4-2	2.92	12.98	0.46	3.20	0.0042	0.107
	L8-1	6.06	26.97	0.48	3.33	0.0045	0.114
	L8-2	5.21	23.17	0.41	2.86	0.0047	0.119
II	EL2-1	2.54	11.32	0.81	5.58	0.0004	0.010
	EL2-2	2.19	9.73	0.70	4.80	0.0003	0.008
	EL4-1	3.31	14.74	0.53	3.64	0.0012	0.030
	EL4-2	3.31	14.71	0.53	3.63	0.0026	0.066
	EL8-1	6.16	27.39	0.49	3.38	0.0020	0.051
	EL8-2	6.26	27.86	0.50	3.44	0.0019	0.048

(All test specimens were failed by pull-out.)

Load vs. free-end-slip responses for Group I (light-weight concrete) and Group II (expansive light-weight) concrete are shown in Figure 5-21 and Figure 5-22. There were two parts in these relationships: one was ascending part, and the other was descending part. It can be seen that for these types of GFRP confined light-weight concrete specimens, the maximum free-end-slips of the bars at peak load were very small.

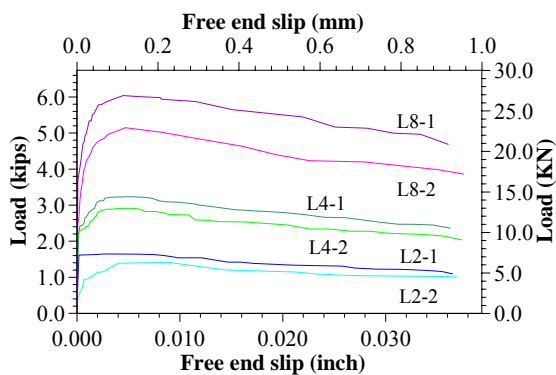


Figure 5-21 Load vs. Free End Slip of Group I

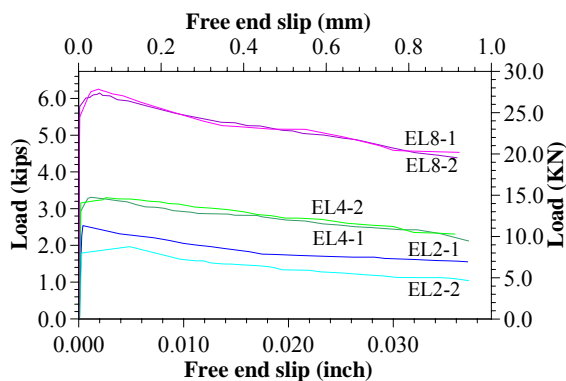


Figure 5-22 Load vs. Free End Slip of Group II

The values of these slips varied from 0.0003in (0.008mm) to 0.009in (0.229mm). Because of this, the load-end-slip calculated from DCVT2, DCVT3 and strain gage was not sufficiently accurate for analyzing the ascending part of the load vs. load-end-slip response. In particular, the following factors were critical: a) Very small slip at peak load. b) Non-perfect flatness of concrete surface. c) Un-straightness of the steel bar. d) Point where DCVT3 measured for concrete deformation could not be the interface between steel bar and concrete. So the loads vs. load-end-slips of the bars were not considered for analysis.

5.3.6. ANALYTICAL MODEL

In this report, only the load vs. free end-slip results were used to calibrate these parameters, according to the analytical model described in section 2.1.4.2. The results from these experimental and analytical studies are shown in Table 5.15, Figure 5-23 and Figure 5-24.

The average local bond-slip relationships for Group I and II considering all the test results were also shown in Figure 5-23 and Figure 5-24. It should be mentioned that the result of specimen EL2-1 was not considered when calibrating all the test results to get the average bond-slip relationship for Group II due to the abnormal peak bond stress value as indicated in Figure 5-24. The local bond-slip relationship between a hot-rolled smooth steel bar and FRP confined light-weight concrete can be computed by Eq. 5.3 (US custom system):

$$\tau(s) = 1.032s^{0.14} \left(1 - \frac{s}{0.0742} \right) \quad \text{Eq. 5.3}$$

And Eq. 5.4 in metric system is:

$$\tau(s) = 4.5s^{0.14} \left(1 - \frac{s}{1.88} \right) \quad \text{Eq. 5.4}$$

The local bond-slip relationship between a hot-rolled smooth steel bar and FRP confined expansive light-weight concrete can be computed by Eq. 5.5(US custom system):

$$\tau(s) = 0.754s^{0.07} \left(1 - \frac{s}{0.0822} \right) \quad \text{Eq. 5.5}$$

And Eq. 5.6 in the metric system is:

$$\tau(s) = 4.16s^{0.07} \left(1 - \frac{s}{2.09} \right) \quad \text{Eq. 5.6}$$

Table 5.15 Calibrated Parameters of mBEP Model

Specimen	C		a	\bar{s}	
	ksi	MPa		in	mm
L2-1	0.821	4.39	0.08	0.079	2.01
L2-2	2.098	5.78	0.29	0.046	1.17
L4-1	1.031	4.78	0.13	0.074	1.89
L4-2	0.740	3.86	0.09	0.085	2.16
L8-1	1.017	4.57	0.13	0.080	2.04
L8-2	1.110	4.36	0.17	0.060	1.52
Average	1.032	4.50	0.14	0.074	1.88
EL2-1	1.148	5.96	0.09	0.079	2.00
EL2-2	1.353	5.50	0.16	0.056	1.43
EL4-1	0.998	4.70	0.12	0.070	1.78
EL4-2	0.779	4.32	0.07	0.081	2.06
EL8-1	0.514	3.45	0.01	0.115	2.91
EL8-2	0.559	3.61	0.02	0.098	2.50
Average	0.754	4.16	0.07	0.082	2.09

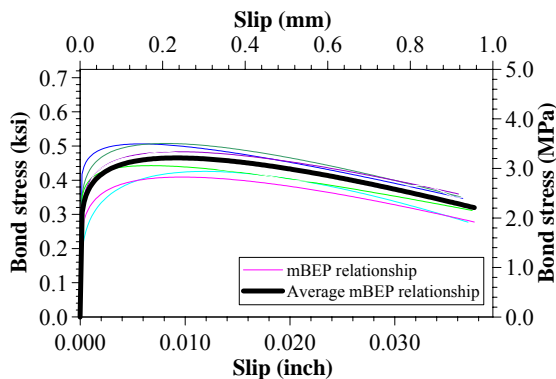


Figure 5-23 mBEP Local Bond Slip Laws for Group I

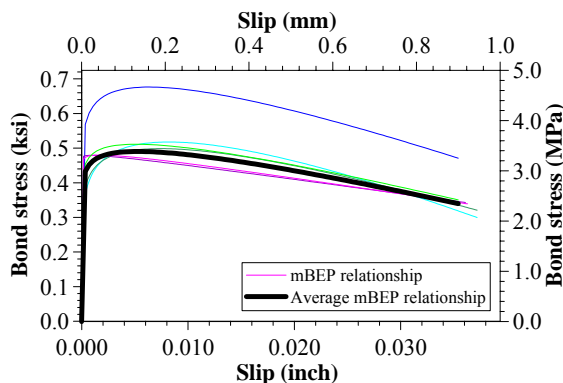


Figure 5-24 mBEP Local Bond Slip Laws for Group II

These bond-slip expressions can be used to solve engineering problems, such as anchorage length of bar in the concrete. For example, a smooth steel bar, with a diameter of 0.5in (12.7 mm), and a modulus of elasticity of 29000ksi (200GPa), is embedded in the above type of FRP confined light-weight concrete. The minimum anchorage length that would be needed to obtain no slip at the free end is 5in (127 mm), when a nominal tensile design force of 2.25 kips (10KN) is applied. If the same type of bar is embedded in the above type of FRP confined expansive light-weight concrete (incomplete sentence). The minimum anchorage length needed to obtain no slip at the free end is 3.6in (91mm), when a nominal tensile design force of 2.25 kips (10KN) is applied, as shown in Table 5.16.

Table 5.16 Anchorage Length Examples

		Group I	Group II
Type of concrete		FRP confined light-weight concrete	FRP confined expansive light-weight
Type of bar		Hot-rolled smooth steel bar	
		Modulus	
		29000 ksi	200 GPa
		Diameter	
		0.5in	12.7mm
Local bond-slip relationship	US	$\tau(s) = 1.032s^{0.14} \left(1 - \frac{s}{0.0742}\right)$	$\tau(s) = 0.754s^{0.07} \left(1 - \frac{s}{0.0822}\right)$
	Metric	$\tau(s) = 4.5s^{0.14} \left(1 - \frac{s}{1.88}\right)$	$\tau(s) = 4.16s^{0.07} \left(1 - \frac{s}{2.09}\right)$
Design tensile load		2.25 kips	10 KN
Anchorage length		4in	127 mm
			3.6in
			91 mm

(Unit conversion: 1kips = 4.45KN, and 1 inch = 25.4mm)

It can be seen that the anchorage length of a smooth steel bar embedded in FRP confined light-weight concrete is shorter than a smooth steel bar embedded in FRP confined expansive light-weight concrete.

5.3.7. CONCLUSIONS

Based on the test results and the local bond-slip relationship between smooth steel bars and FRP confined concrete, the following conclusions may be drawn:

- 1) The expansion of the concrete is helpful to get a better bond behavior between concrete and steel.
- 2) An analytical solution can be obtained for the design of development length.

5.4. FRP RETROFIT SCHEME FOR CORRODED STEEL COLUMNS

5.4.1. OBJECTIVE

This sub-task describes the research program undertaken to determine the feasibility of a proposed FRP retrofit method to strengthen the corroded steel columns. This method consists of two steps: wrapping the corroded steel column with open FRP jacket and filling the jacket with expansive light-weight concrete. Seven steel columns were tested in the laboratory with five strengthened using the proposed technique. The first two were used as control units with one being a virgin shape and the other notched in the center zone to simulate the loss of section due to corrosion. The remaining five, all notched, were wrapped with FRP composite tubes in the damage area and the tubes were filled with light-weight expansive concrete. All specimens were axially loaded to failure while strain and displacement readings were measured to demonstrate the validity of this repair concept. This section presents the experimental results and discusses the findings with preliminary conclusions on the feasibility of the proposed strengthening method.

5.4.2. TEST SPECIMENS AND TEST MATRIX

Seven 10 ft (3.05 m) long S4x9.5 steel columns (ASTM A36) were selected as the test specimens according to the layout depicted in Figure 5-27. The first two specimens were designed as control units. The first one was a virgin steel column without a notch, and the second one was

notched in the center zone to simulate severe corrosion. Test units 3 and 4, both notched, were wrapped with 3 ft (0.91 m) and 5 ft (1.52 m) long FRP composite tubes in the damaged area and the tubes were filled with light-weight concrete. Test units 5, 6 and 7, all notched, were wrapped with 1 ft (0.3 m) , 3 ft (0.91 m) and 5 ft (1.52 m) long FRP composite tubes in the damaged area and the tubes were filled with light-weight expansive concrete to demonstrate the active confinement effects which came from the FRP composite tubes and the expansive concrete. The test specimens are shown in Figure 5-25, and the test matrix is indicated in Table 5.17.



Figure 5-25 Test Specimens

Table 5.17 Test Matrix

Test Unit	Steel Shape	Length		Retrofit Scheme	Retrofit Length		Notch
		ft	m		ft	m	
1	S4x9.5	10	3.05	No	N.A.		No
2	S4x9.5	10	3.05	No	N.A.		Yes
3	S4x9.5	10	3.05	Light-weight Concrete & FRP pipe	3	0.91	Yes
4	S4x9.5	10	3.05	Light-weight Concrete & FRP pipe	5	1.52	Yes
5	S4x9.5	10	3.05	Expansive Light-weight Concrete & FRP pipe	1	0.30	Yes
6	S4x9.5	10	3.05	Expansive Light-weight Concrete & FRP pipe	3	0.91	Yes
7	S4x9.5	10	3.05	Expansive Light-weight Concrete & FRP pipe	5	1.52	Yes

(Unit conversion: 1 ft = 0.3048 m)

After casting of concrete inside the FRP jackets, all the retrofitted specimens were cured in the lab environment for two months until the internal pressures developed in the expansive concrete of test units 5 to 7 were stabilized. The properties of the GFRP jackets (provided by the manufacturer) are shown in Table 5.18.

Table 5.18 Properties of GFRP Pipe

	Inside diameter		Height		Thickness		Modulus of elasticity of hoop direction		Tensile strength	
	inch	mm	inch	mm	inch	mm	ksi	MPa	ksi	MPa
GFRP pipe	6.4	162	13	330	0.1	2.5	4200	28963	70	483

The FRP jackets used in this series of tests were entire FRP pipes, and the purpose was to simplify the construction of test units. In real field situations, the FRP jackets can be easily fabricated with slotted pipes or other open shapes bonded together by epoxy as shown in Figure 5-26. The engineering properties of the light-weight and expansive light-weight concrete confined by the above type of GFRP pipe used in this test program are shown in Table 5.19.

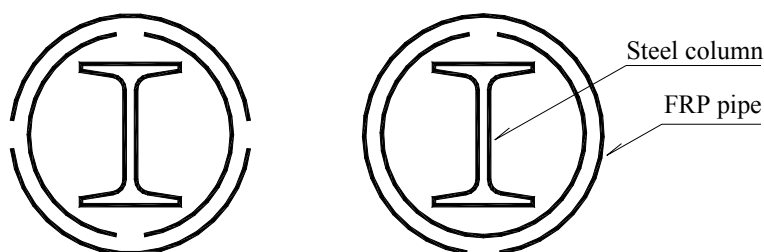


Figure 5-26 Fabrication Schemes of FRP Jackets

Table 5.19 Engineering Properties of GFRP Confined Concrete

	Modulus of elasticity		Ultimate compression strength		Density		Stabilized internal pressure	
	ksi	MPa	ksi	MPa	pcf	kg/m ³	psi	MPa
Light-weight concrete	1300	8965	10	69	105	1683	0	0
Expansive light-weight concrete	1000	6896	10	69	105	1683	350	2.4

(Unit conversion: 1 ksi = 6.896 MPa, 1 psi = 6896 Pa, and 1 pcf = 16.03 kg/m³)

Steel coupons were cut from a specimen and tested to failure to obtain the material properties of the steel. Test results are shown in Table 5.20. The notch of the section was applied in the middle of the steel shape and at either side of both flanges. The notch length was 1 foot (0.3 m) and the notch width was 0.625in (15.9 mm). Notch details are shown in Figure 5-27.

Table 5.20 Properties of Steel Material

Material	Modulus of elasticity		Yield strength	
	ksi	GPa	ksi	MPa
Hot-rolled steel (ASTM A36)	29000	200	60	414

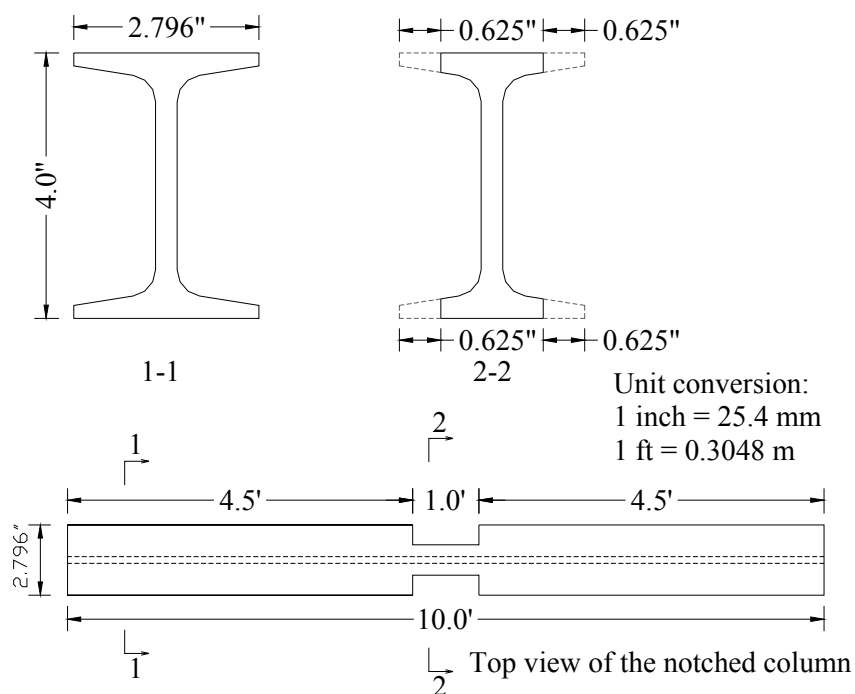


Figure 5-27 Notch Details

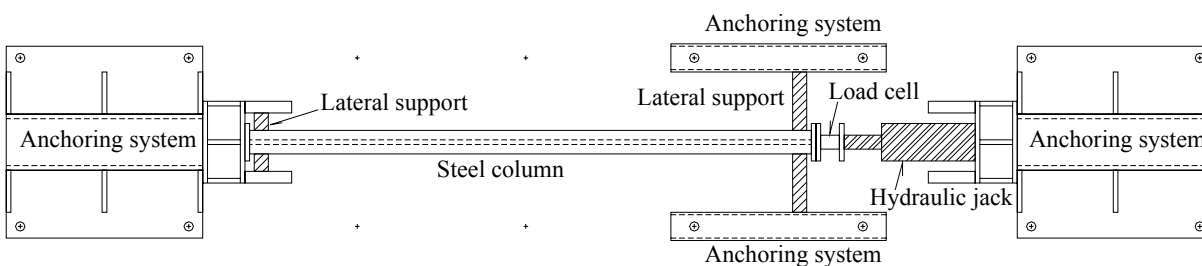
Comparison between area and moment of inertia of the notched cross and original cross sections are shown in Table 5.21. For the notched cross section, the remaining area was nearly 78.1% of the original value and remaining moment of inertia was approximately 21.1% of the original value.

Table 5.21 Notch Details

Section	Area		Moment of inertia along weak axis	
	in ²	mm ²	in ⁴	mm ⁴
Original cross section	2.79	1800	0.903	3.76x10 ⁵
Notched cross section	2.18	1406	0.191	7.95x10 ⁴
Remaining	78.1%		21.1%	

5.4.3. TEST SETUP AND INSTRUMENTATION

The length for all seven test specimens was 10 ft (3.05 m). During testing, all the specimens were set on the ground with the weak axis (y-y axis) perpendicular to the ground. Axial load was applied horizontally by one hydraulic jack, such that the steel columns buckled horizontally. Wood plates were inserted between the steel column and the anchoring systems to assure that the load was applied on the entire cross section. Four lateral supports were installed at both sides of two ends of the steel columns, such that the load could be applied to the cross section center. The top view of the test setup is shown in Figure 5-28.

**Figure 5-28 Test Setup**

For Test Units 1 and 2, the middle lateral deflections were measured by LVDTs. For Test Units 3 to 7, the middle lateral deflections and the lateral deflections at the location where the concrete and steel shape connected were measured by LVDTs. Two strain gages, located 10in (254mm) from the lateral supports, were installed on both sides of the web of the steel columns at one end. Two more strain gages were installed at the same location, but on the opposite end of the specimens. The actual loads applied to the specimens were back-calculated from these measured strains. For Test Units 1 and 2, two strain gages were installed on both sides of the web at the middle locations of the columns. For Test Units 3 to 7, strain gages were installed on both sides

of the web at the middle locations of the columns and the locations where the concrete and the steel shape connected (see Figure 5-29 for the details).

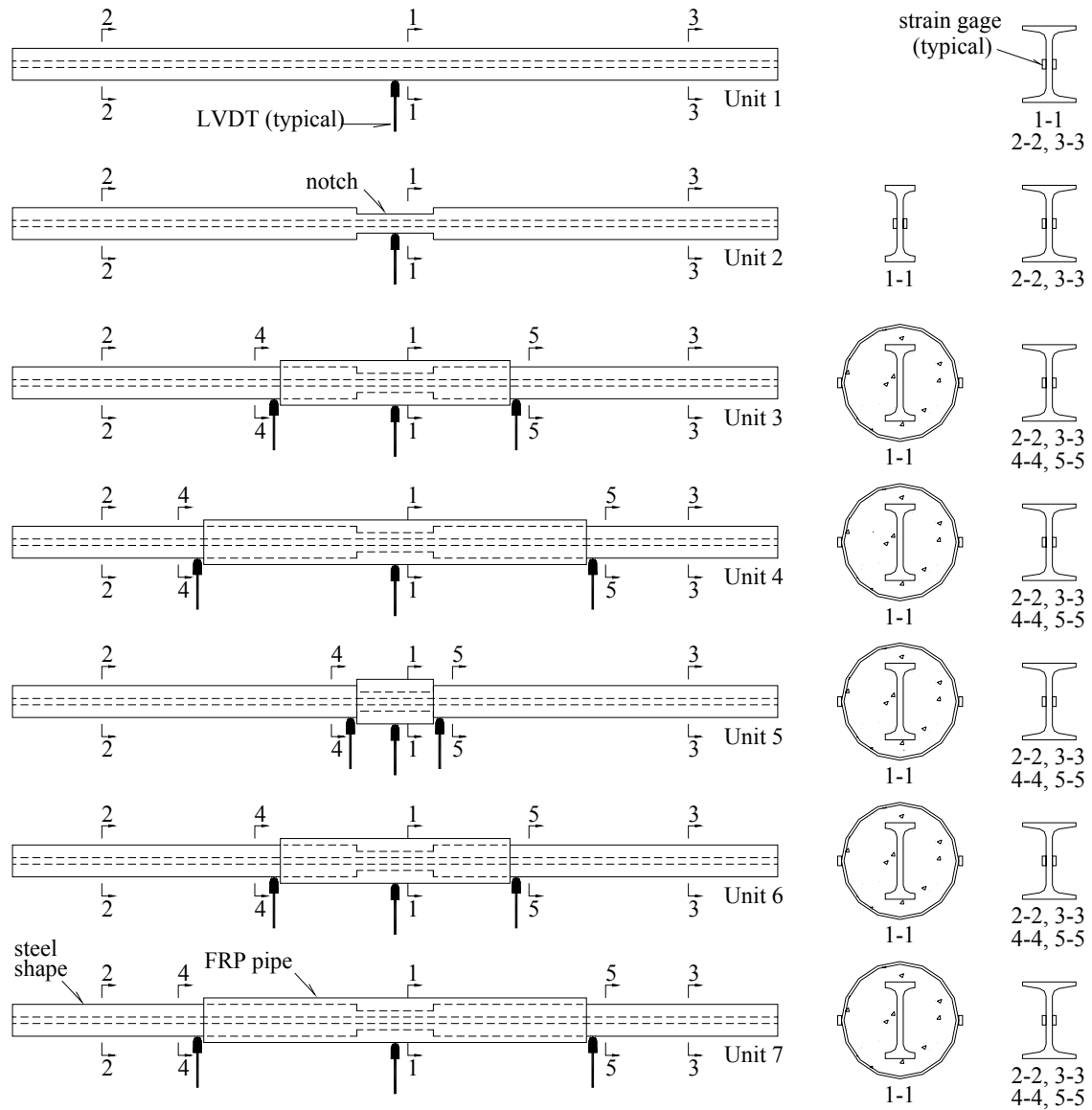


Figure 5-29 Distributions of LVDTs and Strain Gages

5.4.4. TEST RESULTS AND DISCUSSIONS

The failure mode for all the seven specimens was buckling, but the difference between different test specimens was in the buckling location. For test units 1 and 2, the structural shape buckled at its middle part. For test units 3, 4, 5, 6 and 7, buckling occurred at end of the termination of the jacket (see Figure 5-30 for details).



Figure 5-30 Failed Specimens

The test results of these seven columns are provided in Table 5.22. The ultimate load capacities of the notched specimens with different retrofit schemes increased dramatically compared to control unit 2 (notched specimen without retrofit). Test Unit 3 and 6, and Unit 4 and 7 had the same retrofitted length. The difference between them was that Unit 3 and 4 were strengthened with light-weight concrete, and Unit 6 and 7 were strengthened with expansive light-weight concrete. Test results indicated that the specimens retrofitted with expansive light-weight concrete had higher ultimate load capacities than the specimens strengthened with light-weight concrete. This can be explained as the effect of active confinement came from the FRP confining device and expansion of the concrete. The expansion of the concrete was confined by the FRP jacket, resulting in internal pressure and the increase of friction between the concrete and the steel column, thus resulted in higher stiffness of the retrofitted steel columns.

Table 5.22 Test Results

Test Unit	Ultimate load Capacity		Increase of load capacity compared to Test Unit 2	Increase of load capacity compared to Test Unit 1	Difference of theoretical value compared to experimental value
	kips	KN			
1 (virgin)	43.8	194.9	+69%	0%	-3%
2 (notched)	25.9	115.3	0%	-41%	-4%
3	68.2	303.5	+163%	+56%	-9%
4	74.3	330.6	+187%	+70%	+24%
5	41.1	182.9	+58%	-7%	+13%
6	77.3	344.0	+198%	+76%	-16%
7	86.4	384.5	+233%	+97%	+13%

(Unit conversion: 1 kips = 4.45 KN)

The load vs. deflection responses for the seven columns are shown in Figure 5-31. It should be mentioned that this figure shows the load vs. middle location deflection responses of Test Unit 1 and 2, and load vs. buckling location (not in the middle of the columns) deflection responses of Test Unit 3 to 7 due to the different buckling location for these seven specimens as mentioned before. For a perfectly straight column without load eccentricity, there is no lateral deflection before the axial load reaches the buckling load. But in reality, columns are rarely perfectly straight. Geometrical imperfection and load eccentricity, which are unavoidably present in an actual column, will cause the column to deflect laterally at the onset of loading. Consequently, the load-deflection curve of an imperfect column is a smooth curve as shown in Figure 5-31. The shape of the curve depends on the imperfection. It is shown from these load-deflection responses that these seven columns had different imperfections. After the axial loads reached the critical loads (buckling loads), then the capacity decreased as shown in Figure 5-31.

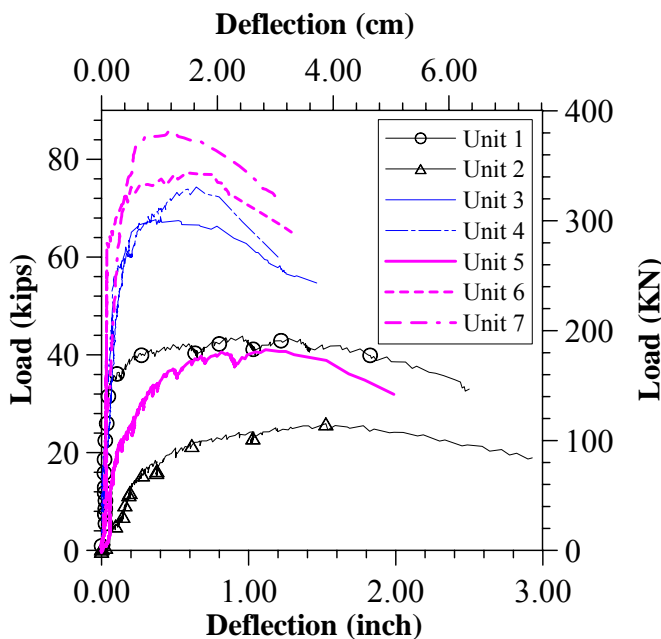


Figure 5-31 Load vs. Deflection

5.4.5. CONCLUSIONS

The following conclusions may be drawn based on the experimental results:

- 1) The proposed FRP retrofit method for corroded steel columns is feasible.
- 2) The active confinement effect resulting from the expansive concrete was helpful to increase the ultimate load capacities of the steel columns by using the proposed FRP strengthening method.

5.4.6. ANALYTICAL MODEL

The elastic buckling load for Test Unit 1 was developed by Euler in 1744, and can be found in any design book. The elastic buckling load for Test Unit 2 (with changes in cross section) can also be found elsewhere (Franke, 1901; Timoshenko, 1908; Maletz, 1932; and Falk, 1956) and shall therefore not be further discussed.

5.4.6.1. Composite Column

The retrofitted specimens (unit 3 to 7) with changes in the cross section were composite columns, and they did not buckle at their middle height location. So, the elastic buckling loads

were determined using energy methods by translating concrete materials into equivalent steel as follows:

$$I = \frac{E_s I_s + \alpha E_c I_c}{E_s} = I_s + \alpha \left(\frac{E_c}{E_s} \right) I_c \quad \text{Eq. 5.7}$$

The contribution of the FRP pipe on the moment of inertia was not taken into account. In Eq. 5.7, α is a factor accounting for the presence of cracks in the concrete. It was assumed $\alpha = 0.4$ for light-weight concrete according to ACI 318-95 and $\alpha = 0.6$ for expansive light-weight concrete. A larger value of α was used for expansive light-weight concrete to take into account that the expansion of concrete increases the friction between the concrete and steel materials.

5.4.6.2. Development Length

The column investigated in this project is a special type of composite column compared to a typical composite column. For typical composite columns, the axial load is directly applied to both the steel shape and the concrete core. But for the type of composite column studied in this project, the axial load is directly applied to the steel shape only. There are two reasons for this: a) the retrofit materials are only needed to strengthen the damaged zone (i.e. severe corrosion area in this proposed FRP retrofit method), b) it is difficult to connect the retrofit materials to the structural members at the extremity of the steel. As explained above, the axial load is transferred to the retrofit materials through a development length, and then the steel shape and the strengthened materials work together. In other words, the strains of the steel shape and the retrofit materials become the same after the development length. The load transfer mechanism is shown in Figure 5-32.

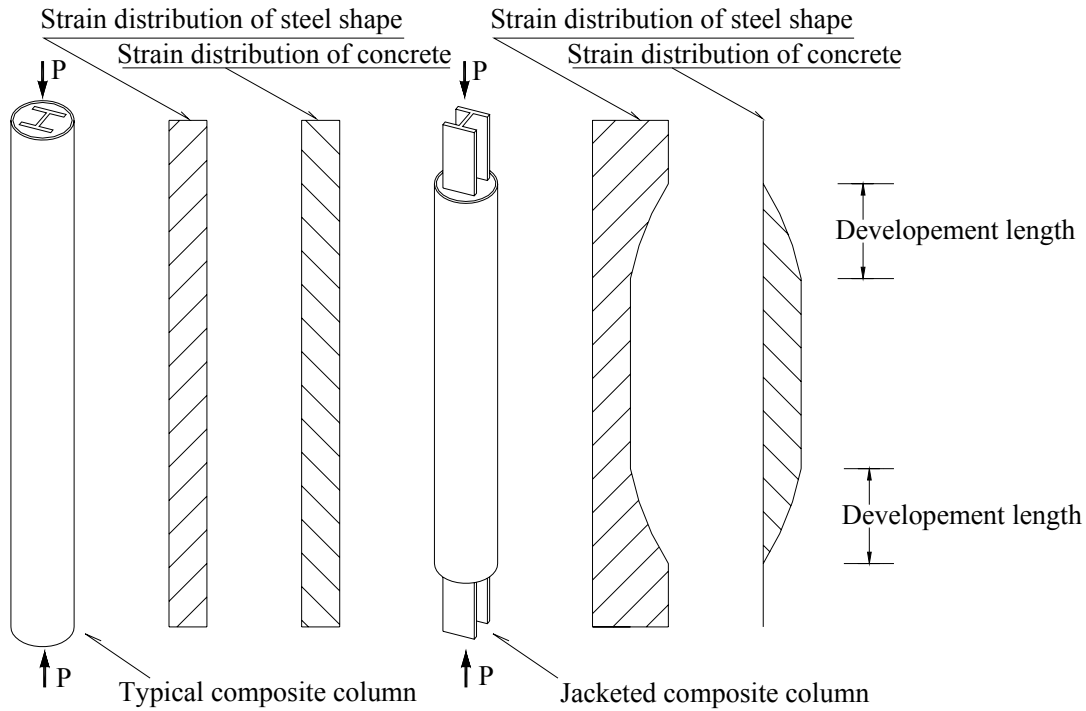


Figure 5-32 Load Transfer Mechanisms of Typical Composite Column and Jacketed Composite Column

The load that has to be transferred from the steel shape to the retrofitted section can be calculated as follows:

$$P_c + P_s = P \quad \text{Eq. 5.8}$$

$$\frac{P_s}{E_s A_s} = \frac{P_c}{E_c A_c} \quad \text{Eq. 5.9}$$

$$P_{transfer} = P_c = \frac{P \cdot E_c A_c}{E_s A_s + E_c A_c} \quad \text{Eq. 5.10}$$

Where P is the axial load applied to the composite column, P_s is the load carried by the steel shape, $P_{transfer}$ is the load needed to be transferred from steel shape to concrete, P_c is the load carried by concrete, E_s is the modulus of elasticity of steel, A_s is the area of steel shape cross section, E_c is the modulus of elasticity of concrete, and A_c is the area of concrete cross section.

Pull-out tests were performed to investigate the local bond-slip relationship between hot-rolled smooth steel bar and light-weight concrete and between hot-rolled smooth steel bar and

expansive light-weight concrete. The local bond-slip relations between steel and concrete from pull-out test results were used to predict the development length of the composite column in this project. These local bond-slip relations work with the following assumptions: a) the local bond-slip relationship between smooth steel bar and concrete is the same as between the corroded steel shape and the concrete; b) there was no reduction factor applied to the bond strength when using these experimental local bond-slip relationships to steel shape with larger cross section compared to steel bar with smaller cross section; c) the local bond-slip relationships between steel and concrete are assumed to be the same for compression and tension.

The method to find the development length for the special composite column was obtained according to the Russo et al., (1990) model between steel shape and concrete of the composite column described in section 2.1.4.2 The development length is then obtained with the following boundary conditions:

$$s(0) = 0 \quad \text{Eq. 5.11}$$

$$\left. \frac{ds}{dx} \right|_0 = \varepsilon(0) = 0 \quad \text{Eq. 5.12}$$

It can be found that the load needed to be transferred from steel shape to concrete is:

$$P_{transfer} = E_s A_s \left. \frac{ds(x)}{dx} \right|_{x=L_D} = E_s A_s \varepsilon_s(x) \Big|_{x=L_D} \quad \text{Eq. 5.13}$$

where L_D is the development length. The above details are shown in Figure 5-33.

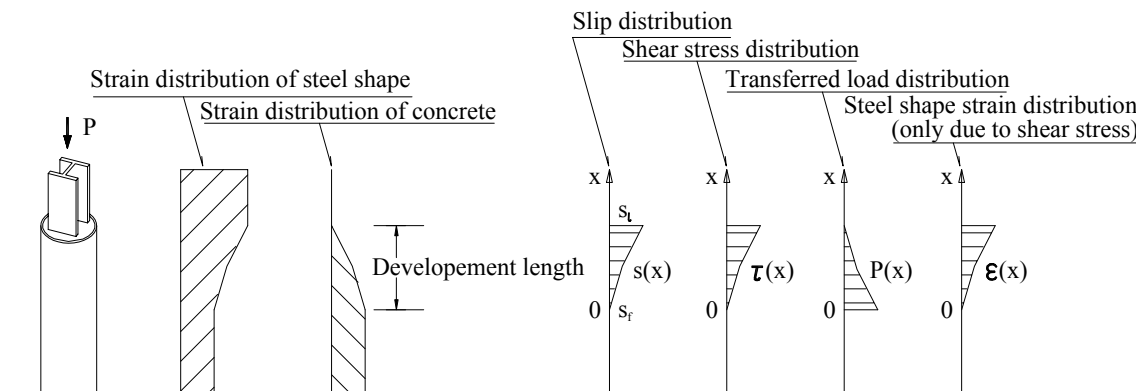


Figure 5-33 Defined Functions

The development lengths for the test specimens are shown in Table 5.23. It can be seen that the development length was very short. This could be the fact that no reduction factor was applied on the local bond-slip relationship when the relationship was applied to a steel column with a larger cross section (longer perimeter) compared to a steel bar with a small cross section (shorter perimeter). More research should be conducted on the local bond-slip relationship between a steel shape with large cross section and concrete.

Table 5.23 Development Length Results of the Specimens

Test Unit	Experimental ultimate load Capacity		Retrofit materials	Load needed to be transferred		Local bond-slip relationship between steel and concrete	Development length	
	kips	KN		kips	KN		in	mm
1 virgin	43.8	194.9	NA	NA		NA	NA	
2 notched	25.9	115.3	NA	NA		NA	NA	
3	68.2	303.5	GFRP pipe Light-weight concrete	23.3	103.7	See Eq. 5.3 and Eq. 5.4	4.41	112.0
4	74.3	330.6		25.4	113.0		4.71	119.6
5	41.1	182.9	GFRP pipe Expansive light-weight concrete	13.9	61.8	See Eq. 5.5 and Eq. 5.6	2.62	66.5
6	77.3	344.0		22.0	97.9		2.98	75.7
7	86.4	384.5		24.6	109.5		3.30	83.8

(Unit conversion: 1 kips = 4.45 KN, and 1 inch = 25.4 mm, 1 ksi = 6.896 MPa.)

5.4.6.3. Elastic Buckling

The energy method to solve for the elastic buckling load of a column can be explained as below. For Test Unit 3 to 7, the stiffness distribution and the deflection shape were assumed as shown in Figure 5-34. Actually, the combined stiffness of the composite column is changing in the development length area from I_1 to I_2 . In order to simplify the calculation procedure, an assumption was made that the combined stiffness was I_1 in half development length area, and the combined stiffness was I_2 in the other half development length area as shown in Figure 5-34. In this figure, L_D is the development length as explained in the previous sections.

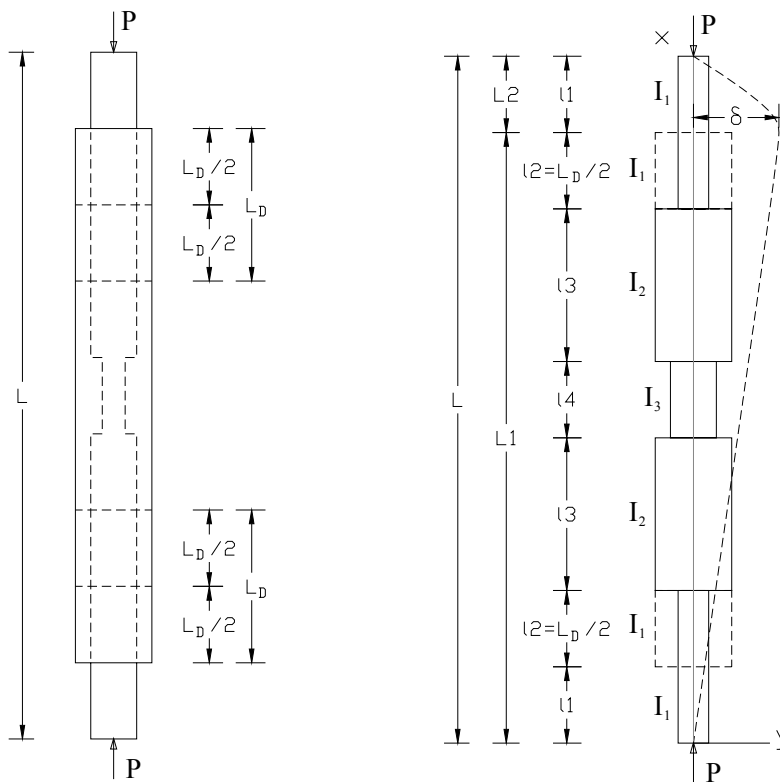


Figure 5-34 Assumed Stiffness Distribution and Deflection Shape for Test Unit 3 to 7

The equation of this deflection curve is:

$$y = \delta \sin \frac{\pi x}{2L_1} (0 \leq x \leq L_1)$$

$$y = \delta \cos \frac{\pi(x-L_1)}{2L_2} (L_1 \leq x \leq L)$$

Eq. 5.14

The strain energy of bending during column bending is:

$$\begin{aligned}
 \Delta U &= \int_0^{l_1+l_2} \frac{M^2 dx}{2EI_1} + \int_{l_1+l_2}^{l_1+l_2+l_3} \frac{M^2 dx}{2EI_2} + \int_{l_1+l_2+l_3}^{l_1+l_2+l_3+l_4} \frac{M^2 dx}{2EI_3} + \\
 &\int_{l_1+l_2+l_3+l_4}^{l_1+l_2+l_3+l_4+l_3} \frac{M^2 dx}{2EI_2} + \int_{l_1+l_2+l_3+l_4+l_3}^{l_1+l_2+l_3+l_4+l_3+l_2} \frac{M^2 dx}{2EI_1} + \int_{l_1+l_2+l_3+l_4+l_3+l_2}^{l_1+l_2+l_3+l_4+l_3+l_2+l_1} \frac{M^2 dx}{2EI_1} \\
 &= \frac{P^2 \delta^2}{2E} \left[\int_0^{l_1+l_2} \left(\frac{1}{I_1} \sin^2 \frac{\pi x}{2L_1} dx \right) + \int_{l_1+l_2}^{l_1+l_2+l_3} \left(\frac{1}{I_2} \sin^2 \frac{\pi x}{2L_1} dx \right) + \int_{l_1+l_2+l_3}^{l_1+l_2+l_3+l_4} \left(\frac{1}{I_3} \sin^2 \frac{\pi x}{2L_1} dx \right) + \right. \\
 &\int_{l_1+l_2+l_3+l_4}^{l_1+l_2+l_3+l_4+l_3} \left(\frac{1}{I_2} \sin^2 \frac{\pi x}{2L_1} dx \right) + \int_{l_1+l_2+l_3+l_4+l_3}^{l_1+l_2+l_3+l_4+l_3+l_2} \left(\frac{1}{I_1} \sin^2 \frac{\pi x}{2L_1} dx \right) + \\
 &\left. \int_{l_1+l_2+l_3+l_4+l_3+l_2}^{l_1+l_2+l_3+l_4+l_3+l_2+l_1} \left(\frac{1}{I_1} \cos^2 \frac{\pi(x-L_1)}{2L_2} dx \right) \right] \\
 &= \frac{P^2 \delta^2}{2E} \left[\frac{1}{I_1} (l_1+l_2) - \frac{1}{2\pi I_1} \left(L_1 \sin \frac{\pi(l_1+l_2)}{L_1} - L_1 \sin \frac{\pi(l_1+l_2+l_3+l_4+l_3)}{L_1} \right) \right] \\
 &\quad + \frac{1}{I_2} l_3 - \frac{L_1}{2\pi I_2} \left(\frac{\sin \frac{\pi(l_1+l_2+l_3)}{L_1} - \sin \frac{\pi(l_1+l_2)}{L_1}}{} \right. \\
 &\quad \left. + \frac{\sin \frac{\pi(l_1+l_2+l_3+l_4+l_3)}{L_1} - \sin \frac{\pi(l_1+l_2+l_3+l_4)}{L_1}}{} \right) \\
 &\quad + \frac{1}{2I_3} l_4 - \frac{L_1}{2\pi I_3} \left(\sin \frac{\pi(l_1+l_2+l_3+l_4)}{L_1} - \sin \frac{\pi(l_1+l_2+l_3)}{L_1} \right) \right]
 \end{aligned}$$

Eq. 5.15

Where I_1 , I_2 and I_3 are the moment of inertias for different column cross sections; l_1 , l_2 , l_3 , l_4 , L_1 and L_2 are the lengths according to the cross section changes as shown in Figure 5-34; L is the total length of the column; δ is the assumed maximum deflection of the column; P is the applied axial load.

The work done by the compressive force P during buckling is:

$$\begin{aligned}
 \Delta T &= \frac{P}{2} \int_0^l \left(\frac{dy}{dx} \right)^2 dx = \frac{P}{2} \left[\int_0^{L_1} \left(\frac{dy}{dx} \right)^2 dx + \int_{L_1}^L \left(\frac{dy}{dx} \right)^2 dx \right] \\
 &= \frac{P}{2} \left[\int_0^{L_1} \frac{\delta^2 \pi^2}{4L_1^2} \cos^2 \frac{\pi x}{2L_1} dx + \int_{L_1}^L \frac{\delta^2 \pi^2}{4L_2^2} \sin^2 \frac{\pi(x-L_1)}{2L_2} dx \right] \\
 &= \frac{P\pi^2 \delta^2 L}{16L_1 L_2}
 \end{aligned} \tag{Eq. 5.16}$$

Equating ΔU and ΔT , the buckling load was obtained:

$$B = E \cdot t \tag{Eq. 5.1}$$

$$\Delta U = \Delta T \tag{Eq. 5.17}$$

$$P_{cr} = \frac{\frac{\pi^2 EL}{8L_1 L_2}}{\left[\frac{1}{I_1} (l_1 + l_2) - \frac{1}{2\pi I_1} \left(L_1 \sin \frac{\pi(l_1 + l_2)}{L_1} - L_1 \sin \frac{\pi(l_1 + l_2 + l_3 + l_4 + l_3)}{L_1} \right) \right.} \\
 \left. + \frac{1}{I_2} l_3 - \frac{L_1}{2\pi I_2} \left(\frac{\sin \frac{\pi(l_1 + l_2 + l_3)}{L_1} - \sin \frac{\pi(l_1 + l_2)}{L_1}}{\right. \right. \\
 \left. \left. + \sin \frac{\pi(l_1 + l_2 + l_3 + l_4 + l_3)}{L_1} - \sin \frac{\pi(l_1 + l_2 + l_3 + l_4)}{L_1} \right) \right.} \\
 \left. + \frac{1}{2I_3} l_4 - \frac{L_1}{2\pi I_3} \left(\sin \frac{\pi(l_1 + l_2 + l_3 + l_4)}{L_1} - \sin \frac{\pi(l_1 + l_2 + l_3)}{L_1} \right) \right] } \tag{Eq. 5.18}$$

The buckling load developed above is for pin-pin end connection columns. For other end conditions, the buckling load can be calculated from the value of P_{cr} from Eq. 5.18 divided by an effective length factor K. Due to the lateral restraint at both ends of the columns in this test program, it was assumed that all the columns were partly fixed at both ends. But in actual situation, the ideal fixed conditions are not perfectly fulfilled. So, the effective length factor was

assumed to be 0.65 ($K = 0.65$) for all these specimens in these tests according to LRFD design manual (AISC, 1998).

5.4.6.4. Inelastic Buckling

Residual stresses exist in a hot-rolled steel member due to the uneven cooling to room temperature, and vary through the thickness of the flanges and the web. Cross-sectional geometry (flange thickness and width, web thickness and depth) influences the cooling rate and residual stress pattern. Typical residual stress distribution of W section hot-rolled steel member is shown in Figure 5-35. The maximum residual stress is typically near $0.3F_y$. If inelastic buckling occurs for this type of composite column, the inelastic buckling load can be calculated from Eq. 5.18 by substituting elastic modulus E with tangent modulus E_t (Shanley, 1947) or reduced modulus E_r (Timoshenko, 1961) of the steel shape. The tangent modulus E_t can be obtained from experimental steel member compression test or calculated numerically by assuming residual stress distribution pattern and magnitude (Chen et al., 1987).

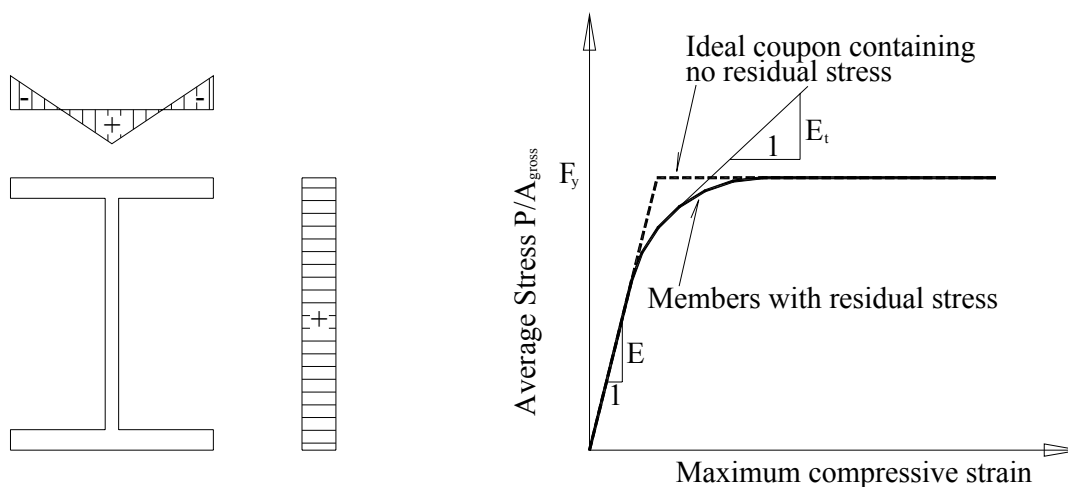


Figure 5-35 Influence of Residual Stress on Average Stress-strain Curve

5.4.6.5. Analytical Results and Conclusions

In this column test series, all the specimens buckled within the elastic range. The theoretical elastic buckling loads calculated by the above method are shown in Table 5.24, and the comparison between experimental and theoretical buckling load is shown in Figure 5-36. During the calculation, the development lengths for all the specimens were calculated directly based on

the experimental buckling loads for convenience. Trial and error procedures can be used during the calculation, i.e. first assume the development to be zero, and then a buckling load can be derived. Next, the development length is calculated based on this buckling load, and then the buckling is calculated again. Repeat the above procedure until the difference between the two adjacent calculated development lengths is small enough. The combined stiffness for different cross sections is calculated using Eq. 5.7, and the properties of steel shape, light-weight concrete and expansive light-weight are provided by Tables 5.18, 5.19, 5.20 and 5.21 and Figure 5-27.

Table 5.24 Theoretical Buckling Load

Test unit	Experimental buckling load		Theoretical buckling load		Difference
	kips	KN	kips	KN	
1 (virgin)	43.8	194.9	42.5	189.1	-3%
2 (notched)	25.9	115.3	24.8	110.4	-4%
3	68.2	303.5	62.2	276.8	-9%
4	74.3	330.6	91.8	408.5	+24%
5	41.1	182.9	46.6	207.4	+13%
6	77.3	344.0	65.0	289.3	-16%
7	86.4	384.5	97.6	434.3	+13%

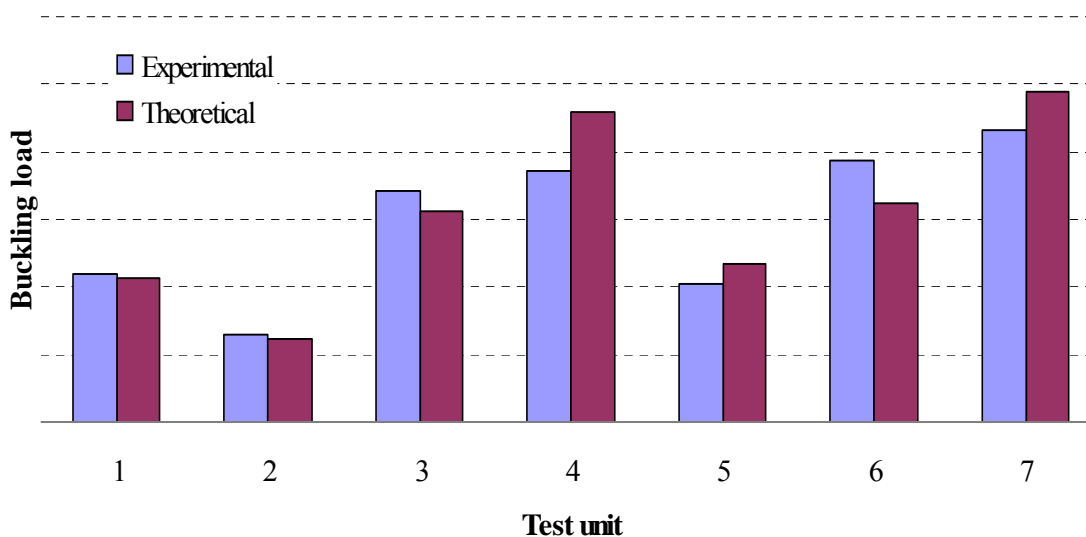


Figure 5-36 Comparison between Experimental and Theoretical Buckling Loads

The difference between the theoretical buckling load and the test load is due to the facts listed below: a) Initial crookedness of the column; b) Eccentricity of the axial load application; c) Difficulties of exact prediction for ideal end restrain conditions; d) The assumption of the value of α ; e) The omission of the contribution of the FRP jacket to the stiffness increase of the

composite steel; and f) The accuracy of the assumed deflection shape of the column. From the analytical and experimental results, the elastic buckling load equation derived in this report is sufficient to calculate the load capacity of this type of composite column investigated in this project.

5.5. SUMMARY

In this report, a new retrofit technology for the upgrading of deficient steel bridge columns using FRP composite material was proposed. The concept is to strengthen a given deficient built-up column with a two-step procedure: (1) wrapping with open FRP jackets and (2) filling these jackets with expansive light-weight concrete. The expansion of the concrete allows the FRP jacket to provide active confinement to the steel column and increase its ultimate load capacity. This retrofit method has many advantages, such as fast and simple implementation in the field, and no need to touch the inside structure. These overcome the disadvantages of the traditional retrofit methods which need drilling, bolting and are labor intensive and time consuming.

Experimental tests were carried out to verify the feasibility of this new strengthening method. The experimental tests included three series: (1) the first test series was to develop a high-expansion light-weight concrete that can provide enough expansion for the FRP jacket to provide active confinement to the steel column. A high-expansion concrete as expected was achieved, but the expansion lower the modulus of elasticity of this type of concrete due to the fact that expansion came from adding gypsum and calcium aluminate to the concrete mixture. More research should be conducted focusing on obtaining high expansion concrete without compromising its modulus of elasticity; (2) the second test series was to determine the local bond-slip relationship between steel and concrete materials because the jacketed composite column in this project is different from ordinary composite column. For this jacketed composite column, the load is directly applied to the steel shape only, for which a development length area is needed to transfer the load to the retrofitted material.

The test results showed that the development length was not so long based on the local bond-slip relationship between hot-rolled smooth steel bars and expansive light-weight concrete investigated in the first test series. Future research should focus on investigating the local bond-slip relationship between steel shapes and concrete, and between corroded steel shapes and

concrete because these are the real situations of a corroded steel bridge column; (3) the third test series was a column confinement test. Deficient columns were strengthened using FRP material according to the proposed retrofit technology, and test results showed that this method can restore the ultimate load capacity of the deficient steel column to the original capacity and even higher. However, just the type of slender steel column was investigated, and further research should be conducted on strengthening deficient stocky steel column using the FRP retrofit technology proposed in this report.

5.6. DESIGN GUIDELINES

The failure mode for steel column is buckling or yielding, which depends on the type (slender or stocky) of column. A stocky column as shown in Region 1 in Figure 5-37 fails by yielding the column, and a slender column as shown in Region 2 in Figure 5-37 fails by buckling the column.

For a stocky steel column, the ultimate load is:

$$P_y = A_s \cdot F_y \quad \text{Eq. 5.19}$$

where A_s is the cross section area of the column; F_y is the yield stress of the steel column; and P_y is the ultimate yield load. For a slender steel column, the ultimate load is a function of stiffness, modulus of elasticity and length of the column:

$$P_{cr} = f(I_s, E_s, L) \quad \text{Eq. 5.20}$$

where I_s is the stiffness of the column; E_s is the modulus of elasticity of the column; L is the length of the column; and P_{cr} is the ultimate buckling load.

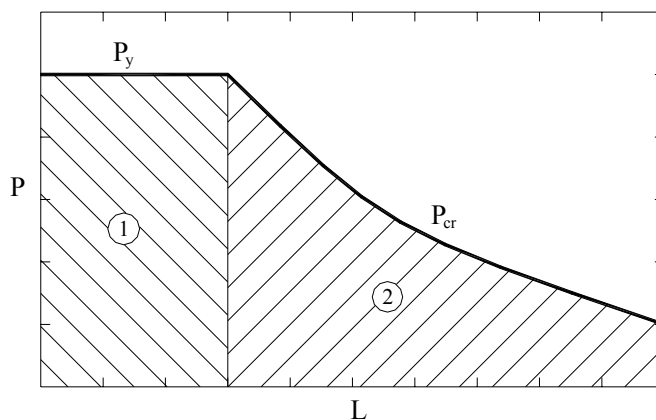


Figure 5-37 Ultimate Load (P) vs. Slenderness Parameter (L) for a Steel Column

For a corroded steel column, corrosion means two items: a) loss of cross section area; and b) a loss of stiffness. So, for a corroded slender steel column, the ultimate load capacity can be restored to the original carrying capacity if the stiffness can be restored to the original value. For a corroded stocky steel column, the ultimate load capacity can be restored to the original capacity if the cross section area can be restored to the original value. It should be mentioned the difference between stiffness and cross section area: stiffness is related to the distribution of the cross section area, e.g. if the cross section area of a corroded steel column is restored to the original, the stiffness may not be restored to the original and vice versa. In addition, if both the cross section area and stiffness of the corroded steel column are restored to the original value, then this retrofitted column will for sure have the same designed original load capacity.

5.6.1. CROSS SECTION OF RETROFIT MATERIAL

5.6.1.1. Area Requirement

For a stocky column, the failure mode is yielding as shown in Eq. 5.19. For this type of column, the cross section area should be restored to the original value:

$$E_s A_s = E_s \cdot (1 - \eta_a) \cdot A_s + E_c A_c \quad \text{Eq. 5.21}$$

The required area of the retrofitted material (concrete) can be derived:

$$A_c = \frac{\eta_a E_s A_s}{E_c} \quad \text{Eq. 5.22}$$

If the confining device is a pipe shape, then the inside diameter of the FRP pipe or the outside diameter of the concrete can be calculated by:

$$d_1 = \sqrt{\frac{4\eta_a E_s A_s}{\pi}} \quad \text{Eq. 5.23}$$

Where E_s is the modulus of elasticity of steel, A_s is the cross section area of the steel column, E_c is the modulus of elasticity of concrete, A_c is the cross section area of concrete, d_1 is the inside diameter of the FRP pipe by area requirement, and η_a is percentage loss of section area, e.g. 20% loss of cross section area.

5.6.1.2. Stiffness Requirement

For a slender column, the failure mode is buckling as shown in Eq. 5.20. For this type of column, the stiffness should be restored to the original value:

$$E_s I_s = E_s \cdot (1 - \eta_s) \cdot I_s + \alpha E_c I_c \quad \text{Eq. 5.24}$$

The required stiffness of the retrofitted material (concrete) can be derived:

$$I_c = \frac{\eta_s E_s I_s}{\alpha} \quad \text{Eq. 5.25}$$

If the confining device is a pipe shape, then the inside diameter of the FRP pipe or the outside diameter of the concrete can be calculated by:

$$d_2 = \sqrt[4]{\frac{64 \eta_s E_s I_s}{\pi}} \quad \text{Eq. 5.26}$$

Where I_s is the stiffness of the steel column, I_c is concrete stiffness, α is a reduction factor of the concrete stiffness contribution to the entire composite column stiffness, d_2 is the inside diameter of the FRP pipe by stiffness requirement, and η_s is percentage loss of stiffness, e.g. 20% loss of stiffness. It should be mentioned that the values of η_a and η_s are different because η_s is accounting for loss of stiffness and stiffness (moment of inertia) is related with the pattern of area distribution. It is recommended that for ordinary concrete $\alpha = 0.4$; for expansive concrete $\alpha > 0.4$, which depends on the expansion degree and the higher expansion the bigger value of α . For the light-weight and expansive light-weight concrete investigated in this project, the values of α are recommended to be 0.4 and 0.6.

5.6.1.3. Structural Requirement

The outside diameter of the retrofitted material (concrete) or inside diameter of the FRP pipe should fulfill structural construction requirement:

$$d_3 = L_{diagonal} + 2 \cdot t_{cover} \quad \text{Eq. 5.27}$$

where $L_{diagonal}$ is the diagonal length of the steel column cross section, t_{cover} is thickness of cover, and d_3 is the inside diameter of the FRP pipe by structural requirement.

The detail is shown in Figure 5-38.

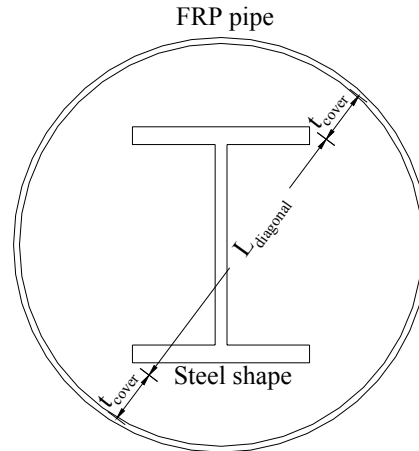


Figure 5-38 Structural construction requirement for the retrofitted material

For the stocky column, the diameter of the FRP pipe and concrete should be the maximum of:

$$d = \max \{d_1, d_3\} \quad \text{Eq. 5.28}$$

For the slender column, the diameter of the FRP pipe and concrete should be the maximum of:

$$d = \max \{d_2, d_3\} \quad \text{Eq. 5.29}$$

5.6.2. LENGTH OF RETROFIT MATERIAL

As discussed above, load is transferred from the steel shape to the retrofit materials through a development length for this type of composite column. The steel shape and retrofit materials have the same deformation after the development length and work together. So the length of the retrofit material should be the length of the corrosion area plus two times the development length as shown in Figure 5-33 and Figure 5-34.

$$L_{retrofit} = L_{corrosion} + 2L_D \quad \text{Eq. 5.30}$$

where $L_{retrofit}$ is the retrofit length, $L_{corrosion}$ is the length of corrosion area, and L_D is the development length.

5.6.3. THICKNESS OF FRP PIPE

Expansive concrete is recommended to reduce the total weight of the retrofit material and to provide active confinement. There are some relations among the diameter, thickness of the FRP

confining jacket and the compositions of concrete. The rule is the internal pressure developed in the concrete or the stress developed in the confining FRP pipe is not too high to result in the fatigue problem of the jacket, for example, the stress developed in the jacket should be less 20% of the jacket's ultimate strength. So, the procedure for designing the FRP confining jacket should be as follows: a) the inside diameter of the pipe is the same as the concrete diameter as calculated according to the presented procedures in this report; b) decide the desired internal pressure, c) then the compositions of the concrete and the thickness of the pipe empirically can be obtained based on the experimental results; d) finally, check the concrete stress to be in the pseudo elastic range of the stress-strain curve of FRP confined concrete.

6. DISPLACEMENT SENSING

6.1. INTRODUCTION

6.1.1. BACKGROUND

Development of health monitoring technologies capable of continuously monitoring the structural performance of civil infrastructure on a real-time basis is becoming a very important research area. In this research program, the main components used in the development of a field deployable remote system for health monitoring of the civil infrastructure consisted of wireless sensors for data collection.

6.1.2. OBJECTIVES

Health monitoring of steel bridges has been identified as a priority area in the FRA's R&D plan. In order to accomplish this objective UMR's researchers have been evaluating the feasibility of the latest technology in Global Positioning Systems (GPS) and other sensors for the wireless monitoring of the performance of steel bridges.

The key issues that are necessary for the proper evaluation of the performance of steel bridges are: (a) temperature induced deformations; (b) wind induced deformations; (c) vibrations induced deformations; (d) long term degradation due to corrosion and/or fatigue induced deformations; and (e) damage impact.

UMR researchers have been evaluating different sensors for the design of a health monitoring system that will address these induced deformations.

6.1.3. RESEARCH FINDINGS

Although Global Positioning Systems (GPS) appear to be a promising solution to obtain accurate relative displacement measurements, due to high costs, their use in this research project was not possible. Instead, research in this project used PVDF vibration sensors in combination with a wireless sensor data acquisition cluster. This system provided reliable data sets for the continuous health monitoring of steel bridges. For future applications the addition of temperature and wind loading sensors may improve the sensor system. The electronic platform required for the wireless PVDF sensor networks has been developed at UMR. This wireless acquisition cluster consisted of Bluetooth-compliant radios, coupled with microcontrollers and a solar power supply.

6.1.4. CHAPTER LAYOUT

Section 6.1 gives some background information on displacement sensing, the objectives of this research project, and the main research findings. The use of relative displacement sensors for the health monitoring of steel bridges is addressed in Section 6.2. Section 6.3 introduces dynamic response sensors, respectively. Section 6.4 deals with wireless instrumentation, henceforth presenting commercially used devices and for this project an in-house constructed smart sensor cluster.

6.2. RELATIVE DISPLACEMENT SENSORS (GPS)

GPS have been successfully used by others for measurement of relative displacement. Accordingly it was decided early in the project to attempt the use of GPS for this purpose. The following sections describe the potential usage of GPS system for the health monitoring of steel bridges.

6.2.1. TEST DESCRIPTION

On August 16, 2001 an experiment was conducted using the Smart Bridge located on the UMR campus to determine the feasibility of using a low-cost GPS receiver to measure the displacement on this bridge. The Motorola Oncore receiver used, is an in-house GPS-box containing an 8-channel receiver; powered with a 12V battery, and a proxim RF-LAN wireless radio as depicted on Figure 6-1. This is capable of using up to 8 satellites to calculate the position of the antenna. A copy of GrafNav/GrafNet version 6.02 software was acquired from Waypoint Consulting Inc. (wpinfo@waypnt.com or www.waypnt.com) in Calgary, Alberta, CA for use during the experiment. The oncore receiver was donated by Synergy through their “GPS for scholars” program. The GPS receiver antenna was set in three different points on the Smart Bridge. Motorola WinOncore software (<http://www.motorola.com>) was used during the monitoring. The first point of the testing was on the top rail of the bridge (see Figure 6-1). At this point, the signal was strong for each of the satellites used in calculating the position of the receiver antenna.

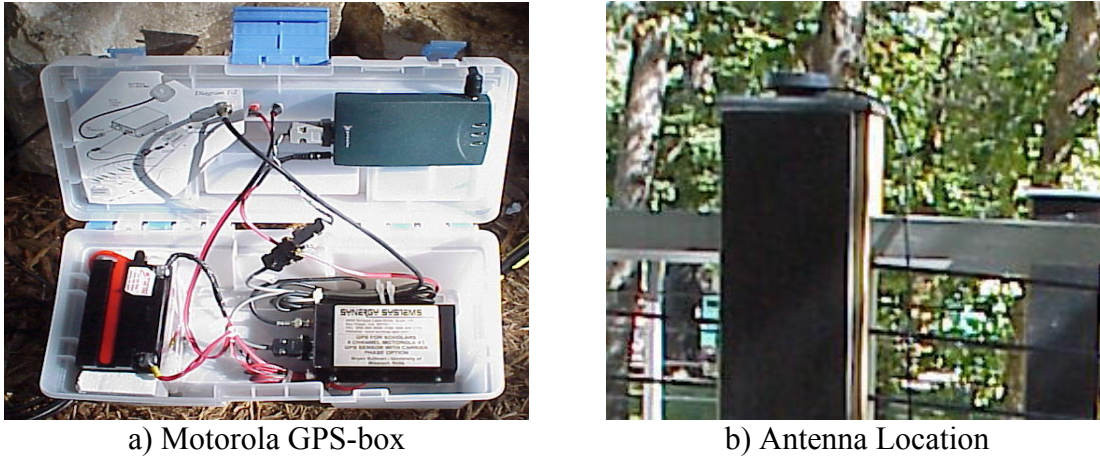


Figure 6-1 UMR Smart Bridge Test

6.2.2. RESULTS

On the top rail of the bridge, 7 satellites were consistently available and at times the maximum of 8 could be reached. The second point of testing was on the walking deck of the bridge. At this point, the antenna did not have a clear view to the sky. The restriction was the railing of the bridge. The signals received were not as strong as on the top railing, but they were strong enough to make an accurate position calculation. On the walking deck, 6 satellites were consistently used to calculate the position. The third and final point was under the bridge on one of the support beams. This position is inconclusive because the antenna could not pick up a signal. The data from successful reception was collected for approximately 45 minutes. It was converted using Waypoint software, which is post processing software. The converted data points were within 16ft (5.9m) of each other. This data can become more accurate when recorded over a longer period of time and augmented with additional receivers using differential corrections. Unfortunately, the equipment used was not able to achieve the desired accuracy, and in the future more powerful receivers should be used.

6.2.3. CONCLUSION

According to the results obtained it can be demonstrated that GPS is currently the best choice for relative displacement sensing but also it is the more expensive solution. Table 6.1 shows the actual cost of this solution for two different companies. These costs were verified in conversations with local USGS staff.

Table 6.1 GPS Displacement Solution Cost

Equipment/Company	Actual Solution Cost
Trimble NT200D GPS Receiver	\$13,200
Leica Geosystems MC500/TCA1800	\$25,050

Although technology has a tendency to drop prices as new more powerful models become available, at present this solution is highly expensive even though it is recommended for its performance and accuracy of results. However, GPS rely on a clear line of view to the sky. While this is not a problem for large outdoor structures like railroad bridges, it would be an issue for structures indoors, in dense urban areas, or heavily wooded areas that are sheltered from the sky.

6.3. DYNAMIC RESPONSE SENSORS

Sensors magazine (www.sensormag.com), an industry trade magazine, lists several types of acceleration sensors. The sensor handbook (Frandon, 1997) categorizes accelerometers as: capacitive, piezoresistive, piezoelectric, and thermal. PVDF material was selected as the vibration sensor due to its low cost and ease of use.

Like some other ferroelectric materials, PVDF is also piezoelectric, producing electrical charge in response to a change in temperature. PVDF strongly absorbs infrared energy in the 7-20 μm wavelengths, covering the same wavelength spectrum as heat from the human body. LDT0 is a commercial version of a PVDF sensor and it is shown in Figure 6-2a. Figure 6-2b shows the equivalent circuit diagram.

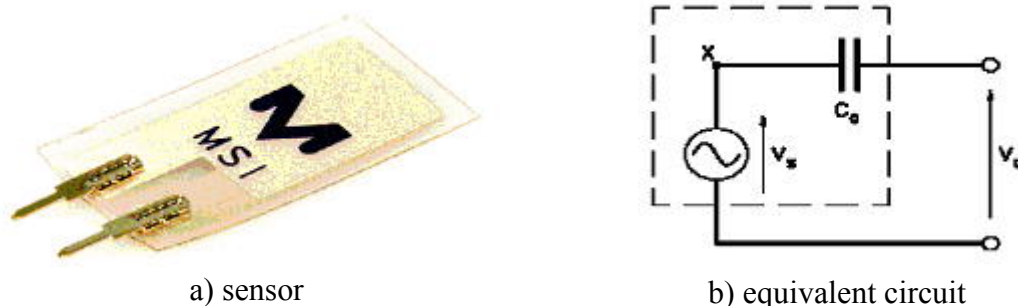


Figure 6-2 PVDF Sensor

PVDF makes a useful vibration sensor, because its properties as a transducer include those shown on Table 6.2.

Table 6.2 PVDF Properties

Parameter	Value
Frequency response	0.001 Hz to 10^9 Hz
Voltage output	0.001 mV to 50 volts
Mechanical strength and impact resistance	10^9 Pascal modulus
High stability	<0.02% moisture absorption
Placement	Glued with most commercial adhesives

6.4. WIRELESS INSTRUMENTATION

A distributed sensor network was selected as the architecture of the wireless instrumentation system. The architecture consists of a number of intelligent sensor nodes or clusters in communication with a central host via a short range radio frequency (RF) communication link. The host in turn is connected to the Internet for remote data acquisition and control via a longer range RF or wired communication link. The next few sections describe each of these components and their testing in more detail.

6.4.1. OBJECTIVE

Steel railroad bridges have been in service for several years and structural engineering researchers have identified the need for a rational and economical method of monitoring the performance and safety of civil structures over their life spans. The current state includes the monitoring of some key parameters on structures in areas of high traffic and loading conditions (i.e. rail road steel bridge). These structures have been identified as special due to the essential role they play in society due to their high everyday demand. The high repair cost and installation of new technologies have been a major concern on the civil engineering community, but such maintenance activities are necessary in order to maintain a safe operation of these engineering structures. A wired network is not suitable for old bridges where wiring just can not be taken into consideration; the main objective in this project was to develop a reliable, easy to install, low cost maintenance, low power consumption wireless network for structural health monitoring.

6.4.2. BACKGROUND

One of the first wireless data acquisition systems considered for this project was the Crossbow Technology LT110, depicted in Figure 6-3. This system is a complete wireless, four-channel, data monitoring and acquisition kit. The system consists of a four-channel, microcontroller-based data acquisition system, 2.4GHz spread spectrum radio (Bluetooth) with a range of 330ft (100m), and a sample rate of 500-1000Hz per channel. The approximate cost for this system is \$2,750. Due to the high costs of this system, and the fact that Crossbow did not support ad-hoc networks, UMR researchers developed an in-house system. The in-house system was first constructed as a prototype from commercial off-the-shelf modules. A custom module was subsequently developed.



Figure 6-3 Crossbow Technology

6.4.3. BLUETOOTH ENABLED DEVICES

Bluetooth is a recently developed technology that uses radio frequency (RF) transceivers to provide point to multipoint wireless connectivity. This new technology limits connectivity to a radius of about 33 to up to 330ft (10 to 100m) with a higher power consumption, which provides a maximum data rate of 723 kbps. Bluetooth represents a wireless communication protocol; it provides support for such communication functions as connection setup, authentication, sending and receiving data, error detection and correction, and similar communications protocol functions. Bluetooth-enabled devices were originally envisioned as replacements for familiar wired desktop computer peripherals such as mice and keyboards and other wired consumer electronic items. It has become a promising technology for low-power, mobile, distributed sensor networks.

The Bluetooth effort began at Ericsson in 1994, and numerous companies began developing products based on this new technology. Then the Bluetooth special interest group (SIG) was formed in 1998. The SIG purpose was to maintain interoperability. In order to truly have various devices communicate into a piconet, a small network consisting of one master and seven slaves is desired to employ a point to multipoint communication functionality in Bluetooth network devices.

Bluetooth is designed to operate on the globally available, 2.45 GHz unlicensed radio band, providing a data transmission rate up to 721 kbps as well as three voice channels. The basic design of Bluetooth results in a complex specification that supports communications even in a noisy frequency environment. Through the use of frequency hopping, the Bluetooth radio module can avoid interference from other signals by hopping to a new frequency after transmitting or receiving a packet.

Bluetooth employs frequency hopping in 79 hops displaced by 1 MHz, starting at 2.402 GHz and ending at 2.480 GHz. Frequency hopping is employed to reduce the affect from signal interference and fading, with the expected range of a typical Bluetooth device being approximately 33 or 330ft (10 or 100m) and the actual range (10 or 100 m) depending on the power level.

The Bluetooth protocol stack is used in conjunction with the Link Manager, the Bluetooth baseband hardware and the Bluetooth RF interface hardware to transmit data over a Bluetooth wireless link. The Link Manager, baseband, and RF are collectively known as the Link control hardware. The Link Manager controls link setup, security, and control, and the Link Managers on two Bluetooth devices communicate with each other via the Link Manager Protocol (LMP). The baseband provides the digital hardware interface and handles the basic low-level Bluetooth communications protocols, while the RF hardware takes care of the actual radio transmission. In most Bluetooth hardware implementations, the Link Manager and baseband functions are combined into a single chip known as the Host Controller, which is often called the "baseband chip", even though it handles both the baseband and Link Manager functions. The RF function is isolated onto a separate radio chip or module (see Figure 6-4).

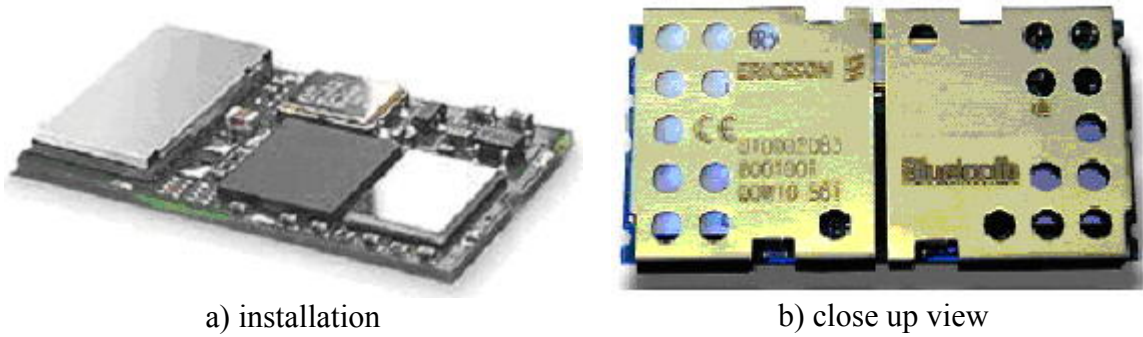


Figure 6-4 ROK 101 007

Under the Bluetooth specification, a device is categorized as either a master or slave for transmission purposes. All packet transmissions commence at the beginning of one of the $625\mu\text{sec}$ time slots.

While the normal duration of a transmission is one slot, a packet can last up to five times the slot length. To support full-duplex communications, Bluetooth employs a time-division multiplexing (TDM) scheme. A master device can commence transmission using an even-numbered slot, whereas a slave can commence transmission through the use of an odd-numbered slot. Full-duplex communication enables transmission of control and configuration data to the sensor controller as well as acquiring data from the controller.

6.4.4. A PROTOTYPE: SMART WIRELESS SENSOR CLUSTER (SWSEC)

After it was determined that a commercial solution was not economically feasible, it was decided to construct a smart sensor cluster in-house. Development kits for Cygnal's C8051F005 processor and Ericsson's ROK module were available and used for this purpose. The Department of Electrical and Computer Engineering has an extensive infrastructure for the development and support of microcontroller-based systems like the Cygnal module that uses the 8051 family. The next several sections describe the development and testing of this first prototype.

6.4.4.1. Microcontroller

The features of the Cygnal C8051F005 development kit are described in this section. Cygnal is a company that develops useful and powerful 8051 variant microcontrollers, and for this prototype, a development kit C8051F005-DK is used. C8051F005 is a powerful, low power, low cost 8051

microcontroller. This microcontroller contains an integral 12-bit multi-channel ADC (used for sensor inputs).

Another important feature is that it has a user programmable gain pre-amplifier and two 12-bit DACs. The memory in this microcontroller is 32Kbytes of flash memory. There is a UART serial interface implemented in the hardware component. Timing is always a concern in software development, and this 8051 variant has 4 general purpose 16-bit timers. The C8051F005 has 2304 bytes of memory RAM, and is able to execute instructions at a rate of 25 MIPS compared to the generic 8051's 1 MIP rate. Currently the program running on SWSeC occupies 494 bytes. This chip contains an internal clock oscillator which reduces parts count and size, but is also able to accept external clock sources for specific needs.

Power can be saved using the user-programmable power management functionality. For real time in-system programming and/or debugging an on-board JTAG is provided. Note that all the included analog and digital peripherals remain fully functional while running in debugging mode using JTAG. C8051F005 comes in a 64-pin TQFP package, which measures 0.5 by 0.5in (12 by 12mm). Resetting the microcontroller is not a problem because of the hard and soft reset sources provided. The power supply required to operate the C8051F005 is in the range of 2.7 to 3.6V with a maximum current consumption of 30mA. These power requirements are for the microcontroller; any extra components included on the development kit are not considered.

The block diagram for the components that are used on the wireless sensor cluster from this family of microcontrollers is depicted in Figure 6-5.

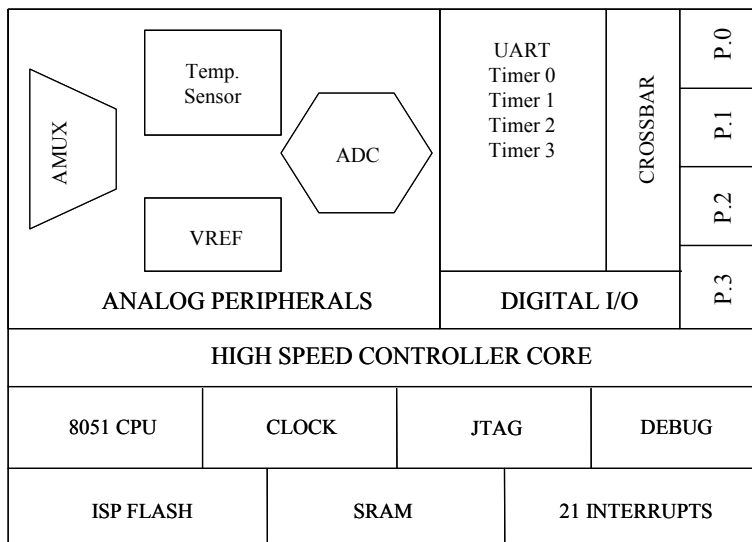


Figure 6-5 C8051 Block Diagram

6.4.4.2. Bluetooth Enabled Radio: ROK 101 007

This Bluetooth radio is an essential part of SWSeC design and Ericsson provides a functional development kit containing an ROK101007 Bluetooth based radio shown in Figure 6-6. ROK101007 is a short range module which is based on Bluetooth wireless technology. This module has an RF output power class 2; this means it is able to establish a communication link to other modules within a range of up to 11yards (10m). The ROK101007 supports a maximum data rate of 460 kbps using the built-in UART interface.

Another of its multiple features is that this module is capable of multipoint operation (scatternet). According to its specification this module is fully compliant with all of the Bluetooth profiles. The ROK101007 consists of three major components which are: (a) a baseband controller; (b) a flash memory; and (c) a radio that operates in the widely available 2.4 GHz ISM band. Extensive testing seems to indicate that scatternet operation with the Ericsson module is not very reliable. This makes it less suitable as a basis for the type of ad-hoc sensor networks envisioned here.

A 50-Ohm “inverter F” antenna is included on the Ericsson development kit printed circuit board. A baseband processor and firmware that manages internal module components is also included.

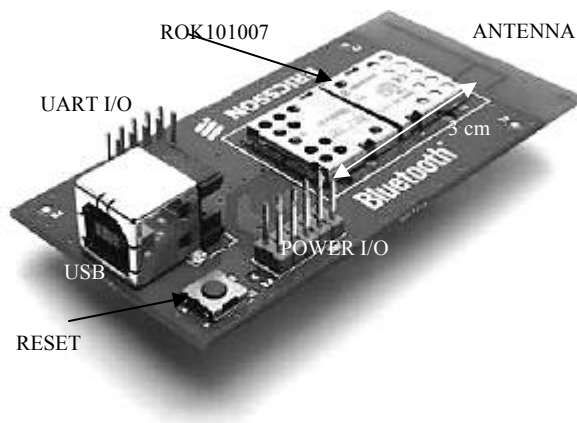


Figure 6-6 Ericsson Development Kit

According to the Bluetooth specification Version 1.1 there are different ACL packets which can be used on the asynchronous links. The information carried can be user data or control data. Including the DM1 packet, seven ACL packets have been defined. Six of the ACL packets contain a CRC code and retransmission is applied if no acknowledgement of proper reception is received, unless in the case where a flush operation is carried out. The 7th ACL packet, the AUX1 packet, has no CRC and is not retransmitted.

The ACL packet type that the prototype utilizes is the DH5. This packet is similar to the DM5 packet, except that the information in the pay-load is not FEC encoded. As a result, the DH5 packet can carry up to 341 information bytes, which includes the two bytes payload header, plus a 16-bit CRC code.

6.4.4.3. Establishing a Bluetooth Connection

In order for 2 Bluetooth devices to pass data, these devices must communicate with each other and create an ACL data connection. There are a few steps that are involved in creating the ACL connection. First, one of the Bluetooth devices must act as a Master while the other acts like a Slave. The purpose of the Master is to scan for Slave devices to which to connect. Scanning is accomplished by transmitting a request concerning the type of device and waiting for a reply. The Inquiry process is performed to locate devices that are within the range of the equipment used. The reply information of the Inquiry Request contains information about the remote

Bluetooth device. The most important piece of information is the Board Address (BD_ADDR) of the remote device.

An Inquiry is performed by issuing an Inquiry Command to the HCI Controller. The HCI Controller can be instructed to stop the scan and report its findings after a determined number of devices are found, or report on the findings only after the entire Inquiry process is complete.

In order for the Slave to receive the Inquiry request, the Slave must be in the Inquiry Scan State. When an Inquiry request is received information about itself is sent to the caller. Sending the HCI Controller the Write_Scan_Enable Command enables inquiry Scan Mode and Page Scan Mode. Note: The current firmware in the Ericsson modules requires the enabling of both Page Scan and Inquiry Scan.

Once the Master has obtained the Board Address of a Slave device and the Slave device is in Page Scan mode the connection process can begin. The Master initiates a connection with a Slave after issuing an HCI_Create_Connection command. The command takes a number of parameters, the most important is the BD_ADDR of the device. The other parameters are values that were determined via the Inquiry process. When the Slave receives the Connect Request, one of two things can happen. The Slave will receive a Connection Request Event, and may examine the Class of Device, callers BD_ADDR and the type of connection that is attempting to be established before accepting the connection by issuing an Accept_Connection_Request, or the Slave can be placed in an Auto Accept mode, by issuing a Set_Event_Filter Command. The Set_Event_Filter can be used to only accept connection from all devices, specific Class of Device or a device with a specific BD_ADDR. Upon completing the connection, the Host Controller will provide a Connection Handle. The Connection Handle will be used when sending data from one device to the other. The connection establishment process is illustrated in Figure 6-7.

6.4.4.4. Interfacing the Controller with Bluetooth

The source code for this wireless data acquisition was written in C using a comprehensive integrated development environment (Cygwin IDE) for unobtrusive real-time debug in your target system and compiled with Keil Pro which is an 8051 compiler.

The firmware that had been programmed into the Ericsson module (ROK 001 007) defaults the UART into 57.6 Kbps after the device is switched on. The C8051F005 device installed on the target board features an internal oscillator which is enabled as the system clock source on reset. After reset, the internal oscillator operates at a frequency of 2.0MHz by default but may be configured by software to operate at other frequencies (4.0 MHz, 8.0MHz or 16MHz). Therefore, in this in-home-system an external oscillator of the value of 22.1184 MHz was used in order to make the ROK 101 007 and the C8051F005 ready to communicate. After the UART in both sides (radio and controller) have been setup into 57.6 Kbps after a hard reset, then the devices are ready to send/receive information.

The next state of the software is to setup the flow control between the two devices. It is necessary to slow down the data transport across the HCI when the Bluetooth module's buffers are overloaded; Bluetooth solves this problem by providing flow control of the HCI. There are three types of flow control: (a) command flow control; (b) flow controlling data from host; (c) and flow controlling data from Bluetooth module. The HCI_Read_Buffer_Size command is used to determine the Bluetooth buffer space Bluetooth module replies with the number ACL packets it can buffer, as well as the maximum size of the HCI ACL data packets. Once the host has pulled up the module's buffer, it must wait for a HCI number of completed packets event from the module. After the flow control has been setup, few parameters that handle time constraints can be established. Such parameters are necessary for device discovery timeout and power conservation issues.

The next task for the software is to start scanning for devices every fixed time, waiting for a master to establish a connection. The commands are Inquiry and Write_Scan_Enable. All aspects of the inquiry process are controlled by the HCI. The host uses the HCI Inquiry command to initiate an inquiry. The HCI_Set_Event_Filter command can be used to set an inquiry result filter. The module utilizes an HCI_Inquiry_Result event to respond to an inquiry from the host.

The inquiry HCI command issued by the host or master will lead to all Bluetooth devices within its vicinity being reported by the Process_Inquire event. The software then automates the Process_Inquire event to establish the connection using the command Create_Connection with the device found. The slave will receive the Process_Connection_Request event when the master issues the Create_Connection command, and the software is setup to automatically accept the connection. When the connection has been accepted, the master and slave will receive a Process_Connection_Complete event, and this means that the connection was established. Finally, the application program can call the HCI_Receive_Data to read the ACL data packets and plot such information. The data type that has been setup by the software is data packets type DH1, which can handle 341 information bytes; when a DH5 packet is sent or received, the hop frequency shall not change for the duration of five time slots.

6.4.4.5. Hardware Design

The circuit design for this prototype is simple and consists of six major components which are: (a) power supply; (b) microcontroller; (c) ROK 101 007; (d) in system programming JTAG (IEEE 1149.1); (e) an external crystal; and (f) the antenna.

The schematic that illustrates the SWSeC hardware design is shown in Figure 6-8.

C8051F005-DK AND ROK101007

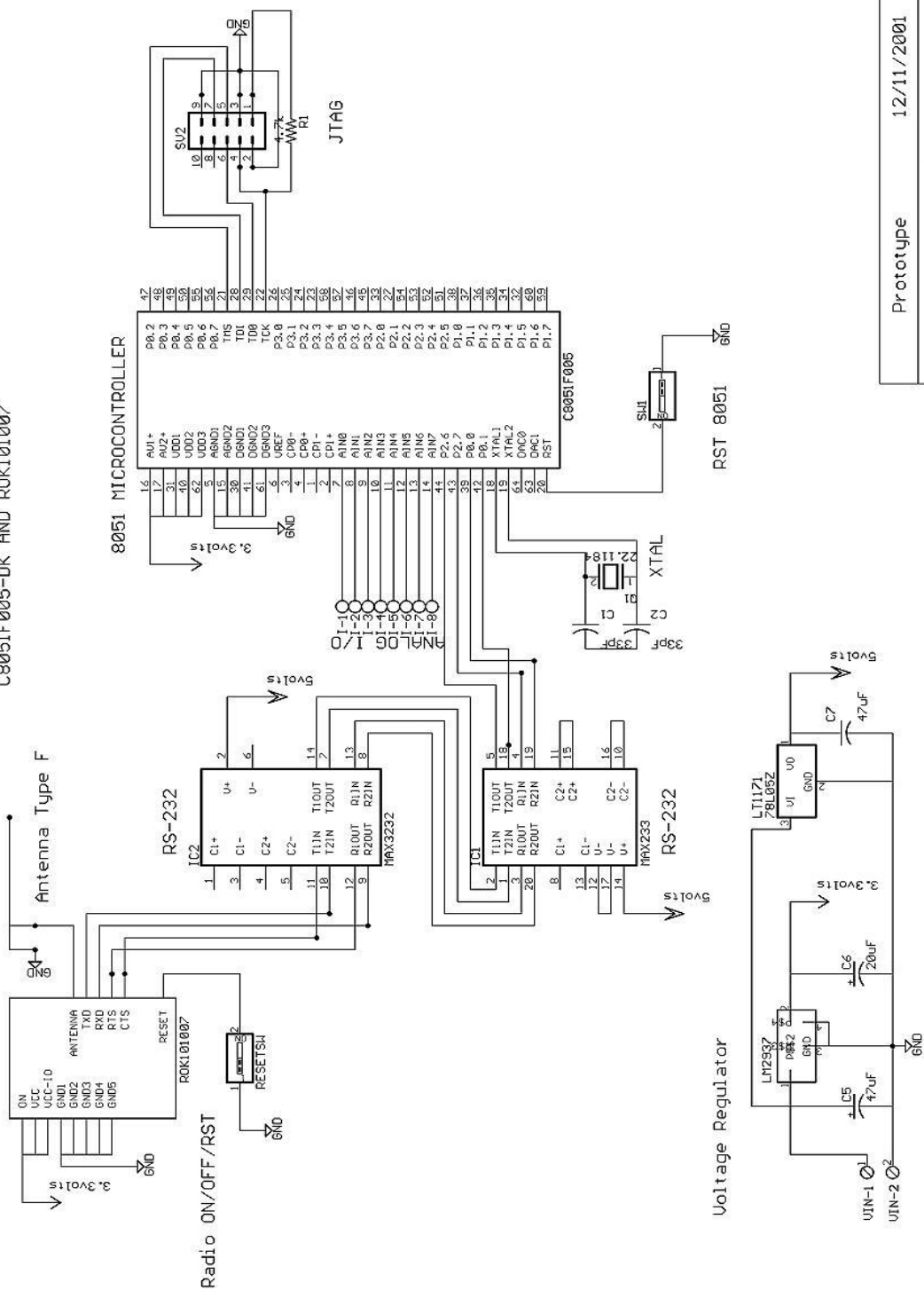
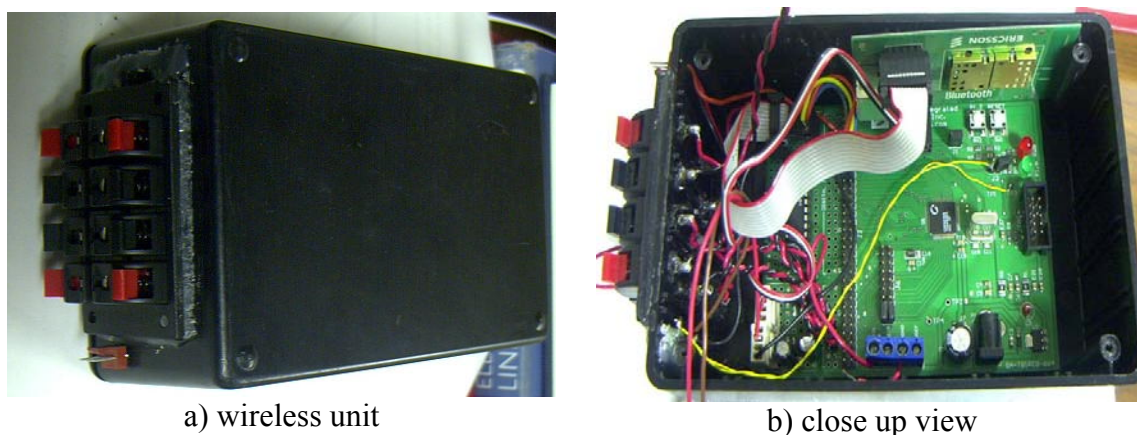


Figure 6-8 Prototype Schematic

Prototype	12/11/2001
Design by Jose H Mata	
University of Missouri - Rolla	

6.4.4.6. Smart Wireless Sensor Cluster

The smart wireless sensor cluster is a prototype of a wireless acquisition unit that is able to handle four differential channels (4 differential analog inputs). The prototype developed in-house is a wireless data acquisition system and consist of a microcontroller (Cygnal C8051F05-DK), Bluetooth radio (Ericsson ROK 101 107), portable power supply, and weatherproof enclosure depicted in Figure 6-9. This subsystem is referred to as a *smart sensor cluster*. The Cygnal processor is an 8051 variant with integrated analog-to-digital converter and a channel analog multiplexer as described in 6.4.4.1. The Ericsson module is shown in Figure 6-4. The size of this module is about 0.7 x 1.3in (17 x 33mm). Smaller Bluetooth complaint solutions such as Taiyo Yuden is currently under development by the industry.



a) wireless unit

b) close up view

Figure 6-9 Smart Sensor Cluster

Standard Bluetooth (<http://www.bluetooth.org>) systems have a range of only 33ft (10m) but can be expanded (like the Crossbow LT110) to 330ft (100m). Multiple Bluetooth-based intelligent sensor clusters can be grouped to form a piconet, and several piconets can then form a scatternet for larger networks. Each cluster will need to be within 33ft (10m) of at least one other cluster or the local host, which will also be equipped with a Bluetooth radio. The ROK101 007 has a built in inverted-F antenna, and since the enclosure is plastic, transmission can be performed successfully.

6.4.4.7. Instrumentation Field Test

6.4.4.7.1. Objective

In order to test the in-house instrumentation, diverse tests were conducted at the Teardrop Bridge, which is a highway steel truss bridge located on the historic old Route 66, 30 miles (48km) from UMR.

6.4.4.7.2. Setup

The teardrop bridge and one of its structural members is shown in Figure 6-10b. Data was collected using the smart sensor cluster within a range of up to 10 meters from a single PVDF sensor temporarily mounted on specific points of the bridge's structural members (see Figure 6-11).



a) location



b) structural member

Figure 6-10 Teardrop Bridge

A driving force was applied to the bridge by simply driving a truck, shown in Figure 6-11b, over the bridge at various speeds (see Chapter 5). Data was captured continuously at several different times. This data was subsequently analyzed off-line; however the analysis is not relevant to the design of the instrumentation system and is not discussed further in this section. Further information is described in Chapter 5. A plot of the data is shown in Figure 6-12.



a) sensor location



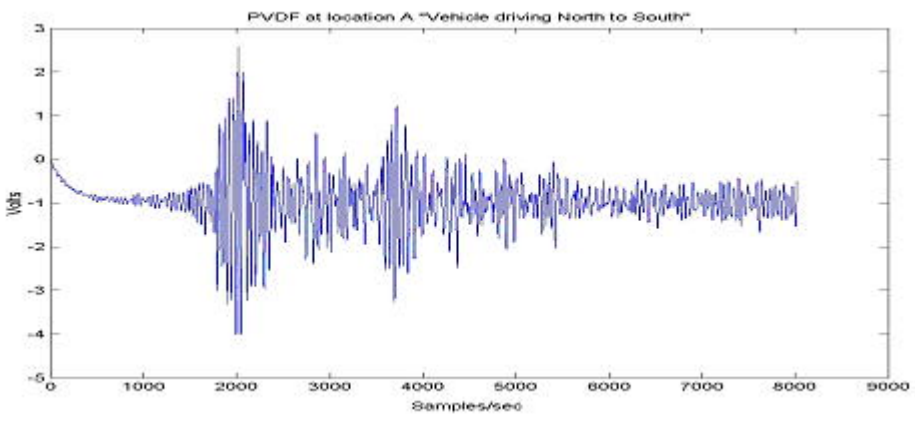
b) applied load

Figure 6-11 Testing Teardrop Bridge

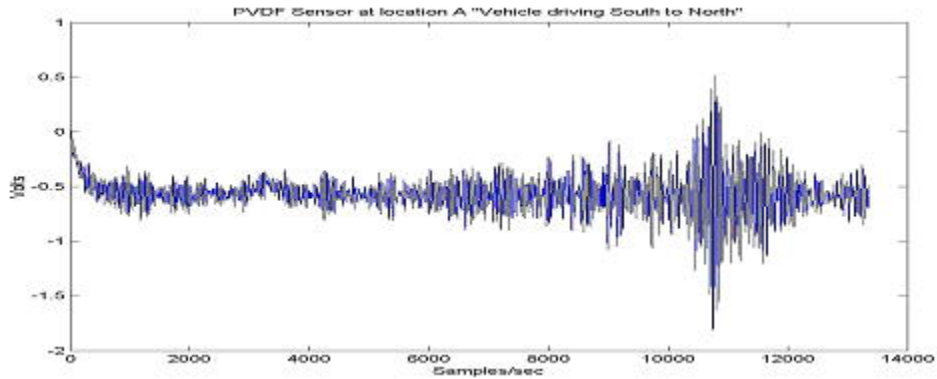
6.4.4.7.3. Results

Bluetooth provides a highly reliable communication and a smooth data transfer. The PVDF sensor was able to extract vibrations at any time it was required. Figure 6-12 displays two plots acquired during this testing. In Figure 6-12a it is clear how the peak vibration occurs when the load (vehicle) enters the bridge from the north side, while in Figure 6-12b it is also clear how the peak vibration occurs when the vehicle had been driven in the opposite direction.

According to the results obtained it is clear to see how reliable the data has been transmitted using the smart sensor cluster as the wireless acquisition cluster and the PVDF as a vibration sensor. The results show how the data collection has been successfully accomplished.



a)



b)

Figure 6-12 Peak Vibration**6.4.5. FINAL DESIGN: ASUL**

For the final design called ASUL, a faster variant of the Cygnal 8051 microcontroller has been used as well a Taiyo Yuden Bluetooth compliant radio. The reason the C8051F123 was chosen, was because it is faster than the C8051F005 and provides a wider range of features. The following section will explain this new microcontroller in more detail.

6.4.5.1. C8051F123 Microcontroller

The C8051F123 can directly access 8448 bytes of internal RAM and 128 Kbytes of in-system programmable flash memory. Currently the software utilized on ASUL uses 1813 bytes of RAM memory. The additional RAM memory in this microcontroller has been reserved for a future implementation of health monitoring algorithms, routing tables, and network organization. In order to enable analog inputs this device has an on-board 10-bit ADC, which is able to handle speeds of up to 100 ksps. Currently Cygnal has the fastest available 8051 microcontroller; in this case ASUL utilizes a controller capable of speeds up to 100 MIPS. The block diagram of the C8051F123 is very similar to the one for the C8051F005 depicted in Figure 6-5.

This controller offers five general purpose 16-bit timers/counters. The software uses four of these timers. This controller has an on-board JTAG (IEEE1149.1) circuitry for allowing in-system programming/debugging. The TQFP package is the way that the 64-pin C8051F123 has been produced by Cygnal, resulting in one of the smaller available sizes for an 8051 microcontroller.

6.4.5.2. Taiyo Yuden EYSF2SAXX

Taiyo Yuden, a rapidly emerging leader in Bluetooth module development and implementation, combines its expertise in multilayered component manufacturing, high-frequency circuitry design, advanced assembly techniques and evaluation technologies with aggressive Bluetooth research, development and strategic partnerships. Taiyo Yuden's certified module is built on the radio modem IC developed by Silicon Wave, Inc., a San Diego-based high-frequency semiconductor research and development company. The single-chip radio modem utilizes Silicon-on-Insulator (SOI) BiCMOS process technology and direct conversion demodulation, resulting in high-isolation, low switching loss, use of fewer subcomponents, e.g., SAW filters or LC filters, and thus lower cost and smaller size. The EYSF2SAXX block diagram is depicted in Figure 6-13a, while Figure 6-13b displays its actual dimension in mm (25.4mm = 1in).

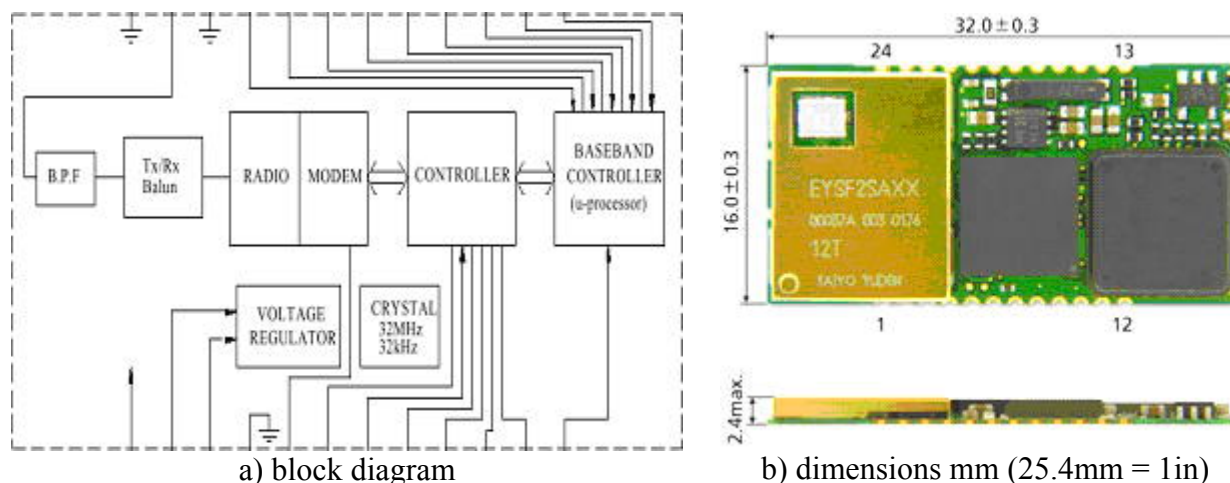


Figure 6-13 Taiyo Yuden EYSF2SAXX

EYSF2SAXX supports all the features the ROK 101 007 has to offer according with the Bluetooth specification Version 1.1, and some of these features are: (a) Bluetooth TM 1.1 Qualified; (b) UART Interface; (c) Baud Rate : 115.2kbps (d) Point-to-Multipoint (7 Slaves); (e) Encryption; (f) Hold, Sniff Mode, Sleep Mode; ACL Supported Link.

6.4.5.3. EYSF2SAXX: Changes to the Source Code

This section will focus on the major source code changes that have been made in order to achieve the same functionality as the ROK 101 007. The major change in the source code has been made in the way that EYSF2SAXX sends packets. Taiyo Yuden module sends packets type

DM1, which is a packet that carries data information only. DM stands for Data-Medium rate. The payload contains up to 18 information bytes (including the 1-byte payload header) plus a 16-bit CRC code. The DM1 packet may cover up to a single time slot. The information plus CRC bits are coded with a rate 2/3 FEC, which adds 5 parity bits to every 10-bit segment. If necessary, extra zeros are appended after the CRC bits to get the total number of bits (information bits, CRC bits, and tail bits) equal a multiple of 10. The payload header in the DM1 packet is only 1 byte long. The length indicator in the payload header specifies the number of user bytes (excluding payload header and the CRC code).

Taiyo Yuden Co. provides a user configurable firmware for the EYSF2SAXX which is very useful since you can change the default UART baud rate after hard reset, encryption, device address, transmitting power, etc.

6.4.5.4. Hardware Design

A schematic of the custom module (ASUL) is shown in Figure 6-14. This module is implemented as a single double-layer printed circuit card that integrates the microcontroller, Bluetooth radio, and solar power supply.

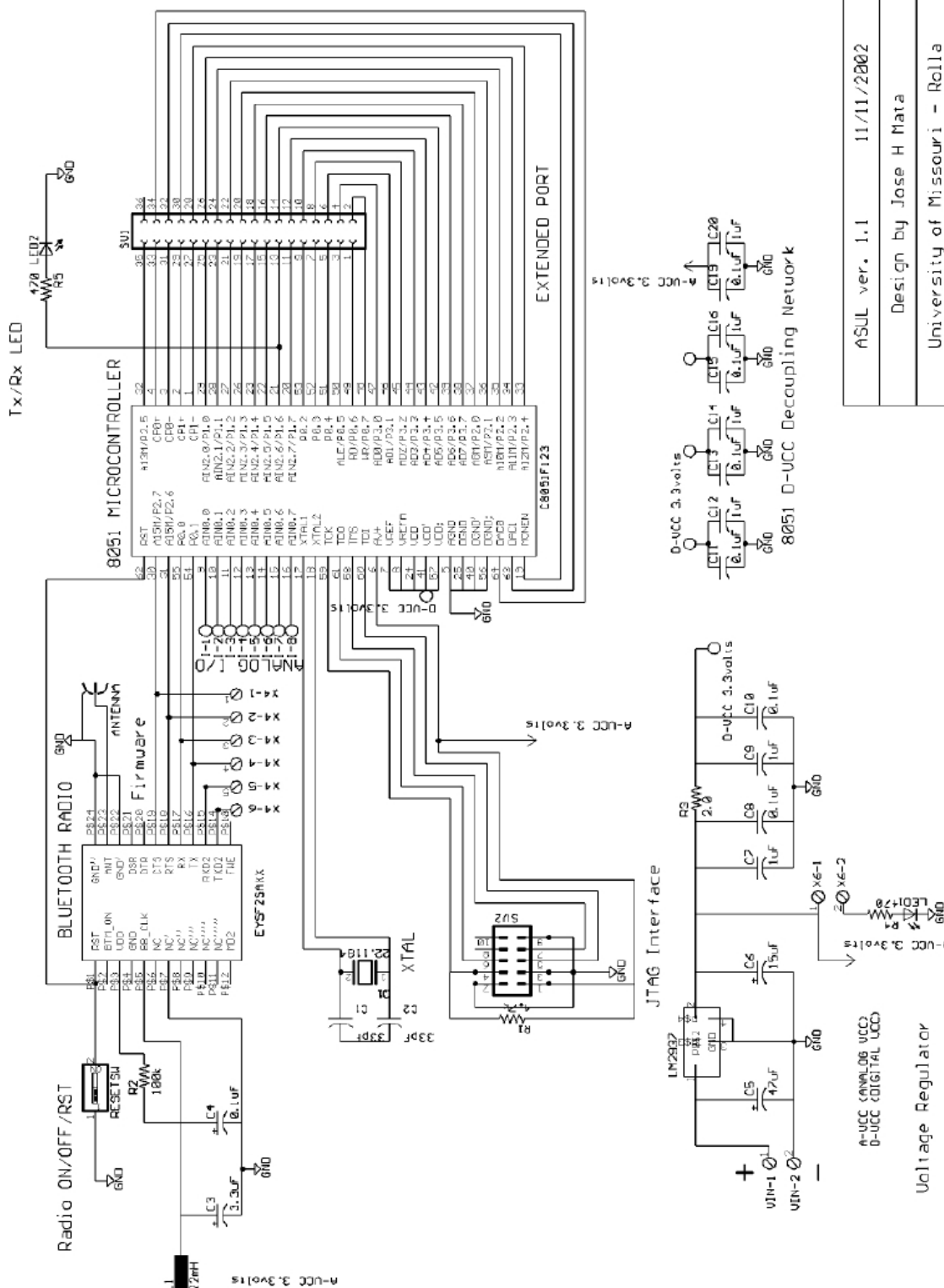


Figure 6-14 ASUL Schematic

ASUL ver. 1.1 11/11/2002
 Design by Jose H Mata
 University of Missouri - Rolla

6.4.5.5. ASUL Cluster

After completion of the circuit layout, including routing and power constraints, assembling the ASUL cluster were completed successfully using a reflow soldering station. Figure 6-15 shows the completed ASUL wireless cluster.

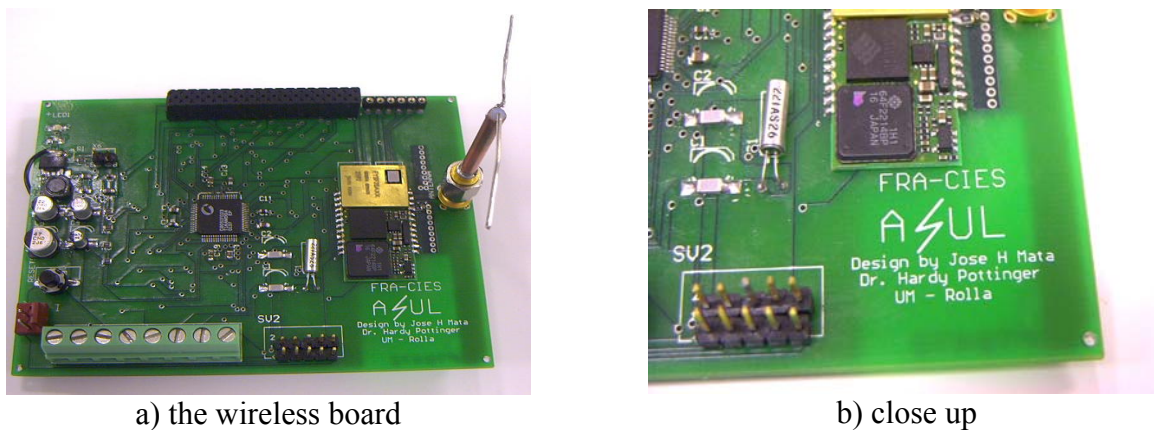


Figure 6-15 ASUL cluster

Soldering each of the components, testing and assembling of the external antenna were accomplished at UMR. After making software modifications for ASUL the board was ready to test. Several tests were performed to ensure the expected functionality. The board worked as expected and no errors were found in the board design. The main test is described in the next section, which describes the testing of the complete wireless solution for its full functionality.

6.4.6. COMPLETE WIRELESS SOLUTION DESCRIPTION

The complete wireless solution consists of three major components which are described as follows: (a) Remote PC containing a small industrial computer with a modified wireless LAN card built in, a weatherproof enclosure with external 2.4 GHz antennas, as well containing an LCD display for on site setup, and finally a Taiyo Yuden Bluetooth device acting as a master device; (b) one or more solar powered clusters containing a wireless data acquisition device “ASUL”; (c) and finally a PC with a standard Internet browser. The remote PC system is depicted in Figure 6-16.

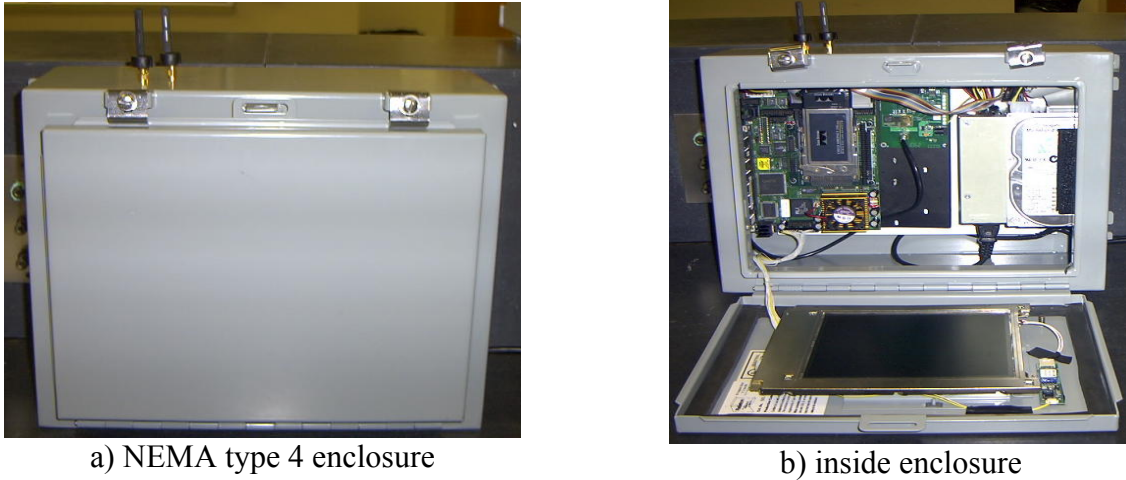


Figure 6-16 Remote PC

6.4.6.1. System Test Setup

The equipment was setup in the senior design lab at the University of Missouri-Rolla in order to use the existing IEEE 802.11 wireless infrastructure. The cluster shown in Figure 6-17 was connected to a signal generator and running on batteries. The cluster was located within a distance of about 9 meters from the remote PC.

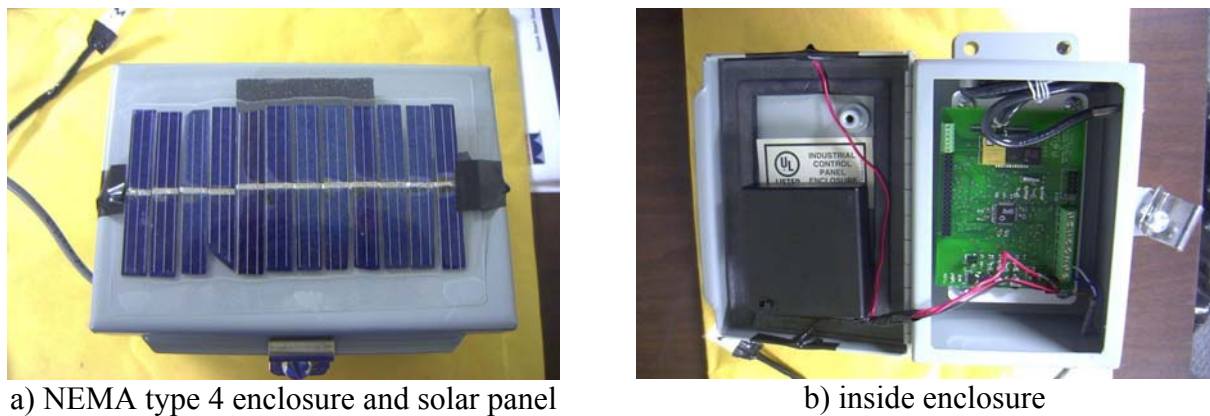


Figure 6-17 Cluster AZUL

The system test was prepared for testing the data transmission from a PVDF (e.g. LTD0) mounted on a predefined structural member of the lab Bridge specimen. The LTD0 served as a vibration sensor and it was connected to channel 4 on ASUL. The test consisted of applying a load at a given time (e.g. hit the Bridge with a hammer); this was done after the ORAP had

established a communication with ASUL, and sampling data from its analog channels. Figure 6-18 shows the lab setup conducted.

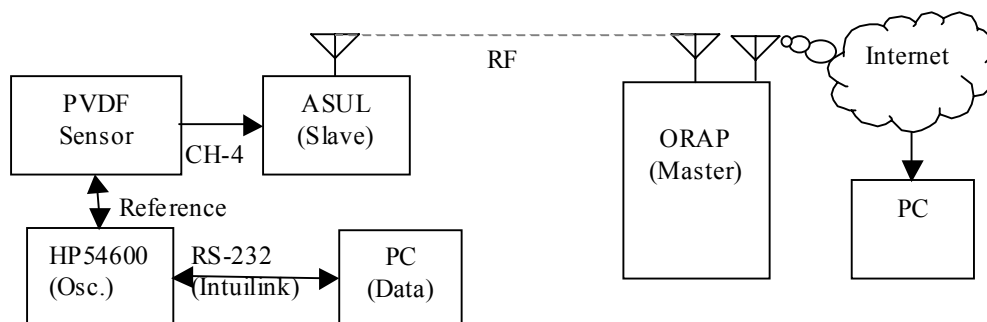


Figure 6-18 ASUL Test Configuration

Data received at the web site was plotted using Matlab. Figure 6-19 shows the sensor output as displayed on an HP54600 oscilloscope. Figure 6-20 shows the same data after it has been sampled, transmitted through the system, and plotted with Matlab. It is easy to see that the plots are the same.

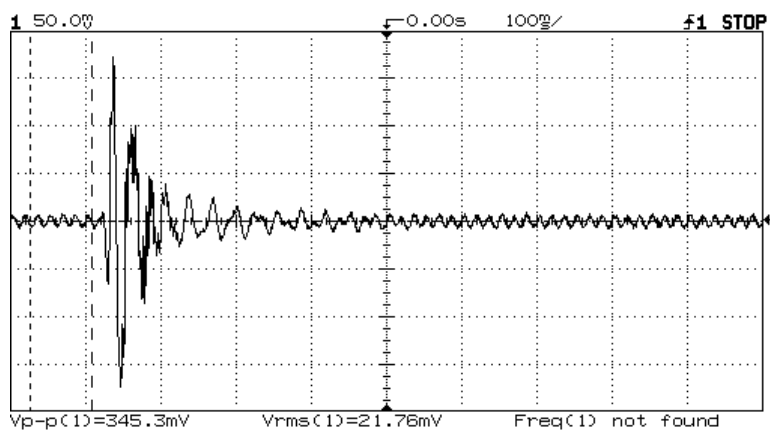


Figure 6-19 HP54600 Test V Plot

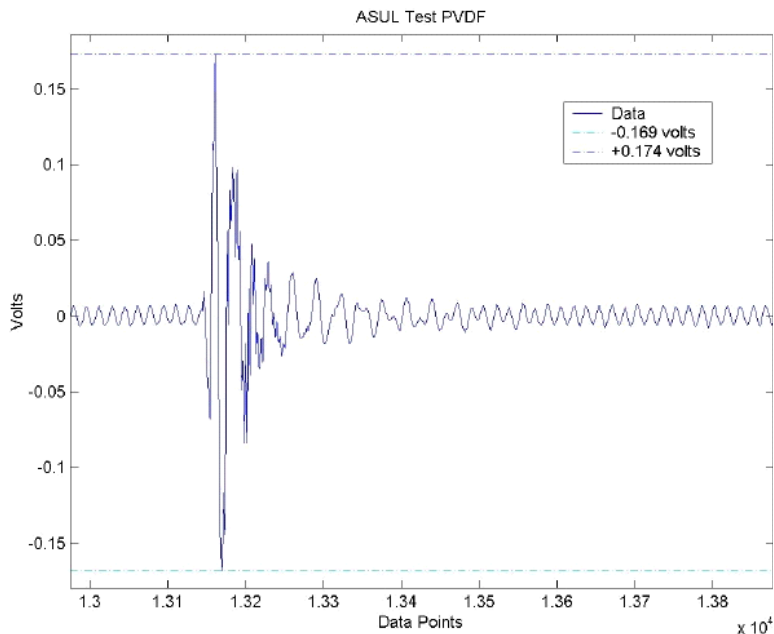


Figure 6-20 ASUL Test V Results

6.5. CONCLUSIONS

GPS appears to be the best solution available for accurate relative displacement measurements of steel railroad bridge displacement. Unfortunately the cost is prohibitive in most applications. A robust platform for constructing wireless distributed sensor networks was developed at UMR. Small, low-power, inexpensive Bluetooth-compliant radios, coupled with a fast microcontroller, and a solar power supply resulted in a low-cost, scalable subsystem on which to built sensor networks that are easy to configure and deploy in the field. While testing was conducted using simple PVDF vibration sensors, other sensors such as temperature and wind loading are simple to add. Software needs to be developed that will take full advantage of the computation capability of these smart sensors.

7. SMART HEALTH MONITORING SYSTEM

7.1. INTRODUCTION

7.1.1. BACKGROUND

Structural health monitoring of steel bridges is in general done using the vibration data collected from the bridge. The basic premise of vibration based structural health monitoring is that damage in the structure or change in its physical properties (i.e., stiffness, mass and/or damping) will, in turn, alter the dynamic response of the system. This change in dynamic response can be detected using smart engineering concepts and tools such as a hybrid neuro-fuzzy architecture and hence the damage can be detected. Soft computing tools like neural networks, fuzzy logic and genetic algorithms are used to solve such problems because of their inherent robustness and their abilities to handle nonlinearities and uncertainties in structural behavior. It is of essential importance to add smart engineering tools to process extensive amounts of data that are collected using the wireless monitoring devices.

7.1.2. OBJECTIVE

Over the past few decades structural health monitoring has received paramount importance. The necessity to develop reliable real-time health monitoring techniques is increasing. These types of health monitoring techniques allow continuous monitoring of the systems, capable of detecting damage, locating the damage and estimating the severity of the damage. The real-time health monitoring system described in this paper meets the following requirements:

- It is a non-destructive evaluation (NDE) technique
- It is capable of monitoring the structure on a global basis
- Initial and operating costs are inexpensive
- It is sensitive as to detect small damage
- It does not cause any disruption to the normal operation of the structure
- The equipment used for collecting data is small, it is easy to replace and is reliable

After an extensive literature review it is reasonable to conclude that vibration-based structural health monitoring is one of the most suitable options, because it has a number of advantages over some other conventional methods (Charles, et al. 2000). Vibration-based structural health monitoring is simple, inexpensive, small and more effective for real-time structural health monitoring (Doebbling et al. 1996, 1997, 1998). Vibration based structural health monitoring

provides continuous data, which can be processed and analyzed by the neuro-fuzzy architecture. Ambient excitation methods are more realistic and accurate for test data collection. Of the various ambient excitation methods a test vehicle based method is simple and reliable to use (Farrar, et al.). A cluster of sensors attached to different structural members can effectively monitor an entire bridge. Therefore a cluster of sensors attached to a bridge structure may be used to monitor for ambient vibrations by driving the test vehicle. Therefore based on this literature information, the research team selected the test vehicle based method to collect data on a bridge structure. This method was used on a bridge located approximately 30 miles from the University of Missouri-Rolla campus, on old route 66, (see figure 7.1).



Figure 7-1 Teardrop Bridge

In order to collect data at different ambient vibrations a test vehicle was driven along the bridge at different speeds. Test data was collected using a wireless sensor developed at UMR under this research program (see chapter 6). Results from this bridge monitoring program are presented and discussed in this report.

7.1.3. RESEARCH FINDINGS

An approach for monitoring the structural health of a bridge on a real-time basis based on vibration data using smart engineering systems and tools has been demonstrated. The demonstrated method has a number of advantages over the conventional methods. This system can monitor the bridge on a global and real-time basis. Data is collected and analyzed continuously. It is an NDE technique and does not cause disruption to the normal operation of the bridge. The sensitivity of the approach is high and it can detect small damages. The use of fuzzy logic and neural network makes it robust and helps in handling the non-linearities

associated with the structural behavior. The initial and operating cost of this system is also less. It is a relatively simple and easy approach, yet it is accurate and reliable.

7.1.4. CHAPTER LAYOUT

This chapter deals with the methodologies used to collect and analyze data from a bridge and to detect damages in the bridge. Section 7.2 gives a birds-eye view of the overall smart health monitoring system. Section 7.3 describes in detail the data acquisition and analysis procedures. Section 7.4 gives a brief description of the damage detection techniques used. Section 7.5 deals with fuzzy logic decision-making systems. Section 7.6 presents the neural network prediction system, which is followed by the possible future work.

7.2. OVERALL SYSTEM

Damage is generally defined as harm or injury to property or people, resulting in loss of value or the impairment of usefulness. In other words, it denotes a state of change, which affects its present or future performance. Implicit in the above definition is the fact that damage detection involves comparison with some initial stage, which is supposed to be the undamaged state.

In this research program wireless sensors were connected to different structural members of the Teardrop Bridge, which was selected in this program for data collection using a test vehicle vibration method. These sensors collect continuous vibration data by wireless means. As a first step some pre-processing was done to the data so that it can be fed to the fuzzy system architecture developed for this project. Details of the pre-processing process can be found in Section 7.3.

The fuzzy logic system developed was a decision-making system. The fuzzy logic basically uses some relationships between the members of the bridge under normal undamaged operational conditions to detect the possibility of damage in the bridge. If there is a possibility of damage, the fuzzy logic gives a list of members, which could possibly be damaged.

This data is fed into the neural network system. The neural network takes speed of the car as the input and tries to predict the vibration value that should occur if the bridge was undamaged. Based on this system the neural network outputs the result. Figure 7-2 shows the block diagram

of the overall system. However it is important that the fuzzy logic and neural network system be trained using data collected from the bridge operating under normal undamaged conditions.

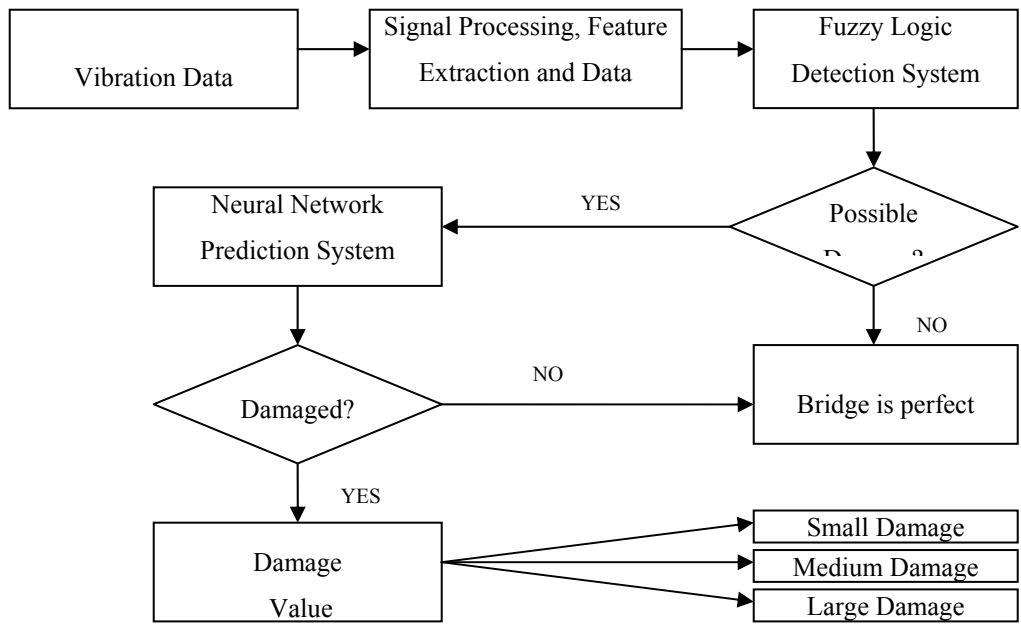


Figure 7-2 Overall System

Fuzzy logic and neural network were trained using the data collected from the Teardrop Bridge. The Teardrop Bridge was constructed by use of hot rivets in 1923 to serve Missouri Route 14. When Route 66 was laid across the country in 1926, the pre-existing bridge served as a convenient and cost saving alignment over the Big Piney River in Missouri. The bridge has a concrete deck and steel trusses. For testing, wireless sensors were attached on steel trusses and data was collected. The next section will deal in detail with the data collection procedures.

7.3. DATA ACQUISITION AND ANALYSIS

All data for this experiment has been collected from the Teardrop Bridge mentioned above. Figure 7-3, shows a sketch of the Teardrop Bridge and the locations where the vibration sensors were mounted.

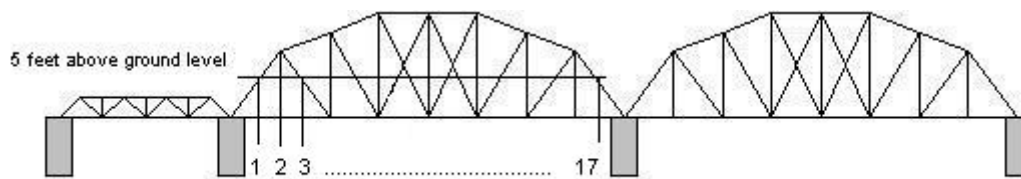


Figure 7-3 Teardrop Bridge – Sensor Locations

As can be seen in Figure 7-3 the sensors were mounted on various truss elements (both vertical and diagonal trusses) in one span of the bridge at a height of 5ft (1.5m) above ground level. With the sensor in Location 1 marked in Figure 7-3, a test vehicle (GMC Pickup) was driven from both directions at speeds of 10, 15 and 20 mph (16.1, 24.2 and 32.2 km/h) and the vibration data was collected. The same procedure was followed with sensors in the various locations marked indicated in Figure 7-3, such as 1, 2, 3 to 17.

The data acquisition part of real-time structural health monitoring can be subdivided into a number of steps. The first step was to decide on the type of data that is to be collected. Based on the above decision, the equipment needed to collect the data was chosen. Then, the type of data transmission was chosen. Two options are available: (1) wired data transmission, or (2) wireless data transmission. Next, a place to install the equipment was chosen. These locations were selected such that sensitive data could be collected and yet no disruption of the regular operation of the bridge occurred. In order to train the network relatively large data was collected. This affected the number of equipments that were used for data acquisition. Finally, the frequency at which data was collected was decided. All these sequential steps directly depend on the type of application.

Extensive literature review was performed (see Chapter 2) to select the best suited data acquisition technique for real-time structural health monitoring. Vibration wireless sensors were chosen and were connected to various truss elements of the bridge. At least one sensor was connected to each of the truss members. The sensors were connected to a blue tooth device, which transmitted the data, by wireless means to the data analyzing computer at the laboratory (see chapter 6 for specific details about the sensors). All analysis was performed in the laboratory at UMR. Data was collected and analyzed continuously.

There are two sets of data acquisition system. The first data acquisition system is an in-field system, which is described in Chapter 6. This system is directly wired to the sensors. It collects and transmits the data continuously by wireless means to the second set of data acquisition system. The second system consists of a PC running on Windows and uses MATLAB (computational software developed by MATHWORKS, Inc.) for data analysis. The neural network and fuzzy logic is also run within the MATLAB. With the sensor mounted on one of the trusses, data was collected continuously by driving a test vehicle at different speeds of 10, 15 and 20 mph (16.1, 24.1 and 32.2 km/h) in both directions.

The data analysis is part of a real-time structural health monitoring and, similar to the data acquisition, it can be subdivided into a number of steps. The first step is the pre-processing step. Feature selection and signal processing usually follow the pre-processing step. Then data cleansing is performed on the selected features of the data. This cleansed data analysis is finally fed into the smart engineering tools. The smart engineering tools then perform the data analysis.

The following section will describe how the data was analyzed. All the data used in the following section was collected by mounting the sensor on the Teardrop Bridge at locations, shown in the Figure 7-3.

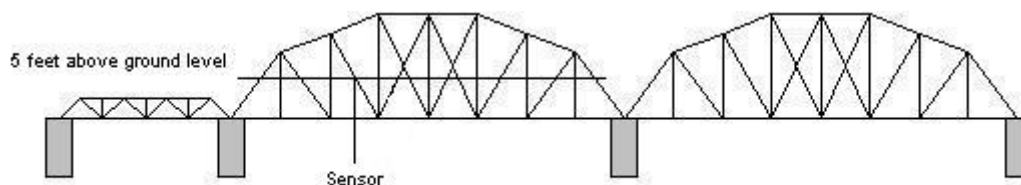


Figure 7-4 Sensor Locations

Figure 7-5, shows the un-calibrated output of the sensor when mounted on the truss of the Teardrop Bridge (see Figure 7-4) and the test vehicle driven at different speeds.

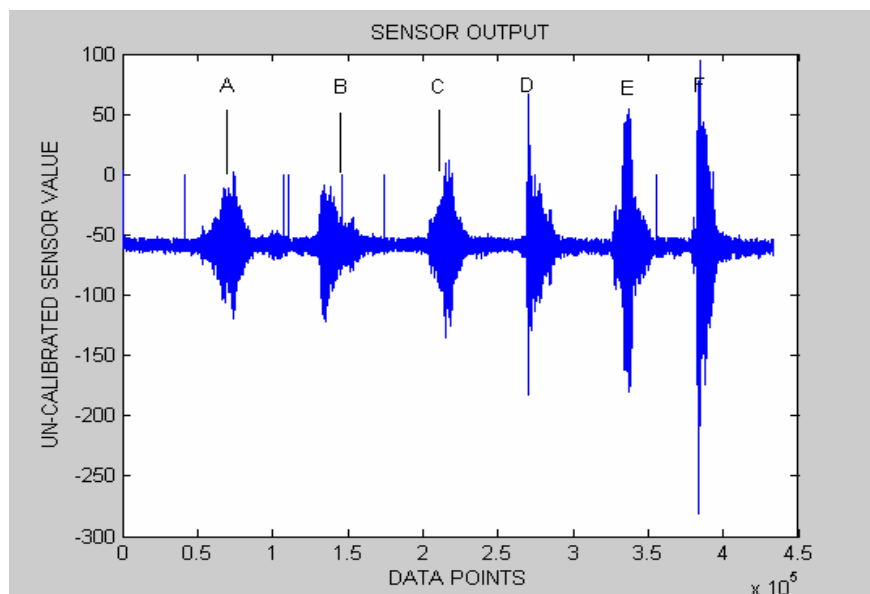


Figure 7-5 Sensor Output

Table 7.1, shows the details of the data presented in Figure 7-5.

Table 7.1 Data Details

Data	File Name	Direction	Speed		Car Type	Comments
			mph	km/h		
A	Testa	N-S Far-Close	10	16.1	Test Vehicle (GMC Pick-up)	5 ft above ground level in a diagonal truss
B		S-N	10	16.1	Test Vehicle	A
C		N-S	15	24.1	Test Vehicle	A
D		S-N	15	24.1	Test Vehicle	A
E		N-S	20	32.2	Test Vehicle	A
F		S-N	20	32.2	Test Vehicle	A

The collected data was obtained continuously and was a rather large set formed by 433280 data points. The first part of data analysis was to separate the vibration data for different speeds and direction. Figure 7-6 shows the separated data for the different speeds and direction.

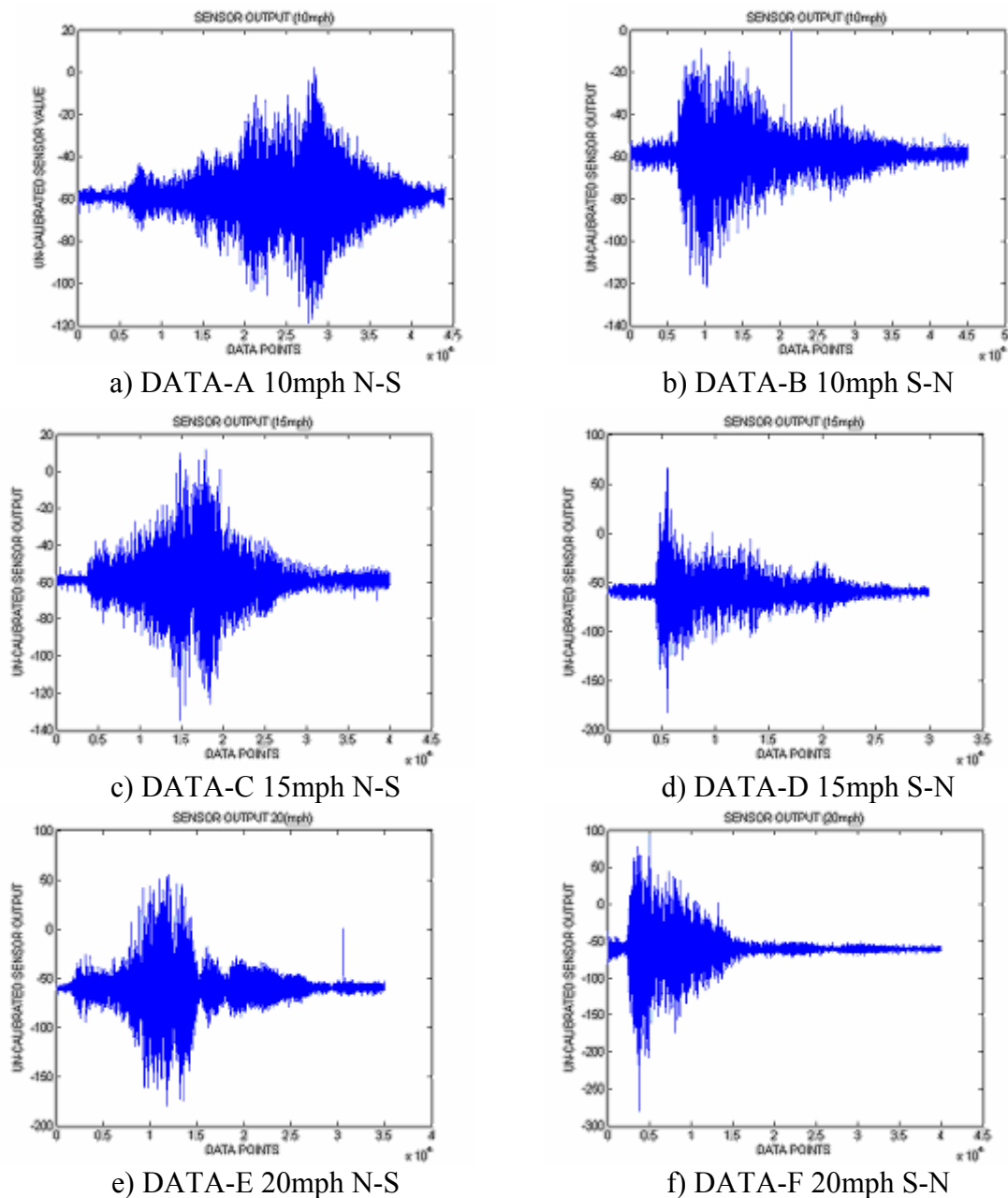


Figure 7-6 Un-calibrated Sensor Output

As can be seen from Figure 7-6, the data collected was not biased against a reference frame and had to be calibrated. The raw output values range between +/- 32767. It is calibrated based on the

sensor specifications and is converted to ± 2.4 volts. Figure 7-7 shows the data values in volts after the calibration process was completed.

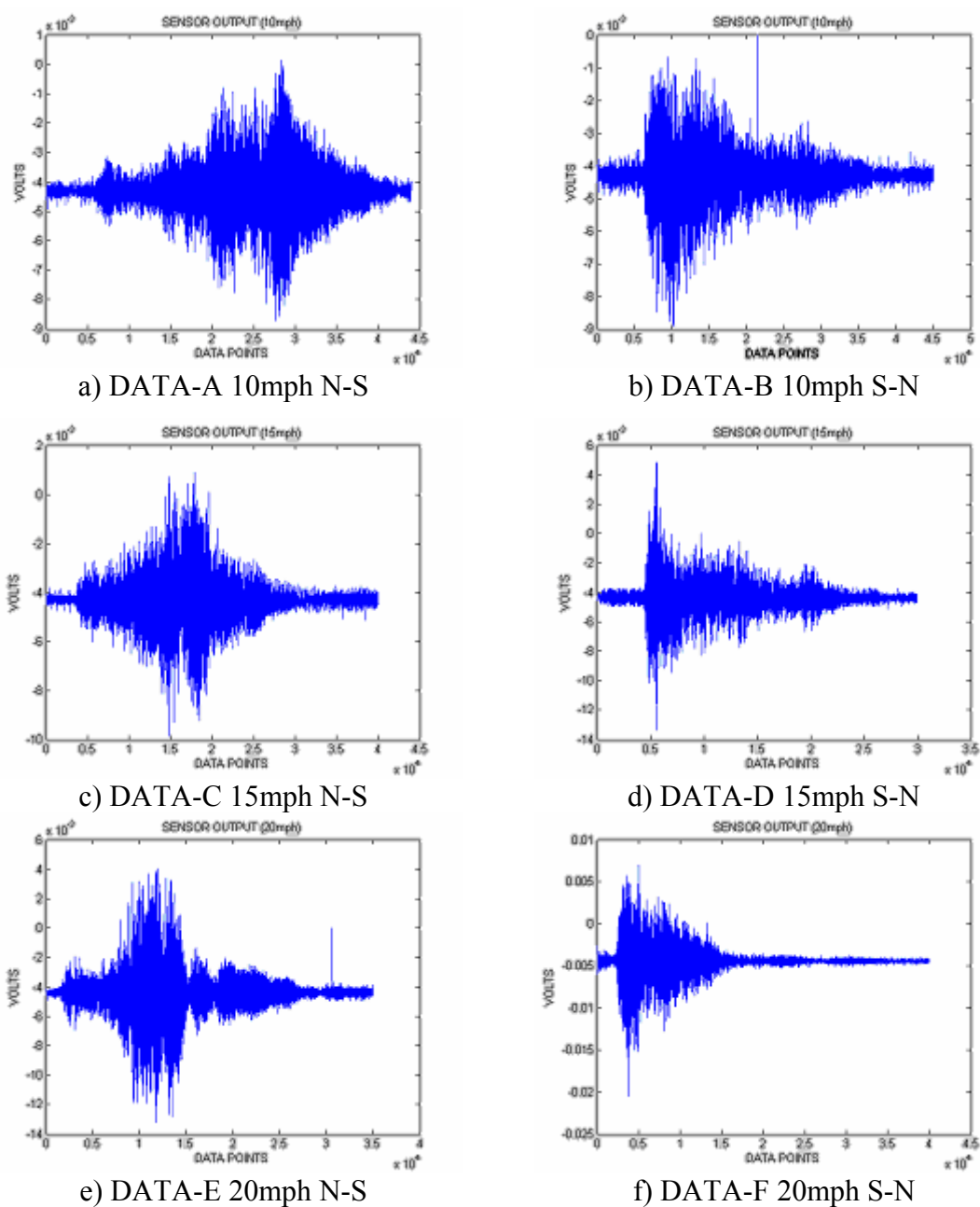


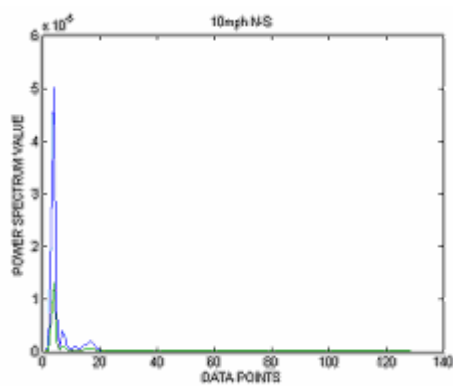
Figure 7-7 Calibrated Sensor Output

However, this data cannot be fed to the smart engineering tools like neural networks and fuzzy logic used in this research program but further data analysis is necessary. The next step in data analysis is called the feature selection. Feature selection involves condensing the data and

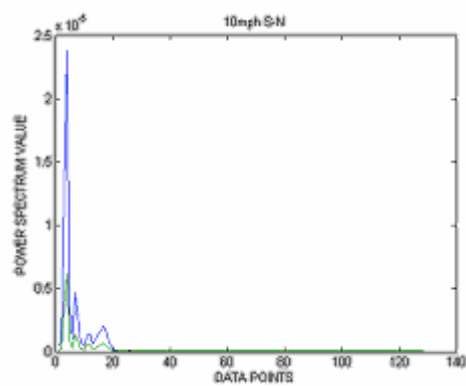
detecting a distinguished feature that can be used as input, to analyze and potentially detect damage. The main idea of feature selection is to reduce the dimensionality of the data. The goal of feature selection is to eliminate a feature if it yields little or no additional information beyond that subsumed by the remaining features. In particular, this will eliminate the irrelevant and redundant features. Thus, the data after feature selection will be reduced in dimension and will not have any redundant and nonrelevant data.

The next step in the data analysis comprises the signal processing. Signal processing involves processing the signal in such a way that useful information from the raw data is collected. This further reduces the dimensionality of the data space. Signal processing involves sampling and quantization in general. One way to look at a signal is in the discrete time domain, which puts a series of values consecutively in time. In this way it is possible to infer the behavior of the signal at every moment in time, and also make some simple statements commenting its long-term behavior. However, it is rather difficult to detect the long-term behavior relationship to the short-term development of the signal.

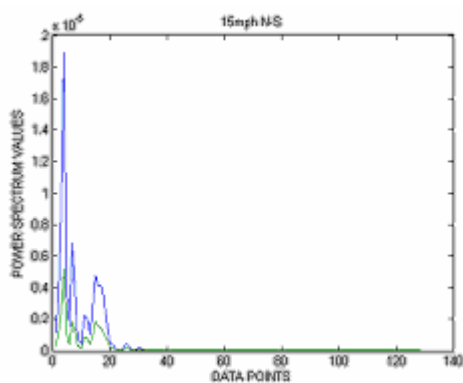
Another way to look at a signal is to view its spectral density (i.e., the Fourier transform of the signal). The Fourier transform views the signal as a whole. It swaps the dimension of time with the dimension of frequency. One can think of the Fourier transform as a combination of slow and fast oscillations with different amplitude. Fast Fourier Transform (FFT) reduces the number of computations needed for N points from $2N^2$ to $2N \lg N$, where \lg is the base-2 logarithm. Once again using FFT was not possible to conclude the nature of the signal and a different technique was employed. The power spectrum analysis was used instead. The power spectrum itself is the Fourier transform of the auto-correlation function. The auto-correlation function represents the relationship of long and short-term correlation within the signal itself. Figure 7-8 shows the power spectrum of the calibrated sensor output obtained at different speeds.



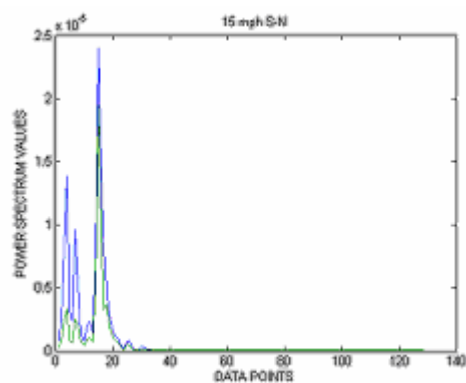
a) DATA-A 10mph N-S



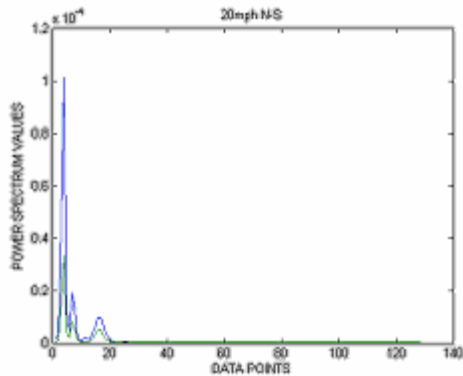
b) DATA-B 10mph S-N



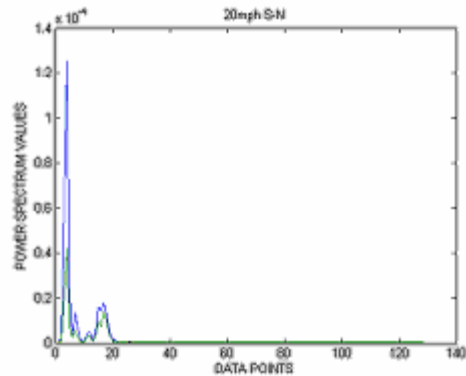
c) DATA-C 15mph N-S



d) DATA-D 15mph S-N



e) DATA-E 20mph N-S



f) DATA-F 20mph S-N

Figure 7-8 Power Spectrum Values

The next step in the data analysis part is the data cleansing. Data cleansing is the process of selectively choosing data to accept for, or reject from the feature selection process. Data cleansing is usually done based on expert knowledge. When previous experience or expert knowledge is not available, data cleansing is done based on a trial and error procedure. Peak values of power spectrum were used as cleansed data. This was done on a trial and error basis

and was best suited for feeding it as input to the fuzzy logic and neural network architectures. The next step relates to damage detection using the power spectrum analysis method.

7.4. DAMAGE DETECTION

This step involves detecting that damage has occurred, then finding the location of damage followed by the severity of damage and finally as how much would this affect the structural integrity of a bridge as a whole. In this condition, the data has to be analyzed in a manner that it can uniquely identify the damage, its location and severity. On extensive analysis it was found that the power spectrum peak values were unique for every different location of the sensor and that they increase with increase in speed. The relationship between the power spectrum values and speed was non-linear. It was also clear that the power spectrum values (indirectly the vibration values) also depends on a number of other parameters such as the mass of the vehicle, type of the vehicle (different types of suspension systems cause different vibrations) and so on.

Even though vibration varies with speed, its relation to a different member remains the same. For example, if the power spectrum peak value of a sensor mounted on a particular truss at a speed of 10mph (16.1 km/h) is greater than the power spectrum peak value of a sensor mounted on another truss at 10mph (16.1 km/h), the relation always holds at all different speed values and directions. This fact will be capitalized to detect if there is any damage in any member. If there is some damage, then based on the various relationships the member that is actually faulty can be detected. Since the speed-power spectrum relationship is a non-linear process the neural network can be used to predict the occurrence and severity of the damage. This method is promising because it is independent of the speed and also the mass of the vehicle.

For simplicity of explanation the above-mentioned technique was investigated by mounting sensors at only the five locations shown in the Figure 7-9. For the real-time testing, sensors were mounted on all the truss members and data was collected. All data was analyzed in a similar manner and the final results are discussed next.

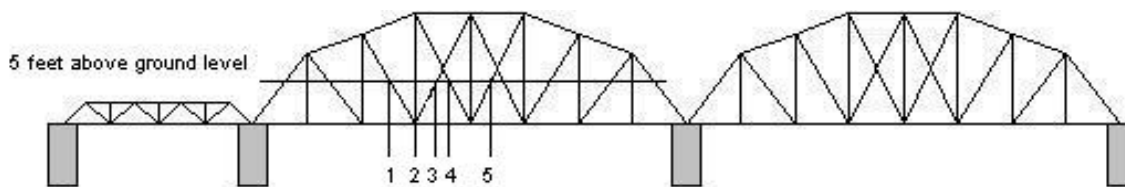


Figure 7-9 Sensor Locations

With the sensors mounted on one of these locations data was collected at speeds of 10, 15 and 20 mph (16.1, 24.1 and 32.2 km/h) in both directions. Table 7.2 shows a summary of the power spectrum values for these five locations at the above-mentioned speeds in both directions after performing all the data analysis.

Table 7.2 Power Spectrum Summary

Member	Power Spectrum Peak *e-4					
	10mph (16.1 km/h)		15mph (24.1 km/h)		20mph (32.2 km/h)	
Starting:	South	North	South	North	South	North
1	0.0614	0.1308	0.1948	0.2058	0.419	0.333
2	0.00395	0.00345	0.00678	0.01993	0.01155	0.02123
3	0.1121	0.2010	0.3760	0.752	0.989	2
4	0.01926	0.0161	0.0534	0.0856	0.0699	0.0857
5	0.0533	0.0338	0.1708	0.1557	0.1944	0.323

Figure 7-10 summarizes the data presented in Table 7.2. It shows the power spectrum values plotted based on the speed of the test vehicle and location of the sensor. From these results it is possible to conclude the following:

With increase in speed there is a non-linear increase in the power spectrum peak values.

At all different conditions the relationship between the members remains the same that is member 3 has the highest power spectrum value in all of the above cases followed by member 1, 5, 4 and 2 respectively.

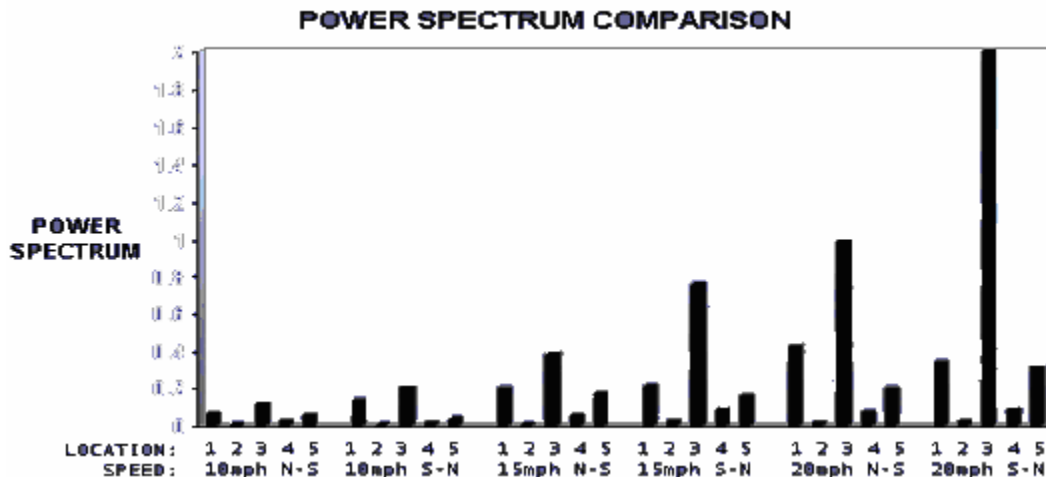


Figure 7-10 Power Spectrum Comparison

At a later data collection if there is some discrepancy in this relationship, it is possible to conclude that there is some damage in the bridge and based on the various relationships it is possible to detect the damaged member. The first step of detecting a possible damage is done using fuzzy logic. If possible damage is predicted by fuzzy logic, then the members that may be possibly damaged are detected and the neural network is used to predict the amount of damage in each of those members. The neural network makes the prediction based on the speed of the vehicle. The speed needs to be entered by the user. It can be collected using a speed gun in real time and fed to the neural network directly. The fuzzy logic system and the neural network architecture are discussed in the following section.

7.5. FUZZY LOGIC DECISION SYSTEM

Vibration based health monitoring using fuzzy logic has attracted the attention of structural control engineers during the last few years (Joghataie and Ghaboussi, 1994; Liba et al., 1994; Subramaniam et al., 1996; Battaini et al., 1998). The main characteristics of fuzzy logic are its effectiveness and ease in handling non-linearities, uncertainties and large collection of data.

Conventional decision making systems and control systems rely on the accuracy and the modeling of the system dynamics. Some complex civil structures are highly non-linear. Designing an accurate dynamic model may not always be possible. However, a fuzzy system does not require accurate dynamic models. Fuzzy logic is much closer to human thinking and

natural language than conventional logical systems. It provides an effective means of capturing the approximate, inexact nature of the real world. The basic idea of a fuzzy logic system is to incorporate the expert experience of a human operator in the design of the controller in controlling a process whose input-output relationship is described by a collection of fuzzy rules involving linguistic variables rather than a complicated dynamic model. The utilization of linguistic variables, fuzzy control rules, and approximate reasoning provides a means to incorporate human expertise in designing the controller.

- Fuzzy systems generally consist of the four principal components:
- Fuzzification Unit
- Knowledge Base
- Decision Making Logic
- De-fuzzification Unit

The first component is the fuzzification unit, which performs the function of fuzzification and converts input data into linguistic values. This basically maps measured inputs of crisp value into fuzzy linguistic values that can be used by the fuzzy decision making system. The second component is the knowledge base. This is a collection of expert control knowledge to take various actions. It consists of linguistic rules. In many cases it is easy to translate an expert's knowledge into such rules. So this type of controller is used to control complex processes when no precise model of the process exists and most of the information is available only in qualitative form. This also provides necessary definitions used to characterize fuzzy control rules and fuzzy data manipulation in the fuzzy logic controller. The next component is the fuzzy decision making logic. This performs various fuzzy logic operations to infer the control action for the given fuzzy inputs. The fourth component is the de-fuzzification unit, which converts the inferred fuzzy control action into required crisp control values to be entered into the system under control.

There is no fixed process for designing a fuzzy system. Also no rules exist for selection of the appropriate fuzzy parameters, and they therefore have to be chosen on the basis of an experimental trial and error approach or based on expert knowledge. The fuzzy system developed in this research program has gone through a number of iterations and the best-suited fuzzy parameters were used and are discussed next.

A fuzzy logic program was written using MATLAB, which performed all the required operations. As described the power spectrum peak values are given as input to the system. The system has been designed using 101 membership functions. The term set used was 0, 1, 2, 3 ... 99, 100. Numerical names were given to the term sets for simplicity. In this system triangular fuzzy numbers were used as membership functions corresponding to the elements in term set. The reason for using triangular fuzzy number was that it is easy to use. The triangular fuzzy number was denoted as follows:

$$f_M(x) = \begin{cases} \frac{(x-a)}{(b-a)}, & a \leq x \leq b, \\ \frac{(x-c)}{(b-c)}, & b \leq x \leq c, \\ 0, & \text{otherwise} \end{cases} \quad \text{Eq. 7.1}$$

Where a , b , and c are real numbers, and $a \leq b \leq c$.

The membership functions are shown in Figure 7-11.

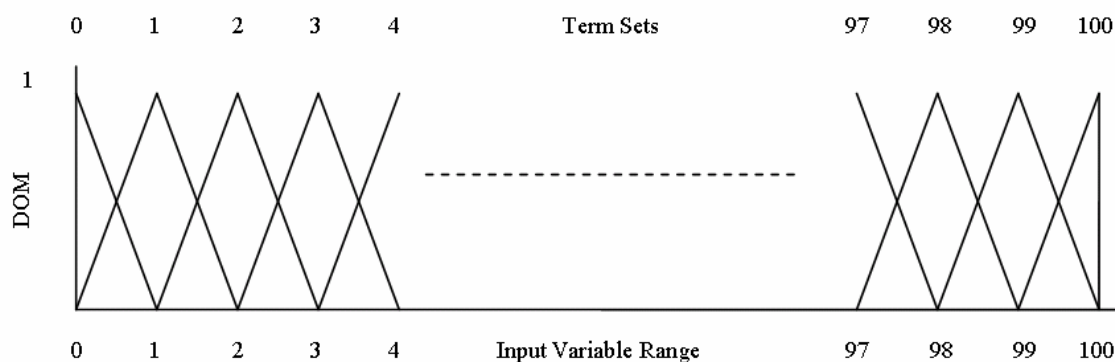


Figure 7-11 Membership Values

The input (power spectrum value) is fuzzified and is converted to a triangular fuzzy number. An input value may belong to two membership functions with different degree of memberships.

In such cases Zadeh (<http://www.cs.berkeley.edu/People/Faculty/Homepages/zadeh.html>) operators listed below are commonly used:

- AND => use the minimum of the options.
- OR => use the maximum of the options
- NOT => use 1-option

According to Zadeh's interpretation, AND operator is used for combining two different input classes. OR operator is used when choosing the membership value that belongs to an output class. NOT operator is used while combining two incompatible input classes. This program mainly used the AND operator. Then will have to order these fuzzy values. The process of ordering fuzzy numbers is called ranking. There are several methods of ranking fuzzy numbers (Chen, 1985; Kim and Park, 1990; Liou and Wang, 1992). In this research project, the total integral value method (Liou and Wang, 1992) was used because of its simplicity and accuracy. Accordingly, the total integral value for triangular fuzzy number $F = (a, b, c)$, was defined as:

$$I_T^\alpha (F) = \left(\frac{1}{2}\right) [\alpha c + b + (1 - \alpha) a] \quad \text{Eq. 7.2}$$

Here, α is an index of optimism that represents the degree of optimism of the decision-maker. It has a value between 0 and 1. A larger value of α indicates a higher degree of optimism. For given fuzzy numbers F_i and F_j , if $I_T^\alpha(F_i) < I_T^\alpha(F_j)$, then $F_i < F_j$; if $I_T^\alpha(F_i) = I_T^\alpha(F_j)$, then $F_i = F_j$; and if $I_T^\alpha(F_i) > I_T^\alpha(F_j)$, then $F_i > F_j$.

As described above the fuzzy system will give a ranked member relation output. This will be compared with the general order member relation got as input from the user. If both these values match perfectly then the bridge is intact. If there are some discrepancies then one or more member may be damaged. Based on the above calculations and comparisons some members may be classified as possibly damaged. This does not mean that all these members actually are damaged. Fact is that if a single member is damaged, it may affect the general relationship order of more than 1 member. So, further analysis will have to be done using neural network.

7.6. NEURAL NETWORK PREDICTION SYSTEM

Neural network is a promising new generation information processing system that demonstrates the ability to learn, recall, and generalize from training patterns and data. They are deliberately constructed to make use of some organizational principle resembling the human brain.

Neural networks have a large number of highly interconnected processing elements (nodes) that usually operate in parallel and are configured in regular architectures. The collective behavior of the neural network, like human brain, demonstrates the ability to learn, recall, adapt and generalize data.

Neural network are excellent for predictions, pattern recognition, classification, conceptualization, filtering and optimization, while traditional computers, because of their architecture, are inefficient at these tasks. There are a variety of architectures and types of neural networks. The Back propagation network and Self-Organizing Maps are Feed-Forward type of neural networks, which are commonly used for predictions. Perceptron is another type commonly used for predictions. Hopfield Network and Hamming Network are commonly used for association tasks. Learning Vector Quantization and Self-Organizing Maps are used for classification problems. Adaptive Resonance theory is used for conceptualization. Hopfield Network is also used for optimization. These are not fixed rules of thumb, but are the most common ways in which the different types of neural network architectures used in various problem-solving areas.

When a car or any other vehicle moves on a bridge, the bridge vibration varies with respect to the speed of the vehicle (assuming all other parameters like the load etc., remain the same). Therefore by training the neural network with different speeds and their corresponding vibration values (power spectrum values of vibration data was used) the neural network was made to predict the power spectrum value of a particular vibration value at a particular speed for a particular member.

The most commonly used Backpropagation network was used for solving this prediction problem. Werbos developed Backpropagation first (Werbos, 1994); however, this work remained unknown for many years. The presentation of Backpropagation by Rumelhart et al. (1986) was probably responsible for the popularization of the algorithm in the areas of science and

engineering. The standard steps in a Backpropagation algorithm are to initialize the network synaptic weights to small random values, form training set (Corresponding input-output pairs) and calculate the network response, calculate the error value (difference between desired and actual output), update the weights, repeat from Step 2 iteratively as long as the predefined level of accuracy is reached. There are a number of variations available to the Backpropagation algorithm. The choice of a type of Backpropagation algorithm depends totally on the application. A number of neural network architectures were tested for this research application and it was found that the Backpropagation network using Levenberg-Marquardt (LM) method was the best.

The next step involved selecting the number of neurons in the input, hidden and output layers. Different number of neurons in the hidden layer were used and tested, with the aim of having minimum possible number of neurons as this will not only ensure better performance and faster training but also will prevent any potential over fitting problems. It finally boiled down to fifteen neurons. Different combinations of transfer functions in the hidden layer and the output layer were tested. Finally tansig in the hidden layer and purelin in the outer layer yielded the best results. The Backpropagation architecture is shown in Figure 7-12.

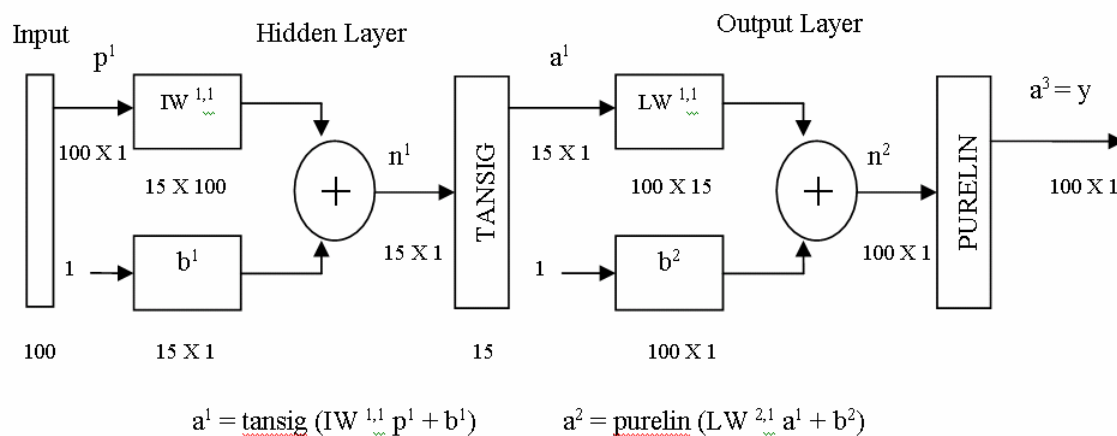


Figure 7-12 Backpropagation Architecture

The Architecture Details are summarized below:

Input:	100 Data Points (speed)
Target:	100 Data Points (Power Spectrum Peak Value)

Algorithm:	Back Propagation (LM Method)
Layers:	2 Layers [15 1]
Transfer Functions:	[Tansig Purelin]
Error Rate:	1e-8
Max Epochs:	1500

In order to overcome the over fitting problem of the BP network and improve its generalization, the early stopping technique was used. In this technique, the available data are divided into three subsets. The first subset is the training set, which was used for computing the gradient and updating the network weights and biases. The second subset was the validation set. The error on the validation set was monitored during the training process. The validation error will normally decrease during the initial phase of training, as also the training set error does. However, when the network begins to over fit the data, the error on the validation set will typically begin to rise. When the validation error increases for a specified number of iterations, the training was stopped, and the weights and biases at the minimum of the validation error are returned. The third set was the testing set.

The user was asked to input the speed of the vehicle. The speed can be collected using a speed gun in real time. The above neural network was run for different members (which were put in the possibly-damaged list by the fuzzy logic system) separately and it predicted a corresponding power spectrum peak value for each one of them. This predicted value was compared with the value entered by the user. Based on the difference between these two values the program outputs the result as:

- a) The Member N is Fine
- b) The Member N has Small Damage
- c) The Member N has Medium Damage
- d) The Member N has Large Damage

As can be seen above the output is a fuzzy linguistic value. The main reason for giving an output like this than giving values like 0.4in (10mm) damage or so is because, 0.4in (10mm) damage may not give the user a good idea of the damage. This value may be very small in the case of a

very large bridge but may be significant in a small bridge. So, fuzzy linguistic variables are used which can be understood easily, so that corresponding actions may be taken.

7.7. CONCLUSIONS

An approach for monitoring the structural health of a bridge on a real-time basis based on vibration data using smart engineering systems and tools has been demonstrated. The demonstrated method has a number of advantages over the conventional methods. This system can monitor the bridge on a global and real-time basis. Data is collected and analyzed continuously. It is an NDE technique and does not cause disruption to the normal operation of the bridge. The sensitivity of the approach is high and it can detect small damages. The use of fuzzy logic and neural network makes it robust and helps in handling the non-linearities associated with the structural behavior. The initial and operating cost of this system is also less. It is a relatively simple and easy approach, yet it is accurate and reliable.

7.7.1. RECOMMENDATIONS FOR FUTURE RESEARCH PROJECTS

Vibration based health monitoring has a number of advantages over other conventional methods. But it does not come without a price. In order to detect damages efficiently and accurately data from damaged bridge is needed, which is generally not available. In such cases generally expert knowledge and experience is used in arriving at this data. The current system relies on this. A better way would be a simulation using finite element analysis to get the damaged data set. Currently fuzzy ranking is used in the decision-making system. For a complex structure with many truss members this type of a method will be very tedious. In such cases Fuzzy clustering will yield better and faster results.

8. CONCLUSIONS AND FUTURE RESEARCH NEEDS

8.1. CONCLUSIONS

The main objectives of this research program were: (1) to demonstrate the use of FRP composites in the repair/rehabilitation of railroad steel bridges with highly corroded steel members, and (2) health monitoring of railroad steel bridges to ensure a safe mode of operation of these bridges. The following discussion lists potential applications of the research program findings and future research needs.

In this research program experimental and analytical studies were conducted to investigate the feasibility of using advanced composites made of fibers embedded in a polymeric resin for the retrofit of highly corroded steel members. Since there are no nationally accepted specifications for the construction process control and structural repairs of bonded FRP composite materials, results from this research program will be used to initiate the development of retrofit techniques for application to highly corroded steel. In addition, in this research program, UMR researchers from the civil, engineering management, and electrical engineering departments have concluded the design of a field deployable remote wireless data collection system for health monitoring. In the next section a summary of major research findings are presented.

8.1.1. REPAIR/REHABILITATION OF STEEL MEMBERS WITH FRP COMPOSITES:

Research findings have an immediate application in the rehabilitation of corrosion-damaged steel structures. Since most of the steel bridges in the railroad inventory are over fifty years old and many have not been painted in many years because of environmental regulations related to lead paint removal, these factors combine to make corrosion a major problem facing railroad bridge maintenance forces. As a result transfer of technology is of urgent need to convert test results into field practice.

Another major issue in the repair rehabilitation of railroad bridges is that the majority of these old steel structures are riveted. Rivets are difficult and time-consuming to remove. This makes repair of corrosion damage by adding steel patch plates or cover plates more difficult. In addition, removal of portions of corrosion-damaged members during repair or replacement can require temporary closure of the structure to train traffic. The resulting train delays can be very costly. The use of FRP composites for repair of corrosion damaged members, particularly if the

composite material can be applied to existing steel surfaces without removal of the field corrosion, could minimize the need for rivet removal and train delay. As a result, future research should address the strengthening of steel structures without the removal of either rivets or surface corrosion.

Many older steel structures were designed for lower live load levels than modern structures. The use of 286,000 lb. (1273 kN) cars is now common on Class I railroads, and becoming an increasing concern on short-line and light density roads. These railroads frequently were originally branch lines of larger railroads, which usually were maintained at a lower level than the main lines. The cost of the strengthening needed to carry these heavier cars can have a major economic impact on a short line. However, their economic survival may require the ability to handle this traffic. The use of FRP reinforcement for supplemental strengthening of railroad structures to safely carry 286,000 lb. (1273 kN) traffic could provide a cost-effective method of allowing short-line railroads to increase their ability to accept and transport these heavier cars.

The retrofit of axially loaded steel compression members using FRP pipes filled with expansive concrete offers possible benefits for structural rehabilitation and strengthening. In addition, in our increasingly security-conscious environment, it may have potential for increasing the blast resistance of steel bridge columns. This application is further described later in this chapter.

8.1.2. HEALTH MONITORING OF STEEL BRIDGES USING NEURAL NETWORKS:

One aspect of the technology demonstrated in this research program could be applied very easily to bridge rehabilitation. Many older steel truss bridges have eyebar tension members, typically consisting of multiple bars in a single member. Over time, wear in the pin joints leads to loosening of these bars. Heat shortening of the bars is then performed to tighten the member components. A problem in this process is the verification that the eyebars in the member are uniformly tight following heat shortening. The current method for checking tightness is to oscillate each bar and manually measure its frequency of vibration, which is mathematically related to its tightness. This check is done by moving a pencil for a given time period along a strip of paper attached to the eyebar, and counting the peaks of oscillation. This method is shown in Figure 8-13.



Figure 8-13 Manually Investigating the Tightness of Eyebars in Steel Bridges

The use of the Bluetooth technology with accelerometers would allow the direct reading of the frequency of vibration of eyebars. The accelerometer could be clipped to the eyebar, which would then be oscillated manually. The frequency of vibration could be read directly from a laptop computer with a data acquisition system. This would be faster and have a higher degree of accuracy than the manual method.

8.2. FUTURE RESEARCH NEEDS

8.2.1. REPAIR/REHABILITATION OF STEEL MEMBERS WITH FRP COMPOSITES:

More research on required surface treatment for application of the FRP composite material to the existing steel member is needed. Particular attention should be paid to the attachment of FRP strengthening to riveted steel structures. Further research on the strengthening of axially loaded compression members with FRP pipe filled with expansive concrete is needed to determine the effects of the reduced modulus of elasticity of concrete on the resulting column strength. Full-scale trials of both of these strengthening techniques should be performed to verify constructability under field conditions. These trials would also be conducive for testing the long-term durability of these repairs.

8.2.2. STRENGTHENING OF TIMBER AND CONCRETE BRIDGE MEMBERS WITH FRP COMPOSITES:

As discussed above, a pressing economic issue facing short-line railroads is the strengthening of structures required for carrying 286,000 lb. rail cars. Short-line railroads typically have more

timber than steel structures, and the capacity of the timber structures are also a concern. Research into the applicability of FRP strengthening to railroad timber structures could be useful.

In addition, many concrete bridges are also found on short-line railroads. It is likely that most of these will have satisfactory capacity for 286,000 lb. traffic. However, FRP strengthening could be applicable to cases where these structures have substandard load capacity.

8.2.3. IMPROVING BLAST RESISTANCE OF RAILROAD BRIDGE MEMBERS WITH FRP COMPOSITES:

The support columns of railroad bridges are probably the elements most vulnerable to attack. This is due to their easy accessibility from ground level. Increasing the blast resistance of these components, particularly on critical bridges, could be a cost-effective way to improve the security of the rail transportation system.

The retrofit of axially loaded steel compression members using FRP pipes filled with expansive concrete described earlier in this report may have some potential application for blast protection. Prior experience has shown that the effectiveness of certain types of explosives is greatly reduced by preventing the explosive from having direct contact with the structural element. The concrete fill in the FRP pipe could help dissipate blast forces, as well.

This potential application would require sophisticated study by a multi-disciplinary team to verify its applicability. Team expertise would be needed in structural behavior, composite materials, and explosive properties and performance.

8.2.4. HEALTH MONITORING OF STEEL BRIDGES USING NEURAL NETWORKS:

Further research into several aspects of this work is needed to improve its applicability to the railroad industry.

First, a determination of the key parameters for structural monitoring must be made. These parameters would likely vary depending on structure type.

Next, criteria for good and poor structural health should be established. These will determine the threshold for sending a warning notice to the appropriate railroad officials on a particular structure's condition.

Finally, a reliable mechanism for sending the information on structure condition should be developed. This could be through the railroad signal system. The importance of the reliability of this information system cannot be overemphasized. The issuance of warnings on poor structural health that cannot then be verified by inspection will rapidly lead to a loss of confidence in the system.

A simple pilot program demonstrating this technology could provide an initial step toward eventual full implementation. Many railroad bridges are located in remote areas. Monitoring of these structures with one or two accelerometers to check for extreme events, such as earthquake, scour damage, or even explosive blast, would provide a warning to railroad officials that the structure needed immediate inspection.

LIST OF REFERENCES

- AASHTO LRFD Bridge Design Specifications (1994), 1st Ed., American Association of State Highway and Transportation Officials (AASHTO), Washington, D.C.
- ACI 440.1R-01 (2001), "Design for the Design and Construction of Externally Bonded FRP Systems for Strengthening Concrete Structures".
- Albrecht, P., and Sahli, A. (1988), "Static Strength of Bolted and Adhesively Bonded Joints for Steel Structures," Proceedings of the International Symposium on Adhesively Bonded Joints: Testing, Analysis, and Design, Baltimore, Maryland, 10-12 September 1986, pp.
- Albrecht, P., Sahli, A., Crute, D., Albrecht, Ph., and Evans, B. (1984), "Application of Adhesives to Steel Bridges," Report FHWA/RD-84/037.
- Al-Saidy, A.H. (2001), "Structural Behavior of Composite Beams Strengthened/Repaired with Carbon Fiber Reinforced Polymer Plates," Ph.D. Diss., Iowa State University.
- Altrock, C. von (1995), "Fuzzy Logic & Neurofuzzy Applications Explained," Prentice-Hall Inc., Upper Saddle River, New Jersey Prentice-Hall, Inc.
- Ammar, N. (1996), "Rehabilitation of Steel Bridge Girders with Graphite Pultrusion," M.S. Thesis, University of Delaware.
- Askegaard, V., and Mossing, P. (1988), "Long Term Observation of RC-bridge Using Changes in Natural Frequencies," *Nordic Concrete Research*, Vol.7, pp.20-27.
- Battani, M., Casciati, F., and Faravelli, L. (1998), "Fuzzy Control of Structural Vibration: An Active Mass System Driven By Fuzzy Controller," *Earthquake Engineering and Structural Dynamics*, Vol.27, No.11, pp.1267-1276.
- Buckley, J.J. (1985), "Ranking Alternatives Using Fuzzy Numbers, Fuzzy Sets and Systems," Vol.15, pp.21.
- "Building Code Requirements for Structural Concrete (318-95)", ACI, 1995.
- Chen, S.H. (1985), "Ranking Fuzzy Numbers with Maximizing Set and Minimizing Set, Fuzzy Sets And Systems," Vol.17, p.113.
- Chen, W.F., Lui, E.M. (1987), "Structural Stability: Theory and Implementation," New York: Elsevier.
- Denton, S.R. (2002), "Analysis of Stresses Developed in FRP Plated Beams Due to Thermal Effects," FRP Composites in Civil Engineering, CICE 2001, (Edited by J.-G. Teng). Proceedings of the International Conference on FRP Composites in Civil Engineering, 12-15 December 2001, Hong Kong, China.

Doebling, S.W., Farrar, C.R., and Goodman, R. (1997), "Effects of Measurement Statistics on the Detection of Damage in the Alamosa Canyon Bridge," Proceedings 15th International Modal Analysis Conference, Orlando, FL.

Doebling, S.W., Farrar, C.R., Prime, M.B., and Shevitz, D.W. (1996), "Damage Identification and Health Monitoring of Structural and Mechanical Systems from Changes in their Vibration Characteristics: A Literature Review," Los Alamos National Laboratory report LA-13070-MS.

Doebling, S.W., Farrar, C.R., Prime, M.B., and Shevitz, D.W. (1998), "A Review of Damage Identification Methods that Examine Changes in Dynamic Properties," *Shock and Vibration Digest*, Vol.30, No.2, p.21

Euler, L. (1744), Appendix "De curvis elasticis," in "Methodus inveniendi lineas curvas maximi minimive proprietate gaudentes", Lausanne and Geneva.

Falk, S. (1956), "Ingr.-Arch.," Vol.24, p.85.

Farrar, C.R., and Doebling, S.W. (2000), "Lessons Learned from Applications of Vibration-Based Damage Identification Methods to a Large Bridge Structure," Proceedings of the International Workshop on Structural Health Monitoring, Stanford, CA.

Farrar, C.R., Doebling, S.W., and Duffey, T.A. (1999), "Vibration-Based Damage Detection," presented at the SD2000 Structural Dynamics Forum.

Farrar, C.R., Duffey, T.A., Cornwell Jr., P., and Doebling, S.W. (1995), "Excitation Methods for Bridge Structures," Proceedings of the 17th International Modal Analysis Conference, Kissimmee, FL.

FHWA (2001), Federal Highway Administration, Report 2001
<http://www.fhwa.dot.gov/bridge/britab.htm> (04/14/03)

Franke, A. (1901), "Z. Math. u. Physik", Vol. 49.

Fuzino, Y., Abe, M., Shibuya, H., Yanagihara, M., Sato, M., Nakamura, S., Sakamoto, Y., (2000), "Forced and Ambient Vibration Tests and vibration Monitoring of Hakusho Suspension Bridge," *Transportation Bridge Record* 1696, pp.57-63.

Ghosh, U.K. (2000), "Repair and Rehabilitation of Steel Bridges," A.A. Balkema Publishers.

Heywood, R., Roberts, W., Taylor, R. and Andersen, R. (2000), "Fitness-for-Purpose Evaluation of Bridges Using Health Monitoring Technology," *Transportation Research Record* 1696, pp.193-201.

Hoff, G. (1972), "Practical Applications of Expansive Cements," CTIAC Report 8, U.S. Army Engineer Waterways Experiment Station, Vicksburg, Mississippi.

Hollaway, L.C. (2002), "The Development and the Future of Advanced Polymer Composites in the Civil Infrastructure," Proceedings of the First International Conference for Advanced

Polymer Composites for Structural Applications in Construction, Southampton University, U.K., 15-17 April 2002, pp.3-21.

http://www.ciria.org.uk/bct_rp645.htm (01/17/03)

<http://xnet.mouchel.com/aesolut> (01/23/03)

Joghatatie, A., and Ghaboussi, J. (1999), "Neural Network and Fuzzy Logic in Structural Control," Proceedings of 1st World Conf. On Struct. Control, Vol.1, Pasadena, Calif., pp.21-30.

Kim, K., and Park, K.S. (1990), "Ranking Fuzzy Numbers with Index of Optimism, Fuzzy Sets and Systems," Vol.35, p.143.

Klaiber, F.W., Dunker, K.F., Wipf, T.J., and Sanders, Jr., W.W. (1987), "Methods of strengthening existing highway bridges," National Cooperative Highway Research Program Report 293.

Klein, A., Karby, T., and Povilka, M. (1961), "Properties of Expansive Cement for Chemical Pre-stressing," *Journal of ACI, Proceedings*, Vol.58, pp.59-79.

Li, T. (2002), "Performance-Assessment of Infill URM Walls Retrofitted with FRP Composites under In-Plane Loads," M.S. Thesis, University of Missouri – Rolla.

Liba, M., Fuzitani, H., Kitagawa, Y., Midorikawa, M., Kawamura, H., and Mochio, T. (1994), "Shaking Table Test on Seismic Response Control System by Fuzzy Optimal Logic," Proceedings of 1st World Conf. on Struct. Control, Vol. 1, Pasadena, Calif., pp.69-77.

Liby, L.W. (1993), "Steel Composite Bridge Sections Strengthened by Carbon Fiber Reinforced Plastic Laminates," M.S. Thesis, University of South Florida, Tampa.

Liou, T.S., and Wang, M.J.J. (1992), "Ranking Fuzzy Numbers with Integral Value, Fuzzy Sets and Systems," Vol.50, p.247.

Liu, X., Silva, P.F., and Nanni, A. (2001), "Rehabilitation of Steel Bridge Members with FRP Composite Materials," Proceedings of the CCC 2001 Composites in Construction, Porto, Portugal, October 10-12, 2001, pp.

Maletz, M. (1932), "Design of Columns of Varying Cross Section," *Trans. ASCE*, Vol.54.

"Manual of Steel Construction, Load & Resistance Factor Design", Second Edition, AISC, 1998.

Masri, S.F., Nakamura, M., Chassiakos, A.G., Caughey, T.K., (1996), "Neural Network Approach to Detection in Structural Parameters," *ASCE Journal of Engineering Mechanics*, Vol.122, No.4.

Matusumoto, S. (1970), "Expansive Additive for Cement," CEER.

- McKnight, S.H., Bourban, P.E., and Gillespie, Jr., J.W. (1994), "Surface Preparation of Steel for Adhesive Bonding in Rehabilitation Applications," Proceedings of the 1994 ASCE Conference – Infrastructure: New Materials and Methods for Repair, San Diego, CA, pp.
- Mehta, P.K. (1986), "Concrete-Structures, Properties, and Materials," Prentice-Hall, Inc., Englewood Cliffs, New Jersey 07632.
- Mertz, D.R., and Gillespie, Jr., J.W. (1996), "Rehabilitation of Steel Bridge Girders through the Application of Advanced Composite Materials," IDEA Project Final Report, Contract NCHRP-93-ID011.
- "MIL-HDBK-17-3E. Polymer Matrix Composites" (1996), DoD Coordination Working Draft, Chapter 5 – Structural Behavior of Joints. <http://mil-17.udel.edu/Pdf/v3ch5e.pdf> (02/12/03).
- Miller, B.D. (1999), "Bond between Carbon Fiber Reinforced Polymer Sheets and Concrete," M.S. Thesis, University of Missouri – Rolla.
- Miller, T.C. (2000), "The Rehabilitation of Steel Bridge Girders Using Advanced Composite Materials," M.S. Thesis, University of Delaware.
- Miller, T.C., Chajes, M.J., Mertz, D.R., Hastings, J.N. (2001), "Strengthening of a Steel Bridge Girder Using CFRP Plates," *Journal of Bridge Engineering*, Vol.6, No.6, pp.514-519.
- Mortazavi, A.A. and Pilakoutas, K. (2001), "Pre-tensioning of Composite by Lateral Pressure," In: FRP Composites in Civil Engineering, Vol.I, J.-G. Teng (Ed.), 2001 Elsevier Science Ltd, pp.345-354.
- Moy, S.S.J., (Ed.) (2001), "FRP Composites: Life Extension and Strengthening of Metallic Structures," ICE design and practice guides. Thomas Telford Publishing.
- Moy, S.S.J., and Nikoukar, F. (2002), "Flexural Behavior of Steel Beams Reinforced with Carbon Fibre Reinforced Polymer Composite," Proceedings of the First International Conference for Advanced Polymer Composites for Structural Applications in Construction, Southampton University, U.K., 15-17 April 2002, pp.195-202.
- Nakagoshi, A., and Shintani, S. (2000), "Steel Tower Reinforcement Using High Modulus Carbon Fiber and Resin Infusion for Prevention of Seismic Buckling Failure," Proceedings of the 21st International Conference of SAMPE, Paris, 19 April 2000.
- Nozaka, K., Shield, C.K., and Hajjar, J.F. (2001), "Rehabilitation of Fatigued Steel Girders with Carbon Fiber Strips," Fifth National Workshop on Bridge Research in Progress.
- Reid, I.L.K., Milne, D.M., and Craig, R.E. (2001), "Steel Bridge Strengthening – a Study of Assessment and Strengthening Experience and Identification of Solutions," Thomas Telford Publishing.

Rosetti, A., Chiocchio, G., and Paolini, A.E. (1982), "Expansive Properties of the Mixture C₄ ASH-2CS Part I - A Hypothesis on Expansion Mechanism," *Cement and Concrete Research*, Vol.12, pp.577-585.

Rumelhart, D.E., Hinton, G.E., Williams, R.J. (1986), "Learning Representations by Backpropagation Errors," *Nature*, Vol.323, pp.533-536.

Russo, G., Zingone, G., and Romano, F. (1990), "Analytical Solution for Bond-Slip of Reinforcing Bars in R.C. Joints," *J. Struct. Engrg., ASCE*, Vol.116, No.2, pp.336-355.

Shanley, F.R. (1947), *J. Aeronaut. Sci.*, Vol.14, p.261.

Sheigh, S.A., Fu, Y., and O'Neill, M.O. (1994), "Expansive Cement Concrete for Drilled Shafes," *ACI Materials Journal*, Vol.91, pp. 237-245.

Subramaniam, R.S., Reinhorn, A.M., Riley, M.A., and Nagarajaiah, S. (1996), "Hybrid Control of Structures Using Fuzzy Logic," *Microcomputes Civil Engineering.*, Vol.11, pp.1-17.

Tavakkolizadeh, M., and Saadatmanesh, H. (2002), "Repair of Steel Bridges with CFRP Plates," Proceedings of the First International Conference for Advanced Polymer Composites for Structural Applications in Construction, Southampton University, U.K., 15-17 April 2002, pp. 211-218.

Timoshenko, S. (1908), "Buckling of Bars of Variable Cross-Section", *Bull. Polytech. Inst., Kiev*.

Tumialan, G. (2001), "Strengthening of Masonry Structures with FRP Composites," Ph.D. Diss., University of Missouri – Rolla.

University of California site 2000, (01/20/03)

<http://www.cs.berkeley.edu/People/Faculty/Homepages/zadeh.html>

Werbos, P.J. (1974), "Beyond Regression: New Tools for Prediction and Analysis in Behavioral Sciences," Ph. D. thesis, Cambridge, MA, Harvard University.

West, T.D. (2001), "Enhancements to the Bond between Advanced Composite Materials and Steel for Bridge Rehabilitation," M.S. Thesis, University of Delaware.